

## Impact of inhibition mechanisms, automation, and computational models on the discovery of organic corrosion inhibitors

Winkler, David A.; Hughes, Anthony E.; Özkan, Can; Mol, Arjan; Würger, Tim; Feiler, Christian; Zhang, Dawei; Lamaka, Sviatlana V.

**DOI**

[10.1016/j.pmatsci.2024.101392](https://doi.org/10.1016/j.pmatsci.2024.101392)

**Publication date**

2025

**Document Version**

Final published version

**Published in**

Progress in Materials Science

**Citation (APA)**

Winkler, D. A., Hughes, A. E., Özkan, C., Mol, A., Würger, T., Feiler, C., Zhang, D., & Lamaka, S. V. (2025). Impact of inhibition mechanisms, automation, and computational models on the discovery of organic corrosion inhibitors. *Progress in Materials Science*, 149, Article 101392. <https://doi.org/10.1016/j.pmatsci.2024.101392>

**Important note**

To cite this publication, please use the final published version (if applicable). Please check the document version above.

**Copyright**

Other than for strictly personal use, it is not permitted to download, forward or distribute the text or part of it, without the consent of the author(s) and/or copyright holder(s), unless the work is under an open content license such as Creative Commons.

**Takedown policy**

Please contact us and provide details if you believe this document breaches copyrights. We will remove access to the work immediately and investigate your claim.



# Impact of inhibition mechanisms, automation, and computational models on the discovery of organic corrosion inhibitors

David A. Winkler<sup>a,b,c,\*</sup>, Anthony E. Hughes<sup>d,e</sup>, Can Özkan<sup>f</sup>, Arjan Mol<sup>f</sup>,  
Tim Würger<sup>g</sup>, Christian Feiler<sup>g,h</sup>, Dawei Zhang<sup>i</sup>, Sviatlana V. Lamaka<sup>g</sup>

<sup>a</sup> Department of Biochemistry and Chemistry, La Trobe Institute for Molecular Science, La Trobe University, Melbourne, Victoria 3086, Australia

<sup>b</sup> Monash Institute of Pharmaceutical Sciences, Monash University, 392 Royal Parade, Parkville 3052, Australia

<sup>c</sup> School of Pharmacy, University of Nottingham, Nottingham NG7 2RD, UK

<sup>d</sup> CSIRO Mineral Resources, Bayview Avenue, Clayton 3168, Australia

<sup>e</sup> Institute for Frontier Materials, Deakin University, Waurn Ponds, Geelong 3216, Australia

<sup>f</sup> Department of Materials Science and Engineering, Delft University of Technology, Mekelweg 2, 2628 CD Delft, The Netherlands

<sup>g</sup> Institute of Surface Science, Helmholtz-Zentrum Hereon, 21502 Geesthacht, Germany

<sup>h</sup> Kiel Nano, Surface and Interface Science KiNSIS, Kiel University, 24118 Kiel, Germany

<sup>i</sup> National Materials Corrosion and Protection Data Center, University of Science and Technology, USTB, Beijing, China

## ARTICLE INFO

### Keywords:

Corrosion inhibitors

High-throughput corrosion inhibition testing

Machine learning

Corrosion inhibitor mechanisms

Organic molecules

Molecular design

## ABSTRACT

The targeted removal of efficient but toxic corrosion inhibitors based on hexavalent chromium has provided an impetus for discovery of new, more benign organic compounds to fill that role. Developments in high-throughput synthesis of organic compounds, the establishment of large libraries of available chemicals, accelerated corrosion inhibition testing technologies, the increased capabilities of machine learning (ML) methods, and a better understanding of mechanisms of inhibition provide the potential to make discovery of new corrosion inhibitors faster and cheaper than ever before. These technical developments in the corrosion inhibition field are summarized herein. We describe how data-driven machine learning methods can generate models linking molecular properties to corrosion inhibition that can be used to predict the performance of materials not yet synthesized or tested. The literature on inhibition mechanisms is briefly summarized along with quantitative structure–property relationships models of small organic molecule corrosion inhibitors. The success of these methods provides a paradigm for the rapid discovery of novel, effective corrosion inhibitors for a range of metals and alloys, in diverse environments. A comprehensive list of corrosion inhibitors tested for various substrates that was curated as part of this review is accessible online <https://excorr.web.app/database> and available in a machine-readable format.

## 1. Introduction

Catastrophic structural failures of engineered structures occur mostly due to a combination of corrosion and stress and can cause death, injury, and major capital loss in a wide variety of industries and application areas [1]. These ongoing, short-term impacts

\* Corresponding author at: Department of Biochemistry and Chemistry, La Trobe Institute for Molecular Science, La Trobe University, Kingsbury Drive, Bundoora 3086, Australia.

E-mail address: [drdavewinkler@gmail.com](mailto:drdavewinkler@gmail.com) (D.A. Winkler).

<https://doi.org/10.1016/j.pmatsci.2024.101392>

Received 7 July 2024; Received in revised form 16 October 2024; Accepted 21 October 2024

Available online 24 October 2024

0079-6425/© 2024 The Author(s).

Published by Elsevier Ltd.

This is an open access article under the CC BY license

(<http://creativecommons.org/licenses/by/4.0/>).

coupled with economic losses due to corrosion, materials loss, failure, and aesthetic damage mean that corrosion control is extremely important and expensive. Recent publications have listed corrosion and stress-corrosion cracking as being by far the most severe cause of loss of longevity and integrity of metal products [3]. It has been estimated this loss equates to 3.4 % of the annual global gross domestic product (US\$2.5 trillion) [4,5]. Clearly, any progress in corrosion control will significantly improve the longevity of metal components. According to the latest NACE report, implementing best practices in corrosion prevention could result in global savings of 15–35 % of that cost, or up to 875 billion dollars [5]. There is also a growing concern over the large amount of energy required to extract and manufacture metals and alloys required to replace corroded components, and the greenhouse gases and pollution this produces. For example, it was estimated by Ianuzzi and Frankel that the steel required to replace only that conservatively estimated to be corroded, contributes 1.9 % to the total world CO<sub>2</sub> emissions [6]. Raabe *et al.* [3] identified ten measures that can reduce these impacts, with corrosion control being the most effective and feasible in the short term (Fig. 1). While adequate corrosion control measures are available, clearly there is room to reduce ongoing economic, health, and environmental impacts through the discovery of better corrosion inhibitors.

A working definition of a corrosion inhibitor is “a substance that, when added to an environment in small concentrations, minimizes the loss of metal, reduces the extent of hydrogen embrittlement, and protects the metal against pitting [7]. Corrosion inhibitors can be used in multiple ways. Inhibitors in aqueous systems reduce corrosion by forming an adsorbed or passivation layer that acts as a barrier, or by retarding cathodic, anodic, or both electrochemical processes. They can also be incorporated into anodic and conversion coatings (industrially applied active barrier coatings [8,9]) and as paint pigments [10]. Chromate has been used as a nearly universal corrosion treatment for a wide variety of metals for a century but is a teratogen, mutagen, and carcinogen [11]. Clearly, it poses an unacceptable risk to workers. It has been estimated that workers exposed to chromate residues when aircraft are repainted have ~ 250,000-fold higher risk of cancer than the public [12,13], thus the use of chromate inhibitors is being phased out in most countries. Other highly effective corrosion inhibitors containing tin and lead also have unacceptable risks and will be banned, or their use will be restricted due to health and safety and environmental concerns.

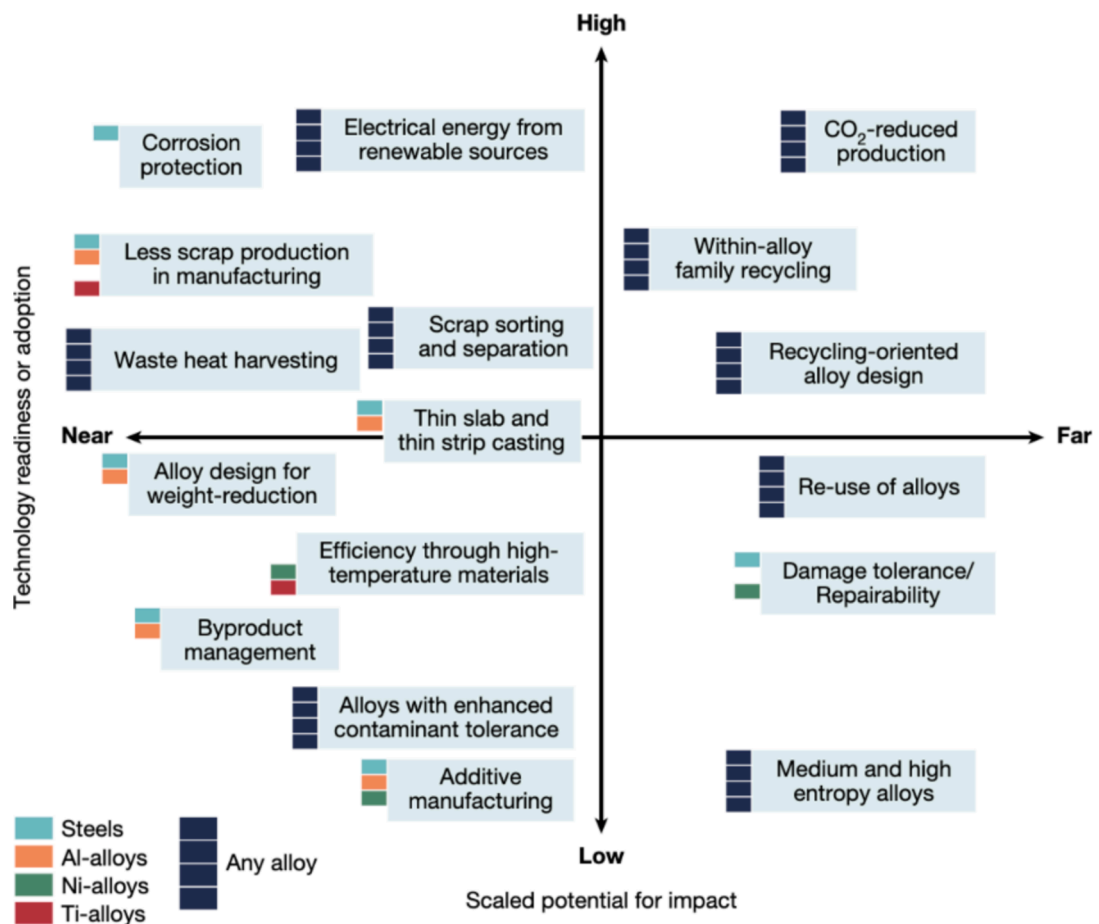


Fig. 1. An impact and technology readiness diagram for measures that can be taken to improve the sustainability of metals in the future. Note that corrosion protection ranks highest for both technological readiness and potential impact. Reproduced from Raabe *et al.* [3] with permission.

### 1.1. The critical importance of replacing chromate corrosion inhibitors

Chromate has been targeted for removal from the metal finishing and coatings industries in many jurisdictions including Europe and the US [13,14]. Some of these jurisdictions may have reduced usage of chromate in conversion coatings, but market reports suggest that chromate-based inhibitors as pigments for paint coatings are a growth area (see for example [15,16]) There are specific issues with chromate withdrawal in some aerospace applications because some parts of airframes may not be inspected for many years and need durable and highly reliable corrosion protection applied at the start of the service life [17].

Another issue with chromate replacement is the availability and cost of alternatives, as has been addressed by Hughes *et al.* [18] for inorganic inhibitors. Any organic inhibitor must match the cost and quantity issues of chromates. Chromate chemicals used in corrosion protection are derived from mineral chromite. However, the main reason for mining chromite is to obtain chromium for the manufacture of ferrochrome and stainless steel. Use in this application has remained steady at around 13 M tons per annum for several years [19]. Over a similar period, around 600,000 to 700,000 tons are converted to sodium dichromate ( $\text{Na}_2\text{Cr}_2\text{O}_7$ ) [20] thus dichromate is a commodity chemical. 224,000 tons were subsequently converted to chromic acid, ~50 % of which was used for metal finishing [20]. Thus, on a purely weight for weight basis, somewhere between 112,000 – 139,000 tons of inhibitor will be required to replace chromic acid used in industry. If replacement inhibitors are less efficient, then the amount required will be larger.

Small organic molecules offer a vast diversity of structures and properties, some of which may be potentially superior corrosion inhibitors for industrial corrosion control and occupational health and safety needs. Organic inhibitors are widely used for multiple industrial applications owing to their selectivity, affordability, and stability under operational conditions. While their danger to humans is generally lower than chromate (by a factor of 10 to 20 as assessed by  $\text{LD}_{50}$  (rats)), they are not without issues. Mercaptobenzothiazoles are a group of commonly studied inhibitors which perform well on a range of metals. However, 2-mercaptobenzothiazole has been declared a potential carcinogen in humans by the WHO, based on studies of worker exposure [21]. There are also environmental issues associated with organic molecules like EDTA due to its strong and persistent complexing of metal ions in natural water [22].

Typically, organic corrosion inhibitors adsorb onto metal/oxide/hydroxide surfaces and form protective films that displace the water and slow down the ingress of aggressive chloride ions. Efficient small organic molecule inhibitors usually contain oxygen, nitrogen, sulfur, and phosphorus atoms with lone electron pairs, along with moieties providing  $\pi$ -electrons, all facilitating adsorption [23]. The number of organic corrosion inhibitors studied to date is approximately 1500 out of 150 million compounds catalogued in Chemical Abstract Service database. Among these organic corrosion inhibitors none, so far, has the effectiveness and wide applicability of chromate.

Here we review important developments likely to impact the discovery of more effective organic corrosion inhibitors. These include automation of the synthesis and characterization of organic inhibitors, AI and machine learning, and mechanism-based inhibitor design. We also provide an overview of the literature on organic inhibitors for metals including copper, iron, aluminium, magnesium, and their alloys. Specifically, we briefly summarize recent developments in high-throughput synthesis and corrosion testing, and the use of quantitative structure–property relationships (QSPR) and advanced machine learning methods to predict the inhibitory properties of organic compounds. The latter allows the corrosion inhibition of compounds not yet synthesized or tested to be predicted [24–29]. Machine learning models can also be used as surrogate fitness functions for the evolutionary design of new corrosion inhibitors with multiple desirable properties [31–33]. We provide a concise summary of current knowledge on relationships between inhibitor structure, mechanisms of inhibition, and efficacy and perspectives for future developments. A database of corrosion inhibitors tested for various substrates that was curated as part of this review, accessible online <https://excrr.web.app/database> and is available in a machine-readable format.

## 2. Impact of automation on synthesis and characterization of organic inhibitors

Discovery of inorganic and organic inhibitors has traditionally followed the one-compound-at-a-time paradigm. This can be accelerated in two ways. First, increasingly science and technology are embracing robotics and automation to dramatically increase the number of materials that can be synthesized and tested. Second, these experimental techniques are expanding data collection by many orders of magnitude over conventional techniques (see sect. 2.5). These data are important for training machine learning models for discovery, design, and optimization of next generation organic corrosion inhibitors. Unlike some other important areas of science and technology, corrosion science has been slow to adopt of these paradigm-shifting technologies. They promise to leverage valuable prior knowledge and technology to accelerate discovery of more effective and safer organic corrosion inhibitors to replace toxic materials that have dominated the field for decades.

Faster methods of synthesis and testing clearly have major advantages over the traditional ways of performing these tasks. The development of these technologies is driven by the recognition of the vastness of the organic chemical space in which inhibitors exist, and the potentially large, paradigm-changing advantages that data-driven AI and machine learning methods (for which Nobel Prizes in physics and chemistry were awarded in 2024) can bring to the field. Increased synthesis and testing rates means that a much larger part of chemical space can be explored than by traditional methods. However, even the most optimistic projections of the capacity of these automated methods suggest that it is possible to explore only a minute fraction of the estimated  $10^{63}$  organic molecules [35–36] (far exceeding the  $10^{21}$  stars in our observable universe) that are synthetically accessible using the known laws of chemistry. Thus, the size of chemistry space represents both a challenge and an opportunity for the discovery of new, safer, more effective corrosion inhibitors. The challenge is the impossibility of exploring the whole of chemical space exhaustively, and the opportunity is that the vast chemical space provides an almost infinite number of candidate materials, many of which will have valuable properties, if we can discover them.

Automated methods will also generate large data sets that can be used to train machine learning models that predict properties of new materials orders of magnitude faster than any automated experimental method. The paucity of high quality, large (> 100 compounds), chemically diverse data sets is one of the main issues holding back the wider application of data-driven machine learning methods described below. Here we briefly summarize the main methods for synthesizing organic corrosion inhibitors and measuring their performance and discuss the current progress towards automation, the value of AI and machine learning in discovery of new organic corrosion inhibitors, and the potential for future improvements in this area.

### 2.1. High-throughput synthesis of organic compounds

The need for high-throughput (HT) synthesis was first recognized by the pharmaceutical industry around 1990 [38]. They developed combinatorial chemistry that increased the rate of synthesis of small organic molecules by orders of magnitude compared to traditional one-molecule-at-a-time approaches. Subsequently, click chemistry facilitated the reliable generation of large libraries of molecules containing nitrogen heterocycles, potentially valuable corrosion inhibitors chemotypes [39], and flow chemistry has provided a pathway to efficient, safe, and at-scale synthesis of chemical compounds [40]. These are now very large and mature research and technology areas, well covered by numerous books and reviews, see, for example [41,42], so they are not discussed further here.

Although high-throughput and combinatorial synthesis of small organic compounds is well established in the pharmaceutical industry, it is yet to be employed in corrosion inhibition research. This is due to the lack of HT corrosion inhibition testing methods, and the existence of very large libraries of virtual, commercially available or make-on-demand organic compounds (billions of compounds) that can be tested or computationally screened for corrosion inhibition without requiring synthesis. An additional factor delaying the development of HT methods for inhibitor testing is the large variety of deployment conditions of metallic structures,

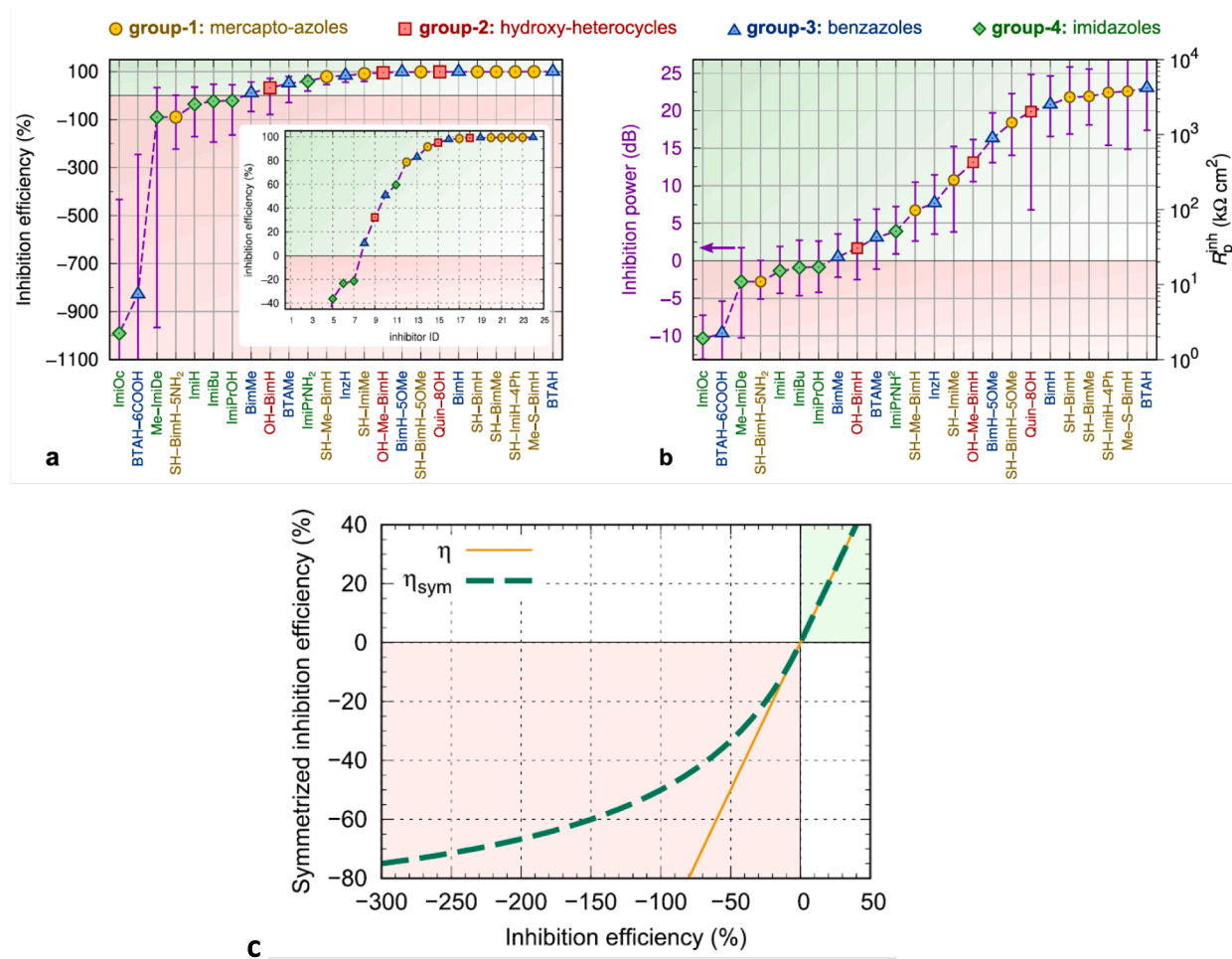


**Fig. 2.** The values of inhibition efficiency a) and inhibition power b) calculated for the identical set of Cu corrosion inhibitors, introduced by Kokalj et al. [43], reproduced from [43] under Creative Commons CC-BY license. Differentiation between highly potent inhibitors is more clearly seen in b), the inhibition power plot. c) Symmetrized inhibition efficiency that penalizes the negative values of inhibition efficiency, keeping all the  $\eta_{sym}$  values within  $-100$  to  $100$  % range, introduced by Kokalj et al. Reproduced from [1] with permission.

resulting in an even larger range of exposure environments and a lack of understanding of the most relevant testing conditions.

## 2.2. Experimental measurements of corrosion inhibition

Corrosion inhibition (CI) can be measured using a range of well-known techniques summarized below, and metrics from these different techniques can often be compared directly to assess performance. Many studies report “inhibitor efficiency”  $\eta$ :

$$\eta = \frac{\gamma - \gamma_{inh}}{\gamma} \cdot 100 \%$$

where  $\gamma$  and  $\gamma_{inh}$  are the parameters of interest (e.g., corrosion current, mass loss, hydrogen evolution, polarization resistance derived from EIS spectra, etc.) in the absence and presence of the inhibitor respectively. Although widely used, this relationship is highly non-linear: for low values of  $\gamma_{inh}$ , a small increase in inhibition causes a rapid increase in inhibition efficiency, whereas for  $\sim \eta > 90 \%$ , further reduction in corrosion only leads to a small increase in  $\eta$ . Clearly,  $\eta$  is more useful for screening poor or modest inhibitors since in such cases  $\gamma_{inh}$  will be of a similar magnitude to  $\gamma$ . However, its ability to distinguish between good inhibitors is poor since  $\gamma_{inh}$  may be two or more orders of magnitude smaller than  $\gamma$ . This means that several orders of magnitude difference in performance between good inhibitors is squeezed into two percentile points at the top of the inhibitor range.

A recently conceived inhibitor performance metric, inhibition power  $P_{inh}$  expressed as

$$P_{inh} = 10 \log_{10} \left( \frac{\gamma}{\gamma_{inh}} \right)$$

enables easier differentiation of the good inhibitors by ranking them in an unbiased way [43]. The unbiased distribution of data is also important in the training of machine learning models for which skewed data results in lower predictive performance. This lack of balance [44] in the data usually generates models with poor predictive performance, specifically for the minority class. Inhibition power delivers more balanced data, hence is expected to improve the predictive power of the models. Fig. 2 illustrates the difference between inhibition efficiency and inhibition power for the identical set of corrosion inhibitors tested on pure Cu by Kokalj *et al.* [43].

An alternative metric for corrosion inhibitor performance, symmetrized inhibition efficiency (Fig. 2c), was also introduced by Kokalj *et al.* [1]. It penalizes negative values of inhibition efficiency, deemphasizing the importance of large negative values that are not always measured with the same precision (e.g. due to difficulties of accounting for change of sample surface area in hydrogen evolution measurements or missing deeper pitting in image analysis). These values can potentially bias machine learning models:

$$\eta_{sym} = \begin{cases} \eta & \text{if } \eta \geq 0 \\ \frac{100\eta}{100 - \eta} & \text{otherwise,} \end{cases} \quad [1]$$

The value of inhibition efficiency and symmetrized inhibition efficiency are virtually the same in the range between 100 to  $-20 \%$ , Fig. 2c, but  $\eta_{sym}$  decreases more slowly below this, asymptoting so that no datapoint can be lower than  $-100 \%$  or greater than  $+100 \%$ . Comparing the applicability of these two recent metrics, the inhibition power ( $P_{inh}$ ) is more suitable for strong corrosion inhibitors, while symmetrized inhibition efficiency  $\eta_{sym}$  is more intuitive and may be better for the datasets of modest corrosion inhibition efficiency [1].

The three metrics quantify total corrosion impact without differentiating between different types of localization of corrosion attack, a potential shortcoming. Mechanical integrity of metallic components that can be compromised by pitting, intergranular and other types of localized corrosion, is of prime concern in practical applications. However, the existing metrics for inhibition efficiency do not elucidate these processes because they assume a homogeneous degradation and evenly distributed corrosion attack. It has been shown for a magnesium alloy that inhibition efficiency does not necessarily correlate with the ability of given inhibitor to prevent localized corrosion and help retain mechanical properties of the alloy [45]. Industrially, many tests are used to assess corrosion performance of bare metals and painted materials. Many of these tests are codified in standards such as ASTM and DIN. Often, tests are based on visual inspections of colour changes in corrosion products or number of pits developed after a defined exposure time, see for example salt-spray exposure according to ASTM B117, ASTM G85 and evaluation according to ASTM D1654, ASTM D714. A detailed description of these is beyond the scope of this review, so we only summarize more common corrosion inhibition test methods here. This is because accelerated testing is a distinct topic, ranging from cyclic outdoor tests to museum environments [46], to the auto industry [47,48], aerospace [49,50,51,52,53,54] and infrastructure industries [55].

One of the biggest issues with accelerated testing is whether acceleration accurately mimics natural corrosion processes. Thus, accelerated tests are often categorised into cyclic or constant stress testing, i.e., where stressors are factors like temperature, electrolyte, UV exposure etc., and cyclic refers to repeated temperature cycles, or wet/dry cycles etc. Cyclic tests tend to be more realistic predictors of performance, particularly those with wet/dry cycles [56]. This is because they account for formation of possible insoluble corrosion products that provide protection to the substrate and allow for electrolytes to become more concentrated during drying, facilitating more aggressive corrosion. Dante *et al.* [49,50] developed an accelerated dynamic corrosion test method that more accurately predicts corrosion of bare or coated alloys and galvanic couples in operational environments. In doing so, they concluded that the relative humidity and its cyclic variations are by far the most important factors in governing the atmospheric corrosion.

The issue of accurate mimicking of natural corrosion processes is, of course, also relevant to high-throughput testing and will undoubtedly be the subject of further debate on how HT tests are designed. Combined stressors, such as corrosion and mechanical impacts, widely encountered together, lead to even faster degradation of material systems in operational environments. The Boeing

company patented two experimental testing designs combining mechanical load with corrosion attack. A cyclic flexing salt-spray chamber [51] is able to exert cyclic mechanical stress (at a frequency between 0.1 to 60 Hz) to metallic panels in controlled salt-fog environment. Another patent describes the perturbed oscillatory kinetics electrochemistry setup suited to record electrochemical response of metallic coupons before and after applying mechanical load [52].

A common method for assessing corrosion is weight loss, which is used in both industrial and research environments. It can be used to assess any type of environment. Coupons are weighed before and after an experiment (preceded by removal of corrosion products following established standards [57]), and the test measures the amount of corrosion product removed or amount of metal or alloy remaining. Hydrogen evolution is usually only employed in Mg corrosion and inhibition research because, unlike Al, Zn, Fe, and Cu-alloys where oxygen reduction is the main cathodic reaction, hydrogen evolution reaction is the main cathodic process during magnesium corrosion, with oxygen reduction being secondary process [58–61]. Galvanic corrosion test methods typically start with manufacturing galvanic test assembly panels comprising, for example, titanium or stainless-steel fasteners in aluminum alloy panels. These are exposed to salt-spray followed by visual inspection [54], and profilometric quantification of material lost due to the galvanic corrosion or galvanic current measurements in full immersion condition [53].

Electrochemical approaches are widely used in the research environment because they provide quantitative measures of corrosion performance. The most common types of tests include electrochemical impedance spectroscopy (EIS), potentiodynamic and potentiostatic polarization, electrochemical noise, and zero resistance ammeter (ZRA) for galvanically coupled dissimilar metals (e.g. Boerstler *et al* [53]). Raw EIS data can be used for qualitative comparisons of the performance of inhibitors. Inspection of these data

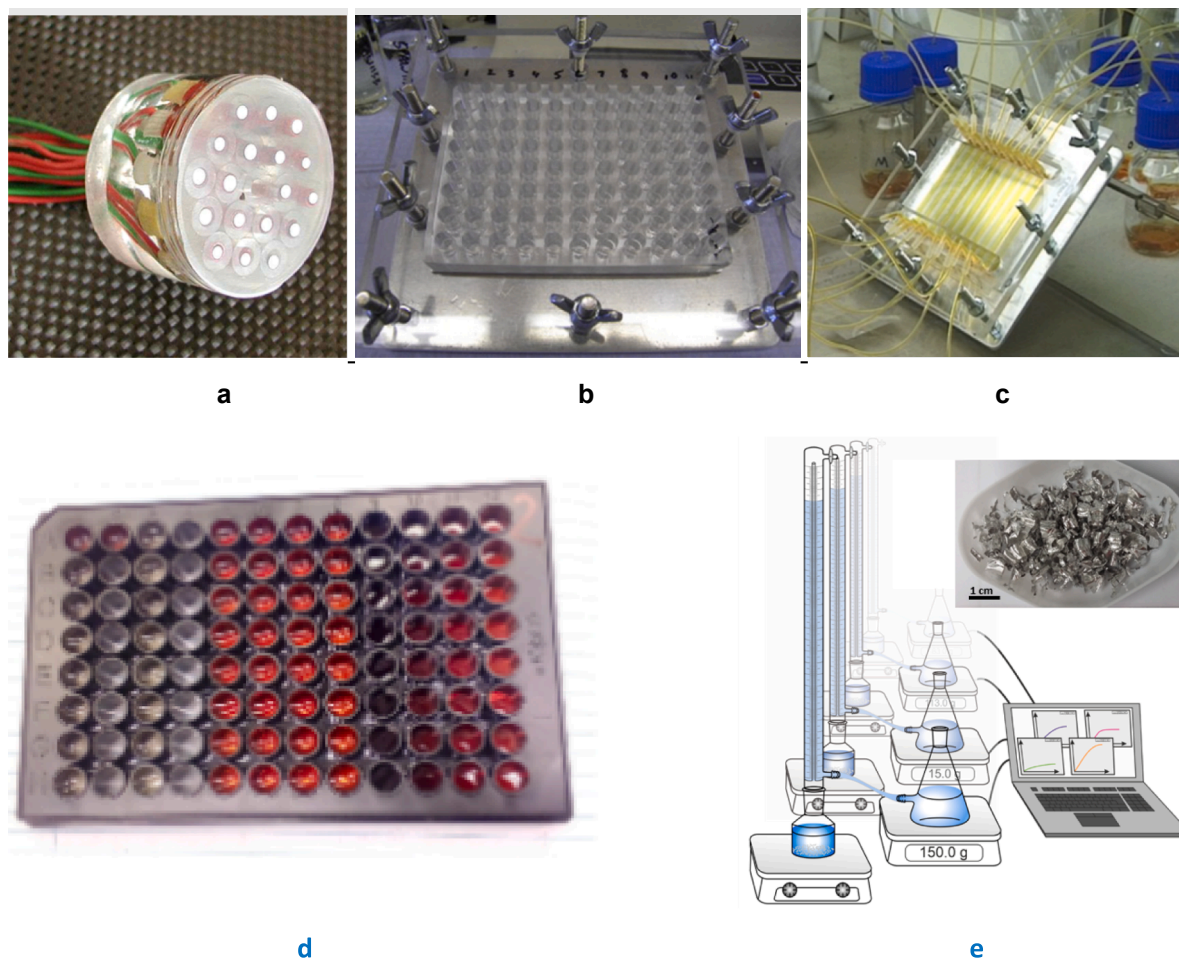


**Fig. 3.** Experimental high-throughput corrosion inhibitor screening setups. a) Multi-electrode assembly showing the layout of wire specimens. Reproduced from Muster *et al.* [72] with permission; b) Multi-well corrosion inhibition setup. Reproduced from White *et al.* and Winkler *et al.* [73,74] with permissions; c) Multi-channel microfluidic arrays adapted from White *et al.* [75]; d) Test-tubes containing of iron-thiocyanate Fe(SCN)<sub>3</sub> complex for spectrophotometric quantification of dissolved Fe concentration, proposed by Zabula *et al.* [76] reproduced with permission; e) Automated eudiometer setup logging volume of released H<sub>2</sub> during corrosion of Mg alloys by weighing the amount of displaced water adapted from [60,77]. The insert shows the visual appearance of the Mg chips used for H<sub>2</sub> evolution measurements reproduced from Lamaka *et al.* [60] with permission.

provides an estimate of the low-frequency impedance, which is usually related to the charge transfer or polarization resistance and is a typical performance indicator for inhibitor studies. The corrosion current is measured by potentiodynamic polarization experiments and is used to calculate corrosion inhibition values that are comparable between samples. Other, more sophisticated techniques are used for laterally resolved corrosion (inhibition) studies, such as the scanning vibrating electrode technique (SVET) used for inhibitor screening for galvanically coupled dissimilar metals [62–64].

### 2.3. High-throughput corrosion inhibition screening

Development of high-throughput direct or surrogate methods for assessing corrosion inhibition is essential to progress this field because collection of inhibitor performance data is the rate-determining step, not chemical synthesis. Although high-throughput assessment methods have become the mainstay of diverse research fields, corrosion science is a slow adopter [65]. However, encouraging progress has been made in the past 10–15 years. The most important consideration in developing these rapid methods is how their results relate to ‘real world’ corrosion inhibition. Currently, electrochemical methods, weight loss, hydrogen evolution, spectroscopic, and photometric methods are still being used to measure corrosion inhibition in medium- to high-throughput formats.

Seminal work by Chambers *et al.* employed the direct current polarization between two aerospace aluminium alloy (AA2024) wire electrodes and a multi-electrode testing system to assess corrosion inhibition of fifty chemistries in just 9 h. The results correlated highly with those from extended testing over 10 days [66]. They extended their work by scoring corrosion using fluorometric detection of  $\text{Al}^{3+}$  levels [67]. They measured corrosion inhibition of 14 compounds over a wide range of initial pH values after 1–7 days [68]. They subsequently developed a system for rapidly assessing inhibition characteristics of 100 diverse chemistries using DC polarization, cyclic voltammetry of re-deposited copper, and fluorometric detection of  $\text{Al}^{3+}$  [69,70]. Muster *et al.* and Garcia *et al.* also reported high-throughput screening techniques for corrosion inhibitors using a multielectrode electrochemical system [71,72]. This allowed 30 electrochemical experiments per hour to be performed, facilitating rapid discovery of inhibitors that protect different metals, and quickly identifying optimal inhibitor concentrations (Fig. 3).

Kallip and coworkers reported a novel procedure using SVET to assess corrosion inhibitors [62]. They determined the percent corrosion inhibition efficiencies (%IE) of four inhibitors for Fe and Zn. He *et al.* described a high-throughput electrochemical impedance spectroscopy (HT-EIS) method for the rapid evaluation of corrosion coatings. They developed a 12-element, spatially addressable electrochemical platform interfaced with a commercial EIS instrument [78].

White *et al.* described a novel multi-well method for high-throughput testing of corrosion inhibition based on image analysis of corrosion surfaces generated after exposure to inhibitor-containing electrolyte (Fig. 3b) [73,74]. Up to 88 simultaneous corrosion inhibition tests could be carried out on a single plate, plus positive and negative controls. After a 24 h assessment period and using the AA2024-T3 aerospace alloy, the amount of white corrosion product was used to assess the extent of corrosion. Corrosion inhibition was assessed using a novel, robust, computerized image processing method. Shi *et al.* reported a similar automated system for corrosion assessment using optical imaging that showed a linear relationship between the apparent grey value of the image and the depth of corrosive pitting in the specimen.[79].

A spectroscopic method for studying metal dissolution using multi-channel microfluidic arrays was reported by White *et al.* (Fig. 3c) [75]. They employed inductively coupled plasma atomic emission spectroscopy to determine Al and Cu levels, visual inspection, and image analysis of pits to quantify the relative performance of AA2024-T3 corrosion inhibitors under flowing electrolyte conditions in 10 parallel channels. The flow conditions accelerated corrosion up to 15-fold, resulting in shorter experimentation times. Different chemistries could also be readily investigated through parallel experimentation. Analogously, Zabula *et al.* [76] (Fig. 3d) determined the amount of dissolved iron formed during corrosion by spectrophotometric measurements of the colour intensity of iron-thiocyanate  $\text{Fe}(\text{SCN})_3$  complex and used this to quantify the inhibition due to the presence of corrosion inhibitors.

For reactive metals like magnesium, hydrogen evolution can also be used to measure corrosion inhibition or acceleration properties of molecules. Here, fixed amounts of Mg-alloys with large ( $180 - 550 \text{ cm}^2/\text{g}$ ) surface areas were exposed to a corrosive agent with, or without added inhibitor or accelerant. Magnesium dissolution and hydrogen evolution occur during aqueous magnesium corrosion. The amount of hydrogen evolved over a given time was used to quantify the performance of inhibitors. Lamaka *et al.* reported a medium- to high-throughput testing rig that used hydrogen evolution to measure the performance of organic inhibitors of magnesium corrosion (Fig. 3e)[60]. They reported the inhibiting properties of 151 chemical compounds on AZ31, AZ91, AM50, WE43, ZE41, and Elektron 21 Mg alloys, and three grades of pure magnesium, generating  $\sim 2000$  corrosion inhibition values. The large surface area and rapid corrosion in the absence of oxygen in these experiments made it possible to ignore the significant contribution of the oxygen reduction reaction (ORR) to Mg corrosion under atmospheric conditions [80] or in air-equilibrated electrolytes [59,81].

Encouragingly, most of these rapid inhibition measurement methods are amenable to substantial scale up. This should be an active area of research going forward, together with more substantial validation of the methods under real world operating conditions.

### 2.4. Potential impact of additive manufacturing technologies

Additive manufacturing (3D printing) is having a large impact in many areas of science, technology and commerce [82]. Metals and alloys can now be deposited by additive manufacturing processes like powder sintering, cold spray, laser, laser powder bed fusion, thermal inkjet printing, electron beams, and wire arc melting [83–89]. These AM approaches provide two types of opportunities. First, new metal alloys can be produced using conventional compositions but with different properties due to the rapid cooling associated scanned beam (laser, electron) processing. Second, they can potentially be used to simulate microstructures of conventionally manufactured materials.



Indeed, in the former case, there is a considerable body of work emerging on the corrosion behaviour of electron and laser beam AM materials [90]. Note that, in this area, the range of metal alloys investigated has been narrow due to the limited number of metal powders that are available commercially. Summaries of the types of materials that have been produced, their microstructures and mechanical properties are available [85,91]. For example, SS316L steel manufactured using laser powder bed fusion (LPBF) has been extensively studied. It has been shown that the microstructure of the as-manufactured material is fundamentally different from conventionally manufactured (CM) material. AM materials exhibit better mechanical properties (microhardness, yield strength, tensile strength), and similar elongations [92–96]. The corrosion behaviour is also fundamentally different because the microstructure is different. Specifically, LPBF SS316L steel has an extensive dislocation cell structure that captures Mn and S (and other elements) thus inhibiting the formation of MnS, which leads to higher breakdown potentials than CM SS316L steel [93,97–98]. These microstructural features may require special inhibitors to interact with the dislocation structures or the Mn and S trapped in them, for example.

Regarding the second opportunity that AM presents, it might be possible to create a large number of small area samples of different alloys and metals for subsequent high-throughput corrosion testing. AM can also create gradients of two or more metal alloys [86] that could also be tested in high-throughput methods, thus expanding the number of metallic systems available for corrosion inhibition studies. New developments in multi-materials AM promise unprecedented control over these systems [99]. For example, a new multi-metal AM technique called electrohydrodynamic redox printing (EHD-RP) overcomes the limitations of small-scale multi-metal AM, allowing direct printing and mixing of multiple, high-quality metals from a single nozzle with high spatial resolution [100].

As additive manufacturing is increasingly adopted because of its parsimonious use of materials, versatility, and low cost for prototyping, the study of corrosion in additively manufactured metals and alloys, and the use of AM to screen larger numbers of these materials for effective corrosion inhibitors will undoubtedly increase markedly in the near future.

### 2.5. Advances in physicochemical characterization for screening

While it may be possible to manufacture artificial microstructures using AM manufacturing processes, an alternative for high-throughput investigations of inhibitor interactions with metals is extensive characterization of the surfaces before and after inhibitor exposure. Here the focus is on obtaining excellent data on inhibitor interactions at the micron scale. This has two advantages over 3D printing: (i) it does not require prior knowledge of the microstructure that is needed to devise the scanning pattern program that allows 3D printers to produce realistic microstructures and (ii) large data mapping (centimetres) can be done at micron scale resolution. In the case of aluminium alloys, this means that hundreds of thousands of intermetallic particles can be characterized in a single experiment (Al-alloys typically have a few hundred thousand particles/cm<sup>2</sup>) [101–103]. This provides primary information, such as their elemental composition, as well as secondary information about their spatial relationships (such as clustering of intermetallic particles that can lead to more active corrosion initiation sites). This approach would be useful for many alloys that have heterogeneous microstructures such as iron and magnesium alloys. Another technique, Electron Backscatter Diffraction, can provide both elemental and structural characterization over large areas of a surface. This means that structural information on intermetallic particles and the matrix in which they are imbedded can be obtained in great detail. Moreover, large scale characterisation can be performed prior to and after exposure to corrosion inhibitors, thus providing site-specific information on inhibitor interactions with the microstructure of the surface at a statistical level. In principle, the information derived from these large-scale characterisation studies can be coupled with scanning electrochemical techniques to provide spatially resolved information on composition and electrochemical activity. This has already been done on much smaller scales [104]. The information gained from these studies may well provide important metrics for assessment of inhibitor interactions with metallic surfaces.

Some of the earliest research on intermetallic particles effects was done on aluminium alloys, which have a highly heterogeneous microstructure comprised of many small intermetallic particles embedded in an aluminium alloy matrix (see for example Table 3). For example, Boag *et al.* [105] measured 82,000 phase domains in 18,000 particles in a 2 mm × 2 mm area of AA2024-T3 alloy. These studies ultimately led to the identification of new structures for some of AA2024-T3 intermetallic particles, plus an assessment of the electrochemical potential differences between the particles and the matrix [104]. On a smaller scale, LaCroix *et al.* [106,107] reported the composition and electrochemical activity of over 300 S-phase particles in AA2024-T3. In other work, Cawley and Harlow [108] investigated the influence of 3D clustering on AA2024-T3 using image analyses on large areas of material. They found that clustering of intermetallic particles had an important role in pit initiation. Similarly, Mao *et al.*, [109] did extensive modelling of optical micrographs to develop realistic 3D microstructures of intermetallic particle distributions in AA7075 plate. Chen *et al.* [110] also performed large scale microstructural characterization and devised a method for generating statistically similar surfaces for modelling.

The breadth of application for these techniques is, however, limited by the intrinsic resolution of the techniques and the amount of data they produce. Resolution is primarily determined by the probe size and the excitation volume. Generally, the best current resolution is of the order of a few hundred nanometres, with most being around the micron scale. Hence, these large area/volume approaches miss many of the smaller features such as segregation at grain boundaries, decoration of dislocation structures, hardening precipitates, and very small inclusions (see section 5 for further details on these microstructural features).

Outside of corrosion, large characterization datasets are being generated for a range of applications by new detectors and the use of synchrotron sources [111]. Apart from allowing exploration of much larger parts of organic chemical space, high throughput corrosion inhibition methods can generate much larger datasets. They are, therefore, ideally matched to the capabilities of AI and machine learning methods. The combination of large datasets with deep learning methods is a rapidly emerging area of research [112].

### 3. Impact of inhibition mechanisms on design and discovery of organic corrosion inhibitors

The scope of this review is confined to organic inhibitors. However, it is important to note that organic inhibitors are not the only potential replacements for chromate. There are numerous inorganic inhibitors and compounds that include an inorganic component (usually a cation) with an organic component (usually anion) whose properties are outside the scope of this review.

Organic compounds with molecular weights below 1000 Da are one of the most promising classes of materials for replacing toxic chromate inhibitors for the following reasons. The size of the accessible chemistry space described above provides vast scope for the discovery of novel, effective organic inhibitors [113]. Organic molecules exhibit very high structural, physiochemical, and redox property diversity, important for effective corrosion control for different metals and alloys and exposure scenarios. Many compounds will have acceptable mill costs and compatibility with components of coatings and treatments. Proof of concept experiments have demonstrated their potential as corrosion inhibitors. Additionally, there are large libraries of organic compounds commercially available for experimentation. As discussed above, these libraries plus the increasing capabilities of automated high-throughput chemical synthesis [114,115], and corrosion inhibition assessment will provide large, rich data sets that can be used to train machine learning models used to discover or design new, more effective corrosion inhibitors [116,117]. Also, as foreshadowed, other data-driven methods like design of experiments [118], statistical QSPR modelling [119], and evolutionary methods [31,32] will become essential to fully exploit data from high throughput synthesis and screening methods, allowing the exploration of much larger regions of chemical space for 'islands of utility'.

Organic corrosion inhibitors largely function by forming films or by inhibiting cathodic or anodic processes, or both. Independently of which reaction is suppressed, most organic inhibitors act by surface adsorption and precipitate film formation (Fig. 4), akin to inorganic chromates, phosphates, and nitrites, the best-known oxide film-forming inhibitors [120]. Molecules exhibiting a strong affinity for metal surfaces often exhibit good inhibition efficiency. However, an optimal value of adsorption energy should not be exceeded. Otherwise, a corrosion inhibitor might turn into a corrosion promoter, as reported by Kokalj, Fig. 5 [121].

Anodic inhibitors perform two main functions, slowing the reaction rate of anodic dissolution and generating sparingly soluble reaction products that form thin films over the anode. Fig. 6.1 shows a potentiostatic polarization plot illustrating the behaviour of an anodic inhibitor. As the anodic reaction is modulated by the inhibitor, the corrosion potential ( $E_{\text{corr}}$ ) of the metal is shifted to more positive values, and the corrosion current ( $I_{\text{corr}}$ ) decreases in the presence of the inhibitor.

Cathodic inhibitors also inhibit corrosion via two main processes, disrupting the cathodic oxygen reduction reactions and generating reaction products that precipitate selectively at cathodic sites. Fig. 6.2 shows an example of a polarization curve of a metal with a solution of a cathodic inhibitor. When the cathodic reaction is affected, the corrosion potential  $E_{\text{corr}}$  is shifted to more negative values. Fig. 6.3 illustrates a theoretical potentiostatic polarization curve showing the effect of a mixed (anodic and cathodic) organic inhibitor. With inhibitor, the corrosion potential  $E_{\text{corr}}$  remains the same, but  $I_{\text{corr}}$  decreases. Inhibitors with functional groups that suppress both anodic and cathodic reactions are the most desirable.

So far, the discussion has centred on inhibitors may operate largely by a single mechanism. In reality, many organic inhibitors have more than one mechanism of interaction with a surface. The introduction of heteroatoms, such as S, N, and O containing lone pair electrons, into organic ring structures often improves the binding capacity (Fig. 7). The electron density around these atoms depends on the electronic configuration of the entire molecular structure and promotes chemisorption of these heteroatoms.

As illustrated in the examples of machine learning modelling of organic corrosion inhibition later in the text, quantum mechanical density functional theory (DFT) calculations can provide valuable information about surface interactions of individual molecules and functional groups. Bonding to a surface may also depend on the separation between heteroatoms, as well as the type and number of intermediate atoms. These types of factors are captured more strongly by molecular descriptors used in machine learning and AI models than those derived from DFT calculations. Molecules can only bind perpendicular to the metal surface if heteroatom sites are adjacent, or at specific angles, to the surface depending on the number of atoms separating the hetero atoms. For carboxylic acids, the

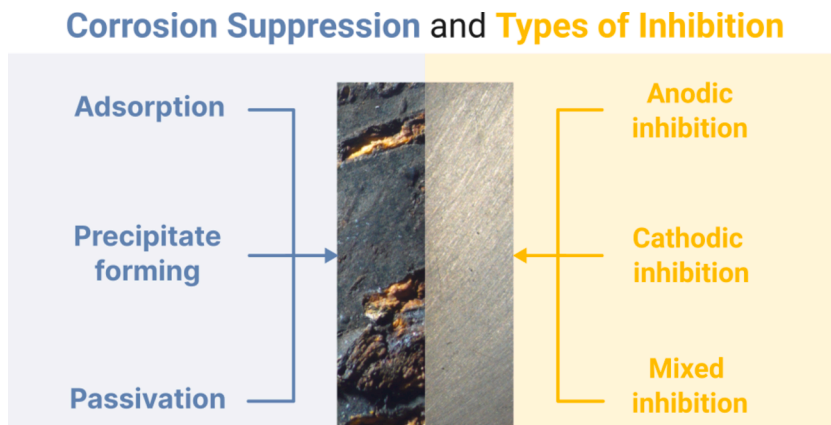


Fig. 4. Diagram of conditional division of corrosion inhibitors into main mechanism groups.

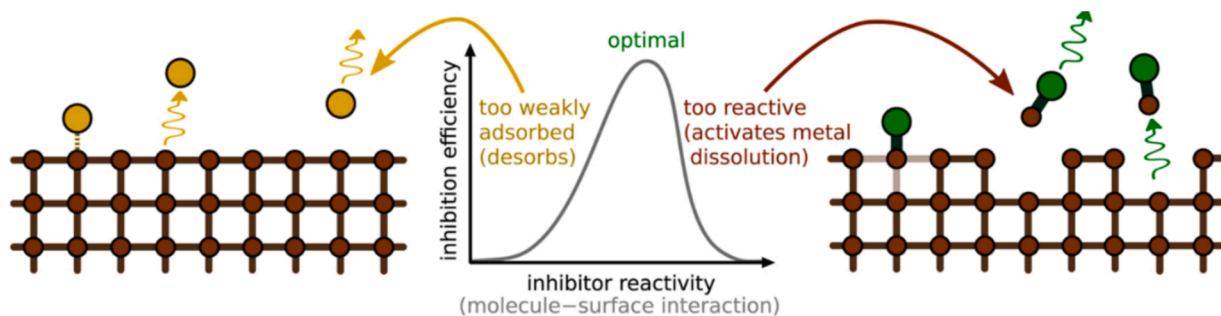


Fig. 5. Schematic illustration of inhibitor-metal interactions. Weak inhibitor-metal interactions result in low inhibiting efficiency, while too strong bonding assists metal dissolution. Reproduced from Kokalj, [121] under Creative Commons CC-BY license.

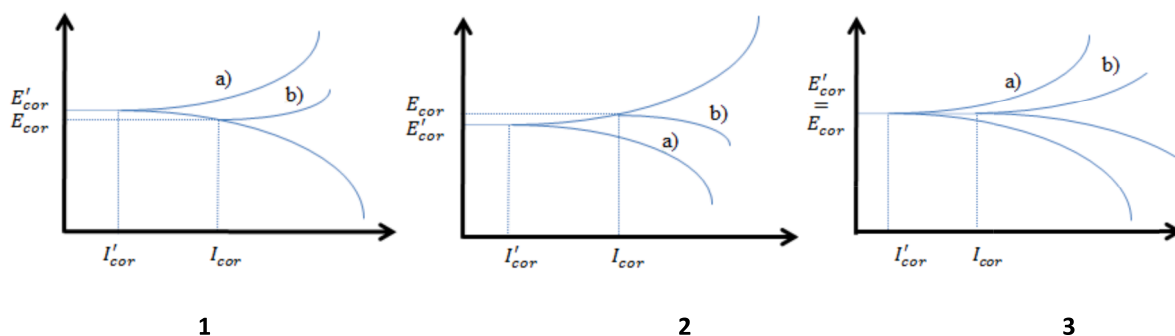


Fig. 6. Potentiostatic polarization diagram showing behaviour of a metal with 1(a) anodic 2(a) cathodic, 3(a) mixed (cathodic and anodic) inhibitor, and without inhibitor (b), respectively. Reproduced from Dariva and Galio [122] under Creative Commons CC-BY license.

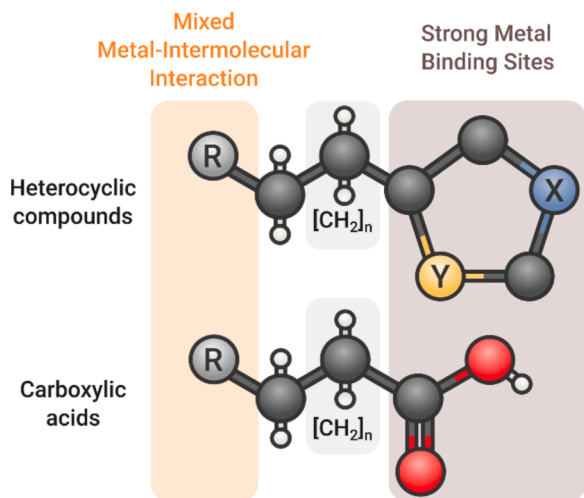


Fig. 7. Many small organic inhibitors exhibit more than one inhibition mechanism. Examples of two classes of inhibitors are shown, a heterocyclic compound and a carboxylic acid both with strong metal binding and R-groups that may exhibit weaker surface interactions. Common heteroatoms for  $\times$  and Y are S, N, and O.

strongest binding site is more localized around the carboxylic acid group. The rest of the inhibitor molecule can also modulate binding to metals. For example, self-assembled monolayers (SAMs) may form by self-organization of molecules on the surface to minimize their interaction energy. Alternatively, where molecules also contain unsaturated, cyclic, branched, or linear hydrocarbons, physisorption can also play an important role in binding to metal surfaces. Thus, molecules may have two or more types of interaction with the surface. For example, more complex branched molecules with additional heteroatoms can, in principle, have multiple points of interaction with the surface and a diverse range of inhibition properties. Ideally, inhibitors with strong absorption characteristics for a

range of different metals will be the most widely applicable.

#### 4. Summary of mechanisms of small organic inhibitors

Here we provide an overview of current knowledge on the mechanism of corrosion inhibitors for several of the most commercially important metals and their alloys. These include the transition metals Cu, Fe and steels, and the light metals Al and Mg and their alloys. We summarize the transition metals before the light metals because transition metals occur as alloying additions and impurities in the light metals. They form secondary phases or inclusions that are a major cause of micro-galvanic corrosion in the light metals. Consequently, small organic inhibitors that perform well on Fe and Cu, in particular, are often good at suppressing corrosion in the light metal alloys. Thus, an understanding of inhibitor performance on Cu and Fe provides a valuable insight into small organic inhibitors for the light metals and alloys.

Environmental factors and inhibitor concentration clearly influence inhibitor performance and mechanisms. pH determines the nature of speciation of ionizable organic molecules. For some poly-hetero-substituted molecules this can be complicated, with a large number of possible stable species coexisting in some pH ranges. Protonated molecules dominate in low pH, which often hinders adsorption [123]. Increasing the pH to  $\sim 8.5$  leads to stronger adsorption and increased protection [124,125].

Inhibition generally increases up to a critical concentration then, in some cases, starts to decrease. The putative mechanism is that after the critical concentration, adsorbed inhibitor molecules desorb because they form oligomers with their soluble forms [126]. An alternative explanation is that oligomers that form in solution reduce the concentration of inhibitor available for adsorption. Due to adsorption reactions being generally exothermic, an increase in temperature most often results in decrease in inhibition. Time-dependent behaviour of the environment-interface may also alter the inhibition [127].

A clear example of concentration and time dependence is surfactants. For short immersion times both chemisorption and electrostatic attraction are observed but, at longer timescales, molecules desorb from the surface and aggregate to form micelles, decreasing surface coverage and inhibition [128]. This effect is also concentration-dependent because an increase after a threshold concentration promotes the formation of micellar aggregates that promote inhibitor desorption from the interface [129]. Micelle formation above the Krafft temperature (the minimum temperature from which the micelle formation takes place) has also been an effective route to loading higher concentrations of inhibitor into porous ceramic-like polyethylene oxide (PEO) conversion layers on Mg alloy [130]. Inhibitor concentrations can even change the dominant inhibition behaviour. It was reported that, up to 1 mM concentration, benzotriazole derivatives exhibit cathodic inhibition. However, with increasing concentration, the main inhibition mechanism switched to copper-benzotriazole passive layer formation [131]. Thiosemicarbazide was seen to inhibit copper surfaces via adsorption at low concentrations ( $<50$  ppm). However, at higher concentrations the nature of protection changes, with formed  $\text{Cu}^+$  complexes subsequently being oxidized to  $\text{Cu}^{2+}$  complexes [132].

##### 4.1. Micro-galvanic corrosion

Micro-galvanic corrosion is one of the most important processes in light metals and alloys. The metallic microstructure of these metals contains transition metal inclusions whose electrochemical activities, at the mixed potential of the metal, results in the separation of anodic and cathodic reactions. These separated electrode sites are where small organic inhibitor play their role. These moieties encompass a range of microscopic structures: –

- (i) Secondary phases in the form of particles composed of alloying elements;
- (ii) Enrichments – Cu in Al-alloys concentrates at many sites due to processing or corrosion. Fe, Cu, and Ni are the most detrimental elements for Mg alloys; alloying and impurity elements can aggregate at ferrous metal grain boundaries;
- (iii) Mixed phase materials, predominantly transition metals, where various forms of Fe can crystallize in steels and Cu brasses and bronzes have different phases;
- (iv) Different grain (small crystallite) orientations at surfaces can lead to differential corrosion;
- (v) Deformed or stressed structures resulting from manufacturing or subsequent processing can be more susceptible to corrosion than areas of lower stress;
- (vi) Concentration gradients of inclusions resulting from thermomechanical processes.

These processes are commonly the source of micro-galvanic corrosion that leads to localized attack. However, much of the reported literature on corrosion inhibition efficiency largely omits this important information. This is due to the three most common ways of measuring inhibition efficiency, impedance, corrosion current, and mass loss, being effectively averages across the surface, so they integrate localised corrosion into general corrosion. High-throughput experiments suffer from the same problem because their aim is to obtain a single performance metric.

In the sections on the transition metals below, the mechanisms described should be transferable to the light metals and their alloys since micro-galvanic corrosion associated with sites where Cu and Fe are often dominant. However, a major caveat is that the background electrolyte is different to that for the transition metal corrosion environments. This is due to pH changes caused by anodic and cathodic reactions and by presence of light metal cations that can hydrolyse (especially  $\text{Al}^{3+}$  and  $\text{Fe}^{2+}$ ) leading to autocatalytic pitting corrosion and precipitation of hydroxides, hydroxychlorides, and hydroxycarbonates that buffer the interface pH.

## 4.2. Corrosion inhibitors for copper

Copper and its alloys are widely used because of their mechanical, thermal, and electrical properties. Public water pipes, electrical transmission wires, consumer electronics, heat exchangers, and shells for safe storage of nuclear waste all rely on the environmental durability of copper [133,134]. Its ubiquitous application makes understanding and controlling copper corrosion critical. Table 1 shows the United Number System classifications and compositions for pure copper and major copper alloys.

Copper is one of the most corrosion resistant metals. It is also one of the noble (corrosion-resistant) elements in the periodic table and, when alloyed with other metals, also has a very low corrosion rate since it tends to be cathodically protected. It is worth noting that Cu is not protected when coupled with high-Ni alloys, titanium, or graphite. While Cu alloys are subject to all forms of corrosion experienced by metals, two types of corrosion stand out: dealloying; and impingement (erosion) corrosion. These forms of corrosion are largely based on microstructure/composition and nature of their applications respectively.

As with any metal, corrosion of Cu alloys (Table 1) is related to the microstructure. In the case of brass and bronze corrosion, dealloying is dominated by differential corrosion rates of different phases and compositional domains within the microstructure, which leads to dealloying. This is particularly prominent in brasses (Cu-Zn alloys) and to a lesser extent in bronzes (Cu-Sn alloys). Small amounts of As, Sb, and P (dealloying inhibitors) are added to these alloys to reduce this process. However, for two-phase  $\alpha$ - $\beta$  brasses they do not prevent de-zincification of the  $\beta$ -phase.

Given the importance of copper corrosion inhibitors, the literature contains many comprehensive reviews of copper corrosion mechanisms and inhibitors [134–140]. Cu corrosion inhibitors can also help suppress corrosion in other alloys. For example, Cu is an alloying component for high strength Al-alloys that forms intermetallic compounds in the microstructure of these alloy classes (principally the 2xxx (Al-Cu-Mg) and 7xxx (Al-Cu-Zn) series). Not all Cu corrosion inhibitors can be directly transferred to Al-alloys since the inhibitors are used for a variety of reasons. However, there are useful examples where this is helpful e.g., Al added to bronzes and brasses to suppress impingement corrosion through the formation of a surface oxide. This can be relevant to Al alloys since many intermetallic inclusions in Al-alloys are Cu-based and the high Al content means surface  $Al_2O_3$  formation can influence the activity of these intermetallics. Dealloying inhibitors (such as As, Sb, P) in Cu alloys might also inhibit cathodic reactions so are of direct interest to Al-alloys researchers when they perform this dual function. While this phenomenon has not been directly reported, dealloying of S-phase particles ( $Al_2CuMg$ ) is the most important reaction in the corrosion activity of AA2024 as it undergoes anodic dealloying following by conversion of the remnants to cathodically active sites. Finally, corrosion inhibitors for copper and its alloys also show corrosion suppression on Cu-containing alloys due to adsorption on Cu-sites and suppression of cathodic activity. In summary, one must be aware of the interrelationships between corrosion inhibitors for one type of metal and its alloys with other metals and alloys.

In summary, this short section on corrosion and compositions of Cu and Cu-alloys is intended to show that there are interrelationships between corrosion inhibitors for one type of metal and its alloys and other metals and alloys. Moreover, there are rich corrosion and inhibitor databases for each of these different metal types. While some research has taken advantage of this, machine learning approaches are likely to deliver a greater insight into inhibitor design by drawing on the embodied knowledge of consolidated

**Table 1**  
Copper and copper alloy United Number System (UNS) designation and composition.

| Name                           | UNS Numbers   | Composition             |
|--------------------------------|---------------|-------------------------|
| Coppers                        | C10100-C15760 | > 99 %                  |
| High-Cu alloys                 | C16200-C19600 | > 99 %                  |
| Brasses                        | C205-C28580   | Cu-Zn                   |
| Pb brasses                     | C31200-C38590 | Cu-Zn-Pb                |
| Sn brasses                     | C40400-C49080 | Cu-Zn-Sn-Pb             |
| P bronzes                      | C50100-C52400 | Cu-Sn-P                 |
| Leaded P-bronzes               | C53200-C54800 | Cu-Sn-Pb-P              |
| Cu-P and Cu-Ag-P alloys        | C55180-C55284 | Cu-P-Ag                 |
| Al-bronzes                     | C60600-C64400 | Cu-Al-Ni-Fe-Si-Sn       |
| Si-bronzes                     | C64700-C66100 | Cu-Si-Sn                |
| Cu-Zn alloys                   | C66400-C69900 | —                       |
| Cu-nickels                     | C70000-C79900 | Cu-Ni-Fe                |
| Ni-silvers                     | C73200-C79900 | Cu-Ni-Zn                |
| Coppers                        | C80100-C81100 | > 99 %                  |
| High Cu alloys                 | C81300-C82800 | > 94 %                  |
| Red & Leaded brasses           | C83300-C85800 | Cu-Zn-Sn-Pb (75–89 %Cu) |
| Yellow & leaded yellow brasses | C85200-C85800 | Cu-Zn-Sn-Pb (57–74 %Cu) |
| Mn and leaded Mn-bronzes       | C86100-C86800 | Cu-Zn-Mn-Fe-Pb          |
| Si bronzes and brasses         | C87300-C87900 | Cu-Zn-Si                |
| Sn and leaded Sn bronzes       | C90200-C94500 | Cu-Sn-Zn-Pb             |
| Ni-Sn bronzes                  | C94700-C94900 | Cu-Ni-Sn-Zn-Pb          |
| Al-bronzes                     | C95200-C95800 | Cu-Al-Fe-Ni             |
| Cu nickels                     | C96200-C96800 | Cu-Ni-Fe                |
| Ni silvers                     | C97300-C97800 | Cu-Ni-Zn-Pb-Sn          |
| Leaded coppers                 | C98200-C98800 | Cu-Pb                   |
| Miscellaneous alloys           | C99300-C99750 | —                       |

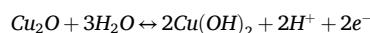
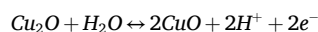
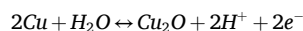
databases. Thus, the following section provides an overview of contemporary mechanistic details of corrosion inhibition rather than comprehensively describing the wide variety of known copper corrosion inhibitors.

#### 4.2.1. Corrosion mechanisms

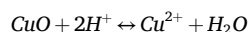
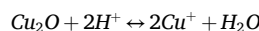
Copper corrosion mechanisms are different in the absence and presence of oxygen and other oxidants such as nitrate, sulfate and chloride species. In anoxic environments, copper surfaces are heterogeneous catalysts that promote water splitting and adsorption of molecular hydrogen on the surface:



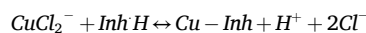
The durability of copper is determined by how well  $\text{H}_2$  is removed [133,141]. This reaction can continue when the dissolved  $\text{H}_2$  can be transported away. However, since  $\text{H}_2$  evolution is not a part of its corrosion process, for most of the practical applications it is accepted that copper does not corrode in non-oxidizing environments. For oxidizing, near neutral, and slightly alkaline environments copper corrosion products form in the order  $\text{Cu}_2\text{O}$ ,  $\text{CuO}$ , and  $\text{Cu}(\text{OH})_2$ :



Corrosion products generate a passive double layer composed of an outer cupric hydroxide and an inner cuprous oxide, which is only stable in the pH range 8–12 [137,142]. The stability of the passive layer is key to the corrosion protection afforded by an inhibitor. A good corrosion inhibitor should prevent both surface roughening via acidic etching at low pH:



and stabilize soluble complexes formed by corrosive species:



#### 4.2.2. Corrosion inhibition mechanisms

Organic molecules prevent copper corrosion by physisorption or chemisorption to the oxide/metal surface, commonly by forming chelates. Physisorbed and chemisorbed inhibitor layers provide barrier protection for metal surfaces. Physical adsorption results from electrostatic interactions between partially charged centres of the molecules and charged oxide or metal surfaces. Physisorption can also occur through hydrogen-bonding and Van der Waals interactions. Depending on the molecule, electrostatic interactions can make an important contribution to the adsorption energies, like chemisorption modes. Chemical adsorption stems from sharing or transfer of charge from the inhibitor to the surface. The vacant d-band of transition metals enables parallel chemisorption of the molecule to a surface via pronounced  $\pi$ -d orbital hybridization, or perpendicular chemisorption via the  $\sigma$ -molecular orbitals of unsaturated heteroatoms. For fully occupied d-bands of copper, weaker perpendicular chemisorption through  $\sigma$ -molecular orbitals is expected [123]. Inhibitor-copper substrate chemisorption frequently occurs by donation of readily available free electron pairs on the inhibitor to the free orbitals on copper.

Aqueous phase adsorption can be considered a substitution reaction that results from several competing interactions: molecule-water; metal-water; water-water; molecule-metal; and similar interactions with corrosive ions and contaminants. The adsorbed layer physically inhibits corrosion by keeping aggressive, corrosion-inducing ions away from the surface. It can also electrochemically inhibit corrosion by slowing anodic and/or cathodic reactions. The entire surface can be covered by an anodic passivation layer, or adsorption can occur on rate limiting cathodic zones.

Protection is achieved through self-assembly of inert, insoluble polymeric inhibitor barrier layers on naturally formed  $\text{Cu}_2\text{O}$ . Stabilizing Cu(I) is the key to inhibiting the copper corrosion reactions. Cu(II) complexes often do not provide protection [143,144]. The stability of these self-assembled monolayers is dependent on the chemical structure of the molecule and the presence of appropriate, active functional groups.

Functional groups containing heteroatoms such as nitrogen, oxygen, sulfur, and conjugated  $\pi$ -bonds facilitate copper corrosion inhibition by coordinating these electron donor species with vacant orbitals of copper. Due to the strong adsorption affinity of sulfur for copper [145], many nitrogen-containing organic molecules with sulfur functional groups have been investigated as copper corrosion inhibitors. Nitrogen- and sulfur-containing molecules (thiazoles, azoles, amines, etc.) improve the copper oxide layer stability by preventing the formation of copper chloride complexes.

Additionally, the introduction of nonpolar functional groups in appropriate molecular positions increases the hydrophobicity of the organic film, improving corrosion protection performance due to stronger surface-electrolyte interactions. For example, increasing an alkyl chain length initially improves inhibition by increasing the hydrophobicity, but eventually the aqueous solubility of the molecule becomes so low that any benefit gained from the protective properties is lost. For 5-alkylbenzotriazoles, protection increases with longer chain lengths up to six carbon atoms, with no improvements beyond that [146]. With alkyl esters of 4- and 5-carboxybenzotriazoles chemisorbed to copper surfaces through the triazole ring nitrogen, the inhibition improves with increasing chain length,

with the 5-octyl derivative showing excellent protection in low/neutral pH [147,148].

The chemical configuration of molecules and steric hindrance effects also play an important role in the effectiveness of protective, self-assembled monolayer barrier films. These factors are exemplified by substituted benzenethiol derivatives. Those containing amino, acetamido, fluoro, methyl, and isopropyl functional groups form protective self-assembled monolayers on copper substrates, whereas unsubstituted benzenethiol provides weaker corrosion protection. Molecules adsorb to copper via thiolate bonds, and substituted benzene rings provide hydrophobic protection, resulting in densely packed monolayer protective films. The effectiveness of thiolate and aromatic substituents depends on their type and position. They can modify the acidity of the thiol proton, change the ligand properties of the thiolate, and improve or degrade the adsorption of the molecule on the copper surface. Sterically crowded substituents may act as a diffusional barrier to the incoming corrosive species and affect the formation of monolayers in some cases. For *para*-substituted benzenethiol molecules it was observed that electron-withdrawing functional groups such as  $-F$  increase the acidity of the thiol hydrogen, which improves bonding to the copper substrate. In comparison, electron-donating substituents such as  $-NH_2$  increase the SH pKa and weaken binding of benzenethiolate to the Cu surface. However, despite being electron-donating, these substituents can also improve inhibition by blocking corrosive species due to their bulkiness and hydrophobicity, as is the case for methyl and isopropyl substituents. Compared to the unsubstituted molecule, substituted benzenethiolate inhibition increases in the order of *para*, *ortho*, *meta* for  $-NH_2$  substitution. Due to mesomeric effects, the electron donating *meta*- $NH_2$  is unable to adversely influence the pKa of the thiol group, so bind more strongly to copper than the *ortho* and *para* substituents. However, the *para* substituent can regain some its binding energy by facilitating formation of a bidentate coordination to Cu through both sulfur and nitrogen moieties, and by forming intermolecular hydrogen bonds not observed for the *ortho* and *meta* isomers [149]. Thus, elucidating the effects of substitution on the performance of certain chemotypes can be complex. Given that barrier formation is the main mechanism for protection of copper and its alloys, we describe the mechanisms of specific chemotypes, rather inhibition mechanisms used for the magnesium inhibitors section.

#### 4.2.3. Azoles

Azoles interact with copper through heteroatom lone pair electrons, forming copper-azole complexes by coordinating with  $Cu^0$ ,  $Cu^+$ , and  $Cu^{2+}$ . The nature of protection can be physical and/or chemical. Molecules can bond to the surface through ring nitrogen

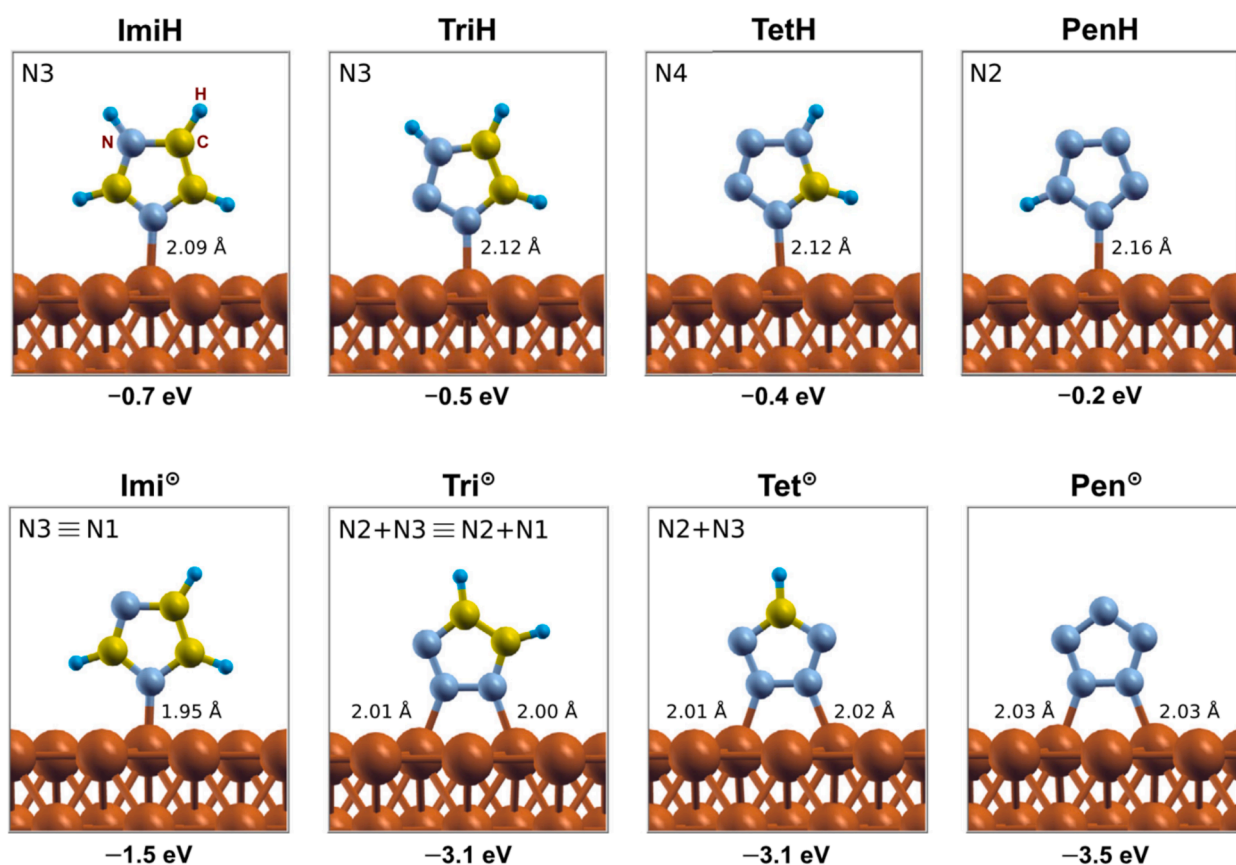


Fig. 8. DFT calculations of most stable gas-phase bonding configurations of imidazole, triazole, tetrazole and pentazole on Cu (111) for top: neutral, and bottom: deprotonated states of molecules. N-Cu bond lengths and adsorption energies are also stated. Reproduced from Kovacevic et al. [154] with permission.

atoms and through metal-hydrogen bonds [150].

Imidazole, triazole, and tetrazole preferentially adsorb to Cu<sub>2</sub>O via a single unsaturated N  $\sigma$ -bond, and a hydrogen bond to a nearby surface O ion [151]. Triazole and tetrazole can chemisorb perpendicular to the surface via two N atoms, however, such a binding mode is unfavourable for imidazole. This is due to its molecular geometry that places the two N atoms on opposite sides of the imidazole ring. Instead, dissociative cleavage of C–H bond leads to adsorption perpendicular to the surface. On the other hand, bonding through two N atoms to the Cu surface results in adsorption parallel to the surface, with the former being more thermodynamically favourable than the latter [152].

Fig. 8 summarizes the most stable bonding configurations for imidazole, triazole, tetrazole, and pentazole. Increasing the number of nitrogen atoms in the ring causes the molecule to be more electronegative and chemically harder, which makes hybridization with the metal states and molecule-surface contact more difficult, reducing adsorption by decreasing the adsorption energy in the order of imidazole < triazole < tetrazole < pentazole [153].

Azoles in their protonated and deprotonated forms interact strongly with water due to their charged nature and hydrogen bond donor/acceptor properties. However, despite strong solvation, deprotonated molecules bind so strongly to the surface that they result in superior adsorption compared to neutral forms. The aqueous-phase adsorption free energies of 1,2,3-triazole, tetrazole, and pentazole are considerably more exothermic for their deprotonated forms. However, due to its high pKa, imidazole binds with similar energy in its protonated and neutral forms [154].

Fig. 9 displays the molecular structure of azoles commonly used as copper corrosion inhibitors. The complexes of such molecules are likely polymeric, forming adherent protective films on the surface and blocking aggressive ions such as chlorides. When cuprous ions interact with these azoles, they are chemisorbed on the copper surface and form a protective film that inhibits anodic dissolution of copper. Corrosion inhibition of common azoles increases in the order of imidazole < benzimidazole < mercaptobenzothiazole < benzotriazole for neutral pH in saline environments [155], and benzotriazole < benzimidazole ~ mercaptobenzimidazole < benzothiadiazole < mercaptobenzothiazole for alkaline borate buffer environments [125].

Imidazole derivatives exhibit increasing inhibition in the order of 1-methyl-imidazole < imidazole < benzimidazole < 2-mercapto-1-methyl-imidazole < 2-mercaptobenzimidazole. Mercapto- and benzene groups *improve* inhibition, whereas methyl groups can accelerate corrosion with increasing concentration. While methyl and phenyl groups reduce solvation free energy, and hence increase the relative adsorption to the surface, electronegativity is increased by the phenyl group and reduced by the methyl and thiol substituents [156]. Imidazole and 1-methyl-imidazole form soluble cupric corrosion products, but only the cuprous compounds were detected for the other inhibitors. Thiol and phenyl substituents have a weaker tendency to form soluble complexes with Cu<sup>2+</sup> ions and result in stable adsorbed layers [157,158].

Thiadiazoles have strong inhibition properties due to sulfur in the ring and presence of thiol functional groups. 2-amino-5-ethyl- and 2-amino-5-ethylthio- derivatives of 1,3,4-thiadiazole prevent formation of soluble CuCl<sub>2</sub>/Cu<sub>2</sub>(OH)<sub>3</sub>Cl species in acid and saline environments [159–162]. Protective 1,3,4-thiadiazole-2,5-dithiol-Cu<sup>+</sup>/Cu<sup>2+</sup> complexes are formed by spontaneous substitution of surface water molecules with inhibitor [162].

Benzimidazoles chemisorb and form an insoluble Cu(I)benzimidazole anodic passivating polymeric film [155]. 2-mercaptobenzimidazole binds to the surface strongly due via the thiol moiety. At low surface concentrations the molecules lie flat, with both S and N atoms bound to the copper. At higher concentrations, molecules adsorb with S and one N tilted away from the metal surface, creating a denser protective monolayer [163].

2-mercaptobenzothiazoles (MBT) inhibit copper corrosion by forming a thin water-insoluble polymeric film of Cu(I)MBT. It is not formed by precipitation of MBT from the bulk solution but by an anodic corrosion product formed by a surface reaction of cuprous ion. Chemisorption occurs through the thiocarbonyl group coordinated to cuprous ions. The formation of chelate structures is not likely because of high formation strain. An S-bridged polymeric structure results in nearly parallel adherent films with an outer dibenzothiazolyl-disulphide (DBDS: oxidation product of MBT molecules) and an inner Cu(I)MBT film. The protective Cu(I)MBT film forms over the Cu<sub>2</sub>O surface during the initial corrosion stage and grows at the Cu<sub>2</sub>O/ Cu(I)MBT or Cu(I)MBT/DBDS interface via diffusion of cuprous ions to the interface [164–167].

Triazoles may adsorb by displacing water molecules on the surface and by sharing the triazole nitrogen lone pair electrons. The protection offered by triazoles is due to formation of an insoluble, semipermeable, polymeric copper-triazole film formed by covalent

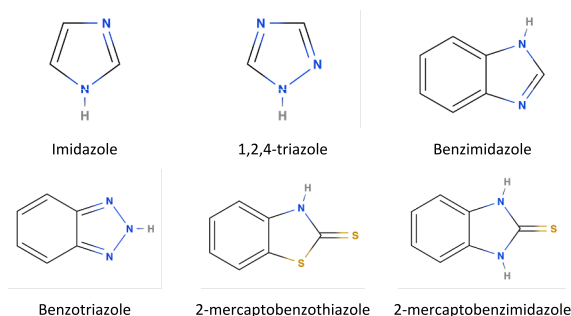


Fig. 9. Structure of azoles commonly used for copper corrosion inhibition.



or coordinate bonds. 3-amino-1,2,4-triazole inhibits corrosion by forming complexes with Cu(I) and preventing dissolution of the soluble  $\text{CuCl}_2$  [167,168]. Introduction of amine groups at position 3 results in reduced cathodic currents in HCl medium by increasing the fraction of transferred electrons during chemisorption; this effect further increased by *second* amine substitution at position 5 [169]. For 3-amino-1,2,4-triazole, introduction of a thiol group in position 5 increases inhibition due to additional bonding by sulfur, while introduction of a methylthio moiety increases inhibition because of higher electron donation by the methyl group [170]. However, when the positions of thiol and amino groups are swapped, the trend reverses where 5-amino-3-mercapto substitution has higher inhibition than the 5-amino-3-methylthio analogue. This was thought to be due to the methylthio moiety preventing the formation of C–S bond tautomers [171]. 5-phenyl substituted analogues exhibited  $\sim 99\%$  inhibition efficiency due to the formation of Cu-inhibitor( $-\text{H}_2\text{O}$ ) complexes [172]. Among 1,2,4-triazole phosphonate derivatives, maximum protection was observed for the electron-donating methoxyphenyl group, and minimum protection for the electron-withdrawing p-nitro substituents. Electron donation results in increased basicity of the coordinating atoms, assisting in electron transfer during chemisorption. 5- and 6-membered Cu(II)-phosphonate ring complexes formed through Lewis acid-base electron exchange were the main inhibiting structures [173].

*Benzotriazole* (BTA) derivatives have been used since 1947 [143] to slow down degradation of copper. Both physisorption ( $<0.1$  eV) and weak chemisorption ( $\sim 0.4$  eV) play roles in the protection mechanism [174]. Chemisorption takes place through the triazole ring  $\text{N}$   $\text{sp}^2$  lone pair electrons. Protection occurs by the formation of Cu(I)BTA complex, which retards both the cathodic oxygen reduction reaction and anodic oxidation of metal [137]. The bonding can be parallel or perpendicular to the substrate, with parallel orientation resulting in better inhibition due to the interaction of d-orbitals of Cu with of  $\pi$ -electrons of the benzene ring and intermolecular bond formation [137]. An increase in coverage makes parallel physisorption to the surface more stable than perpendicular chemisorption [175].

BTA only binds the surface strongly enough to compete with Cl–Cu surface interactions in its deprotonated form [176–179]. Deprotonation can occur by release of hydrogen atoms on the copper surface or by classical dissociation in the electrolyte [179]. Complex formation generally increases with increasing pH, but protection decreases in highly alkaline and acidic media, or environments containing highly aggressive ions. In alkaline environments, inhibition results from substitution of the  $-\text{NH}$  hydrogen and coordination with the lone pair of nitrogen electrons [180]. In acidic environments, thicker but more oxygen-permeable and less protective films are formed [181]. The combined effect of potential, pH, Cl<sup>-</sup>, and BTA concentrations on thermodynamic stability of copper-BTA systems can be usefully elucidated by Pourbaix diagrams [182].

Molecular structure investigations of methyl-benzotriazoles reveal that methyl substitutions at positions 1 and 2 hinder bonding due to steric effects, while substitutions at positions 4 and 5 improve protection due to increased hydrophobicity [183]. Functional group substitutions in position 5 enhance the inhibition performance, with electron acceptor groups having a stronger effect than electron donor groups [146]. Substitution of methyl groups in position 4, 5, and 6 increases film hydrophobicity and is responsible for the increased inhibition performance of tolyltriazole [184]. Increasing linear chain length also increases hydrophobicity. Alkyl group substitutions at the 5 position increase protection by increasing chain length up to an alkyl chain with 6 carbons [146]. Adding carboxy group chains to BTA increases inhibition due to additional hydrophobicity of the chain, and electron-withdrawing effect of carboxy group. This is less apparent for 5-substituents than for 4-substituents, which has stronger chemisorption [147]. Compared to

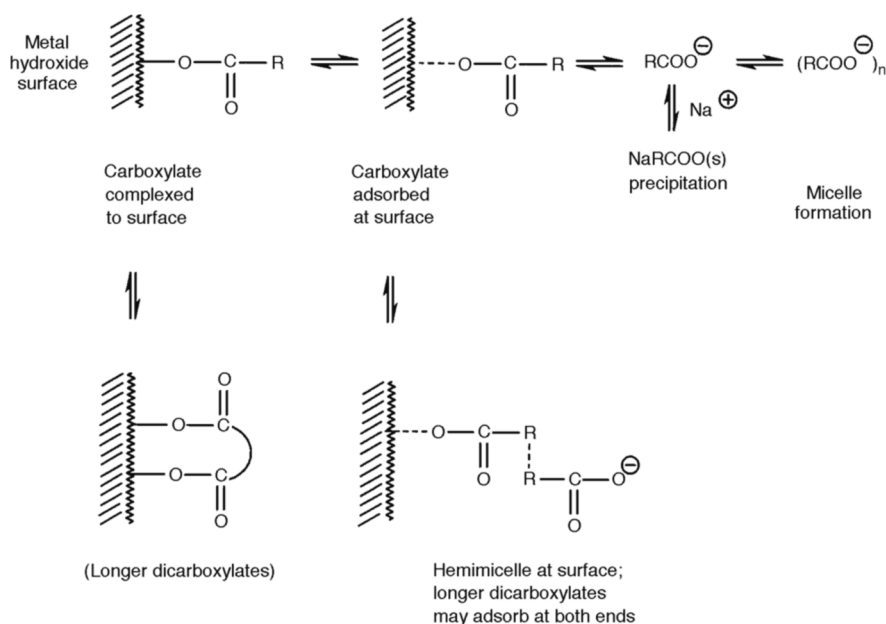


Fig. 10. Mechanisms of corrosion inhibition for mono and di-carboxylates. Reproduced from Hefter et al. [187] with permission.

unsubstituted BTA, the electron-withdrawing 5-Cl substituent enhances inhibition, whereas the electron-donating 5-NO<sub>2</sub> group decreases protection due to stronger dissociation of the molecule to its anion [185]. Despite having similar electronic properties, 3-hydroxyl BTA has a non-planar structure which results in a thick, porous film that does not provide corrosion protection [126].

Tetrazoles also have the potential to replace current inhibitors. 1-Phenyl-5-mercaptotetrazole (PMTA) has a much higher corrosion inhibition performance than other tetrazoles, and protective abilities increase in the order hydroxybenzotriazole < imidazole < aminopyrimidine < mercaptobenzimidazole < mercaptobenzothiazole < benzotriazole < tetrazole. A Cu(I)-PMTA film forms over Cu<sub>2</sub>O, where every PMTA molecule binds to two or more Cu(I) ions through N and S atoms. The hydrophobic phenyl backbone assists inhibition by blocking access of hydrated corrosive ions to the copper surface [144].

#### 4.2.4. Carboxylates

Carboxylate layers limit the interaction of copper with the environment. Fig. 10 provides a summary of the general corrosion inhibition mechanisms for mono- and dicarboxylates. Formation of a hydrophobic diffusional barrier is the basis of inhibition. Adsorption occurs through the COO<sup>-</sup> group, heteroatoms and unsaturated  $\pi$ -bonds. Protection can be increased by linear alkyl chains [186,187] or aromatic [188,189] moieties. Protected surfaces show a micro textured hydrophobic plate-like morphology [190].

Increased chain length results in thinner layers with coarser morphologies and better corrosion protection. Copper carboxylate surfaces created by linear alkyl carboxylates show inhibition that depends on a critical chain length. Long chain tetradecanoic and octadecanoic acids are better inhibitors than shorter decanoic and hexanoic acids [190]. Electrochemically deposited copper decanoate/dodecanoate increase polarization resistance, whereas heptanoate films exhibited no change [186]. This shows that a critical chain length is required for inhibition.

Monocarboxylates with chain lengths smaller than 10 exhibit weak copper corrosion inhibition. There was no significant dependence on chain length until a chain length of 10 (decanoate), where a significant increase in polarization resistance was observed. Resistance remained high but dropped at  $n = 11$  (undecanoate) and increased with further increases in chain length. Abrupt decline in resistance was related to decreased aqueous solubility, increased micellization of carboxylate anions, or both. For  $\alpha$ ,  $\omega$ -dicarboxylates the resistance increased gradually with increasing chain length, increased significantly at  $n = 11$ , and resistance continued to increase gradually with growing chain length. The oxalate (zero chain length) accelerated corrosion [187]. These suggest that copper complexation increases with increasing carboxylate bonding and decreasing chain length, but hydrophobicity/surface-coverage offered beyond a critical chain length was necessary for protection.

$\pi$ -bonds from heterocycles and unsaturated carboxylates with long chains can also assist inhibition. 1,2,4-triazole-3-carboxylic acid binds strongly to copper in a perpendicular orientation through N<sub>1</sub>, N<sub>2</sub> and one of the carboxylate O atoms [189]. Carboxylated indoles physisorb in their neutral form and chemisorb through Cu–N bonds in deprotonated form [191]. Sodium oleyl sarcosinate and sodium oleate have lower free adsorption energies than the widely used BTA, which suggests chemisorption [192]. Hydrophobic tails form a polymolecular film which provides high protection [193]. The dicarboxylate dimegin stabilizes Cu(I) oxide by forming carboxyl bridges over several copper cations, resulting in a self-organized dense protective layer, despite being present in less than 1 mM concentration [194].

**Amino acids and nucleobases:** Biological molecules are promising, environmentally friendly alternatives to current effective but toxic inhibitors, such as benzotriazole and benzimidazole derivatives. Amino acids and nucleobase derivatives interact with copper surfaces via their benzo/azole moieties, carboxyl groups, and heteroatoms present in other functional groups. Cysteine, glutamic acid, glycine, and glutathione coordinate to copper surfaces through N, O, S atoms [195]. A comparison of electrochemical performance shows that cysteine exhibits better binding than lysine, arginine and alanine due to its thiol moiety. A lack of heteroatom means glycine, alanine, and valine have no inhibition properties [196,197]. In acid environments, glutamic acid is a better inhibition in comparison than serine and threonine, attributed to improved electrostatic interaction between positively charged copper surface and negatively charged oxygen adsorption centres of the protonated amino group [197]. Physical adsorption increases with more active N heteroatoms i.e., aspartic acid < glutamic acid < asparagine < glutamine [198]. The presence of an aromatic ring allowed more efficient surface coverage through parallel physisorption of tyrosine and tryptophan, which resulted in higher performance compared to glycine, alanine, valine, proline and phenylalanine [199,200]. Both cysteine [201] and tryptophan [202] act as promising corrosion inhibitors for acidic environments. For sulfate media, the main rate limiting corrosion product was seen to be Cu(I)-cysteine, which was used up in the formation of slightly soluble copper-amino acid complex and limited the Cu<sup>2+</sup> electrooxidation. A similar mechanism was observed for methionine, where inhibition succeeds by prevention of oxidation of Cu<sup>+</sup> into soluble Cu<sup>2+</sup> [203]. The formation mechanism of the self-assembled monolayers of cysteine is different for copper and copper oxide, where adsorption occurred through N for bare copper, and via S for Cu<sub>2</sub>O, which was also easier to adsorb to due to its lower adsorption energy [204].

Purine and adenine inhibit corrosion reactions in sulfate [205] and nitrate [206] environments by forming a chemisorbed Cu(I)-inhibitor complex. A substituted electron donating amino group improved adenine inhibition relative to purine. Purine chemisorbs perpendicular to the copper surface through nitrogen donor electrons, and CuCl<sub>2</sub> reacts with purine to form a protective film [207]. Uracils with hydroxyl, thiol and methyl substituents inhibit corrosion in saline environments, with dithiouracil exhibiting the highest inhibition. This is due to complexation with copper ions through delocalization of aromatic ring, nitrogen electron pairs from the thioamide moiety, and the presence of two thiol groups [208].

#### 4.2.5. Other organic molecules

**Surfactants** inhibit corrosion due to their amphiphilic nature. They physisorb or chemisorb to the surface through covalent coordination by the polar group, while the long non-polar carbon chains form a hydrophobic barrier that protects surfaces from aggressive environments. Common surfactants like sodium dodecyl sulfate [128,170], sodium dodecyl benzene sulfonate [129], ammonium

dodecyl sulfate [209], cetyl trimethyl ammonium bromide [128,170], sodium oleate [128], polyoxyethylene sorbitan monooleate [128] can inhibit copper corrosion in acidic media, mainly by electrostatic interactions of adsorbed ions.

*Ionic liquids* are room temperature molten salts with a high self-assembly capability. They are comprised of organic cations with a hydrophobic tail, a linear chain branch, and a hydrophilic polar head. Ionic liquids inhibit corrosion by blocking the active sites on the copper surface by forming a protective film. As we have noted, this mechanism is common to many inhibitors. In acidic chloride environments, (1-butyl-3-methylimidazolium) chloride or bromide chemisorbs to the surface via the imidazoline ring to form stable, insoluble films [210]. The presence of the chloride anion results in higher performance. In phosphate environments, 1-butyl-4-methylpyridinium tetrafluoroborate exothermically physisorbs to the surface [211]. The inhibition increases with increasing carbon length of the alkyl chain connecting N<sub>3</sub> of imidazolium ring by modifying the electron donor properties and covering the surface better [212]. Investigation of two new protic (PIL) and four aprotic (APIL) room-temperature ionic liquids revealed that di-[bis-(2-hydroxyethyl) ammonium] adipate (DAD) and 1-hexyl-3-methylimidazolium hexafluorophosphate (HMH) have strong inhibiting properties [213]. HMH forms a uniform solid layer on a copper surface due to reactions with the hexafluoro-phosphate anion. DAD formed adsorbed layers, but no corrosion products.

*Schiff bases* also possess good corrosion inhibition properties. Inhibition stems from the coordination of copper ions with azomethine nitrogen [214], resulting in adsorbed inhibitor forming a thin protective film. These interactions are crucial, as the presence of unoccupied  $\pi$ -orbitals enables electron back-donation from the copper d-orbital. The benzene ring, combined with unpaired electrons, enables stable chelate formation through multisite chemical adsorption [140]. It was observed that the geometry of the Schiff bases

**Table 2**

Iron and iron alloy UNS designation and composition [225]. UNS assigns a letter followed by 5 numbers. D denotes carbon steels and alloy casting steel, F denotes cast irons, G denotes carbon and alloy steels, H denotes AISI and SAE H steels, J denotes cast steels, K denotes miscellaneous steels and ferrous alloys, S denotes heat and corrosion resistant steels, and T denotes tool steels.

| Name  | UNS Numbers | Composition  |
|---|-------------|--|
| Cast irons                                  | F33800      | C3.2-4.1, Mn 0.1-1.0, P0.015-0.1, Si1.8-3.0, S 0.005-0.035   |
| Carbon steel (Mn < 1 %)                     | G10xxx      | C0.06-1.04, Mn 0.25-1.00   |
| Carbon steel (Mn 1.00 to 1.65 %)            | G15xxx      | C0.18-0.55, Mn 1.05-1.65   |
| Re-sulfurized carbon                        | G11xxx      | C0.08-0.55, Mn0.30-1.65, S0.08-0.20  |
| Re-sulfurized re-phosphorized carbon steels | G12xxx      | C0.09-0.13, Mn0.6-1.15, P0.04-0.12, S0.10-0.35   |
| Mn steels                                   | G13xxx      | C0.28-0.48, Mn 1.6-1.9, P < 0.35, S < 0.4  |
| Ni Steels                                   | G23xxx      | Ni 3.5   |
|   | G25xxx      | Ni 5.0   |
| AISI and SAE H-steels                       | H10380      | C0.34-0.43, Mn0.50-1.0, Si 0.15-0.30   |
|   | H15220      | C0.17-0.25, Mn1 - 1.5, Si 0.15-0.30  |
|   | H94301      | C0.27-0.33, Mn0.7-1.05, Si 0.15-0.30, Cr0.25-0.55, Ni 0.25-0.65, Mo 0.08-0.15                                    |
| Cast stainless steels                       | J92605      | C < 0.5, Cr26-30, Ni < 4, Si < 2   |
|   | J93005      | C < 0.5, Cr26-30, Ni4-7, Si < 2  |
|   | J94065      | C < 0.35-0.75, Cr13-17, Ni 33-37, Si < 2.5   |
| Cast steels                                 | K11510      | C < 0.15, Mn < 1, P < 0.45, S < 0.05, Cu > 0.20  |
|   | K11856      | C 0.15-0.21, Mn 0.80-1.1, P < 0.35, S < 0.04, Si < 0.3, Cu > 0.20  |
|   |             | C < -.7, Mn0.40-0.70, P < 0.25, S < 0.25, Si < 0.35, Cr 0.6-0.9, Ni 0.7-1.0, Mo 0.15-0.25, Cu 1.0-1.3, Nb > 0.02 |
|   | K20747      |  |
| Ni-Cr steels                                | S31xxx      | Ni 1.25 - 3.5; Cr 0.65-1.57  |
|   | S32xxx      | Ni 1.25 - 3.5; Cr 0.65-1.57  |
|   | S33xxx      | Ni 1.25 - 3.5; Cr 0.65-1.57  |
| Mo steels                                   | S40xxx      | C 0.13-0.50, Mn 0.4-1.0, P < 0.35, S < 0.4, Cr 0.3-1.1, Ni 0.7 to 2.0, Mo 0.08-0.45                              |
|   | S44xxx      |  |
| Ni-Cr-Mo                                    | S43xxx      | Ni 1.82; Cr 0.50 and 0.80; Mo 0.25   |
|   | S43BVxx     | Ni 1.82; Cr 0.50; Mo 0.12 and 0.25; V > 0.03   |
|   | S47xxx      | Ni 1.05; Cr 0.45; Mo 0.20 and 0.35   |
|   | S81xxx      | Ni 0.30; Cr 0.40; Mo 0.12  |
|   | S86xxx      | Ni 0.55; Cr 0.50; Mo 0.20  |
|   | S87xxx      | Ni 0.55; Cr 0.50; Mo 0.25  |
|   | S88xxx      | Ni 0.55; Cr 0.50; Mo 0.35  |
|   | S93xxx      | Ni 3.25; Cr 1.20; Mo 0.12  |
|   | S94xxx      | Ni 0.45; Cr 0.40; Mo 0.12  |
|   | S97xxx      | Ni 0.55; Cr 0.20; Mo 0.20  |
|   | S98xxx      | Ni 1.00; Cr 0.80; Mo 0.25  |
| Tool steels                                 | T11301      | C 0.78-0.88, Mn 0.15-0.4, Cr 3.5-4.0, Ni < 0.3, Mo 8.2-9.2, W 1.4-2.1, V 1-1.35, Si 0.2-0.5                      |
|   |             | C 0.65-0.80, Mn 0.1-0.4, Cr 3.75-4.5, Ni < 0.3, W 17.25-18.75, V 0.9-1.3, Si 0.2-0.4                             |
|   | T12001      | C 0.95-1.05, Mn < 1.0, Cr 4.75-5.5, Ni < 0.3, Mo 0.9-1.4, V 0.15-5.0, Si < 0.5                                   |
|   |             | C 0.44-0.55, Mn 0.1-0.4, Cr 1.0-1.8, Ni < 0.3, Mo < 0.5, W 1.5-3.0, V 0.15-0.30, Si 0.15-2.0                     |
|   | T30102      | C 0.7-1.5, Mn 0.1-0.4, Cr < 0.15, Ni < 0.2, Mo < 0.1, W < 0.15, V < 0.1, Si 0.1-0.4                              |
|   |             |  |
|   | T41901      |  |
|   | T72301      |  |

influences the inhibition efficiency of N,N'-o-phenylen-bis(3-methoxysalicylideneimine) (~90 %), N,N'-p-phenylen-bis(3-methoxysalicylideneimine) (~80 %), and N-[(2-hydroxy-3-methoxyphenyl)methylene]-histidine (~40 %). While Schiff bases can form chelates with both Cu<sup>+</sup> or Cu<sup>2+</sup> ions, the structure of the molecules determines whether stable chelates are possible with Cu<sup>2+</sup> ions. More stable chelates result in better inhibition of anodic dissolution [215]. The influence of molecular structure was also observed for N,N'-ethylene-bis(salicylideneimine), N,N'-isopropylene-bis(salicylideneimine), and N,N'-ortho-phenylene acetyl acetone imine (2-hydroxybenzophenone imine), where a coplanar conformation provides increased interaction of aromatic  $\pi$ -electrons with the copper surface [216].

Caffeine and its derivatives theobromine and theophylline have been investigated as inhibitors in sulfuric acid [217], nitrate, [218] and chloride [219] environments. The simulated adsorption energy distributions of caffeine and water were distinct from each other, whereas for theobromine and theophylline they were overlapping [220]. This is consistent with experimental results, where caffeine alone showed minor inhibiting activity by creating a hydrophobic film consisting of Cu(II)-caffeine complex [217,219].

Other plant-based compounds were also studied due to their non-toxic, environmentally friendly nature. Extracts of cannabis [221] and *Azadirachta indica* (Neem) [222] were among the most efficient compounds. For example, 1 g/l cannabis inhibited carbon steel corrosion in 1.0 mol/L HCl at by > 90 %, while Neem provided 95 % protection of steel reinforced concrete after 182 days. Compounds with higher inhibition efficiency often contained tannins, flavonoids, and phenolic species, which physisorbed to the surface through N and O heteroatoms, and carbonyl and hydroxyl functional groups [223,224]. The mode of action in most cases was blocking surface interactions by creating a diffusional barrier.

#### 4.3. Corrosion inhibitors for iron and steel

Iron is used both in its pure form and in alloys, of which there are a vast number. There are over 3,500 steels that are given grade numbers according to various steel bodies. Table 2 shows the UNS classifications and compositions for some typical iron alloys. [225].

In practice, pure iron is most used in wrought iron for applications where complex shapes with high load-bearing properties are required. More commonly, iron is alloyed with other metals and elements. Iron and steels have complex microstructures containing many phases as seen in the Fe phase diagram. Alloying is often used to improve mechanical properties and corrosion resistance. Often, the alloying additions are designed to stabilise particular phases e.g., high temperature austenite at room temperature, which can be stabilised by alloying with Mn, Ni, Co and Cu.

As with Cu alloys, Fe alloys are subject to all forms of corrosion generally experienced by metals. These are related to the underlying microstructure/composition and types of applications. Iron is intermediate in the electrochemical series but is susceptible to galvanic corrosion when coupled with more noble metals (e.g. Cu). Iron corrosion is generally attributed to the properties of the corrosion product that develops on its surface. It forms a loose product that allows ingress of corrodents that can easily generate more corrosion product. Iron oxidation has been extensively investigated [226]. Other steels, for example stainless steels and weathering steels, owe their corrosion resistance to additional Cr, Cu, Ni, P, Si, Mn and sometimes rare-earth elements, which form passive films or compact corrosion products on the surface of the steel.

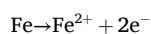
In steels corrosion can occur between the different polymorphs of iron as well as through local galvanic corrosion, such as between inclusions and the metal matrix. There are several polymorphs of iron in carbon steel including, bainite, austenite, pearlite, ferrite, and ledeburite [227]. There are a range of inclusions, with sulphides, carbides, and oxides being the major types. Martensite is an Fe-C *solidi* solution and cementite is a ferrous carbide. Bainite and pearlite are mixes of two phases: carbide and ferrite. Corrosion on, or between different polymorphs of Fe, or between inclusions and the Fe matrix, has completely different chemistry than aluminium, for example. Clearly, this is important when considering inhibitor performance metrics (e.g. %IE) for one metal compared to another, or even between different phases in the same metal.

Precipitates in steels are a major source of localised corrosion [228]. Although inhibitors for steels are often reported, differences in inhibition on inclusions/precipitates/different phases (i.e., the effects of microstructures on corrosion inhibition) are very much overlooked. Carbides are among the most common precipitates, formed by reaction with a number of alloying elements; carbo-nitrides are also formed [229]. The sulphides are also very active inclusions that can form from any of the transition metal alloying additions and with iron itself. Oxides are another type of inclusion and are more prevalent in additively manufactured materials. Corrosion inhibitors that perform well on the light metals may not perform as well in suppressing carbide corrosion. The chemistry of inhibition of corrosion of a carbide will be different the intermetallic particles found in light alloys.

##### 4.3.1. Corrosion mechanisms

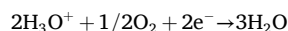
Compared to other metals, the corrosion of steel is very prevalent. Specifically, carbon steels and low-alloy steels exhibit the most obvious corrosion because of their rusty colours. During corrosion, iron undergoes the following reaction:

Anodic Reaction:

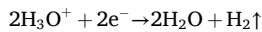


Cathodic reactions vary depending on the solution environment [230].

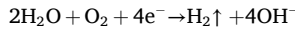
In an acidic aqueous environment with dissolved oxygen:



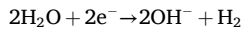
In an acidic aqueous environment without dissolved oxygen:



In a neutral aqueous environment with dissolved oxygen:



In a neutral aqueous environment without dissolved oxygen:



The corrosion products of iron are complex, comprising multiple constituents. Their composition depends on factors such as the nature of the medium, pH, oxygen concentration, transport conditions, and the presence of other chemical substances such as chlorides and sulfates. Misawa [231] *et al.* conducted a systematic study of the formation processes of iron corrosion products in aqueous solutions, and established the relatively complicated reaction system summarized in Fig. 11.

In neutral environments, typical corrosion products of iron include hematite ( $\alpha\text{-Fe}_2\text{O}_3$ ), magnetite ( $\text{Fe}_3\text{O}_4$ ), iron trihydroxide ( $\text{Fe}(\text{OH})_3$ ), goethite ( $\alpha\text{-FeOOH}$ ), akageneite ( $\beta\text{-FeOOH}$ ), lepidocrocite ( $\gamma\text{-FeOOH}$ ), feroxyhyte ( $\delta\text{-FeOOH}$ ), and iron hydroxide ( $\text{Fe}(\text{OH})_2$ ). [232] Notably,  $\text{Fe}_3\text{O}_4$  and  $\alpha\text{-Fe}_2\text{O}_3$  are dense and very stable [233]. However, in aqueous environments, corrosion products often manifest as  $\text{FeOOH}$  forms. These products possess a porous structure that not only fail to prevent corrosive ions from reaching the metal substrate, but also serves as a reservoir to store these ions and moisture that further intensifies the corrosion reaction [234]. This behaviour contrasts markedly with the protective role of the dense alumina film formed on the surface of aluminium [235]. In acidic solutions, iron oxide on the surface cannot maintain stability and is predominantly present as iron ions in the solution, with hydrochloric acid as an example [236].

Anodic Reaction:

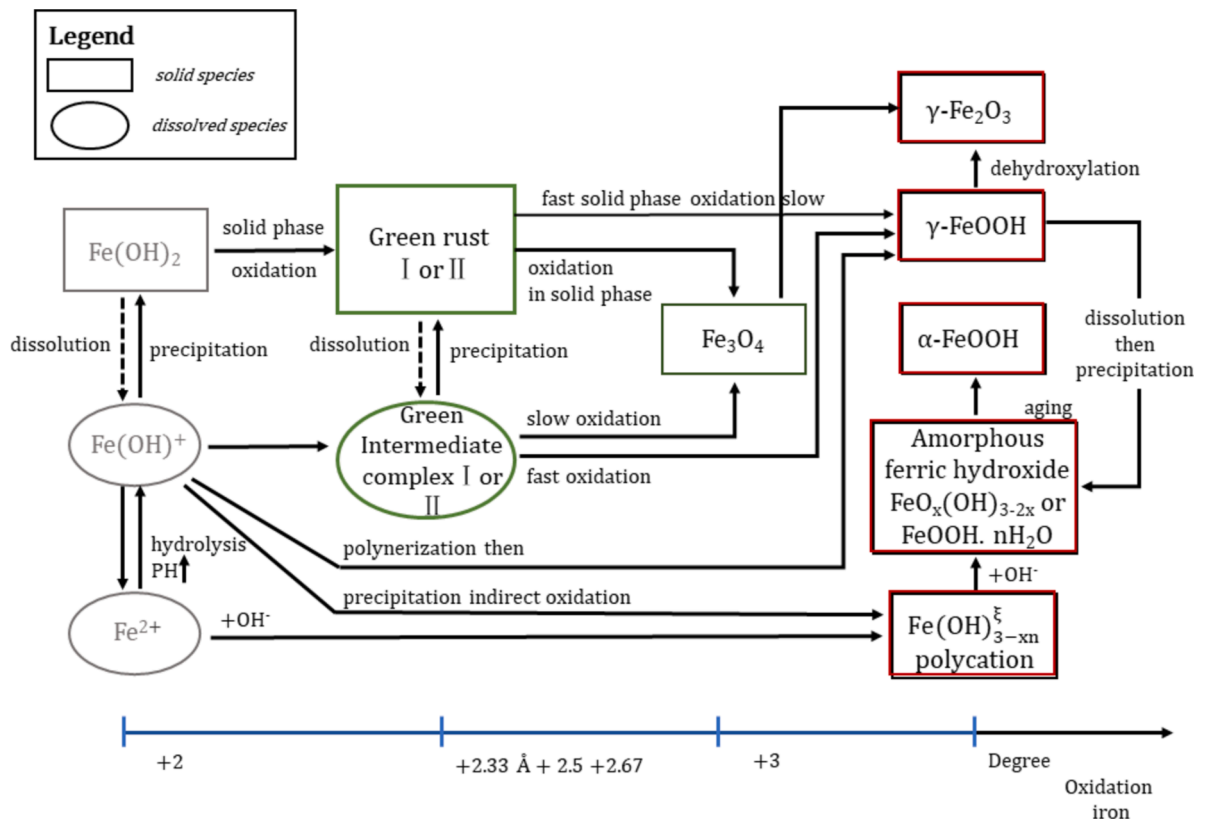
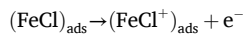
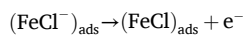
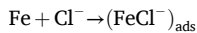
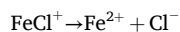
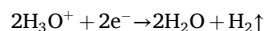


Fig. 11. Reaction scheme governing the appearance and evolution of species in aqueous solution during the iron oxidation process. Reproduced from Misawa *et al.* [231] with permission.



Cathodic reactions:



#### 4.3.2. Corrosion inhibition mechanisms

Different types of corrosion inhibitors exhibit distinct mechanisms when interacting with the surface of steel. They fall into three categories: oxide film-forming, precipitation film-forming, and adsorption film-forming inhibitors. Among these, oxide film-forming and precipitation film-forming inhibitors are commonly used in neutral environments, where they form stable and compact protective films that enhance corrosion resistance of the metal surface [234]. Specifically, oxidizing film inhibitors can directly act on the steel surface or use the dissolved oxygen in the solution as an oxidizing agent, thereby transforming the loose rust layer into a robust passive oxide film. Common oxide film-forming inhibitors are primarily inorganic molecules, such as chromates, molybdates, nitrites, and tungstates [237]. Precipitation film-forming inhibitors generate a precipitated film on the metal surface, mostly on the cathodic regions [238]. Common precipitation film-forming inhibitors include zinc salts, cerium salts, phosphate salts, and others [239].

Small organic molecules can inhibit corrosion of iron and steels via an adsorption film-forming mechanism and are widely used in industrial acid pickling processes. As for other metal corrosion inhibitors, they can be classified into physisorbed inhibitors and chemisorbed inhibitors. The mechanism of physical adsorption relies primarily on electrostatic interactions between organic molecules and the metal surface [240]. This is influenced by the solution properties and the surface charge of the metal. This type of adsorption usually occurs in two ways. One applies to ionic surfactants or ionic liquids that carry a positive charge and are easily adsorb onto areas of the steel surface with a negative charge [241]. The other is via heteroatoms of organic corrosion inhibitors that are easily protonated and converted into cationic forms in acidic solutions [242]. The steel surface accumulates a negative charge due to the adsorption of anions such as  $\text{Cl}^-$ . Species with positive and negative charges interact electrostatically, resulting in physical adsorption. It is important to note that physical adsorption is unstable, reversible, and fairly weak.

In chemical adsorption, organic molecules attach to the iron surface through atoms with high electron density, forming a protective film that prevents the attack by corrosive ions [243]. In general, the adsorption centre involves unsaturated bonds, such as in alkene, alkyne, nitrile, carbonyl, imine, thione etc. [244,245]. These ligands donate  $\sigma$ -electron density to the metal and the metal donates  $\pi$ -electron density to the ligand, so-called “back-bonding” interactions. More importantly, some functional groups composed of polar heteroatoms, such as  $-\text{OH}$ ,  $-\text{NH}_2$ ,  $-\text{COOH}$  [246,247], can chemisorb by transferring non-bonding electrons to the d orbital of Fe to form coordination bonds. Thus, chemisorption between organic molecules and steel is not a simple one-way transfer of electrons. When the heteroatom in the organic molecule transfers electrons to the empty orbital of iron, because of the large number of electrons in iron, there can be backdonation from the iron to the organic molecules. This process of mutual electron transfer enhances the adsorption process and is the essence of the chemical adsorption of corrosion inhibitors to iron [248,249].

#### 4.3.3. Physisorbed inhibitors

*Ionic surfactants* are well known to physically adsorb onto the steel surface. In acidic solutions, the surface tends to carry a positive charge, enabling anions with a negative charge to preferentially adsorb onto it. These negatively charged areas due to the adsorption of anions, attract cationic surfactants through electrostatic interactions, resulting in physical adsorption [250]. Elaraby [251] and his colleagues synthesized a tetra-cationic surfactant CS4 (1,N1'-(ethane-1,2-diyl) bis (N1, N2—didodecyl-N2-(2-(((E)-3-hydroxy-4-methoxy-benzylidene)amino)ethyl)ethane-1,2-diaminium) chloride), and studied its corrosion inhibition on carbon steel in 1 M HCl. Their electrochemical studies showed that, at a concentration of 50 ppm, the %IE reached ~ 96 %. Further theoretical studies indicated that the electrostatic interaction between the N (cationic head) of CS4 and the negatively charged areas on the carbon steel surface aided the adsorption of the inhibitor molecules to the carbon steel surface. Aiad and colleagues [241] prepared three cationic surfactants based on alginic acids with varying alkane chain lengths. They found that the corrosion inhibition efficiency was directly proportional to the hydrophobic chain length and the inhibitor concentration and decreased at higher solution temperatures. Specifically, the quaternary ammonium group ( $\text{N}^+$ ) adsorbs onto cathodic sites on the steel to reduce hydrogen evolution, while Br<sup>-</sup> adsorbs onto anodic sites to reduce steel anodic dissolution. Achouri and colleagues [252] synthesized a series of 1,2-ethane bis (dimethyl alkyl ammonium) bromide surfactants with different chain lengths. These surfactants exhibited corrosion inhibition in 1 M HCl, with increased inhibition efficiency also observed as the chain length increased. The authors proposed that the corrosion inhibition mechanism involved electrostatic interactions between the two positively charged ammonium groups in the surfactant structure and  $\text{Cl}^-$  ions adsorbed on the steel surface.

*Ionic liquids*, as discussed in the copper section, are composed of complex cations and anions. Fadhel [253] and colleagues synthesized three ionic liquids (i.e. 1-methyl-3-propylimidazolium iodide (MPIMI), 1-butyl-3-methylimidazolium iodide (BMIMI), and 1-hexyl-3-methylimidazolium iodide (HMIMI)) to assess their ability to inhibit mild-steel corrosion in 1 M HCl. These inhibitors all used iodide as the anion and alkyl imidazolium as the cation. HMIMI exhibited an %IE of 93 % at a concentration of 5 mM due to the  $\text{Br}^-$  ions being preferentially adsorbed on the surface of the positively charged steel by electrostatic action, with the alkyl imidazole cation adsorbing to the surface of steel by electrostatic interactions with  $\text{Br}^-$ .

Oliavres [254] and colleagues reported four ionic liquid corrosion inhibitors derived from ammonium (free-halide ionic liquids) that exhibited %IE of up to 89 %. Potentiodynamic polarization results indicated that these inhibitors suppressed both cathodic and anodic processes. Their adsorption followed the Langmuir adsorption isotherm consistent with physical adsorption on the steel surface. Likhanova [255] and colleagues synthesized two ionic liquids with different anions, N-ethyl-N,N,N-triethylammonium adipate

(CPA6), and N-ethyl-N,N,N-trioctylammonium ethyl sulfate (ESA8), to study the impact of anionic ionic liquids on corrosion inhibition. The results revealed that ESA8 was a more effective corrosion inhibitor than CPA6, attributed to the superior corrosion inhibition properties of the ethyl sulfate anion compared to the adipate anion.

#### 4.3.4. Chemisorbed inhibitors

Chemisorbed inhibitors encompass a diverse array of compounds including Schiff bases, amine-based organic molecules, imidazoles, and their derivatives [256–259]. Outstanding chemical organic inhibitors possess polar functional groups that usually include heteroatoms such as O, S, or N. These functional groups chemically adsorb onto the steel surface, forming a protective layer that shields the metal from the intrusion of corrosive ions. Unlike some inorganic corrosion inhibitors, chemisorbed organic inhibitors often exhibit excellent corrosion inhibition performance in harsh acidic environments [259].

Schiff base derivatives are widely used to mitigate the corrosion of carbon steels in various electrolytes due to their low cost and ease of synthesis. The imine group ( $RC=N$ ) can coordinate strongly with iron. Hanane and coworkers [260] synthesized three Schiff base derivatives containing quinoline-derived moieties: 4,4-oxybis(N-[(E)-quinoline-2-ylmethylidene]aniline), 4,4-ethane(N-[(E)-quinoline-2-ylmethylidene]aniline), and 4,4-methylenebis(N-[(E)-quinoline-2-ylmethylidene]aniline). All three displayed corrosion inhibition efficiencies exceeding 90 % in 1 M HCl for steel. Theoretical studies indicated that the imine groups, together with electron donation and back-donation between Fe 3d orbitals, drive chemical adsorption. 4,4-oxybis(N-[(E)-quinoline-2-ylmethylidene]aniline) exhibited the highest corrosion inhibition efficiency due to its additional oxygen atoms. Recently, Cao and colleagues [261] studied green synthesized vanillin derivatives, vanillin TRIS imine (VTRIS), vanillin cyanoguanine imine (VCNG), and vanillin tosylade imine (VTOS), that achieved corrosion inhibition efficiencies of up to ~ 93 % for steel in acidic environments. Electrochemical studies revealed them to be mixed-type corrosion inhibitors. Ansari and his colleagues [262] developed salicylaldehyde-chitosan Schiff base (SCSB) as a corrosion inhibitor for carbon steel in 3.5 % NaCl solution saturated with  $CO_2$ . At a concentration of 150 ppm, the %IE reached ~ 95 %. Theoretical studies suggested that this organic molecule exists in both protonated and neutral forms in acidic solutions, which spontaneously chemically adsorb onto the metal surface by transferring electrons from heteroatoms (O, N) and their conjugated systems to the empty orbitals of iron.

Imidazoline derivatives, known for their excellent corrosion inhibition performance and low toxicity, find widespread application in the petroleum, natural gas storage, and transportation industries for mitigating steel corrosion. Solomon [263] synthesized an imidazoline derivative, N-(2-(2-tridecyl-4,5-dihydro-1H-imidazol-1-yl)ethyl)tetradecanamide (NTETD), using myristic acid and diethyleneamine as raw materials. At a concentration of 300 ppm, NTETD exhibited a minimum %IE of over 93 % on steel in a 15 % HCl solution. Potentiodynamic polarization results indicated that NTETD was a mixed-type inhibitor, primarily inhibiting cathodic corrosion. The exceptional corrosion inhibition was attributed to the strong chemical adsorption between the active N, O, and imidazoline ring moieties in the NTETD structure and the iron surface. Zhang *et al.* [264] studied the influence of the number of imidazoline rings and the alkyl chain length of imidazoline derivatives on %IE. Three inhibitors, lauric acid imidazoline (SAI), tetralauric imidazoline (LAI), and symmetric stearic imidazoline (SPI) were synthesized. These inhibitors followed the Langmuir adsorption model, adsorbing on the steel surface through chemical adsorption. Increasing the number of imidazoline rings and alkyl chain lengths of the derivatives enhanced corrosion inhibition. Zheng *et al.* [265] synthesized two imidazoline derivatives, oleic imidazoline (OI) and mercapto-oleic imidazoline (MOI). MOI demonstrated %IEs of up to ~ 96 % at an extremely low concentration of 20 ppm. Conspicuously, the strong corrosion inhibition was maintained even after an immersion time of 144 h. Using the GFN-XTB method, they discovered that MOI is strongly adsorbed on the steel surface by bonding with Fe via the N and S atoms in the molecular backbone.

#### 4.3.5. Chemical conversion film-based inhibitors

Protective films can be formed on the surfaces of metals by irreversible reactions with the corrosion product, or by commercial conversion coatings [8]. While there has been a recent trend to call all these types of coatings conversion coatings, here we refer to the former as protective coatings and the latter as conversion coatings. The formation mechanisms of the chemical conversion coatings and protective films differ from the common physical or chemical adsorption mechanism of organic substances. Instead, like inorganic inhibitors, they protect the steel substrate by stabilizing the rust layer. A common member of this class of substances is phosphate derivatives. It has been reported that alkyl phosphate esters can form P-O-Fe bonds in water, resulting in the formation of insoluble protective films on steel surfaces [266]. Additionally, alkyl phosphate ester derivatives possess active functional groups that can attach to oxide surfaces. Hu and colleagues [266] investigated the corrosion behaviour of bis(2-ethylhexyl) phosphate (BEP) on carbon steel in a  $CO_2$ - $O_2$  environment. They showed the %IE reached 93 % at a concentration of 500 ppm. Further studies revealed that the excellent corrosion inhibition effect was due to the formation of P-O-Fe bonds and the production of  $FePO_4$  protective layers. Furthermore, BEP can interact with  $Fe^{3+}$ ,  $Fe^{2+}$ , and iron oxides, resulting in a thicker and more compact corrosion product layer. Phytic acid (PA) is another commonly used phosphate derivative. It is a six-fold dihydrogen phosphate ester of inositol. Cao *et al.* [267] investigated the corrosion inhibition effect of phytic acid on 20SiMn steel in simulated carbonated concrete pore solution contaminated with Cl ions. The addition of PA resulted in the formation of a dense deposited film with a three-layer structure on the surface of 20SiMn steel. The inner layer consisted of  $Fe_3O_4$  and  $FeOOH$ , the middle layer contained  $Fe_3O_4$ ,  $FeOOH$  and  $FePO_4$ , and the outer layer comprised  $Fe_3O_4$ ,  $FeOOH$ ,  $FePO_4$ , and  $Fe(II)$ -IP6.

Hu *et al.* recently reported the strong corrosion inhibition properties of bis(2-ethylhexyl) phosphate (BEP) in  $CO_2$ - $O_2$ -containing solution and proposed putative inhibition mechanisms [266]. Corrosion was almost eliminated in 1 % NaCl solution in a  $CO_2$ - $O_2$  solution by 500 ppm BEP. The inhibitor forms P-O-Fe and P-Fe bonds to generate a barrier layer that is responsible for the protective performance. Similarly, Mandal *et al.* reported a study of 1–3 % of 0.5 M ammonium phosphate monobasic (APMB) as a corrosion inhibitor for steel rebar [268]. EIS results showed that 2 % inhibitor in SCP plus 3.5 wt% NaCl solution inhibited 90 % of the corrosion

after 1 h. XPS and Raman spectroscopy showed that the inhibition was due to the formation of a thermodynamically stable, insoluble mixed goethite ( $\alpha\text{-FeOOH}$ ), maghemite ( $\gamma\text{-Fe}_2\text{O}_3$ ), and iron phosphate ( $\text{FePO}_4$ ) passive film on the steel rebar surface.

Other phosphonic acid-based inhibitors have been reported recently. Shaban, Felhosi and Telegdi studied a phosphonic-acid based inhibitor blend (Corin P22SU), composed of a mixture of potassium hydroxy-ethane-diphosphonate (HEDP), inorganic additives, and potassium phosphates), on mild steel corrosion in simulated cooling water (SCW) containing chloride ion using electrochemical methods and visual characterization [269,270]. Different concentrations of nitrite ion synergized the inhibition efficiency of the P22SU inhibitor. The inhibition of mild steel corrosion at  $\text{pH} \geq 6$  increased with soaking time. The mechanism of action of P22SU on mild steel corrosion inhibition in SCW was found to be the formation of a robust inhibitor film that blocks the active sites of the metal surface to a large extent.

Another class of substances that can react with rust to form protective films is tannins. Tannins interact with iron oxide through their polyphenolic structure, converting rusted iron into a deep blue coating, which is sparingly soluble in solution and effectively protects the substrate [270,271]. Gust and colleagues [272] conducted Mossbauer spectroscopy studies and found that there is an interaction between the rust phase components in aqueous solution and oak tannins, resulting in a mixture of mono and bis-complexes. Flores Merino *et al.* [273] used tannic acid as a corrosion inhibitor for low-carbon steel in a 0.1 M NaCl solution. Infrared spectroscopy (IR), scanning electron microscopy (SEM) and energy dispersive spectrometer (EDS) studies revealed the transformation of rusted portions into tannin-iron compounds. Inspired by functional mangrove tannins, Cui and colleagues [274] developed a corrosion inhibitor for protecting Q235 carbon steel in an acidic 3.5 wt% NaCl solution. Mangrove tannin inhibitors significantly slowed the cathodic corrosion process and exhibited a better corrosion inhibition performance than commercial tannins.[270,271].

Wang *et al.* investigated 2-(5-mercapto-1,3,thiadiazole-2-yl)-(4-methylbenzene) as an inhibitor for steel. Inhibition efficiency and adsorption behaviour of the inhibitor film was assessed using electrochemical and theoretical methods [275]. The results showed that corrosion is initiated under a microzone without the inhibitor film but is prevented when the protective film was present. Electrochemical studies showed increasing inhibitor concentrations up to 40 ppm generated a positive shift in the corrosion potential and reduced the corrosion current density. The derived  $\Delta G_{\text{ads}}$  implies that the physisorption of inhibitor molecules on the stainless-steel surface is the main mechanism of action.

Other novel organic species have also been reported to be potent inhibitors of steel corrosion. Glycine, N-[N-[(phenylmethoxy) carbonyl] glycol]-, 4-nitrophenyl ester, N alpha,omega-dicarbobenzoxy-L-arginine, N-(2-benzoylphenyl)-1-benzyl pyrrolidine-2-carboxamide, ethyl(E)-3-(4-(((E)-4-methoxybenzylidene)amino)-phenyl)acrylate, and 2-amino-3-(5-hydroxy-1H-indol-3-yl)propanoic acid were shown to be inhibitors of N80 steel in 15 % (wt) HCl solution [276]. Inhibition mechanisms were deduced from electrochemical impedance spectroscopy and polarization measurements as adsorption to the metal surface and passivating formation that limits the transmission of ions and reduces the corrosion current density. Quantum chemistry revealed that electron transfer from the metal surface atoms to the inhibitor molecules was key to suppressing corrosion. The same group also reported the protective efficiency of a new triazole inhibitor for carbon steel, (2-sulfhydryl)-(5-phenmethyl)-(1-(4-phenol)-methanimine)-triazole (SPMT) [277]. The inhibitor readily formed a protective film on the carbon steel surface.

As an atomic-level insight into the organic molecule corrosion inhibition mechanisms is still lacking, and DFT is ill-equipped to handle large inhibitor-metal adsorption systems, a density functional based tight-binding (DFTB) approach was used to investigate the adsorption properties of three large chalcone derivative inhibitors on an iron surface [278]. Guo *et al.* studied the molecular activity of these chalcone derivatives using frontier molecular orbital theory. The growth characteristics of alpha-Fe, adsorption parameters such as charge density difference, the density of states, and changes of molecular orbital were reported.

#### 4.3.6. Plant-based green corrosion inhibitors

As seen above, many organic compounds can inhibit corrosion of metals. However, some chemicals can be expensive and environmentally harmful. In recent years, there has been significant interest in the discovery, extraction, and synthesis of non-toxic and potentially cost-effective plant-based corrosion inhibitors. Research has shown that saponins, flavonoids, organic acids, and various organic substances present in plant roots, stems, and leaves contribute to corrosion inhibition [279]. These types of inhibitors typically follow a mixed adsorption mechanism involving both physical and chemical adsorption.

Gowraraju and colleagues [280] evaluated the corrosion inhibition efficiency of biopolymer Iota-carrageenan (IC) on low-carbon steel in 0.5 M  $\text{H}_2\text{SO}_4$  solution using weight loss tests, potentiodynamic polarization, and EIS. They found that at a concentration of 1000 ppm, IC exhibited a corrosion inhibition efficiency of 96 %, and its adsorption followed the Langmuir isotherm. The presence of heteroatoms such as oxygen and electronegative sulfate atoms as IC adsorption centres results in high %IE. Wang *et al.* [281] utilized an *Oxalis corniculata L.* extract (OCLE) as a green corrosion inhibitor for carbon steel in 1 M HCl. Electrochemical test results indicated that OCLE achieved a %IE of  $\sim 94$  % at a concentration of 500 ppm. High-performance liquid chromatography (HPLC) confirmed that the main components of this extract were monosaccharides. Quantum chemical calculations and MD simulations suggested that monosaccharide molecules present in OCLE could form an adsorption film on carbon steel through O and N to inhibit corrosion. Maizia and colleagues [282] investigated the corrosion inhibition effect of *Urtica dioica L.* extract (NE) on X80 low-carbon steel in 0.5 M  $\text{H}_2\text{SO}_4$  solution. NE achieved a corrosion inhibition efficiency of 95 % at a concentration of 4 g/L. Further research indicated that the corrosion inhibition effect was due to the synergistic adsorption of various chemical components present in NE extract (quercetin and kaempferol, serotonin and histamine) on iron. Typically, plant extracts are multi-compound mixtures that for corrosion inhibition might mean cooperative inhibition effects. Further plant extract studies need to include efforts for unravelling their chemical composition for tracing down the origin of the inhibition effect.



#### 4.3.7. Effects of corrosion inhibitors on different structures of steel

Corrosion inhibition mechanisms can be also influenced by the nature of the metal adsorption sites. Due to differences in manufacturing processes and compositions, the microstructures and structures of different types of steel vary. Consequently, when corrosion inhibitors act on different microstructures, their inhibiting mechanisms may also differ. López [283] and his colleagues used electrochemical methods to study the corrosion inhibition effect of three imidazoline inhibitors on steel with two different microstructures in a CO<sub>2</sub> environment. Their research revealed that the inhibitors were more effective on annealed samples than quenched and tempered samples. They proposed that Fe<sub>3</sub>C is the adsorption site of corrosion inhibitor molecules, and the layered Fe<sub>3</sub>C in annealed samples is more stable than the spherical Fe<sub>3</sub>C in quenched and tempered samples, with respect to corrosion. Spherical Fe<sub>3</sub>C is more easily removed from the sample surface, resulting in a decrease in adsorption sites. In contrast, Zhang *et al.* [284] recently synthesized a new imidazoline corrosion inhibitor and studied its corrosion behaviour on two types of steel with different microstructures in a CO<sub>2</sub> environment. They showed that steel treated by quenching and tempering has a pronounced homogeneous distribution of pearlite (globular and short rod-shaped) and a low density of dislocations, allowing corrosion inhibitor molecules to adsorb more closely on the surface, resulting in better corrosion inhibition. In contrast, annealed steel may preferentially dissolve iron atoms in the pearlite region, facilitating the desorption of corrosion inhibitor molecules from the pearlite. Overall, although the importance of the microstructure of steel on corrosion mechanisms and effects has been recognized, the current research remains limited.

### 4.4. Corrosion inhibitors for aluminium

#### 4.4.1. Corrosion mechanisms

Aluminium forms a passive oxide or barrier layer that is stable between pH 4 and pH 9 but is soluble at lower and higher pH values [285]. The structure of the passive oxide layer is still not clear. Some reports suggest it is amorphous while others state that it is crystalline  $\gamma$ -Al<sub>2</sub>O<sub>3</sub>, with different formation processes on each crystal face [286,287]. Hydration of the passive oxide layer by water generates terminal hydroxyl groups. This results in thickening of the surface oxide, with an outer, more porous layer covering the barrier layer. Aluminium ions generated at the metal/oxide interface migrate to the outer surface to form a hydrated surface oxide. This can also be viewed as cation vacancies migrating from the outer surface, where they are filled by Al<sup>3+</sup> cations. The terminal hydroxyl groups can react with inhibitors forming layers that can block corrosion.

The most detailed and precise computational studies have involved single crystal surfaces (Al(111)) with various levels of oxidation and hydroxylation [152,291,292]. The Al(111) surface is most often modelled because it has a high density of surface atoms that provide a large atom coordination surface (Fig. 12) and a low surface energy [288]. The Al(110) [290] and Al(100) [291,292] surfaces, and Al clusters [293,294] have also been studied [152,291,292]. Al(111) is also one of the most frequently occurring grain orientations in experimental studies, along with Al(001) and Al(101) [295,296]. These crystal orientations occur most frequently because of the way deformation is manifest through mechanical processing. Due to its dense packing, Al(111) is also one of the more difficult orientations to oxidize (Fig. 12) [297]. Open structures tend to be more reactive because, if an adsorbate sits in an empty site, the back donation of electrons promotes bond lengthening and dissociation. This mechanism has been amply modelled by DFT calculations of N≡N on Fe single-crystal surface [295,296].

Aluminium forms alloys with elements having specific materials properties. Table 3 summarizes the main classes of wrought aluminium alloys, exemplifies alloys in each class, and lists typical application areas. Aluminium alloys present entirely different problems for corrosion inhibition compared to pure aluminium. Alloying results in microstructure development via particle formation at multiple scales. This can range from hardening precipitates at the smallest scale (nm), through dispersoids at intermediate scales (submicron), to primary intermetallic particles (IMP) at the micron scale and above. Alloys also contain levels of Fe, Si, Cu, and other transition metals. Intermetallic particles generate galvanic couples with the aluminium matrix to form nano- to micron-sized galvanic

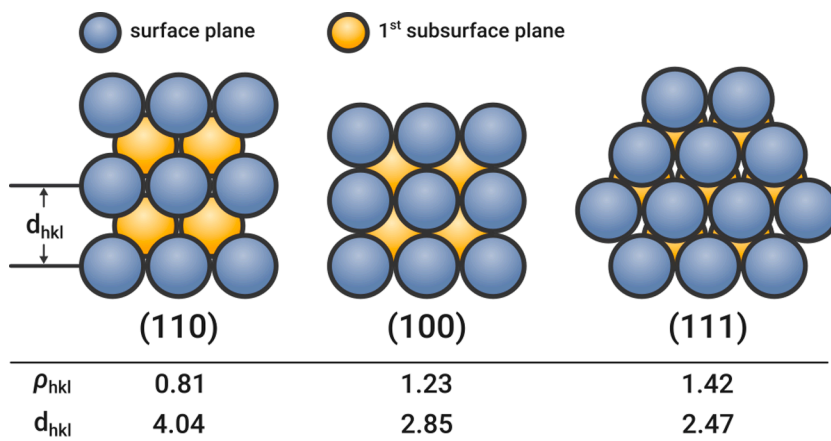


Fig. 12. Hard-sphere models for the three main faces of Al with suggested adsorption sites. The table shows surface density  $\rho_{hkl}$  and stacking distance  $d_{hkl}$  for low index faces of Al. Adapted from Martinson et al. [297] with permission.

**Table 3**

Categories of aluminium wrought alloys, major alloying elements, examples, common usage, and Cu content. Cu is a noble alloying element and is the biggest driver of micro-galvanic corrosion.

| Series      | Alloying Metal             | Examples             | Common Usage for class  | Cu (wt%)          |
|-------------|----------------------------|----------------------|---|-------------------|
| 1xxx        | –                          | AA1100<br>AA1200     | aluminium foil<br>food handling, packaging containers               | 0.05–0.20<br>0.05 |
| 2xxx        | Cu, Mg                     | AA2024               | high strength, aerospace  | 3.8–4.9           |
| 3xxx        | Cu, Li                     | AA2099               | high strength, aerospace  | 0.05–0.20         |
|             |                            | AA3003               | beverage cans   |                   |
| 5xxx        | Mn                         | AA3104               | beverage cans   | 0.15              |
|             |                            | AA5005               | structural alloys, automotive, decorative, marine                   | < 0.2             |
| 6xxx        | Mg                         | AA5052               | “   | < 0.1             |
|             |                            | AA6060               | structural alloys, general purpose, automotive, marine              | < 0.1             |
| 7xxx        | Si, Mg                     | AA6061               | aerospace   | 0.15–0.4          |
| 8xxx        | Zn, Mg, Cu                 | AA7075               | high strength, aerospace  | 1.2–2.0           |
| AM tailored | Other, including Li, Ni    | AA8081               | high strength   | 0.7–1.3           |
| Al-Mg       | Mg, Sc, Mn, Zr, Si, Fe, Zn | Scalmalloy [309–314] | Processed by LPBF, high strength, aerospace, defence, automotive    | 0.1               |
| Al-Si-Mg    | Si, Mg, Mn, Fe,            | AlSi10Mg [310,312]   | Processed by LPBF, high thermal conductivity, aerospace, automotive | 0.05              |

cells that accelerate corrosion [233,301–311]. Table 4 lists common primary intermetallic particles that are produced during processing.

Characterisation of intermetallic particles was first reported in the middle of the twentieth century (e.g., Phragmen [316] and Mondolfo [317]). Recent studies show that modern alloys contain intermetallic particles with different compositions and crystal structures compared to the earlier reports and these will have slightly different electrochemical activity, with Fe and Cu increasing activity and Mn reducing it [318]. The small micro-galvanic cells formed in the matrix act as cathodic sites that, in most cases, are electrochemically active. (Fig. 13)[319–326]. Table 5 summarizes the hardening precipitates that form during alloy aging. These give rise to the high strength properties of alloys. Copper in solid solution is also enriched as a thin layer just under the surface oxide due to etching caused by corrosion or metal finishing processes [324–333] (Fig. 14).

**Table 4**

Typical constituent particles reported in wrought Al-alloys and recent electron microprobe compositions (N.D. = not detected, both calibrated electron microprobe and EDS in TEM are presented in the last column).

| Alloy | Constituent Particles   | Actual Compositions Microprobe (atom %)  |
|-------|---|--|
| 2024  | Al <sub>7</sub> Cu <sub>2</sub> Fe  | Al <sub>79</sub> Cu <sub>13</sub> Fe <sub>5</sub> Mn <sub>2</sub> Mg <sub>0.7</sub> Si <sub>0.2</sub> [104]              |
|       | Al <sub>12</sub> (Fe,Mn) <sub>3</sub> Si  | –  |
|       | (Fe,Mn) <sub>x</sub> Si(Al,Cu) <sub>y</sub>   | Al <sub>67.6</sub> Cu <sub>3.36</sub> Fe <sub>14.89</sub> Mn <sub>6.87</sub> Mg <sub>0.43</sub> Si <sub>6.27</sub> [313] |
|       | α-Al <sub>19</sub> Fe <sub>4</sub> MnSi <sub>2</sub>  | Al <sub>77</sub> Cu <sub>10</sub> Fe <sub>7</sub> Mn <sub>5</sub> Si <sub>2</sub> [104]                                  |
|       | Monoclinic Phase  | Al <sub>76</sub> Cu <sub>6</sub> Fe <sub>7</sub> Mn <sub>5</sub> Si <sub>6</sub> [104]                                   |
|       | Al <sub>2</sub> CuMg  | Al <sub>61</sub> Cu <sub>20</sub> Mg <sub>15</sub> [101]   |
|       | Al <sub>2</sub> Cu  | Al <sub>51.62</sub> Cu <sub>24.0</sub> Mg <sub>23.52</sub> Zn <sub>0.75</sub> [313]                                      |
|       | Al <sub>6</sub> (Cu,Fe)   | Al <sub>52.8</sub> Cu <sub>24.5</sub> Mg <sub>22.7</sub> [313]   |
|       |   | Al <sub>70</sub> Cu <sub>27</sub> [101]  |
|       |   | Al <sub>62.98</sub> Cu <sub>33.83</sub> [313]N.D.  |
| 2X19  | Al <sub>7</sub> Cu <sub>2</sub> Fe, Al <sub>12</sub> (Fe,Mn) <sub>3</sub> Si  | –  |
|       | Al <sub>2</sub> Cu  | –  |
| 6013  | Al <sub>12</sub> (Fe,Mn) <sub>3</sub> Si  | –  |
| 7075  | Al <sub>7</sub> Cu <sub>2</sub> Fe, Al <sub>6</sub> (Fe,Mn), Al <sub>12</sub> (Fe,Mn) <sub>3</sub> Si, Mg <sub>2</sub> Si | –  |
|       | Al <sub>23</sub> CuFe <sub>4</sub>  | –  |
|       |   | Al <sub>79.6</sub> Cu <sub>2.46</sub> Fe <sub>15.0</sub> Mn <sub>0.72</sub> Zn <sub>0.74</sub> Mg <sub>0.34</sub> [313]  |
|       |   | Al <sub>79.3</sub> Cu <sub>2.38</sub> Fe <sub>15.66</sub> Mn <sub>0.77</sub> Zn <sub>0.75</sub> Mg <sub>0.38</sub> [313] |
|       |   | Al <sub>79.2</sub> Cu <sub>4.3</sub> Fe <sub>13.6</sub> Zn <sub>1.3</sub> Mg <sub>1.6</sub> [314]                        |
| 7X50  | Al <sub>7</sub> Cu <sub>2</sub> Fe, Al <sub>2</sub> CuMg, Mg <sub>2</sub> Si  | –  |
| 7055  | Al <sub>7</sub> Cu <sub>2</sub> Fe, Mg <sub>2</sub> Si  | –  |
| 2090  | Al <sub>7</sub> Cu <sub>2</sub> Fe  | –  |
| 2099  | Al <sub>7</sub> Cu <sub>2</sub> Fe  | Al <sub>87.8</sub> Cu <sub>7.9</sub> Fe <sub>0.2</sub> Mn <sub>1.1</sub> Zn <sub>1.9</sub> Mg <sub>0.4</sub> [315]       |
|       | Al <sub>3</sub> Fe (Al <sub>13</sub> (Fe,Mn) <sub>4</sub> )   | Al <sub>75.6</sub> Cu <sub>11.5</sub> Fe <sub>6.9</sub> Mn <sub>3.9</sub> Zn <sub>2.0</sub> [315]                        |
|       | Al <sub>12</sub> Fe <sub>3</sub> Si   | Al <sub>75.2</sub> Cu <sub>9.3</sub> Fe <sub>6.8</sub> Mn <sub>7.0</sub> Zn <sub>1.7</sub> [315]                         |
|       | A <sub>6</sub> (Fe,Mn)  | N.D.   |
|       | Al <sub>37</sub> Fe <sub>12</sub> Cu <sub>2</sub>   | Al <sub>83.9</sub> Cu <sub>3.4</sub> Fe <sub>7.1</sub> Mn <sub>4.4</sub> Zn <sub>1.1</sub> [315]                         |
|       |   | Al <sub>76.2</sub> Cu <sub>14.6</sub> Fe <sub>5.5</sub> Mn <sub>1.3</sub> Zn <sub>2.1</sub> [315]                        |
| 2095  | Al <sub>7</sub> Cu <sub>2</sub> Fe, Al <sub>2</sub> CuLi, Al <sub>6</sub> CuLi <sub>3</sub>                               | –  |
| 8090  | Al <sub>3</sub> Fe  | –  |

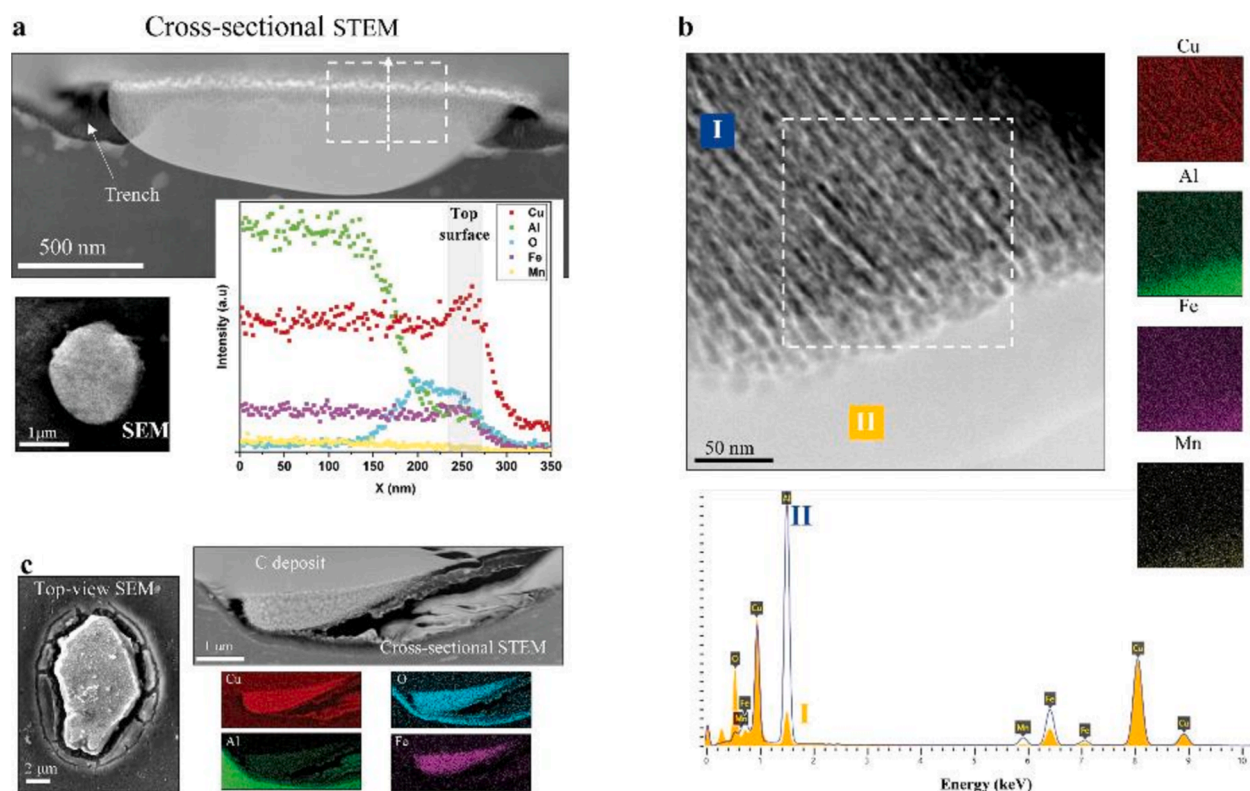


**Fig. 13.** TEM analysis of local corrosion induced by Al<sub>7</sub>Cu<sub>2</sub>Fe(Mn) phase. (a) Top-view SEM and cross-sectional STEM image of an Al<sub>7</sub>Cu<sub>2</sub>Fe(Mn) particle immersed in 0.01 M NaCl for 15 min. Elemental scan lines were reconstructed from the rectangular region in the image, showing preferential dissolution of Al and Mn and formation of a Cu-, Fe-rich layer on top. (b) Magnified cross-sectional STEM/EDS analysis of a dealloyed Al<sub>7</sub>Cu<sub>2</sub>Fe(Mn) particle exposed to 0.01 M NaCl for 6 h. The spectra show the chemical composition of corroded (I) and intact (II) regions. (c) Top-view SEM and cross-sectional STEM/EDS analysis of an undercut Al<sub>7</sub>Cu<sub>2</sub>Fe(Mn) particle immersed in 0.01 M NaCl for 6 h. Reproduced from Kosari et al. [302] under Creative Commons CC-BY license.

**Table 5**

Compositions of Hardening Precipitates.

| Alloy Type | Precipitate Composition  | Precipitate Nomenclature<br>(Includes coherent, semi-coherent and incoherent particles) |
|------------|--|---|
| Al-Cu      | Al <sub>2</sub> Cu   | θ   |
| Al-Mg      | Al <sub>8</sub> Mg <sub>5</sub>  | β   |
| Al-Si      | Si   | —   |
| Al-Cu-Mg   | Al <sub>2</sub> CuMg   | S   |
| Al-Mg-Si   | Mg <sub>2</sub> Si   | β   |
| Al-Zn-Mg   | MgZn <sub>2</sub> (Al <sub>1</sub> (Cu,Zn)<br>) <sub>49</sub> Mg <sub>32</sub> | ηT  |
| Al-Li-Mg   | Al <sub>3</sub> Li   | δ   |
|            | Al <sub>2</sub> LiMg   | —   |
| Al-Li-Cu   | Al <sub>3</sub> Li   | δ   |
|            | Al <sub>2</sub> CuLi   | T <sub>1</sub>  |

#### 4.4.2. Corrosion inhibition mechanisms

Understanding alloy microstructure is important for corrosion inhibitor design and discovery. For example, intermetallic particles containing transition metals, particularly copper, act as cathodes for oxygen reduction (see section 4.3.1). Activating cathodic reactions creates anodic sites is facilitated by consumption of electrons produced at the anodic reaction. This translates into localized attack around intermetallic particles, dissolving the surrounding aluminium matrix (called trenching) [323,332]. Thus, an important role of inhibitors is to suppress cathodic reactions with Cu as well as the anodic reactions adjacent to these sites. Organic inhibitors containing S, O, or N have delocalized  $\pi$  electrons and lone pair electrons that can interact with the 3d electrons of Cu (and other transition metals) [333] (refer to discussion in the copper inhibitor section 4.3). Aluminium alloys also form a passive oxide layer across the matrix that is only stable in the pH range of 4 to 8 [285]. As cathodic sites have higher, and anodic sites lower pH values than

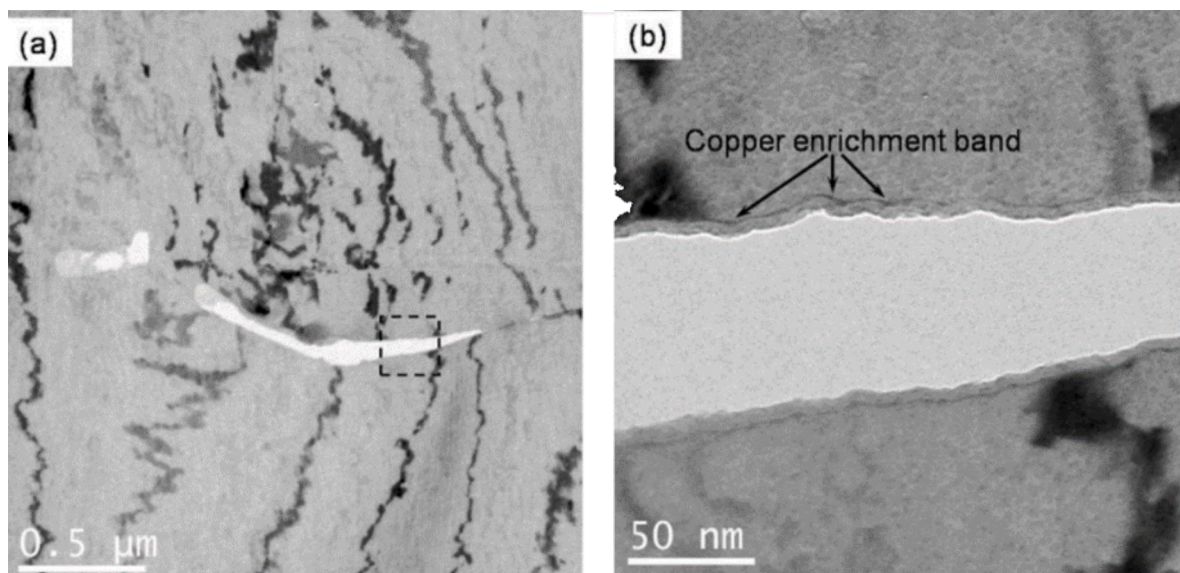


Fig. 14. Cu enrichment band between corrosion product and Al in 2A97 alloy. Reproduced from Luo et al. [331] with permission.

this range, additional inhibition modes are required, *i.e.*, inhibition under acidic and alkaline conditions.

#### 4.4.3. Physisorbed inhibitors

DFT calculations on Al and its alloys suggest donation from the HOMO orbitals of inhibitors to the empty Al 3p states, and back donation from the Al 3s states into the LUMO orbitals occurs [334,335]. This generates weak physisorption, unlike the transition metals where the 3d levels are involved. Organic inhibitors may also interact with metal surfaces by forming complexes with the aluminium ion surrounded by its waters of hydration ( $\text{Al}\cdot 6\text{H}_2\text{O}^{3+}$ ) [335]. However, modelling this process does not provide information on the molecule's interaction with the surface. Multiple studies have used a range of physics-based approaches to understand the interactions between pure metal surfaces and inhibitors, [335–343] or to support experimental data [341–362] by predicting inhibitor efficiencies using a variety of DFT-derived descriptors [342]. Most studies perform calculations *in vacuo*, so, clearly, a one-to-one correlation cannot be expected because, under vacuum, a surface will be neither partially oxidized nor hydroxylated. Some studies do account for the aqueous environment using explicit or implicit solvent models [339,340,357,359].

**Carboxylate inhibitors:** Mechanistically, organic inhibitors containing carboxylates react with terminal hydroxyl groups on the oxide layer to form monodentate or bidentate bonds. For carboxylate interactions with Al(111) surfaces, Poberznik *et al.* provide a more detailed picture of surface interactions [289]. They found that the  $\mu_1$  and  $\mu_2$  monodentate forms are the only ones that exist on a hydroxylated oxidized Al- surface, along with hydrogen bonds between the other carboxylate O and adjacent surface hydroxyl groups (Fig. 15). Poberznik *et al.* reported that the stability of the  $\mu$ -bonded species is modulated by the difference ( $\Delta E$ ) in the binding energy of Al-OH versus the carboxylate, both of which are of the order of 5–6 eV, with their difference being in the range –0.4 to 0.25 eV (Fig. 16 a). Increasing the length of the R group leads to a higher degree of self-assembly of the adsorbates, as described in section 4. This produces a denser protective layer with a tilt angle that depends on the surface structure (Fig. 16 b), where the angle of the R-group will depend on the details of the bonding at the surface. The bidentate form was not found to be stable on fully hydroxylated surfaces and only possible in specific cases.

**Azole inhibitors:** Kovacevic and Kokalj [153] reported that imidazoles and tetrazoles adsorb in a similar way through a single nitrogen atom, while 1,2,3-triazole binds using two nitrogen atoms in a bridged configuration. Lashkari and Arshadi also reported that pyridine and methyl-substituted pyridines bind perpendicular to Al and Fe surface clusters through the lone pair electrons on N, with some additional  $\pi$ -bonding with Fe possible but not preferred [293]. Kovacevic and Kokalj [153] also reported that for azoles, due to the absence of d band back donation that occurs with Cu, Al(111) and Cu(111), surfaces behave quite similarly. This suggests that

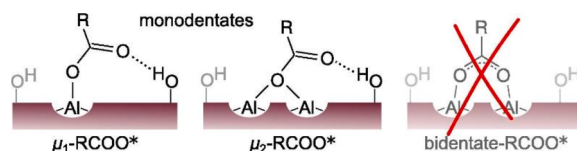
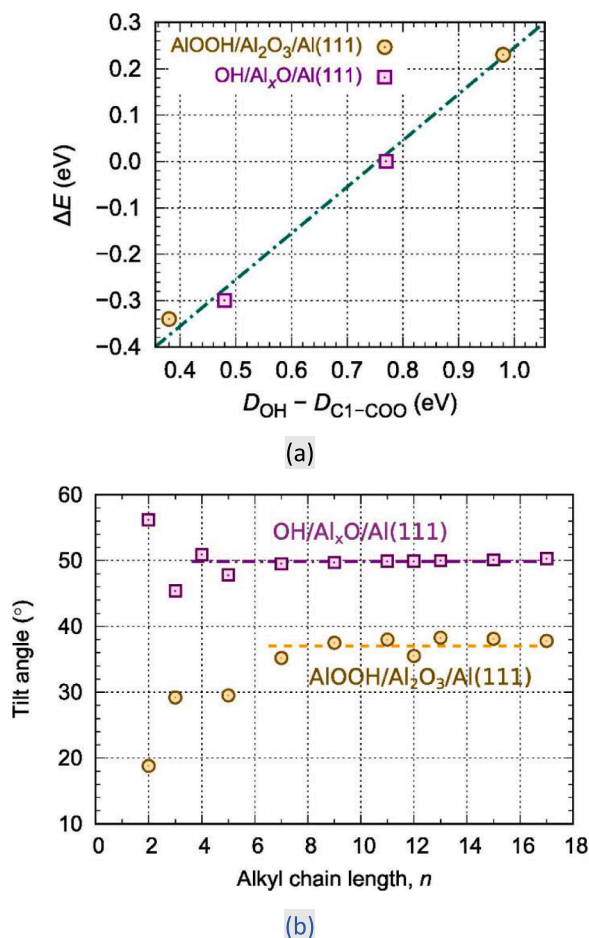


Fig. 15. Representation of monodentate adsorption bonding configurations of carboxylate to a hydroxylated, oxidized Al substrate (left and middle). The bidentate configuration (right) where both carboxylic O atoms bind to Al does not occur on fully hydroxylated surfaces, only near OH vacancies. Reproduced from Poberznik et al. [289] with permission.



**Fig. 16.** a) Correlation between adsorption energy of standalone C1-COO and the difference between the adsorbate-surface bond strengths of substituted OH group and the C1-COO. b) Calculated tilt angles of C<sub>n</sub>-COO as a function of chain length at full molecular coverage for two surface models. Molecular density is larger and the interchain distances are smaller for AlOOH/Al<sub>2</sub>O<sub>3</sub>/Al(1 1 1), leading to tilt angles that are smaller than those on OH/Al<sub>x</sub>O/Al(1 1 1). Reproduced from Poberznik et al. [289] with permission.

chemical hardness may correlate better with adsorption. Kokalj *et al.* [152] later reported that for dissociative adsorption imidazole, 1,2,3-triazole and tetrazole behave quite differently because the nitrogen atoms in imidazole are opposed and cannot adsorb productively end-on using both atoms. DFT calculations showed that dissociative adsorption via cleavage of an N—H bond is less favourable than cleavage of a C—H bond at an oxygen vacancy site on Cu<sub>2</sub>O(111). The cleavage of the C4—H bond leads to a more stable adsorbate since it also involves the adjacent N lone pair electrons, as opposed to N—H cleavage that occurs only through the nitrogen atom. This reaction is also favourable on iron surfaces [360] but much less favourable on Al surfaces, highlighting the possible differences between reactions occurring on the aluminium matrix and IM particles.

For N-thiazolyl-2-cyanoacetamide derivatives, Zhang *et al.* [288] reported that benzene and thiazole rings were the most reactive centres in the derivatives. They found that the LUMO orbitals for back donation were most important for explaining differences in corrosion inhibitor performance. They also found that solvation (compared to *in vacuo*) resulted in a lowering of inhibitor efficiency. MD calculations showed that conformational flexibility in the inhibitors reduced their self-diffusion and improved their inhibitor efficiencies.

#### 4.4.4. Chemisorbed inhibitors

**8-hydroxyquinolines:** Adsorption of 8-hydroxyquinalone (8-HQ) on Al(111) has been studied extensively [361,362]. It is widely reported to be a good corrosion inhibitor for several alloys, including Al alloys [363,364]. Marcelin and Pebere showed that in mixtures with benzotriazole, good corrosion inhibition was provided for the AA2024 alloy. They concluded that it interacted with the aluminium matrix to form a stable surface complex that competed strongly with chloride ions [365]. A computational study by Chiter *et al.* examined several 8-HQ species including 8HQ, its tautomer, fully hydrogenated 8HQ, and the full deprotonated form (Fig. 17) [361]. Native 8HQ is chemisorbed, forming covalent bonds through the N and C (C<sub>4</sub>) atoms [362]. These studies were performed at low coverage ( $\theta = 0.1$ ) and with adsorption parallel to the Al(111) surface at neutral pH, on which only the native and tautomer species was

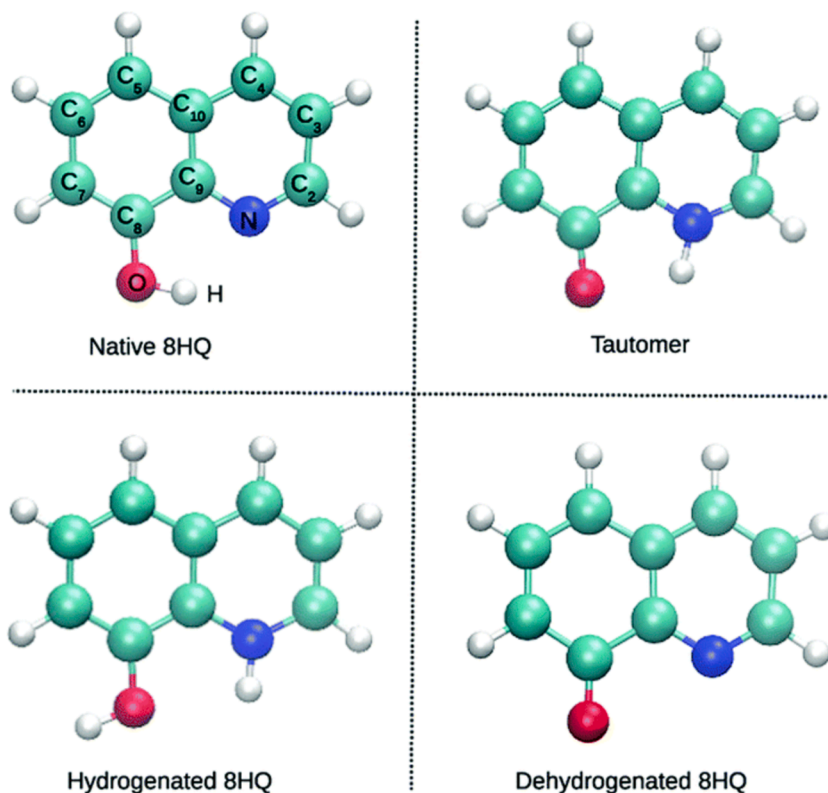


Fig. 17. Native 8HQ ( $\chi$ ), tautomer ( $\tau$ ), hydrogenated ( $\eta$ ) and dehydrogenated ( $\delta$ ) species. Reproduced from Chiter et al. [361] with permission.

adsorbed [363,364].

A more detailed study by Chiter *et al.* examined a range of 8HQ species that exist in aqueous solution as a function of surface coverage [362]. The speciation was driven by the  $pK_a$ , with the protonated form existing below pH 5.3 and the deprotonated form above pH 9.9. For the native 8HQ and the tautomer, bonding is largely through the N and C<sub>4</sub> sites up to  $\theta = 0.66$  (Fig. 18). The tautomer is more strongly adsorbed via a strong O interaction with the surface. However, at  $\theta = 1$ , neither species remains flat, with a preference for bonding through the N and C<sub>2</sub> sites (based on electron density and the C<sub>2</sub>-Al and C<sub>4</sub>-Al bond lengths) and possible interaction through the O site. Similar results to the native 8HQ were obtained for the protonated form. Only the deprotonated form remained bonded through the N and C<sub>4</sub> sites for all surface coverages.

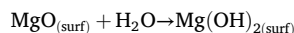
The adsorption energies of 8HQ species were all negative (attractive) in the absence of deformation of the Al(111) substrate and interaction energies (cohesive energy) between adsorbed molecules at high coverage. Between  $\theta = 0.5$  and 1.0 the cohesive energy stabilized the layer, up to 32 % for 8HQ and its fully protonated species, 16 % for its tautomer and 8 % for its deprotonated species. The van der Waals (vdW) interaction between 8HQ and the surface decreases at high coverage due to molecular distortion, but this is compensated by vdW interactions between the adsorbed molecules.

**Thiourea inhibitors:** Weder *et al.* performed extensive studies of a series of thiourea derivatives on Al terminated  $\alpha$ -Al<sub>2</sub>O<sub>3</sub> surfaces in concentrated HCl [367]. The derivatives were chemisorbed, dominated by electron transfer through the S atom to the surface and the first few layers of the surface. The adsorption energy did not correlate directly with the inhibitor efficiency but correlated well with the integrated electron density difference. Weder *et al.* concluded that thiourea derivatives were cathodic inhibitors, generating a net positive surface charge that repelled protons thus inhibiting hydrogen reduction.

#### 4.5. Corrosion inhibitors for magnesium

##### 4.5.1. Corrosion mechanisms

The free energy of MgO formation drives the rapid oxidation of Mg and its alloys. The magnesium oxide layer, reported to be of ~0.5 to 6 nm thick, does not offer adequate corrosion protection. For example, in humid atmosphere or under immersion in aqueous saline solution, native MgO transforms into a MgO/Mg(OH)<sub>2</sub> bilayer film due to hydroxylation



This bilayer structure is a diffuse mixed film defined by a thin/dense MgO-rich inner layer and a thick/porous Mg(OH)<sub>2</sub>-rich outer layer. The change in the compactness from a dense inner to a porous layer is a consequence of a volume change in the crystal structure

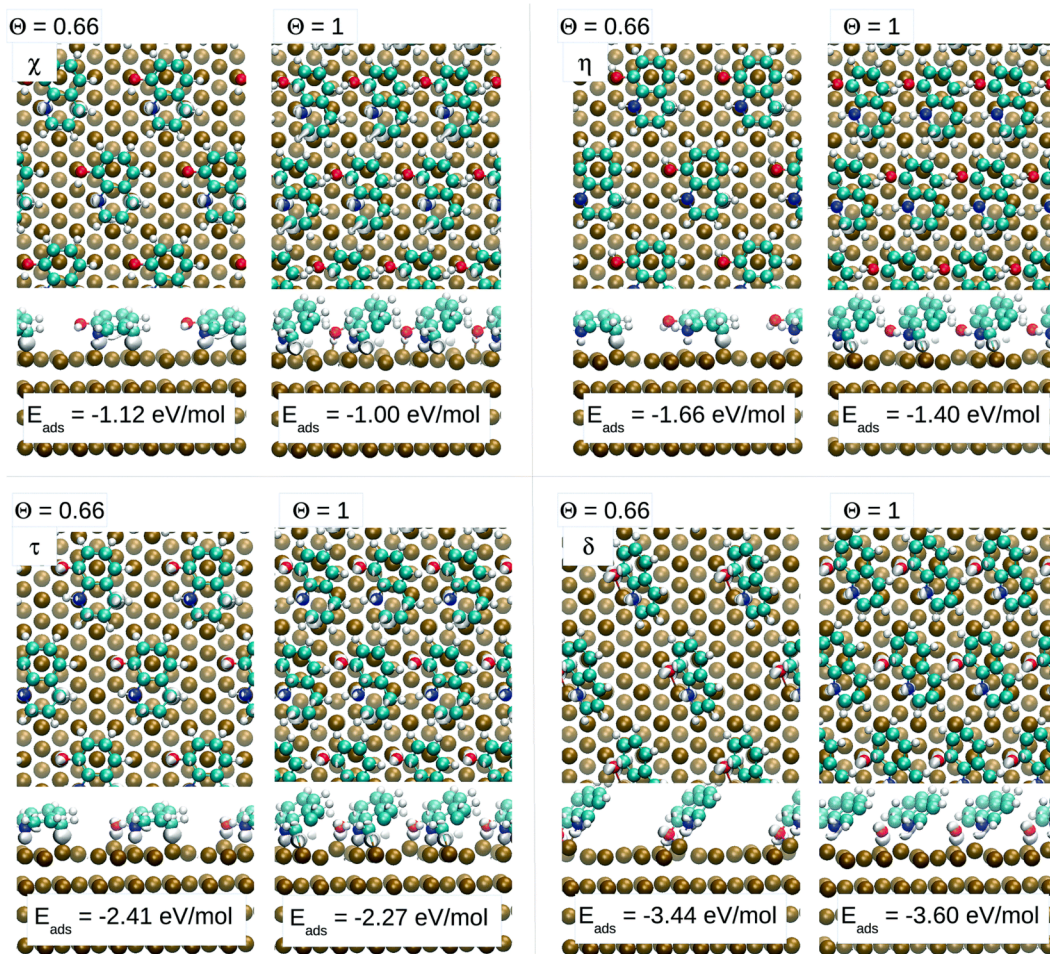
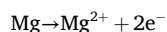


**Fig. 18.** Adsorption topologies and electronic density variation ( $\Delta\rho$ ) at two coverages ( $\theta = 0.66$  and  $\theta = 1$  for 8HQ ( $\chi$ ), tautomer ( $\tau$ ), hydrogenated ( $\eta$ ) and dehydrogenated ( $\delta$ ) species. Each coverage frame shows both the top view and side view. Reproduced from Chiter et al. [366] with permission.

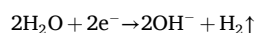
from the transition from Mg-O to Mg-OH and the continuous dissolution-precipitation processes occurring in the bilayer [368–373]. The thickness of the bilayer film varies between 20 – 300 nm and several microns. Mg surface layers are defective and incompletely cover the underlying metal due to a Pilling-Bedworth ratio (the ratio of the volume of the elementary cell of a metal oxide to the volume of the elementary cell of the corresponding metal) being less than 1. This metric can be used to determine whether a metal is likely to passivate in dry air by creation of a protective oxide layer. Additionally, Mg(OH)<sub>2</sub> (brucite) possesses relatively high solubility that increases as pH decreases [371]. This leads to a partially passivated surface that cannot block the contact with the immersion electrolyte, even though the contribution of the oxygen reduction reaction to the total cathodic process decreases with increasing thickness of Mg(OH)<sub>2</sub> [59]. The secondary phases, IMPs, and impurities in Mg alloys are typically covered with even less effective protective surface films and induce micro-galvanic corrosion. Given the highly electronegative potential of Mg, most of the alloying elements (e.g. Al, Zn, Mn) and impurities (Fe, Cu, Ni) act as local cathodes promoting anodic dissolution of Mg matrix. Table 6 presents selected examples of well-studied Mg alloys with industrial applications in aerospace, automotive, motorsport, defence, consumer goods and biodegradable implants. Table 7 presents the corrosion potentials of most common second phases.

In aqueous electrolytes, the main corrosion reactions for magnesium are [81,375,376].

Anodic oxidation:



Cathodic reduction:



the primary process, hydrogen evolution reaction (HER) and the secondary, oxygen reduction reaction (ORR)

**Table 6**  
Selected magnesium alloy codification [372] and examples.

| Codification    | Examples      | Main alloying elements   | Common usage   |
|-----------------|---------------|--|--|
| A – aluminum    | AZ31AZ91      | Al 2.5–3.5, Zn 0.6–1.4, Mn 0.2–1.0<br>Al 8.3–9.7, Zn 0.4–1.0, Mn 0.1–0.5   | Automotive, consumer goods, aerospace  |
| E – rare earths | Elektron 21   | Nd 2.6–3.1, Gd 1.0–1.7, Zn 0.2–0.5   | Aerospace and motorsport   |
| K – zirconium   | ZK40          | Zn 3.5–4.5, Zr 0.4–0.9   | Aerospace, biodegradable Implants  |
| L – lithium     | LA 141LA91    | Li 13–15, Al 0.7–1.9<br>Li 8–10, Al 0.6–1.5  | Aerospace  |
| M – manganese   | AM50,<br>AM60 | Al 4.4–5.4, Mn 0.2–0.6, Zn 0.2–1.0<br>Al 5.5–6.5, Mn 0.2–0.6, Zn 0.2–1.0   | Automotive (e.g. wheels)   |
| Q – silver      | QE22          | Ag 2.0–3.0, (Nd, Pr) 1.8–2.5, Zr 0.3–1.0   | Aerospace and defence (landing wheels, gear box housing)   |
| W – yttrium     | WE43<br>WE54  | Y 3.7–4.3, Nd 2.0–2.5, (Gd, Dy, Yb, Er) 1.9, Zr 0.2–1.0, Zn 0.2<br>Y 4.7–5.5, Nd 1.5–2.0, (Gd, Dy, Yb, Er) 2.0, Zr 0.4–1.0, Zn 0.2 | Aerospace (engine parts, rotor heads), defence, automotive (wheels, gearbox, frames), biodegradable implants; suitable for LPBF AM |
| X – calcium     | Mg-0.1Ca      | Ca 0.05–0.2, Mn 0.03   | Anode for Mg-air batteries; biodegradable implants   |
| Z – zinc        | ZE41          | Zn 3.7–4.8, (Ce, La, Nd, Pr) 1.0–1.75, Zr 0.3–1.0  | Automotive, electronic equipment, biodegradable implants   |



**Table 7**

Representative corrosion potential values for pure Mg, impurities and common Mg second phases. Original data was published in [373] and [374].

| Intermetallic composition             | Corrosion potential<br>V SCE<br>NaCl 0.1 M (0.6 %)[373] | Corrosion potential<br>V SCE<br>(after 2 h in de-aerated NaCl 0.86 M (5 %) solution saturated with Mg(OH) <sub>2</sub> , pH 10.5 [374] |
|---------------------------------------|---|--|
| Mg <sub>2</sub> Ca                    | -1.75   |  |
| <b>Pure Mg</b>                        | <b>-1.65</b>  | <b>-1.65</b>   |
| Mg <sub>24</sub> Y <sub>5</sub>       | -1.60   |  |
| Mg <sub>12</sub> La                   | -1.60   |  |
| Mg <sub>3</sub> Nd                    | -1.55   |  |
| Mg <sub>2</sub> Si                    | -1.54   | -1.65  |
| Mg <sub>12</sub> Ce                   | -1.50   |  |
| Mg <sub>17</sub> Al <sub>12</sub> (β) | -1.35   | -1.20  |
| Al <sub>6</sub> Mn                    |   | -1.52  |
| Al <sub>4</sub> Mn                    |   | -1.45  |
| Al <sub>8</sub> Mn <sub>5</sub>       |   | -1.25  |
| Al <sub>8</sub> Mn <sub>5</sub> (Fe)  |   | -1.20  |
| Al <sub>6</sub> Mn(Fe)                |   | -1.10  |
| Al <sub>6</sub> (MnFe)                |   | -1.00  |
| Mn                                    | -1.28   |  |
| MgZn <sub>2</sub>                     | -1.03   |  |
| Mg <sub>2</sub> Al <sub>3</sub>       | -1.01   |  |
| Al <sub>3</sub> Fe(Mn)                |   | -0.95  |
| Al <sub>3</sub> Fe                    |   | -0.74  |
| Fe                                    | -0.60   |  |
| Ni                                    | -0.22   |  |
| Cu                                    | -0.15   |  |

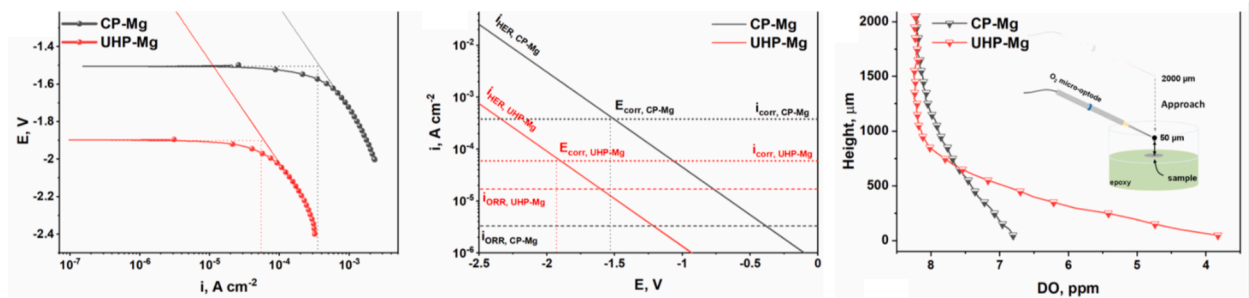
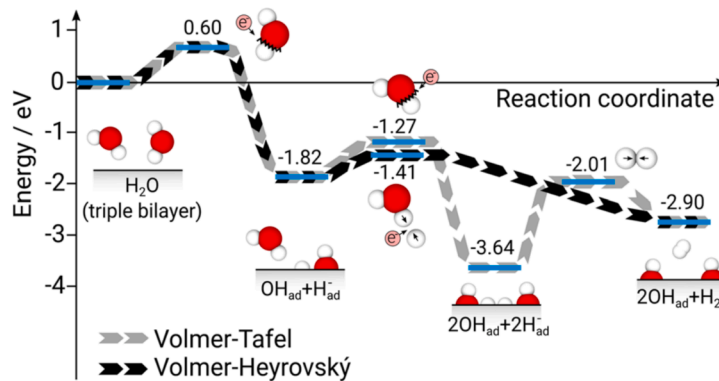
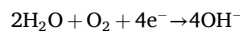
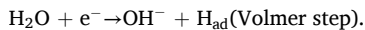
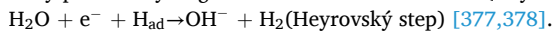


**Fig. 19.** Upper: comparative energy barriers of for the Volmer-Tafel and Volmer-Heyrovský pathways of HER on Mg surface, reproduced from Würger, et al. [378] under Creative Commons CC-BY license; Lower: from left to right: experimental potentiodynamic polarization curves for ultra-high (UHP) and commercial (CP) purity Mg, mixed potential diagram where  $i_{\text{ORR}}$  were calculated based on experimentally measured concentration of dissolved oxygen (DO) deduced from the approach curve of O<sub>2</sub> sensitive micro-optode, adapted from Wang et al. [382] under Creative Commons CC-BY license.

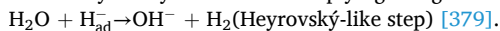
HER starts with water reduction in the Volmer step, associated with atomic hydrogen adsorption on magnesium:



The HER can continue by recombination of two adsorbed hydrogen atoms (Tafel step) or by the adsorbed hydrogen reacting with a partially positive hydrogen atom in a water molecule (Heyrovský step):



or the Heyrovský-like reaction implying a negative charge on the adsorbed hydrogen atom, a hydride:



This is supported by experimental evidence, as magnesium hydride formation has been observed experimentally [380,381]. With the help of DFT calculations, the Volmer-Heyrovsky pathway was found to be more energetically favourable [377 381–384] and is predominant mechanism of hydrogen formation during Mg degradation, Fig. 19.

Traditionally, the HER has been regarded as the only cathodic reaction during Mg corrosion under immersion conditions. The contribution of ORR, as a secondary cathodic process was identified quite recently [59,61,63,81,383,384]. Counterintuitively, the ORR is stronger for slower degrading magnesium of higher purity, with ca. 29 % of total cathodic process accounted for by the ORR. For the much faster corroding commercial purity magnesium (CP-Mg), the ORR contribution was only around 1 % [384]. This was observed during immersion in saline solution and explained by the faster growth of the Mg(OH)<sub>2</sub> layer on CP-Mg that impedes diffusion of molecular oxygen to the metal interface. In a model atmospheric condition with wet-dry cycles, the contribution of the ORR to the total cathodic process could approach 60 % for the AZ91 alloy [80]. Recent first principles DFT calculations of ORR and HER contributions to Mg corrosion showed excellent agreement with experimental results [385]. For a more detailed description of Mg corrosion, interested readers should refer to a seminal review by Esmaily *et al.* [369] and other recent publications [378,388–393].

#### 4.5.2. Corrosion inhibition mechanisms

Development of new corrosion inhibitors for magnesium alloys is an active research topic, with multiple international research groups contributing to the field. The organic corrosion inhibitors for Mg can be categorized into adsorption and precipitation groups. The cathodic inhibitors are a distinct class due to their iron-binding or tailored adsorption on Fe-rich impurities. The chemotypes of organic inhibitors are broad, from the simplest organic anions like acetate and formate, to long chain (C8-C18) saturated and unsaturated fatty acid anions like caprylate and oleate, surfactants such as dodecylsulfate and dodecylbenzenesulfonate, and large ionic liquids such as 1-n-butyl-2-decylpyrazole bis(trifluoromethylsulfonyl) ([BOPz][NTf<sub>2</sub>]). The largest Mg inhibitor performance database was generated by Lamaka *et al.*, [60] with > 1000 values of inhibitor efficiency measurements for 151 individual chemical compounds on six magnesium alloys and three grades of pure Mg. An overview of the most efficient corrosion inhibitors is given in Fig. 20 for the group of aluminium-containing Mg alloys (AZ31, AZ91 and AM50), rare-earth-containing alloys (WE43, ZE41 and Elektron 21) and two grades of pure Mg. Apart from identifying a number of promising inhibitors, this database is a valuable collection of consistent data acquired under the same experimental conditions and well suited to computational methods that correlate inhibitor performance with the molecular properties of the inhibitor (see section 5.2 of this review). As noted earlier in the review, many highly performing inhibitors may have undesirable toxicities or adverse environmental impacts, hence the search for new more benign, efficient candidates. Further details of specific interaction of inhibitors with magnesium alloys are given below. Unlike other sections in this review that describe mechanisms of inhibition for other metals in terms of the major chemotypes, here we discuss Mg corrosion inhibitors in terms of their diverse inhibition mechanisms. Two comprehensive reviews on magnesium corrosion inhibitors have been published recently [391,392].

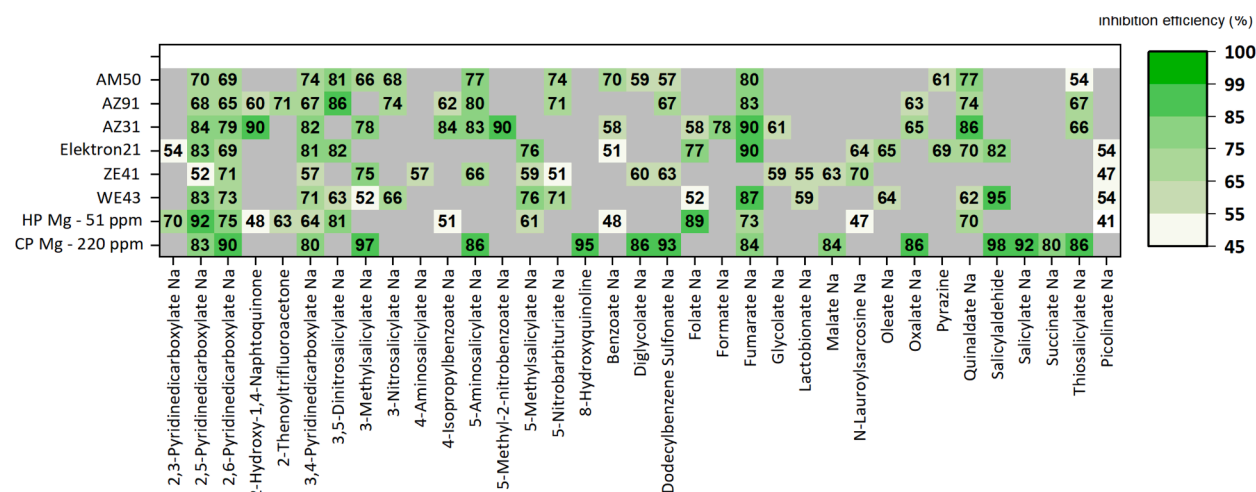
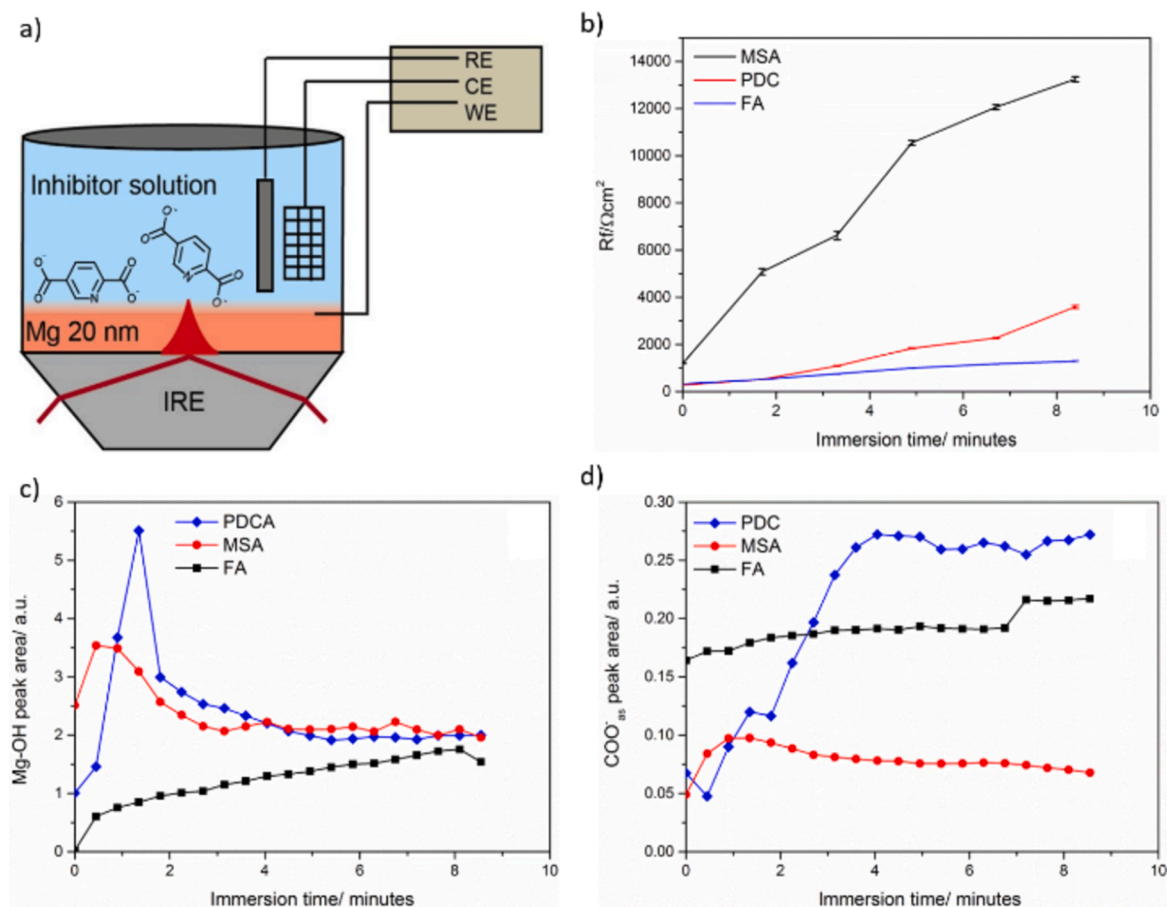


Fig. 20. Most efficient organic corrosion inhibitors with corresponding values of IE for eight Mg substrates. under Creative Commons CC-BY license. The original values of corrosion inhibition were published by Lamaka *et al.* . Adapted from Vaghefinazari *et al.* [391][60]

#### 4.5.3. Adsorption inhibitors

An early suggestion by Guo *et al.* was that adsorption inhibitors may not strongly inhibit the corrosion of magnesium alloys [393]. This opinion was based on the notion that the interaction of these inhibitors with Mg surfaces plays a crucial role in establishing an adsorptive layer that prevents access of corrosive species. While unoccupied *d* orbitals of Fe and Zn can accept  $\pi$  electrons and lone-pair electrons of O, N, S atoms of inhibitor molecules to form adsorbed films, the energy of 3*d* orbital of Mg is much higher and barely able to accept electrons from inhibitor molecules. Yet, multiple reports have shown that adsorptive inhibitors can be highly effective for various Mg alloys [60,397–403]. This apparent paradox can be explained either by adsorption on cathodic phases and impurities that often contain *d* elements (Mn, Zn, Fe), [397] or formation of much denser Mg(OH)<sub>2</sub> in presence of adsorption inhibitors. The high reactivity of Mg results in fast formation of magnesium hydroxide upon immersion. An inhibitor adsorbed onto nano-sized Mg(OH)<sub>2</sub> flakes prevents their further growth, promoting formation of smaller flakes that eventually result in much denser layer of Mg(OH)<sub>2</sub>. This prevents further ingress of Cl<sup>-</sup> to the surface of Mg/MgO/Mg(OH)<sub>2</sub> interface and decreases the corrosion rate. This mechanism was first proposed by Maltseva *et al.* for salicylate, 2,5-pyridinedicarboxylate and fumarate [401].

Carboxylates, fatty acids, and anionic surfactants are potent inhibitors of magnesium corrosion, and their properties are well described for many magnesium alloys in recent publications [60,395,398,401,402]. Organic moieties such as carboxy- or amino groups bind to heterogeneous alloy surfaces by electric dipoles. The adsorptive nature of the organic moiety is modulated by the overall polarizability of the functional group and the electron density of its heteroatoms. A continuous layer of adsorbed organic corrosion inhibitor at the electrolyte-metal interface slows down the electrochemical dissolution of the metal and prevents access of corrosive anions like chlorides, inhibiting corrosion. Chemisorption occurs on MgO and Mg(OH)<sub>2</sub> layers which typically get thicker during exposure to aqueous electrolytes, also contributing to decrease of surface reactivity and increase of inhibiting effect. By coupling ATR-FTIR with an electrochemical cell, Fockaert *et al.* observed both phenomena Fig. 21 [403]. A dynamic equilibrium between growth of a hydroxylated MgO/Mg(OH)<sub>2</sub> layer and its consumption due to interaction with corresponding carboxylate was identified during immersion in 2,5-pyridinedicarboxylate (PDC), 3-methylsalicylate (MSA), and fumarate (FA) solutions, Fig. 21.



**Fig. 21.** (a) Coupled ATR-FTIR and EIS setup for simultaneous measurements; (b) protective outer film resistance evolution retrieved from EIS spectra during immersion in 2,5-pyridinedicarboxylate (PDC), 3-methylsalicylate (MSA) and fumarate (FA) solutions; (c) Mg-OH and (d) asymmetric carboxylate peak area evolution calculated from in situ ATR-FTIR results. Reproduced from Fockaert *et al.* [403] under Creative Commons CC-BY license.

These were in contact with a 20 nm thin layer of pure Mg produced by physical vapour deposition on germanium internal reflection element.

The adsorption structures of tested carboxylates were computed by DFT on a partially hydroxylated MgO(100) surface (Fig. 22). Interestingly, salicylate tested under the same conditions accelerated corrosion. This is explained by strong cation binding ability of salicylate that can caused either corrosion inhibition or acceleration depending on the prevalence of iron-impurity binding (at high content of impurities) or magnesium binding for high purity materials. This aspect is addressed in more detail in section 4.2.2.3 of this review. Surfactants [404] are the most common and efficient small-organic corrosion inhibitors for magnesium alloys. These include the sodium salts of N-lauroylsarcosine, N-lauroyl-N-methyltaurine, dodecylbenzenesulphonic acids, and dodecyl (lauryl) sulphate [60,398–400,405]. According to Frignani *et al.*, the mechanism of inhibition of AZ31 magnesium alloy corrosion in NaCl or Na<sub>2</sub>SO<sub>4</sub> containing aqueous electrolyte is a two-stage process. Firstly, surfactant is adsorbed to the metallic surface, decreasing the area available for anodic and cathodic reactions. This step is followed by the precipitation of a Mg-inhibitor compound that strengthens the ability of the layer to inhibit the anodic process [395]. Similarly, sodium salts of stearic, palmitic, and myristic acids inhibited ZE41 magnesium alloy corrosion in NaCl and Na<sub>2</sub>SO<sub>4</sub> containing electrolyte by forming a physisorbed layer that obeys the Langmuir adsorption isotherm. Moreover, these alkyl carboxylates chemically adsorbed onto the intermetallic phases and inhibited cathodic reactions, while anodic inhibition was due to densification of the magnesium hydroxide layer by precipitates of Mg-inhibitor salts [406]. Many corrosion inhibiting surfactants act at least partially by precipitation. Zucchi *et al.* studied sodium salts of linear, long-chain monocarboxylic acids such as capric, lauric, and myristic acids as inhibitors of AZ31 corrosion in synthetic cooling water. Here, the inhibition was due to the formation of an insoluble magnesium carboxylate layer that forms a barrier on the Mg surface [394]. Following the work by Frignani *et al.* [395], Lu *et al.* further investigated the inhibition mechanism of sodium dodecyl sulfate (SDS, also known as sodium lauryl sulfate) [396,397]. Inhibition of cathodic and anodic activity was attributed not only to the adsorption layer formed on cathodic sites and Mg matrix, but also to thickening of the passive inner oxide layer (the effect disappeared in de-aerated electrolyte). However, the inhibiting effect of surfactants diminishes once they are incorporated in the protective

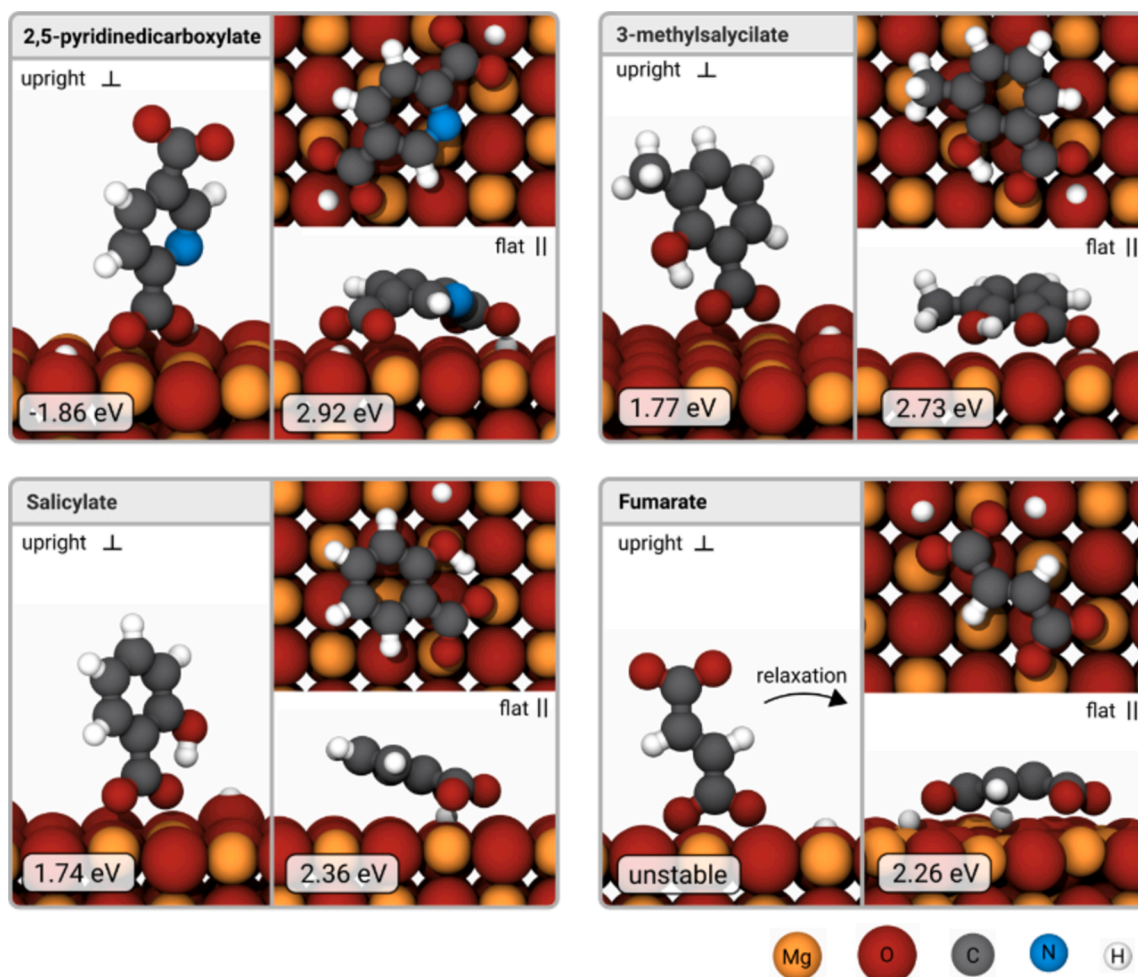


Fig. 22. The DFT-computed adsorption structures and respective adsorption energies of selected carboxylate molecules on the partially hydroxylated MgO(100) surface for a coverage  $\theta = 0.25$  ML. Reproduced from Fockaert et al. [403] under Creative Commons CC-BY license.

coatings or primers. Indeed, they were primarily developed for applications when an alloy could be employed in continuous contact and in a closed system with the inhibitor solution [395].

#### 4.5.4. Precipitation film-forming inhibitors

These are typically anionic compounds (e.g., phosphates and fluorides) and are especially relevant to magnesium [400,411–413]. The reaction is initiated by the slight dissolution of the magnesium substrate. The increase in local pH generates fast precipitation of a magnesium-inhibitor compound. This forms a continuous barrier film on magnesium with corrosion products of low solubility. The most relevant organic example is 8-hydroxyquinoline that, in aqueous electrolytes, forms a sparingly soluble chelate complex with Mg that is a barrier layer on Mg surface [60,410,411].

Apart from the above-described surfactants that often combine adsorption and precipitation corrosion inhibition mechanisms, several other organic compounds form passivating precipitate films on the surface of magnesium alloys. 2-Hydroxy-4-methoxy-acetophenone (paeonol) was reported as precipitation type Mg corrosion inhibitor [412], lowering the rate of anodic dissolution of AZ91D alloy. Mg-inhibitor chelate compounds precipitated along with  $\text{Mg}(\text{OH})_2$ , providing the inhibiting efficiency of 88 % at the optimal concentration of 50 ppm. Later, paeonol was incorporated in silica nanoparticles and dispersed in a silane coating that released the inhibitor upon alkalization of local increase of  $\text{Mg}^{2+}$  concentration [413]. Similarly, it was shown that 5,10,15,20-tetraphenylporphyrin forms Mg-Inh chelate complexes that precipitate together with  $\text{Mg}(\text{OH})_2$  reducing the porosity of the surface film and decreasing the corrosion rate by up to 90 % [393].

8-hydroxyquinoline (8-HQ) is probably one of the most efficient and most studied magnesium corrosion inhibitors reported to date. It was first shown to be an efficient corrosion inhibitor for zinc [414] by forming insoluble chelates with Zn and copper [415,416] particularly by precipitating Cu-inhibitor polymeric layers on the surface. Following this, 8-HQ was tested as a corrosion inhibitor for pure Al and AA2024 alloy where it effectively inhibited localized corrosion of S-phase particles  $\text{Al}_2\text{MgCu}$  [417,422–244]. Dissolution of Mg from S-phases was inhibited in presence of 8-HQ, suggesting its potential use as a Mg corrosion inhibitor [410,423–425 415]. The corrosion inhibition of 8-HQ on Mg alloys is typically described by a combination of adsorption and precipitation, likely coupled with  $\text{Fe}^{2+/3+}$  binding [60]. 8-HQ forms sparingly-soluble chelate complex with Mg,  $\text{Mg}(\text{8-HQ})_2$ ,  $K_s = 6.8 \cdot 10^{-16}$  that is stable between pH 9.4 – 12.7. Precipitation of Mg-inhibitor chelates is accompanied by slow adsorption of 8-HQ, thus preventing the access of chloride ions. It was also noted that 8-HQ is efficiently inhibiting corrosion of pure Mg with a high level of iron impurities. The same effect was observed for 8-hydroxy-5-quinoline sulfonate and 8-hydroxy-7-iodo-5-quinolinesulfonate [60].

Apart from classifying inhibitors by the way they interact with Mg surfaces, corrosion inhibitors can be also categorized by their interactions with anodic or cathodic processes on Mg alloy surface. Anodic corrosion inhibition results in the formation of a uniform barrier film across the magnesium surface, and specifically above local anodic sites. Metal oxidation and dissolution are restricted at the inhibited locations. This is manifested by a decrease in anodic currents on the PD polarization curve. Eventually, diminished anodic

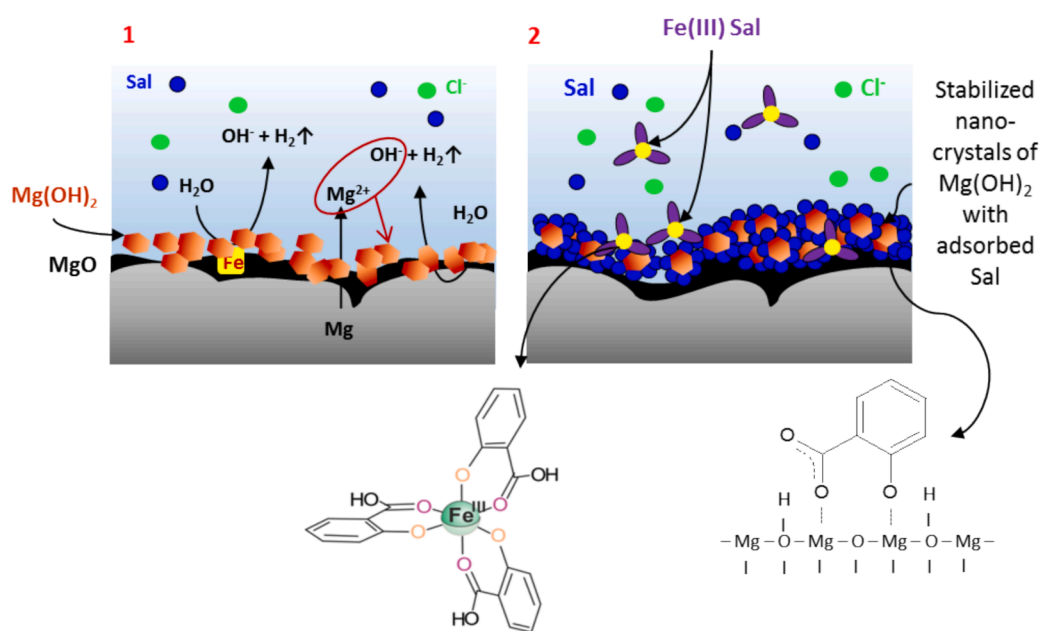


**Fig. 23.** Schematic representation of inhibition mechanism suggested for salicylate. Corrosion starts with cathodic HER (and possibly ORR) on noble Fe-rich impurities accompanied by anodic dissolution of Mg with  $\text{Mg}(\text{OH})_2$  nucleation. Its further growth is restricted by adsorbed salicylate that prompts precipitation of dense layer of corrosion products. Concurrently,  $\text{Fe}(\text{III})$  ions generated due to undermining and dissolution of iron-rich impurities, are bound in  $\text{FeSal}_3$  complex preventing Fe-redeposition and stifling cathodic activity. Reproduced from Maltseva et al. [401] with permission.

reactions lead to the decay of cathodic activity. Cathodic corrosion inhibition occurs by blockage of local sites where hydrogen evolution or oxygen reduction takes place. This can be achieved by selective adsorption on more noble cathodic phases, formation of precipitates on cathodic sites due to fast increase of local pH, prevention of enlargement of cathodic areas (due to enrichment or re-deposition [60,401,422,423]) or even poisoning of hydrogen atoms recombination [424]. In practice, mixed-type corrosion inhibitors are often found where: both partial reactions, anodic and cathodic are suppressed in the presence of an inhibitor (e.g. 2,5-pyridinedi-carbocylate in [401,402]); or adsorption is combined with active cathodic inhibition (e.g. salicylate in [401]), Fig. 23; or the initial adsorption layer is reinforced by precipitation of sparingly-soluble products (e.g. anionic surfactants in [395]).

#### 4.5.5. Cathodic inhibitors

Like copper in aluminium alloys being activator of cathodic reactions, iron-rich impurities are known to be critical active sites of local cathodic activity [423,430–432] in pure Mg and its alloys. Therefore, tolerance limits are introduced for Fe impurities and also for Ni, Cu, [58] and Si, because they promote the growth of Fe-rich nano- and micro-intermetallic particles in Mg matrix [428]. Iron-binding organic compounds, which prevent enlargement of cathodic sites and block existing locations of cathodic reaction by selective adsorption on Fe-rich intermetallic particles or binding dissolved  $\text{Fe}^{2+}/\text{Fe}^{3+}$  species, effectively inhibit corrosion of Mg. This was proposal was first based on indirect evidence (correlation between increasing %IE with increase of stability constants of Fe-inhibitor complexes) [60,402,422] and experimentally confirmed by identifying Fe-salicylate soluble species in [401].

Amino-, methyl-, thio-, nitro-, and dinitro- derivatives of salicylate have high inhibiting efficiencies (up to 97 %) for three grades of pure Mg and AZ31, AZ91, AM50, WE43, ZE41 and Elektron 21 alloys. Similar corrosion inhibiting properties were identified for oxalate, diglycolate, and folate that are known to form strong iron complexes [60]. However, citrate, with a similar iron-binding ability, accelerated corrosion in most Mg alloys as it does with Al-alloys. The inhibiting effect is low or even negative if substances forming  $\text{Fe}^{3+}/\text{Fe}^{2+}$  chelates also bind  $\text{Mg}^{2+}$  to form soluble complexes [422,429]. This balance between the ability of a compound to bind  $\text{Mg}^{2+}$  and  $\text{Fe}^{3+}/\text{Fe}^{2+}$  with different stability constants was demonstrated recently [34]. Fig. 20 lists 15 most efficient corrosion inhibitors for each of the six Mg alloys, high and low (i.e. commercial) purity Mg [391]. Note, that on average the highest values of inhibiting efficiencies were for CP-Mg that contains the highest amount of Fe impurity, 220 ppm, while on average the lowest values are characteristic for HP-Mg with the low content of Fe impurities, 51 ppm.

The electronic properties of 2, 2' bipyridine, a strong  $\text{Fe}^{2+}$  binding agent (but also binds other cations, including  $\text{Mg}^{2+}$ ), were tuned by introducing electron-donating or electron-withdrawing functional groups (methoxy and dimethylamino, or carboxylic and methylcarboxylic) [34]. These additional moieties changed the partial negative charge on the nitrogen atoms of bipyridine and the distance between the nitrogen atoms in the central metal atom in the coordination compound. A shorter distance is indicative of stronger interaction with the metal ion ( $\text{Mg}^{2+}$  or  $\text{Fe}^{2+}$ ). Thus, the methoxy derivative accelerates Mg dissolution and the carboxyl derivative of bipyridine strongly inhibits corrosion. This study combined DFT calculations with experimental validation on two grades of pure Mg.

Mercier *et al.* suggested blocking the HER on iron-rich cathodic impurities and Mg by treating it with a solution of hydrogen sulphide [430]. Highly insoluble adsorbed sulphides restrict H adsorption on Fe-rich sites and thus inhibit the HER on these cathodically active areas. Consequently, the corrosion inhibition effect of organic molecules containing thiol groups should be investigated. So far, the reports on this approach are limited to thiosalicylate, 2,3-dimercapto-1-propane, and 1,3,4-thiadiazole derivatives. These have some positive effect on corrosion while for sulphonate containing compounds, such as tiron, 5-sulphosalicylate, and quinolinesulfonates the inhibiting effect was weaker [60].

Another way to suppress the cathodic HER on Mg was proposed by Williams and co-workers. They reported that arsenic species poison hydrogen recombination and thus inhibit the HER [431,432]. (It is interesting to note that arsenic oxide was used to suppress  $\text{H}_2$  evolution during electrochemical hydrogen charging of pipeline steels [433,434]). A similar effect was for Mg alloyed with Ge, Sn, and In [431,432,440–444]. Although interesting phenomenologically, we do not consider these effects in further details as it is out of scope of this small organic molecule review and arsenic is a highly undesirable material toxicologically.

The protective effect of several ionic liquids on magnesium alloys was also explored [440–450]. In a recent report, an inhibitor efficiency of almost 92 % was achieved by octadecyl triphenyl phosphonium bis(trifluoromethylsulfonyl)amide for AZ31B magnesium alloy [442]. The inhibition effect, primarily cathodic, is explained by several factors, including chemical adsorption, formation of protective film blocking corrosive species, and chemical reaction with Mg forming the composite layer. Ionic liquids are a highly versatile yet barely investigated class of organic compounds that are very promising for Mg corrosion inhibition.

It is noteworthy that conflicting data on the inhibition efficiency of many organic compounds exist in the literature. Although potentially worrying, this can be understood in terms of the multiple factors affecting inhibition. Firstly, no organic corrosion inhibitor can be universal, i.e., efficient for a wide range of magnesium alloys, see Fig. 20. This is due to different corrosion susceptibilities of Mg substrates, alloy composition, microstructure, and distribution of the cathodic sites, the kinetics of surface alkalization, the composition and location of precipitate formation. Multiple additional factors affect the inhibition mechanism for each specific alloy, such as amount and distribution of impurities, the ratio of electrolyte volume to the surface area of the tested material, the concentration of the inhibitor and the aggressiveness of the corrosion medium, aeration and amount of dissolved  $\text{CO}_2$ , temperature, immersion time and hydrodynamic condition of the electrolyte, surface preparation condition, etc. These factors need to be accounted for when comparing the absolute values of inhibitor efficiencies derived by different methods and under potentially varying experimental conditions (by different research groups). This again highlights the need for reliable high-throughput inhibitor testing, so that large datasets can be collected under the same experimental conditions, yielding consistent values.

#### 4.5.6. Conversion coatings and primers containing corrosion inhibitors

While most papers report inhibition efficiency for full immersion in aqueous electrolytes, only a few real-world applications like

heat-exchanger coolants have distributed corrosion inhibitors into an electrolyte in contact with a metallic magnesium part [446]. In most applications, metallic parts are exposed to corrosive electrolytes intermittently or, more commonly, to an atmospheric condensation electrolyte thin film. In the latter case, corrosion inhibitors are combined with other protection strategies. Often, corrosion inhibitors are added to conversion layers or primers directly in contact with a metallic part. A recent comprehensive review summarized several ways of combining magnesium corrosion inhibitors with other protection strategies [447,448]. These include direct inhibitor admixing to sol-gel coatings [419,449], inhibitor impregnation in porous anodic layers produced by PEO (plasma electrolytic oxidation) [421,450,451], incorporation via ion-exchange in LDH (layered double hydroxide) [452–459], and encapsulation in other inorganic or polymeric reservoirs followed by their distribution in sol-gel or primer [413]. A combination of these strategies provides even stronger barrier and active protection effects: e.g., inhibitor-containing PEO sealed with sol-gel coating [410,457–461], and encapsulation in other inorganic or polymeric reservoirs followed by their distribution in sol-gel or primer [413] and PEO loaded with inhibitor containing reservoirs [457,458]. Nevertheless, a wide gap remains between the number of corrosion inhibitors tested on bare magnesium alloys in full immersion and those tested in protective coatings.

#### 4.6. Synergistic inhibition by binary inhibitor mixtures

Synergy occurs when the corrosion inhibition of a combination exceeds the sum of the performances of the individual components. The synergistic effect (S) can be quantified in different ways, the most common of which is that reported by Aramaki and Hackerman [459]:

$$S = \frac{(1 - IE_{1+2})}{(1 - IE_{12})}$$

$$IE_{1+2} = (IE_1 + IE_2) - (IE_1 \cdot IE_2)$$

$IE_1$  and  $IE_2$  correspond to the inhibition efficiencies for inhibitors 1, 2 tested individually and  $IE_{1+2}$  is the inhibition efficiency of the mixture of two inhibitors. S values above 1 indicate the existence of synergies between the selected combination, while S value below 1 indicate antagonistic effect of two inhibitors, also often observed.

Recently, Kokalj [460] took a critical look at Aramaki–Hackerman approach and cautioned that it may predict synergies incorrectly if a compound with stand-alone negative inhibition efficiency (corrosion accelerant) is used in a mixture. Several other equations for quantifying synergistic effects have been proposed using a “corrosion activity” (CA) parameter. It is the complement to inhibition efficiency ( $CA = 1 - IE$  or  $CA, \% = 100 \% - IE, \%$ ) and used to define new synergistic models. It is worth noting that the data for inhibitor mixtures are much less reported in the literature than that for single inhibitors.

From a machine learning perspective, examining mixtures of inhibitors may provide guidance on synthesizing new inhibitor molecules by combining the selected functionalities of the individual inhibitors into a single molecule. Many small organic molecules already have dual functionality arising from different parts of a molecule (e.g. both physisorption and chemisorption).

Typically, inhibitors with different inhibition mechanisms are combined, e.g., anodic and cathodic inhibitors. For example, the combined effect of dodecylbenzenesulphonate and 8-HQ on the corrosion of AZ91D magnesium alloy was 98 % inhibition. This was explained by the adsorption of dodecylbenzenesulphonate on the layer of precipitated Mg-8-hydroxyquinolate [411]. Qiu *et al.* tested a binary mixture of sodium fluoride and DL-malate as a corrosion inhibitor for AM50 magnesium alloy [461]. The inhibiting effect varied between –31 % and +95 %, depending on the concentration of each component. The highest inhibition, with a synergy factor of 3.82, was achieved by equimolar concentrations of both components at 0.05 M.

Several publications explored the effect of binary inhibitor mixtures on AA2024 alloy. 8-hydroxyquinoline mainly protects the aluminium matrix, while benzotriazole inhibits the cathodic activity of Cu-rich intermetallic particles [365]. Additionally, binary mixtures of  $Ce^{3+}$ , 8-HQ, salicylaldoxime, and 2,5-dimercapto-1,3,4-thiadiazolate (DMTD) were tested for their abilities to inhibit corrosion of bare or coated AA2024. For bare alloy, the most effective mixtures were 8-HQ with salicylaldoxime, and 8-HQ with 2,5-dimercapto-1,3,4-thiadiazolate. For alloys with epoxy-based coatings containing  $CaCO_3$  microparticles impregnated with corrosion inhibitors, the best effect was achieved by 8-HQ with salicylaldoxime and  $Ce^{3+}$  with salicylaldoxime inhibitor combinations. The synergy factor, reflecting the extent of improved inhibition of a mixture compared to that of performance of individual inhibitors was highest (above 15 after 2 weeks of immersion) for  $Ce^{3+}$  with salicylaldoxime and coated AA2024 [462]. A binary inhibitor mixture of 3-amino-1,2,4-triazole-5-thiol with  $CeCl_3$  demonstrated synergistic improvement of inhibition for this alloy. This effect was explained by the reinforcement of more specific localized inhibition in cathodic sites by  $Ce^{3+}$  and a relatively uniform mixed-type inhibition by 3-amino-1,2,4-triazole-5-thiol at cathodic and anodic sites [463].

Synergism between 2-mercaptobenzimidazole and potassium iodide on copper was observed in acidic media. Iodide anions facilitated copper-inhibitor bonding by reversibly adsorbing on copper, hence decreasing the positive surface charge and easing adsorption of protonated 2-mercaptobenzimidazole on the surface [464]. This was also the case for physical adsorption between multiple amino acid species and copper surfaces in the presence of potassium iodide additions [198]. The highest amino acid inhibition efficiencies were consistently seen in environments with  $Zn^{2+}$  and iodide ions [257]. Iodide also showed synergistic effects with benzotriazole in sulfuric acid media, where iodide ions adsorbed on cuprous ions preferentially adsorb a protonated benzotriazole overlayer, creating a thicker, more robust polymeric film [465]. A similar synergism mechanism occurs for the surfactant sodium dodecylsulfate with benzotriazole and 3-amino-5-methylthio-1,2,4-triazole [170], and sodium dodecylbenzenesulfonate with 2-mercaptobenzimidazole [466]. It is postulated that surfactants modify the electrostatic interaction of the main inhibitor molecule and, at an optimum concentration, lead to interfacial co-adsorption [129]. Similarly, results have been reported for co-adsorption of iodide

ions and organic inhibitors on ferrous metals [467,473 474–478] and aluminium [474,480 474] and with cerium ions on both types of metals [474–482]. Synergism can also result in reversal of the electrochemical behaviour. It was observed that in acidic media ethylene diamine acts as a corrosion accelerator due to autocatalytic CuCl formation. However, introduced into an already Na<sub>2</sub>S-containing environment, strong chemisorbed HS<sup>-</sup> layer covering the entire copper surface facilitates adsorption of protonated ethylene diamine and prevent dissolution of Cu<sup>+</sup> ions. Although inhibitor mixtures often possess a synergistic inhibitor effect, experimental testing is onerous as it requires matrix testing of at least two inhibitors at multiple concentrations. High throughput testing methods and combinatorial matrix design methods need to be part of the solution. Synergies are believed to be non-linear and hence hard to predict *a priori*. Machine learning methods can overcome this limitation if sufficiently large experimental databases become available.

#### 4.7. Synergy by n-ary inhibitor mixtures

Beyond binary and ternary combinations, there haven't been systematic studies of organic corrosion inhibitor mixture predictions due to rapidly increasing complexities. However, the potential of combinatorial space is vast. Combining compounds at different concentrations in n-dimension ways (n = 2 binary, n = 3 ternary, etc.) results in an explosion of possibilities, with  $(c n)^c - c^2 n$  combinations for a combinatorial grid chemical space where c is the number of selected concentrations and n the number of selected molecules. The challenge and opportunity resulting from such a vast chemical space were previously displayed in the optimisation of corrosion inhibition of a quaternary combinatorial matrix of rare earth mixtures [478].

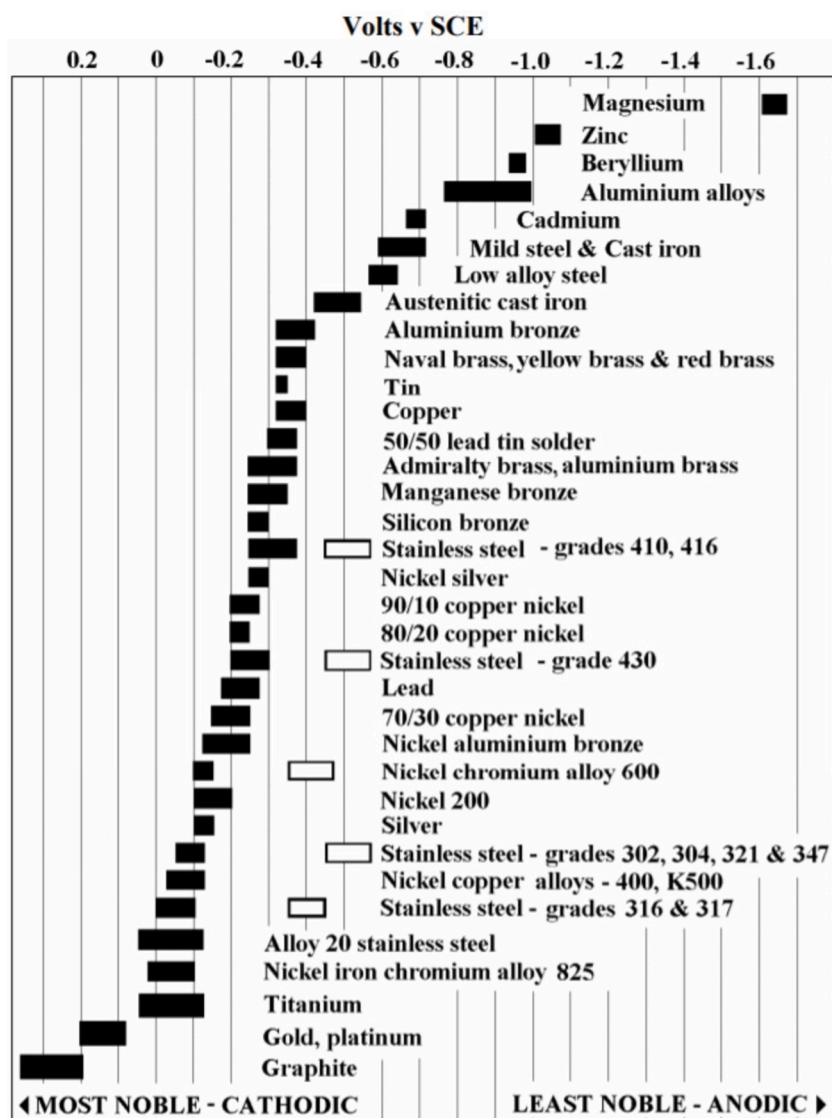


Fig. 24. Galvanic series for metals in seawater with moderate flow. Reproduced from Tugsataydin, under Creative Commons CC-BY license, via Wikimedia Commons.



The first challenge in mixture-based analysis starts with its definition. A good description of the combined chemical space is necessary to convey the mixture system to the computer accurately. To tackle digitizing mixture of compounds in an automated accurate fashion, a text-to-mixture open-source file format MixFile was created. This converts chemical mixture descriptions into a markup form that is well suited for informatics purposes [479]. In addition, chemical descriptors need to move beyond pure components and have the ability to include any reactions that occur between the individual components. It should not be influenced by the arbitrary representation of this n-ary chemical space. A recent approach to build such a description was based on concatenating permutationally invariant encodings of individual molecular descriptors. It resulted in improved H<sub>2</sub>O<sub>2</sub> concentration prediction for formulations with a maximum of 20 mixed-in ingredients [480]. Another review explored combining physical modelling of pair-wise interactions with machine learning to develop hybrid models for prediction of thermodynamic properties of fluid mixtures [481].

Recent studies from other fields show the potential of mixture-based corrosion inhibition predictions. Machine learning predictions of compound mixtures have been undertaken for toxicity of mixed pollutants [482], bioavailability, toxicity of organic and metal(load) compound mixtures [483], toxicity of seven engineered nanoparticle mixtures at 22 binary combinations [484], viscosity of ionic liquid–water mixtures [485], thermodynamic properties of pure H<sub>2</sub>O, CO<sub>2</sub>, H<sub>2</sub> and their mixtures [486], viscosity of binary liquid mixtures as a function of temperature [487], and physicochemical properties related to phase transformation of liquid hydrocarbon mixtures [488], among others.

#### 4.8. Inhibition of galvanic couples

In the previous section, localized corrosion around the intermetallic particles embedded in a metal matrix was highlighted. These intermetallic particles may be intentionally formed (e.g. in high strength Al-alloys or precipitate hardened steels) or form from impurities in the alloy. This type of local corrosion is called micro-galvanic corrosion, a subset of galvanic corrosion. Another unconventional definition is based on corrosion developing where the open circuit potential (OCP) of one conductor is different from another conductor in the same electrolyte. It is most frequently invoked where dissimilar metals are connected to each other and exposed to an electrolyte. The different metals will individually have OCPs in the electrolyte and in the mixed potential of the couple one will inevitably experience net anodic reactions and other net cathodic reactions (Fig. 24 lists a series of potentials for metals in sea water [489,490]). The degree of corrosion resulting from this metallic couple will depend on the electrolyte and the ability of the surface oxide to resist dissolution (i.e. the durability of the passive layer). Three further points need to be made: –

- (i) at the beginning of this paragraph the definition of galvanic corrosion involved conductors. The use of this term includes, in addition to metals, non-metallic conductors but also extends to low bandgap materials. In the former case materials like carbon fibres, are used extensively in some industries such as the aircraft industry, to manufacture composite materials. Carbon fibres can be considered as conductors, and they introduce the possibility of galvanic corrosion in metal-matrix composites.
- (ii) Narrow band gap oxides can also form galvanic couples with metals. Cu(I) oxides are a good example since these can form n- and p-narrow band gap oxides which can couple with metals (particularly the underlying Cu in this case) to form galvanic couples.
- (iii) Galvanic couples can also exist between nominally the same metal. This is because alloying elements in a metal can have different microstructures depending on processing which can change how these elements are distributed. For example, Cu can be in solid solution in precipitate hardened Al-alloys, or it can be incorporated into the precipitates ([318,332,491,492]). These two different configurations for Cu will mean that the alloy will have slightly different OCPs in an electrolyte and this will establish a slightly different galvanic couple.

**Table 8**  
Examples of types of metallic couples in a selection of industries.

| Feature                   | Common couples   | Comments  |
|---------------------------|--|---|
| Storage tanks             | Ni-steel/Steel   | Problems mainly related to environmental issues with siting of the tank |
| Auto                      | Steels/aluminium alloys/Mg-Alloys                            | Lightweighting – Mg alloys Transformation to EVs                        |
| Aircraft                  | Al- Alloys<br>Al-Alloys-composites<br>Al-steels<br>Mg-steels | Fasteners, joints<br>Clad materials                                     |
| Wind turbines             | Steels/CFRP/Aluminium  | Aggressive environment  |
| – Offshore                |  |   |
| – Onshore                 |  |   |
| Pipelines                 | Steels/Weld joints   | Huge legacy issues  |
| – Oil & gas               | Copper/steel/brass   | Being replaced by PVC   |
| – Domestic                |  |   |
| Infrastructure            | Fasteners/Joints   | Internal concrete environment   |
| – Bridges                 | Steel  |   |
| – Reinforcements          |  |   |
| – Ports                   |  |   |
| Heavy Industry            | Carbon Steel/ Stainless steel                                | Aggressive environments   |
| – Metals Manufacture      |  |   |
| – Oil & Gas               |  |   |
| Power Generation & Supply | Cu and Al alloys   | Aggressive environments   |

Historically, large scale galvanic couples are most prevalent in fastened, jointed structures where dissimilar metals meet each other [489,493]. This also extends to other types of joins such as welded joints. Here both, microstructure through regions such as heat affected zones, and the weld material (which can have a different composition to the metal to be welded) may cause galvanic corrosion. Recently, newer methods of joining such as friction stir welding and advanced manufacturing techniques have the potential to create graded materials that will have their own galvanic corrosion issues. Table 8 provides some examples of the types of mixed metal components that might be encountered in joints in selected industries. This table is not intended to be an exhaustive review of all potential galvanic sites, but to show that galvanic corrosion is pervasive across many industries. This area represents a huge challenge for corrosion prevention, particularly in finding inhibitors that can suppress galvanic corrosion. It also presents a great opportunity for AI to explore the complex variable space associated with discovering inhibitors in multi-metal, multi-environment situations.

The specific challenge for small organic inhibitors is to make an impact in this area by finding, ideally, a universal inhibitor that inhibits both cathodic and anodic processes or, more realistically, a combination of inhibitors that deals with each aspect of the galvanic couple. Currently, there is no single formulation that addresses this issue, but there are formulations used in specific industries. In the aerospace industry corrosion prevention compounds are used regularly to suppress and prevent corrosion. These formulations are applied by spraying and typically contain a solvent and a chemical that can form a film. Gui [494] noted that formulations are generally proprietary. Conspicuously, one typical formulation contained barium petroleum sulfonate and alkyl ammonium organic phosphate as corrosion inhibitors. The solvent serves to spread these chemicals across the surface where they form a protective oily film, after solvent evaporation, which prevents corrosion including galvanic corrosion. Other types of corrosion in joints are crevice corrosion, often facilitated by fraying surfaces that disrupt the protective coating, and filiform corrosion, facilitated by defects in the paint coating particularly around fasteners. This type of formulation may be applicable to many metals and metal couples, since the sulphonate group can interact with the surface of many metals and the phosphate forms insoluble metal-phosphate compounds so a reaction that can happen on the metal surface, thus providing a barrier.

The need for either universal inhibitors to cover all these applications, or higher performing inhibitors for specific applications, is an active area of research. Clearly, exploring large chemical spaces (mixes of chemicals, solvents, electrolytes and environments) is a challenge that is best tackled by high throughput experimentation for candidate formulations and machine learning to model this rich

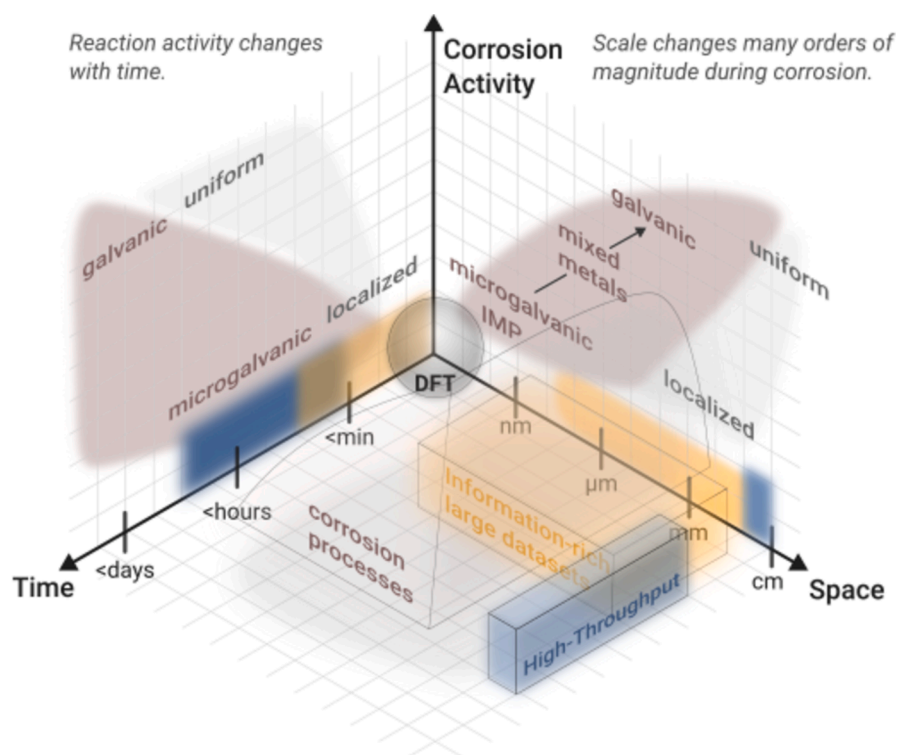


**Fig. 25.** Qualitative schematic outlining regions where the approaches described in this paper best apply in terms of space and time scales, relative to general corrosion processes. This figure aims to identify potential gaps in information on inhibition processes. For example, for HTP a single performance metric (e.g., %IE) has no meaningful representation in the spatial domain because it averages over the material, however, it does in the time domain because time is measured in the experiment. HTP taken over shorter times require more experiments to cover the time scale, thus compromising the *high-throughput* aspect. Alternatively, data rich characterisation sets (microprobe, EBSD etc), cover orders of magnitude in size or scale, but obtaining kinetic information requires registration of sites before and after exposure, limiting the time domain. Additionally, DFT models the molecular scale, but the computational complexity severely limits the time scale, meaning outcomes only relate to very fast surface interactions not real-world corrosion process time frames.

dataset, but also by efficiently leveraging current performance databases. Neither of these avenues is currently an intensive area of research. There are, of course, some research efforts examining the effects of inhibitors on multi-material systems. For example, 24 individual inhibitors and their mixtures were tested for AA2024-graphite (representative of CFRP) galvanic couples by Coelho *et al.* [64]. A ternary mixture containing, 2-mercaptobenzothiazole, Tween 80 (a non-ionic surfactant) and either benzotriazole or triethanolamine exhibited the strongest inhibition. Quantification was based on local current density measurements by SVET or ZRA. The high dependence of outcomes on specific experimental conditions (anode/cathode ratio above all) was emphasized. The Al-CFRP galvanic couple is commonly encountered in aerospace applications and wind turbines and remains problematic to overcome. The adsorption-based anodic inhibitor, 1,2,3-benzotriazole, was combined with the cathodic inhibitor  $\text{Ce}(\text{NO}_3)_3$  to generate effective inhibition of corrosion activity of Zn and Fe galvanic couples [495]. The synergistic effect of binary mixtures was lower for stand-alone Zn or Fe but reached over 30 with inhibition efficiencies above 90 % for the galvanically coupled Zn + Fe. In another report, the inhibiting effect of binary mixtures of organic inhibitors, or with cerium nitrate, was studied for a model galvanic couple representing  $\text{Al}_2\text{CuMg}$  S-phase [63]. The highest value of synergistic parameter for inhibiting the cathodic process on Cu, anodic process on Mg and anodic + cathodic processes on Al, was achieved in presence of 8-hydroxyquinoline (8HQ) and 2,5-dimercapto-1,3,4-thiadiazolone (DMTD). Both were earlier shown to be efficient corrosion inhibitors for Cu, Al and Mg alloys. An Al-Cu multi-electrode system was developed to simulate the galvanic activity of dealloyed S-phase of AA2024 alloy by Catubig *et al.* [496]. The addition of sufficient praseodymium mercaptoacetate ( $>10^{-3}\text{M}$ ) significantly reduced the corrosion process. This effect was ascribed to deposition of a thin protective film. Similarly, a combination of  $\text{CeCl}_3$  and 1,2,3-benzotriazole was shown to be effective in suppressing corrosion of an Al and Cu galvanic couple [497]. Although these studies were aimed at better understanding of micro-galvanic mitigation, and the results are relevant for addressing the galvanic corrosion of Al-Cu joint busbars used for automotive applications, especially with the rapidly increasing number of electric vehicles.

In addressing these issues, it is important to recognize the limitations on using high throughput data derived by AI from these experiments. All approaches discussed in this review have their limitations. This as elaborated below in relation to Fig. 25 which qualitatively places the strengths of different approaches according to length and time scales thereby identifying gaps where further research can bridge these gaps. Here we attempt to establish where most corrosion process occur in terms of location (space), duration (time) and corrosion activity. This volume defined by the light and dark grey regions which fills the space between these three axes. Of course, any part of this volume can be probed by specific, one-off experiments, but here, we are interested in the extent to which the data derived from information-rich experiments, such as HTP or large-scale characterisation, overlaps with this space, i.e., how it samples this space. As projected onto the space/corrosion activity plane, corrosion goes from lower activity associated with micro-galvanic corrosion to high activity associated with generalised corrosion, often driven by galvanic corrosion domain by a change in length scale from large scales reactions to much finer scales. A similar projection is made onto time-corrosion activity plane of Fig. 25. Generalised corrosion can occur over a range of timescales and, under galvanic control, can be quite active. Localised corrosion can occur at low activity very early, starting with activity on the nanoscale, but micro-galvanic corrosion may need a short time for localised corrosion to develop the active anodes and cathodes to develop significantly.

The approaches that have been the focus of this paper sit in different places in the volume depicted space–time–corrosion activity axes depicted in Fig. 25, which identifies the “sweet spots” for optimum outcomes for these approaches. Importantly, they do not have full coverage of the volume. For example, DFT is useful at the atomic to molecular scale and its strength is in revealing aspects of adsorption rather than dissociative reaction and formation of reaction products related to the molecule under examination, as well as the electrolyte and underlying metal. It can't include galvanic reactions over larger spatial dimensions under potential gradients. DFT calculations have also not generally investigated adsorption over different timescales. At the other end of the length scale, high throughput experimentation commonly integrates large areas through visual or digital assessment of optical images or  $\text{H}_2$  evolution from a large area of a magnesium sample compared to the scale of individual molecular adsorption. Currently, the sweet spot for HTP is often confined to specific timescales depending on the type of measurement; 24 h is often reported to get a quick before/after assessment of corrosion performance. So HTP generally “averages out” micro galvanic corrosion because the length scale of these reactions is much smaller than the sampling scale used in HTP and the timescale is shorter. Thus inhibition events may not be adequately encompassed by a typical HTP experiment. This has been observed in Al- and Mg-alloys corrosion, where the anodic reaction must be activated prior to cathodic inhibition because the inhibitor reacts with the corrosion product to suppress corrosion. Of course, there is no in-principle reason why HTP needs to be confined to these scales but longer times (e.g. days) or finer spatial scales come at the cost of quick and reliable outcomes, i.e. high-throughput becomes low throughput. Characterization can cover reactions from the submicron to millimetre scales and can be applied over different timescales, capturing both adsorption and any subsequent reactions. However, large, information-rich datasets (hundreds of gigabytes to terabytes, such as microprobe compositions or EBSD analyses) from which statistically significant data is obtained, performed over a several orders in magnitude on the space scale (microns to centimetres) are uncommon. Electron or proton microprobes can, in principle, sample large areas being only limited by the sample stage movement (probes scan the sample under the beam so they can sample large areas at fine detail without any change in beam conditions – this is one reason why quantitative analysis is so good in microprobes). These types of measurements are often limited in the time domain by the need to register features before and after exposure to an inhibitor. Without this registration information, reaction information of specific corrosion initiation sites can be lost. Thus, the reason for the short timescales on these data-rich datasets is due to the need for registration. Of course, longer timescales can potentially be examined, but as corrosion product builds up the features of the underlying metal microstructure are lost; hence the timescales are limited to minutes in the figure (extending to hours may not be unreasonable depending on the specifics of the reaction). It should also be noted that while the corrosion inhibition experiment may only take a few minutes the mapping exercise may take several days. Clearly, the approaches described in this review only sample portions of the total volume in the space–time–corrosion activity volume. The implications of this

have yet to be determined.

In summary, Fig. 25 shows there is scope to use existing tools to explore different spatial and temporal scales, thereby probing the properties of inhibitors under expanded sets of conditions. The insight provided through these experiments will be valuable for human interpretation as well as for training machine learning models.

## 5. Impact of machine learning on organic corrosion inhibitor discovery

As discussed above, even the most optimistic projections of the capabilities of high throughput experimental methods cannot explore more than an infinitesimal fraction of small organic chemistry space. Data-driven machine learning methods can leverage available experimental inhibition datasets into larger regions of chemical space. However, the generation of large datasets of corrosion inhibitors, development of data-driven machine learning models, and the use of models to design or optimize novel organic inhibitors is still limited and recent. The few reported models are overwhelmingly related to a single metal or alloy, and a significant number of these studies are flawed because they are based on very small datasets.

Before examining this topic in detail in the context of small organic inhibitors, it is useful to provide an overview of the inter-relationships between the different modelling approaches to illustrate the types of information they provide. The purpose here is to identify possible knowledge gaps in our endeavour to find a universal inhibitor akin to the family of chromates, or, at least, a small number of inhibitors that can be applied to a large number and variety of metal alloys. This process is summarized in Fig. 26.

Currently, machine learning models of organic corrosion inhibitors are trained on molecular features and performance metrics such as %IE. There are several gaps between model predictions and real-world performance that are summarized in Fig. 26. On the left of Fig. 26, there are three boxes describing (a) molecules, (b) electrolytes and (c) surfaces. The first conceptual gap is the assumption in all

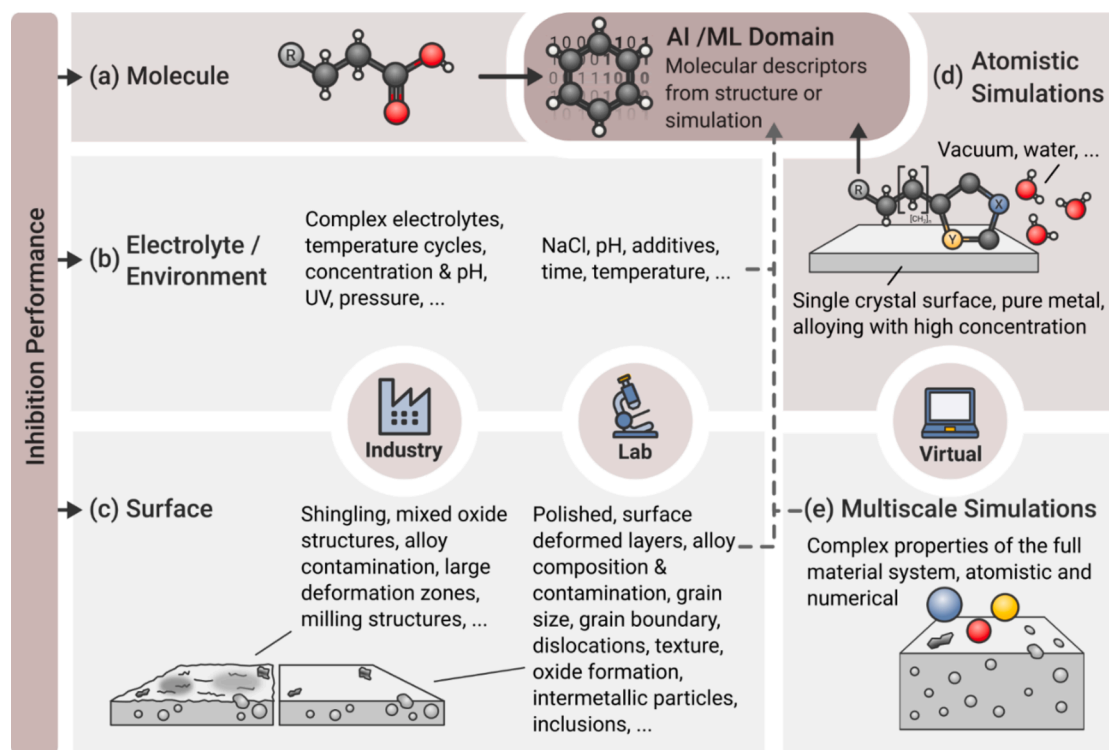


**Fig. 26.** Flow chart for generating machine learning models of corrosion inhibition from chemical structures and experimental inhibition data. The figure identifies the types of features used in current modelling approaches (grey boxes and dashed lines) and identifies other important factors that are currently captured by one parameter (e.g. %IE). (a) machine learning features are largely defined by structures and DFT studies and use %IE to cover many other variables or metrics related to the electrolyte and the surface. (b) Ideally, models should use features related to real world electrolytes, which contain many different ions, have variable volume and concentrations due to wet/dry cycles and experience variable temperature, UV exposure, and pressure etc. Laboratory electrolytes have constant concentrations of simple salts. (c) The surface where the inhibitor reacts is also complex. Manufactured surfaces are quite different to carefully prepared, highly polished, well characterised laboratory surfaces. They have features such as surface deformed layers with a range of gradients from the surface to the bulk, as well as surface oxides and corrosion products. Laboratory surfaces are often single crystal used to observe surface oxidation and inhibitor adsorption. (d) Quantum chemical simulations generate features for training machine learning models. Most published work uses highly simplified systems (e.g. *in vacuo* simulations of free molecules) due to the cost of the calculations and calculates frontier orbital or adsorption energies for pure metal substrates. (e) Studying more realistic systems on different scales (e.g., accounting for impurities or simulation of the inhibitors in a coating matrix) have great potential to link lab-scale experiments to the real target applications.

AI/ML models is that inhibitor performance is related to molecular features or descriptors. The algorithms are initially trained on a limited set of data using those features to generate a mathematical relationship between them and the inhibition performance. The trained model is then applied to another, often larger dataset for predictive purposes. Everything related to the electrolyte (box (b)) and the surface (box (c)) are collectively captured only by the inhibition performance. This means that there is a loss of information about the electrolyte characteristics (such as wet/dry cycles, local concentrations, temperature, diurnal cycles) and the surface (e.g. number of phases, distribution of phases, number of intermetallic particles, surface roughness, etc. (see Fig. 26 (c)). This gap does not represent a fundamental problem with the machine learning approach since these characteristics can potentially be included in the models as additional features if they are available, but currently this is not the case and represents a gap. The second conceptual gap is that inhibition performance data is generally collected under constant stress i.e. static conditions (one concentration, fixed temperature and often initial pH, one time point, etc.) whereas cyclic stress is the most common environment for real world performance, see Fig. 26 (b). These limitations need to be front of mind when considering model outcomes.

A third issue depicted in Fig. 26 (d) is related to the use of quantum chemical approaches such as density functional theory (DFT). These types of calculations are very time- and resource-intensive. Hence, they are necessarily performed on greatly simplified model systems, the simplest being an isolated molecule in a vacuum and more complex systems incorporating an averaged aqueous environment and a single crystal surface (usually a small metal cluster). In these models, molecular features can be calculated for a series of similar compounds and their trend compared to the inhibition performance for a particular metal to establish relationships between the two. It is important to remember that the molecular features derived from DFT are for an idealized model system that is not the same as a real-world electrolyte or surface. The potential of simple computed properties (like frontier orbital energies, dipole moments, electron density at certain atoms) to contribute to an accurate prediction has been highly metal dependent so far. As discussed below, the correlation with the corrosion inhibition performance of small organic molecules for Al or Cu has been reported to be essentially zero, while a correlation has been observed for Mg and Fe. The lack of correlation between DFT properties and the inhibition performance for Al, Cu and other materials might be overcome by simulating more complex systems. Moreover, performing simulations on different scales (e.g. numerical modelling) to determine the mobility of the inhibitors in a coating matrix, or how they are released in case of corrosion, will yield highly relevant input features for training machine learning models.

Clearly, the electrolyte in real-world applications is very complex due to the presence of multiple anions and cations, temperature cycles, wet/dry cycles, and many other factors. There is much more control of the electrolyte in a laboratory environment. The surface condition of the metal may be even more complex than the electrolyte, depending on surface preparation, composition, contamination, microstructure, and deformation structures to name a few variables. Everything about the electrolyte and the surface are rolled into a single value of inhibition performance, clearly a very large approximation. For example, >50-year-old weathered and new polished AA2024-T3 may be exposed to 0.1M NaCl and inhibitor under the same conditions but give entirely different inhibition performance values because of small differences in composition leading to different aggregations of intermetallic particles. The old aggregations are often much more electrochemically active [498] (note this is a real example.) Another example is the determination of inhibitor efficiency of a particular compound for a Mg alloy where, in one case, the alloy is polished and in the other, a residual oxide layer remains. The inhibition performance values again will be quite different. In both examples, the difference in inhibitor performance values might be attributed to errors whereas, in reality, it is the surface condition that is the cause of the variation. Current experimental approaches often do not report the details mentioned above, so extracting trends using only one metric (e.g., %IE) to model a surface/inhibitor combination can be problematic.

### 5.1. Machine learning models for predicting organic corrosion inhibitor performance

The diverse mechanisms by which organic compounds inhibit corrosion on multiple alloys is largely, but not completely, understood as described above. Mechanism-based *de novo* design of bespoke organic corrosion inhibitors for a given metal and application is not yet possible, except in very limited cases. Fortunately, the recent developments in high throughput experimentation discussed above, the availability of very large libraries of small organic molecules, and recent step changes in the power of machine learning modelling methods have provided a robust, useful paradigm for discovery and optimization of next-generation organic corrosion inhibitors. Quantitative structure–property relationship (QSPR) methods have amply demonstrated their capacity to model and accurately predict complex materials properties [119]. These data-driven methods are very well matched to high throughput experimental methods.

Although machine learning and pattern recognition methods often do not provide direct insight into inhibitor mechanisms at the molecular level, they are nonetheless very useful for generating quantitative predictions of performance in real-world situations where molecules interact with metal and alloy surfaces in very complex environments. Machine learning methods are not devoid of mechanistic insight as they describe the relationships between the molecular properties of the inhibitors and their efficiencies, but this information is usually not straightforward to extract. The application of machine learning-based QSPR methods to small organic molecule corrosion inhibitor design has been comprehensively reviewed recently by Winkler [499] so only the main methods and results are summarized in this section.

Clearly, the structures and physicochemical properties of organic inhibitors directly affect their abilities to inhibit corrosion, and machine learning-based computational models have been shown to capture these relationships quantitatively, as discussed below.

The predictive power of machine learning models is critically dependent on the quantity, quality, and molecular diversity of the set of molecules used to train them, and on the relevance of molecular descriptors (features) used to encode them. Descriptors are mathematical representations of the structural, physicochemical, and sometimes provenance properties of inhibitors in the training set. [24,26,119,499] They may be derived computationally from the molecular structure, predicted by other models (e.g., lipophilicity,

water solubility, acid-base properties, redox properties), or may be measured experimentally.

QSPR modelling involves several unit operations, summarized in Fig. 27 [500]. A set of molecules is first screened for their ability to inhibit corrosion. The larger and more chemically diverse this training set of molecules is, the more accurate and widely applicable the resulting machine learning model will be. Thousands of molecular descriptors can be calculated or measured, so it is essential that only the most relevant ones are used in the model. If too many descriptors are used relative to the number of training examples, the model may be overfitted and will not make reliable predictions of the properties of new molecules. Even if overfitting does not occur, the presence of too many irrelevant features (noise) will degrade model quality and efficiency. Optimally sparse models make the best predictions, and sparsity also aids model interpretation. There are diverse methods for selecting relevant features from a larger pool of possibilities. This must be done carefully to avoid chance correlations, apparently good models that can occur by chance if enough subsets of descriptors are investigated. Common methods for reducing the dimensionality of descriptors include removing those with high correlations with other descriptors, stepwise elimination of descriptors from models until significant model degradation occurs, stepwise addition of descriptors until model quality does not improve, and the use of genetic algorithms to select the best subsets of descriptors that generate the most predictive models. However, sparse feature selection methods such as multiple linear regression with expectation–maximization (MLR-EM), LASSO, and the sure independence screening and sparsifying operator (SISSO) are particularly useful because they select the most relevant features in a context-dependent way and generate very sparse models [501–508]. Description of these latter methods is beyond the scope of this review and interested readers are referred to the cited references for more details.

Statistical modelling methods such as multiple linear, polynomial, and kernel regression and efficient machine learning methods like random forest (RF), support vector machines (SVM), recursive partitioning (RP), and artificial neural networks (ANN) are commonly used to decipher the relationships between descriptors and corrosion inhibition. The application of these machine learning methods to modelling and prediction of the properties of materials has been comprehensively reviewed [119,509–511].

It is important to assess the abilities of models to predict the properties of new molecules not used to train them. The best way is to employ an independent set of inhibitors (a test set) not used to train the model [507]. This set is usually drawn from the available data set, either randomly or by choosing members from representative clusters of similar molecules (not completely independent but is reproducible and covers the same chemistry space as the training set). Every machine learning model has a specific domain of applicability defined by the properties of the molecules used to train it. Predictions of properties of molecules that lie outside of this domain are less reliable than those made within the domain because new molecules often have novel chemical features that the model has not seen.

Models can be analysed to gain an understanding of which inhibitor features improve or degrade performance, potentially also providing mechanistic understanding. Models can be used to predict the properties of putative inhibitors not yet synthesized or tested using computational virtual screening, or by using models to identify promising compounds in existing chemical libraries (e.g., ChEMBL > 2.3 M compounds, ChemBridge > 1.3 M molecules, Available Chemicals Database > 3.2 M compounds, ZINC-22 > 37Bn make-on-demand compounds) [508,509]. Clearly, screened molecules must lie near the domain of applicability of the models for the predictions to be useful.

New machine learning methods such as active learning (adaptive experimental design) can minimize the number of molecules required to be synthesized to expand the domain of applicability of models [510]. This involves training a model using a relatively small number of molecules and predicting the properties of a larger set of molecules with unknown corrosion inhibition that lie outside of the domain of the model. Those with the largest prediction uncertainties are synthesized, their inhibition determined, and they are added to the training set. This process proceeds iteratively until the required prediction accuracy in the new chemical domain is achieved.

The rise of deep learning algorithms (multiple layers in a neural network) within the last five years has stimulated more widespread use of neural network and machine learning approaches [116,117,511]. Generative deep learning models and encoder-decoder networks can, for the first time, take machine learning predictions of desirable corrosion properties and convert them directly into chemically synthesizable molecules, effectively inverting the QSPR problem [505,517–519]. This innovation is of great importance for the future design of drugs and materials, and should extend to corrosion inhibitors. In a recent example, a generative model was developed based on variational autoencoder to produce novel molecular structures of corrosion inhibitors for carbon steels with potentially improved performance at lower concentrations. Nine attributes, comprising seven molecular descriptors, the counts of N, O, S, and P atoms, inhibitor concentration, and inhibitor efficiency were employed in the model [515]. This kind of research is only possible in strong collaboration between researchers with a strong background in material science, chemistry, physics and computer science.



Fig. 27. Steps involved in QSPR modelling using statistical or machine learning methods.

## 5.2. Summary of successful and unsuccessful corrosion inhibitor models

A substantial number of papers have reported correlations between corrosion inhibition and molecular properties of small organic molecules, particularly those calculated by quantum chemical methods. Molecular modelling methods applied to prediction for corrosion inhibitors have been reviewed very recently by Ebenso and coworkers [516] and Verma *et al.* [517]. Some of the common techniques they reviewed included DFT, molecular dynamics (MD) and MC simulations, ANNs, and QSAR modelling.

Unfortunately, early studies employed very small data sets with limited chemical diversity. The workflow to model training data and predict the performance of untested corrosion inhibitors is exemplified for Mg in Fig. 28. Structural features of molecules in the training set must be encoded before training the learning algorithms. The accuracy and robustness of the models is assessed by an independent test set or, ideally, by subsequent experimental blind testing. The domain of applicability and accuracy of the models can be improved by methods such as active learning.

The frontier orbital energies (highest occupied molecular orbital  $E_{\text{HOMO}}$  and lowest unoccupied molecular orbital  $E_{\text{LUMO}}$ ) or the HOMO-LUMO gap ( $E_{\text{HOMO}} - E_{\text{LUMO}}$ ) derived from quantum mechanical calculations are often cited as being important for corrosion inhibition. For example, Sastri and Perumareddi found correlations between corrosion rates of iron and  $E_{\text{HOMO}}$ , the HOMO-LUMO gap, and Hammett's  $\sigma$  parameter for a small set of organic compounds [518]. Ozcan and Dehri also found a correlation between frontier orbital properties of thiourea, thioacetamide, and thioacetamide and corrosion inhibition for steel [519]. They later found similar correlations for corrosion inhibition for three additional small organic compounds with high corrosion inhibition and similar structures. The low chemical diversity and small range of inhibition values (93–97 %) throw doubt on the validity and generalizability of these relationships [520]. Sastri *et al.* also reported that corrosion inhibition in copper and iron was driven by  $E_{\text{HOMO}}$ , HOMO-LUMO gap, the chemical softness of inhibitors, and the chemical potential and degree of charge transferred to the metal surface from the inhibitor [521]. However, inhibitor ionization, speciation, and solvent effects were not accounted for, and the training data set was very small. In most early studies, the predictivity of models was not assessed by an independent test set because the data sets were too small. Bedair [522] used DFT, ab initio, and semi-empirical quantum chemical methods to study the corrosion inhibition properties of pyridine, quinolone, acridine and their n-hexadecyl derivatives on steel. He found that the dipole moments,  $E_{\text{HOMO}}$ ,  $E_{\text{LUMO}}$ , and HOMO-LUMO gap correlated significantly with corrosion inhibition. Again, small data sets and a lack of broad chemical diversity compromises the validity of these relationships [499].

Recent studies that use larger, more chemically diverse sets of organic corrosion inhibitors suggest that frontier orbitals and other properties calculated by quantum chemical methods by themselves are often not useful for modelling corrosion inhibition of aluminium and its alloys by small organic molecules [43,523,524]. One of these larger studies found essentially zero correlation between the frontier orbital or any other quantum chemically derived parameters and aluminium corrosion inhibition [73,524]. Even when speciation of organic molecules is considered, there was a very low correlation between ionization potential, HOMO or LUMO

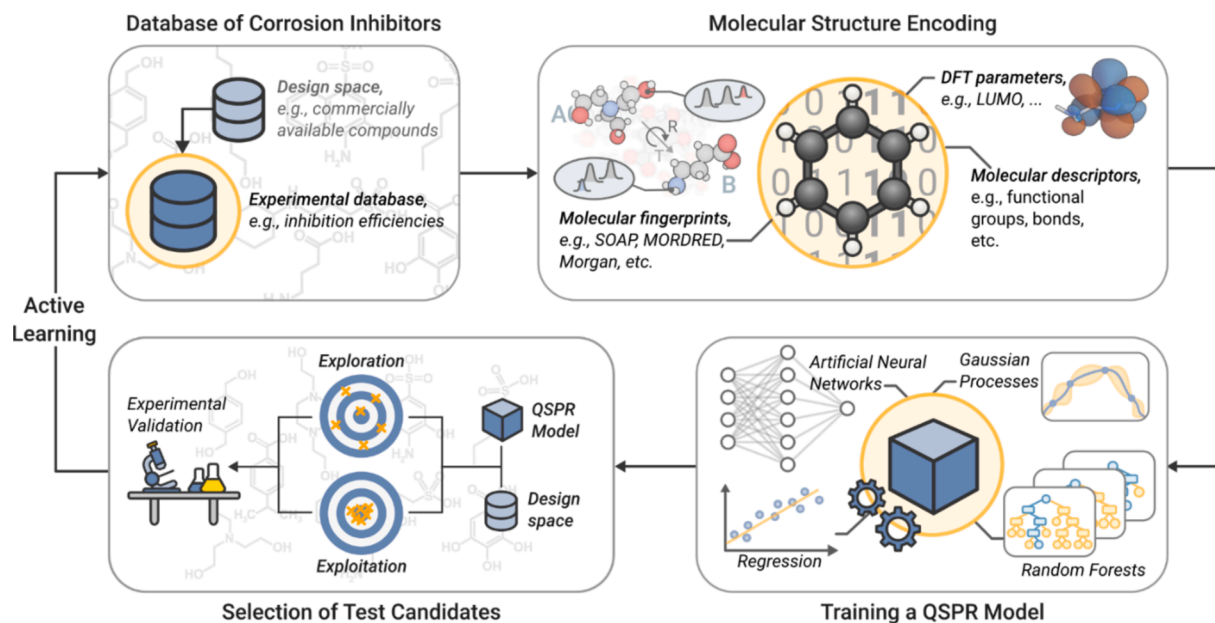


**Fig. 28.** General workflow to predict the performance of untested corrosion inhibitors for Mg using QSPR. First the structural features of the small organic molecules in the database must be encoded before they can be used as input for different (un)supervised learning approaches. In a last step, the accuracy and robustness of the models is assessed by experimental blind testing. Suitable test candidates are selected based on the model uncertainties, either following a more explorative (high uncertainty) or exploitative approach (low uncertainty). After multiple interactions of this workflow and the associated continuous increase in available training data, the domain of applicability and accuracy of the predictive models can be improved by active learning and new corrosion inhibitors can be discovered.

energies, or any other quantum chemically derived descriptors and corrosion efficiency [524]. These conclusions were confirmed in a later study of 100 diverse organic inhibitors, using data from novel high-throughput corrosion inhibition experimental methods. On the other hand, more recent studies have suggested that combining QM-derived descriptors with other types of descriptors can improve the quality and robustness of machine learning models of corrosion inhibition properties [525].

Intrinsically, quantum mechanical calculations should be able to generate descriptors that are effective in modelling corrosion inhibition by small molecules. The current failure to universally do so may be due to several factors:

1. As mentioned, a substantial number of studies use *very small data sets* with limited chemical diversity and range of inhibition values. The apparent significance of frontier orbital properties on corrosion inhibition in studies using small training sets may be due to chance correlations not indicative of causal relationships between the QM-derived properties of compounds and corrosion inhibition.
2. Greatly *simplified models of the inhibitor-alloy system* are necessarily used because of the computational demands of current quantum chemical methods. It is not tractable to model a complete alloy surface with metal inclusions, dislocation structures, electrochemical couples, water, air, ions etc. using quantum chemical methods with chemical accuracy. Innovative solutions to this dilemma are beginning to emerge so more computationally efficient DFT methods (or machine learning surrogates), and more realistic model systems should improve the accuracy of prediction and allow quantitative, or at least semi-quantitative predictions of corrosion inhibition [526].
3. The role of frontier orbitals in corrosion inhibition are likely to be *both metal and alloy dependent*. For example, Feiler *et al.* found that frontier orbitals were important factors in modelling the inhibition of magnesium corrosion [527].

In earlier machine learning studies of corrosion inhibitors, statistically significant and robust models were developed using general molecular descriptors calculated by software packages such as Dragon. These descriptors include atom and functional group counts, physicochemical property predictions, descriptors generated from the chemical graph or adjacency matrix (how atoms in molecules are connected) and many thousands of other more arcane but effective descriptors. Models of corrosion inhibition efficiency generated from these general molecular descriptors made reliable, quantitative predictions of the corrosion inhibition of inhibitors not used to train the model (Fig. 29)[73]. Clearly, the most reliable machine learning models are those trained on larger, more chemically diverse sets of inhibitor molecules across a broad range of inhibition values and concentrations.

Many measured and computed molecular descriptors are available for modelling organic corrosion inhibitors, leveraging the long history of QSAR/QSPR modelling of small, drug-like molecules in the pharmaceutical and agrochemical industries. Molecular descriptors may encode properties of the chemical graph (the way the atoms are connected in a molecule), the existence of molecular fragments and fingerprints, atom types and their properties, molecule physicochemical properties such as dipole moment, pKa of ionizable groups, lipophilicity (polarity), water solubility and many other molecular characteristics. More than 5000 different types of descriptors can be generated for molecules using packages such as the open-source solution RDKit, or commercially available packages such as [528] Dragon[529] and its successor alvaDesc, [530]. Robust, predictive QSPR models for corrosion inhibition by small molecules can be generated using these numerous, general molecular descriptors. However, the models may be difficult to interpret

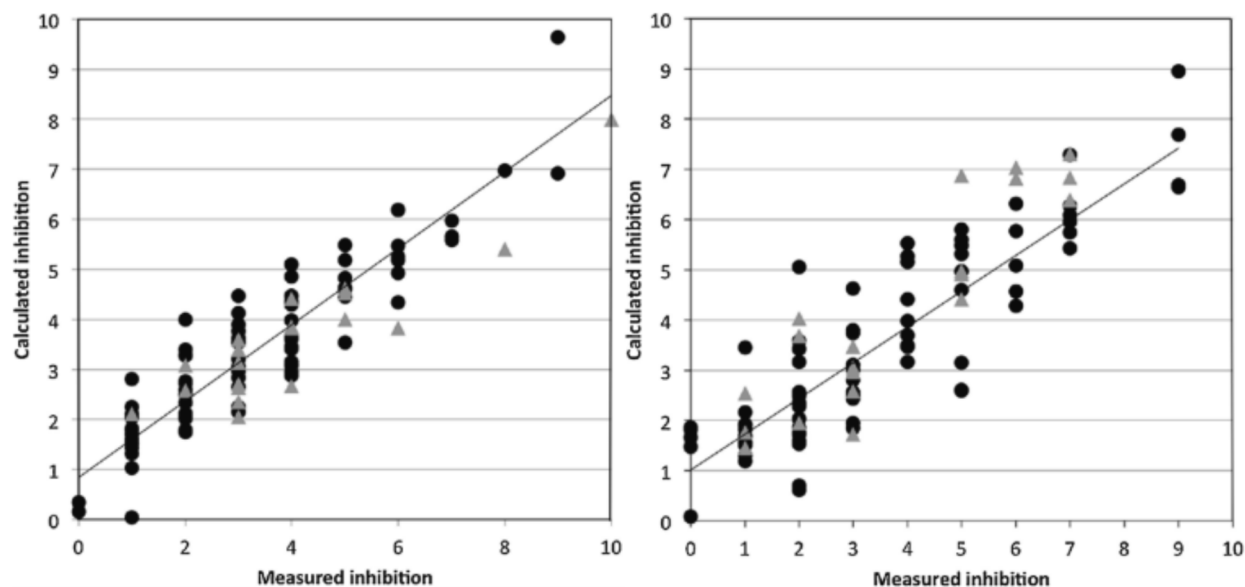


Fig. 29. Quantitative prediction of corrosion inhibitory properties of organic compounds for aerospace alloys AA-2024 and AA-7075 generated using molecular descriptors. Inhibition is scaled between 0 (no inhibition) and 10 (highest inhibition). Circles denote model prediction of training set inhibitors and triangles denote predictions for test set inhibitors. Reproduced from Winkler et al. [73] with permission.



because the descriptors are often arcane and hard to relate to chemical structures.

An example of easy-to-correlate descriptors is given by Fernandez *et al.*, who used a 3D-QSPR method (comparative molecular surface analysis, CoMSA) to model the aluminium corrosion inhibition efficiencies of 28 small organic molecules [531]. They employed distributions of electronegativity, polarizability, and van der Waals volumes from DFT calculations to map QM properties onto molecular surfaces used to model inhibition. This qualitative computational approach identified high-performing corrosion inhibitors.

Some studies have combined molecular descriptors generated by quantum chemical methods with other types of descriptors. Horner and Meisel reported the %IE on Al of 400 organic corrosion inhibitors in 1978 [532] (these are included in a data base containing several thousand inhibitors collected during preparation of this review paper, at <https://excrr.web.app/database> [533] and presented some simple QSAR models. Jayalakshmi and Muralidharan [534] generated QSPR models for iron and nickel corrosion inhibition by four candidate organic corrosion inhibitors. They identified inhibitor concentration, hydrophobicity, and  $\pi$  electron density as important properties influencing inhibitor efficiency. Again, the very small data set size is an important limitation of this study. A steel corrosion inhibition model for substituted imidazoles and benzimidazoles was reported by Keshavarz *et al.* [535]. They generated a simple multiple linear regression model for 34 diverse organic inhibitors:

$$\eta = 38.47 + 20.21n(N) - 7.98n(O + NH_2) + 14.94 \eta_+ - 17.93 \eta_-$$

where  $\eta$  is the corrosion inhibition efficiency (i.e. IE%),  $n(N)$  is the number of nitrogen atoms;  $n(O + NH_2)$  is the sum of the number oxygen atoms and amino groups;  $\eta_+$  and  $\eta_-$  are related to positive and negative structural parameters. The structural factors are complex indicator or 1-hot descriptors. Hydrogen bond donor and extended  $\pi$  electron substituents in the structure of an organic inhibitor are considered positive ( $\eta_+=1$ ) while hydrogen bond acceptor and electron withdrawing substituents or steric crowding have a negative effect ( $\eta_-=1$ ). Model prediction efficiency was assessed by a separate test set of 11 compounds and was higher than two QSPR models that employed quantum chemical descriptors reported by Zhang *et al.* [536]. However, the range of inhibition values for the training and test sets was small (60–95 % for test set) and how the  $\eta_+$  and  $\eta_-$  parameters were derived was unclear. The models Zhang *et al.* reported for the same compounds [536] used the quantum chemical descriptors electron density,  $E_{HOMO}$ ,  $E_{LUMO}$ , frontier orbital properties, partial charges, and polarizability plus  $nX$  and  $\delta_i^+$  topological indices derived from the chemical graph of each inhibitor and log octanol–water partition coefficients (a measure of lipid solubility). Their two 6-parameter models predicted the inhibition of the 34-molecule data set with an  $r^2 = 0.81$  and a standard error of 10 %. However, they did not use an independent test set to assess the ability of the models to predict new data.

More recently, interest in the application of machine learning methods to the design and discovery of organic corrosion inhibitors has increased substantially. Liu *et al.* reported a machine learning model for corrosion inhibition efficiency of benzimidazole derivatives that encoded energy, electronic, topological, physicochemical and spatial properties of the 3-D structures by 150 descriptors [537]. They used feature selection methods to identify 47 descriptors, subsets of which were used to train support vector machine (SVM) models for corrosion inhibition. They did not use a test set but validated their models by leave-one-out cross-validation. The best model had an  $r^2$  value of 0.96 and RMSE of 4 % IE and was used to identify six new benzimidazoles with high predicted inhibition values.

El Assiri and colleagues also used DFT-derived descriptors to model corrosion inhibition of organic compounds for steel [538]. They used  $E_{HOMO}$ ,  $E_{LUMO}$ , the energy gap, dipole moment, hardness, softness, absolute electronegativity, ionization potential, electron affinity, fraction of electrons transferred, log P, molecular mass, and several other QM-derived properties as descriptors. PLS, PCR, and ANN were used to build the models. The leave-one-out cross-validated  $r^2$  values for their PCR and ANN models were 0.92, and 0.90 respectively, and they predicted the inhibition of compounds in an external test set with  $r^2$  values 0.94 and 0.92.

A machine learning algorithm correctly classified organic inhibitors (> 50 % efficiency) and non-inhibitors (< 50 % efficiency) for aluminium, even for different alloys at different pH values [539] that allowed an increase in the size of the training set for the model. These authors devised new descriptors encoding the self-association of the molecules, but the predictive power of the models was limited. Later these authors, together with several co-authors of this review, released a database (CORDATA <https://datacor.shinyapps.io/cordata/>) comprising several hundreds of corrosion inhibitors [540]. The database is continuously growing as new compounds are added by the authors and anyone in possession of a reliable data.

Obot *et al.* studied eight pyrazine derivatives as mild steel corrosion inhibitors in a simulated oil field environment [541]. Using descriptors derived from DFT calculations they showed that all derivatives protected steel to a greater of lesser extent. An MLR model correlated the inhibition efficiency with the molecular descriptors with an  $r^2$  of 0.90. They reported inhibition efficiencies of the pyrazine derivatives were mainly modulated by  $E_{LUMO}$ , dipole moment, and molar volume, although the small data set size and lack of test set are significant limitations in this study. Four new pyrazine derivatives were designed that had good, predicted inhibition efficiencies.

Four imidazole derivatives were assessed for corrosion inhibition in 1020 carbon steel in an acidic medium by Costa and coworkers [542]. Gravimetric and electrochemical tests ranked the four inhibitors consistently. DFT-derived global hardness and inhibition efficiency were found to be inversely correlated. Monte Carlo methods calculated the adsorption energies in water and the Compass force field estimated the solvation energy between inhibitors and the metallic surface. The solvation energy was inversely correlated with corrosion inhibition. Again, the very small data set size left the conclusions at risk of chance correlations.

Sadik *et al.* employed MLR, kernel PLS, and Pharma-RQSAR to model the relationship between chemical descriptors for thiadiazole derivatives and their corrosion inhibition [543]. Classical descriptors and binary fingerprints that represented the inhibitor properties were used to train the models. The resulting contribution maps identified the optimum substitution patterns for the thiadiazole

derivatives.

Molecular fingerprints were also used by Dai *et al.* to create a generalizable %IE prediction model independent of theoretical calculations and expert-crafted features [544]. SMILES (a simple text-based description of organic molecules) was used to create molecular graph structures of 270 corrosion inhibitors used to train a three-level direct message passing neural network. Integrated atomic, chemical bond, and molecular level features enabled cross-category prediction. The accuracy of the model (10-fold validation  $r^2 = 0.46$ ) was higher than the support vector machine, random forest and single level direct message passing neural network counterparts that incorporate atomic and chemical features. Because of the high generalization ability, the model was able to predict molecules of diverse categories, which was demonstrated by validation using 27 molecules outside the training domain (23 from literature studies and 4 experimentally tested). With an expanded training dataset, the same group further improved this approach by incorporating 3D structural characteristics of molecules and corrosion inhibitor concentration information (0.005 to 5 mmol/L) [545]. This model was particularly good at predicting the %IEs of large molecules and recommending lowest effective concentration of cross-category corrosion inhibitors.

The role of quantum chemical descriptors relative to other descriptors was highlighted in studies of Mg alloys. From a dataset of 71 small organic molecules, Feiler *et al.* discovered a moderate correlation between the frontier orbital energy gaps and their corrosion inhibition effect on commercially pure Mg (containing 220 ppm iron) [527]. They trained a backpropagation ANN with a shallow architecture using chemical intuition to select the input features for the model. They combined the calculated HOMO-LUMO gaps with structural features that provide the model with information on the number of carboxylic acid moieties present in the molecules. They subsequently assessed the robustness of their model by experimental blind testing of seven corrosion inhibitors that were not part of the training dataset. The correlation between the predicted and measured values had an  $R^2$  of 0.74 and an RMSD of 33 % where the Pearson test indicated statistical significance of the correlation. Moreover, the authors demonstrated that the trained model could also be used to predict the corrosion inhibition efficiencies of the untested molecules for a Mg-based substrate with a similar composition to the one that was used to train the model.

Starting from the same seed dataset, Li *et al.* [546] developed predictive models for the Mg alloy AZ91 using kernel ridge regression (KRR) and support vector regression (SVR) following a two-step feature selection. First, the pool of available features was converted to a 25-tuple using RFE, which was subsequently screened for the best n-tuple to train the predictive model. Two blind testing compounds were found to be strong accelerators, with IE values of  $-563\%$  ( $IE_{\text{pred,SVR}} = -172\%$ ,  $IE_{\text{pred,KRR}} = -108\%$ ) and  $-517\%$  ( $IE_{\text{pred,SVR}} = -195\%$ ,  $IE_{\text{pred,KRR}} = -109\%$ ) that are far outside of the domain of the available training data. However, the models could still predict that they are both strong accelerators. For the remaining eight compounds, the SVR-based model made robust estimates for the inhibition performance for four and the KRR-based model for six. The SVR predictions were closer to the experimental results while the KRR model generalized better.

Schiessler *et al.* [30] used the measured corrosion inhibition of 60 small organic molecules to the Mg alloy ZE41 as a metric to train an ANN model. Here, a pool of 1260 input features (1254 calculated using alvaDesc and six derived from DFT) was used to encode the structure of the molecules under investigation. As there are no ANN-based feature selection techniques available, the pool of calculated descriptors was processed by two sparse feature selection approaches based on analysis of variance (ANOVA) and recursive feature elimination (RFE) to identify those most relevant to the target property. The authors claim that it is important to take the interactions between a group of selected features into account when selecting a subset of features for training a predictive model as single feature selection based on ANOVA fails to capture complex dependencies between variables. The accuracy and robustness of models using 3, 5, and 63 input features derived from ANOVA, RFE, and from a randomly picked set was assessed by predicting the %IE of six members of the dataset that were withheld from the training process (test set). The best performing model had an  $R^2$  of 0.94 and an RMSD of 26 % and employed five input features, including frontier orbital energies calculated by DFT. However, the model has not yet been evaluated by experimental blind testing. Interestingly, the authors also described how the encoder part of an autoencoder can be used to generate a lower dimensional representation of the input data, that can be displayed as 2D maps of molecular similarities and can detect

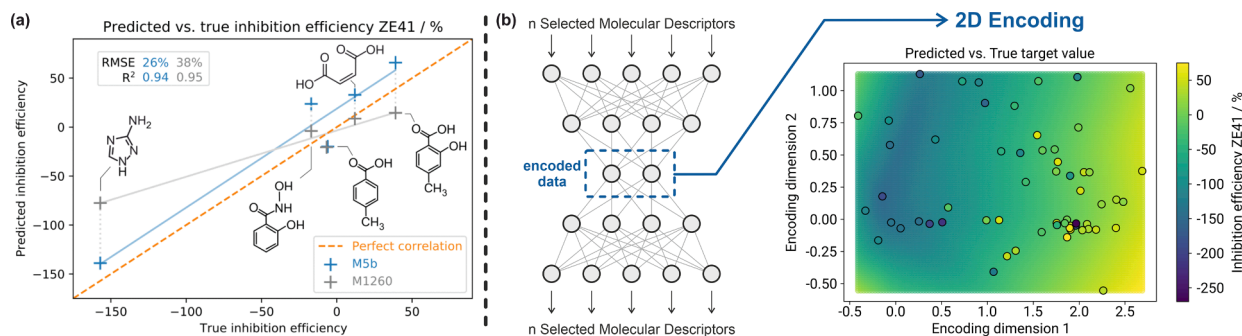


**Fig. 30.** (a) Predicted versus actual corrosion inhibition responses for the validation set used by Schiessler *et al.* [30]. A sparse model using only 5 input features selected by RFE (M5b) clearly outperforms a model that uses all available features (M1260). (b) An autoencoder was used to visualize the five-membered input feature set in two dimensions. The decoder part in combination with an appropriate predictive model (such as a deep neural network) can be subsequently used to generate contour maps across the space spanned by the dimensions of the two-dimensional code to detect outliers in the model. Figure adapted from Schiessler *et al.* [30] under Creative Commons Attribution 4.0 International License.

anomalies in the training dataset (Fig. 30). Sparse and recursive feature selection methods have suggested that the information contained in only a few molecular descriptors can generate efficient and reliable predictive models for the identification of effective small organic molecule corrosion inhibitors. However, a critical concern is how well predictive models trained on the original data can generalize and capture the properties of completely unseen (i.e., blind testing) data. In a follow-up to Schiessler *et al.*'s study [547], the generalization capability of the previously reported deep neural network model [29] was assessed by predicting the performance of additional 15 corrosion inhibitors and subsequent experimental testing. The model trained on the original data and feature set confirmed that the originally selected descriptors showed moderate correlation between predicted and experimentally determined %IE values, as only 9 out of 15 compounds were accurately predicted. A comparison was made between a model trained on sparse features selected for the original data set (60 compounds), the blind test set (15) compounds, and for all 75 compounds. It concluded that these sparse feature sets are not yet able to sufficiently cover enough of chemical space. Selection of molecular descriptors is a crucial step in developing predictive models for corrosion inhibitor discovery even when there are limited data available to train them. However, this work suggests that the modelling approaches used may be scalable. Feiler and Schiessler *et al.* have also provided strong evidence that DFT parameters can be a useful addition to a feature set when modelling %IE models for Mg based on QSPR methods. Furthermore, consistent with the universal approximation theorem, shallow network architectures (a single hidden layer) are usually sufficient and deep neural network approaches (multiple hidden layers) do not improve the accuracy of the models, at least with the limited training data available [547]. However, deep neural networks can be highly effective in converting simple representations of molecular structures to latent features that can generate accurate predictive models of corrosion inhibitor performance. *This is a major advantage of these novel methods.*

A common challenge for researchers using ANNs to model properties is selection of the best network architecture. For shallow neural networks this means how many hidden layer neurons to use, and what kind of transfer function each layer should use. If the network is too large, the number of adjustable weights is also large, risking overfitting of models. If the number is too small, the model may not capture complex, nonlinear relationships in the data. This is known as the bias-variance trade off. Use of model regularization methods, such as sparse prior Bayesian, weight drop out, or ReLU transfer functions can minimize overfitting for large architectures [548].

Instead of using distinct molecular descriptors, molecular structural features can also be encoded by molecular fingerprints, such as the SOAP (Smooth Overlap of Atomic Positions) kernel [549–556]. This kernel defines a global similarity matrix for chemical compounds in the dataset. Applying dimensional reduction techniques, the high-dimensional similarity space can be mapped onto two or three dimensions to help visualize structure–property relationships. These methods attempt to retain the multidimensional distance relationships in the lower dimensional representation of chemical space. Thus, close/distant, i.e., similar/dissimilar, structures in the high-dimensional space maintain this relationship in lower dimensions. Pattern recognition capabilities of these unsupervised learning techniques make it possible to visualize the relationship between molecular structures and the corresponding inhibition performance in a structure–property landscape, where all experimentally tested structures exist as landmark points. Clusters in these similarity maps indicate correlations between the inhibition efficiency and associated molecular structure, identifying key structural features that drive dissolution modulating properties. Here, dissolution modulators are the organic molecules that either inhibit corrosion for structural applications or promote even dissolution of magnesium as anode material of Mg-air batteries [28,60,552].

Following this approach, Würger *et al.* used out-of-sample embedding to qualitatively predict the inhibition efficiencies of Mg corrosion inhibitors [27]. Subsequently, six structures of interest were projected onto the structure–property landscape generated from 74 small organic molecules. These authors showed how mapping structural features to specific clusters helps to qualitatively assess the potential impact on the corrosion rate of the projected compounds, thus helping choose which untested candidate inhibitors require further experimental validation. This reduces the amount of time and resources required to find better inhibitors, compared to a purely experimental screening approach.

The SOAP kernel can also be used to train supervised machine learning methods such as kernel ridge regression (KRR) to obtain quantitative predictions of the corrosion inhibition efficiency of small organic molecules. Using the same database the previous ANN study of Feiler *et al.*, Würger *et al.* showed that a KRR model based on SOAP features achieved similar prediction accuracy, with an  $R^2$  of 0.79 and an RMSD of 36 % [28]. Although the statistical metrics of the predictions derived from the KRR and ANN model are very similar overall, they show distinct differences in the predicted IE values for two compounds in the blind test set. This highlights the potential of committee (consensus) models to mitigate the drawbacks of a single approach and provides guidance on how models can be extended to describe larger chemical spaces (e.g., by adding input features that improve the prediction of outliers, see active learning discussion above). These models allow many potential candidates to be virtually screened for their associated corrosion inhibition efficiencies. Using a database of experimentally measured Mg corrosion inhibitors, Würger *et al.* predicted the %IE of > 7000 commercially available small organic molecules. To help identify potent Mg corrosion inhibitors in very large chemical spaces, the authors developed ExChem (<https://www.exchem.de>). Using the underlying SOAP similarities of the combined dataset allows selection of candidates for further testing that show significant similarity to an already tested compound of interest. If a structure–property relationship exists, the proposed structure has a high chance of yielding similar results on experimental testing. This is particularly important for identifying alternative candidate inhibitors similar to those that have been identified as useful but are expensive or potentially toxic. Limited experimental blind testing of such candidates has validated this approach. In this example, the model showed high accuracy with an  $R^2$  of 0.84 and an RMSD of 36 %. The reason for the relatively high RMSD values is that 2 out of 5 compounds of the 5-membered blind test set were not correctly predicted. These molecules are outliers possibly because of the method used to encode the molecular structures. The SOAP kernel contains information on the local environments of the atoms. However, it does not encode the electronic structure of certain functional moieties (nitro in this case), which subsequently leads to false prediction for compounds with a nitro group in *ortho* or *para* position. Clearly, augmenting the model training data with more nitro

compounds will enable the model to learn the electronic contribution of the functional group and link it to the inhibitor performance.

By changing the target value used to train the machine learning model, the ExChem method can be extended to fields other than Mg corrosion. In another study, Würger *et al.* trained a kernel principal covariates regression (KPCovR) model on a dataset of electrolyte additives for primary aqueous Mg-air batteries [552]. The target was the measured discharge potential and utilization efficiency of a Mg-Ca working electrode against an Ag/AgCl reference electrode. Starting from an initial seed database of 49 compounds, the authors used ExChem to select potential candidates in the chemical space of structurally similar, commercially available compounds that might improve the Mg-Ca anode performance. The small training set size resulted in low prediction accuracy for the test set of only five compounds. Model performance improved significantly for a second test set when an active learning-based design of experiments scheme, illustrated in Fig. 28, was used. Using a sub-sampling approach, the authors additionally provided uncertainty estimates for the predictions, allowing selection of compounds for testing likely to further improve the model performance. Based on the predictions for both target parameters, Würger *et al.* developed a multi-objective optimization method that identifies new electrolyte additives that maximize the battery anode performance for target applications.

Aghaaminiha *et al.* [553] reported a model for corrosion rates of carbon steel that included scheduled dosing of corrosion inhibitors. A Random Forest model that included environmental variables was found to best predict the time-profile of corrosion rates in presence of corrosion inhibitors.

To deal with small corrosion dataset sizes, some research groups added virtually generated data points using methods such as Virtual Sample Generation (VSG) to mitigate data scarcity, class imbalance and enhance the prediction accuracy of machine learning models. In a study by Sutojo *et al.* [554], a K-Nearest Neighbour algorithm was combined with VSG based on bush topology to predict the %IE of inhibitor compounds when trained on six datasets. Similarly, Akrom *et al.* [555] enhanced the model performance by leveraging a kernel density estimation (KDE)-based VSG. Iyer *et al.* [556] built an ANN-based QSAR model to predict the inhibition efficiencies of 2-alkyl benzimidazole scaffold-based corrosion inhibitors for mild steel in 1 M HCl. They used VSG based on conditional GANs to generate synthetic data, thus enhancing the model towards recognizing relationships between chemical features and %IE. Although VSG can have a positive impact on the predictive performance of machine learning models, it has to be treated with care. It is easy to introduce biases, e.g., when the data distribution is not captured correctly, leading to overfitting or the model working well on synthetic data but failing to generalize for real-world data. Aside from that, the quality of data plays an important role. Validation of generated samples is difficult as a ground truth often does not exist. Additionally, since corrosion data is usually afflicted with rather large noise, VSG can further amplify uncertainties, thus impairing the quality of predictions. In worst cases, bad practices such as splitting data into training and test sets after VSG would leak test set information into the training set, resulting in an artificial spike in prediction accuracy for the test set. However, VSG for corrosion inhibitors shows some promising potential and developments of the underlying model architectures (e.g., GANs) may further improve the quality of the generated data in the future if due care is taken.

Quantum computing (next generation computers using quantum properties like superposition and entanglement to solve complex problems faster than on classical computers) and quantum machine learning (classical machine learning methods trained on data generated by high level quantum chemical calculations) are still in very early stages of development. The advantages of this approach suggest they will play a significant role in advancing corrosion control strategies and improving the understanding and mitigation of corrosion-related issues in the near future. Quantum materials science has the potential to become a paradigm shifting technology in scientific research [557]). It is highly likely that quantum computing approaches will be able to simulate the electronic structure and behaviour of materials in corrosive environments more accurately so these larger systems will become accessible to quantum machine learning (QML) methods. Such highly complex material systems are currently intractable for classical quantum chemical modelling approaches. Understanding the very fundamental processes of corrosion on the atomistic and quantum level will naturally enable the design of materials that are more resistant to degradation and protective coatings and may enable researchers to identify promising candidates without the need for expensive and time-consuming experimental testing. QML techniques can help identify and optimize processes as well as novel materials with desired properties more efficiently than the most sophisticated deep learning approaches that are available today. These algorithms can analyse complex data sets related to materials' properties, environmental conditions, and corrosion rates much faster with more complex architectures and pseudo first principles quantum chemical methods. The application of QML in natural sciences already shows great potential e.g. for the simulation of catalytic cycles [558] as well as for the evaluation of corrosion inhibitors [559] whereas the author used a dataset consisting of 94 pyrimidine-type molecules to provide a proof of concept for the integration of QML with traditional QSPR. High potential of quantum computing for materials science and beyond has been already recognized by large industries: Airbus and BMW have announced a "Quantum Computing Challenge" in 2024 [560]. Modelling the process of inhibitor adsorption on an aluminium surface using quantum methods is one of four challenges proposed by the industrial consortium.

### 5.3. Evolutionary methods

Given that the chemical space of small organic molecules, like that of potential drug-like molecules, is huge ( $>10^{60}$ ), there are a vast number of organic molecules that may exhibit useful corrosion inhibition properties. Clearly, accelerated testing using automation, and leveraging of these data into larger areas of chemistry space using machine learning methods, will undoubtedly uncover new corrosion inhibitors. However, these approaches can still only explore a minute fraction of possible chemical space. Evolutionary methods, like biological evolution, are more efficient ways to explore very large solution spaces. These approaches are being adopted for drug and materials discovery, as reviewed recently.[31,32] These methods involve converting the relevant structural, physico-chemical, and prevalence properties of molecules into a bit string, a type of chemical genome. A small initial population of molecules is selected using leads, chemical intuition, or randomly and their fitness (e.g., corrosion inhibition) determined by experiment. The

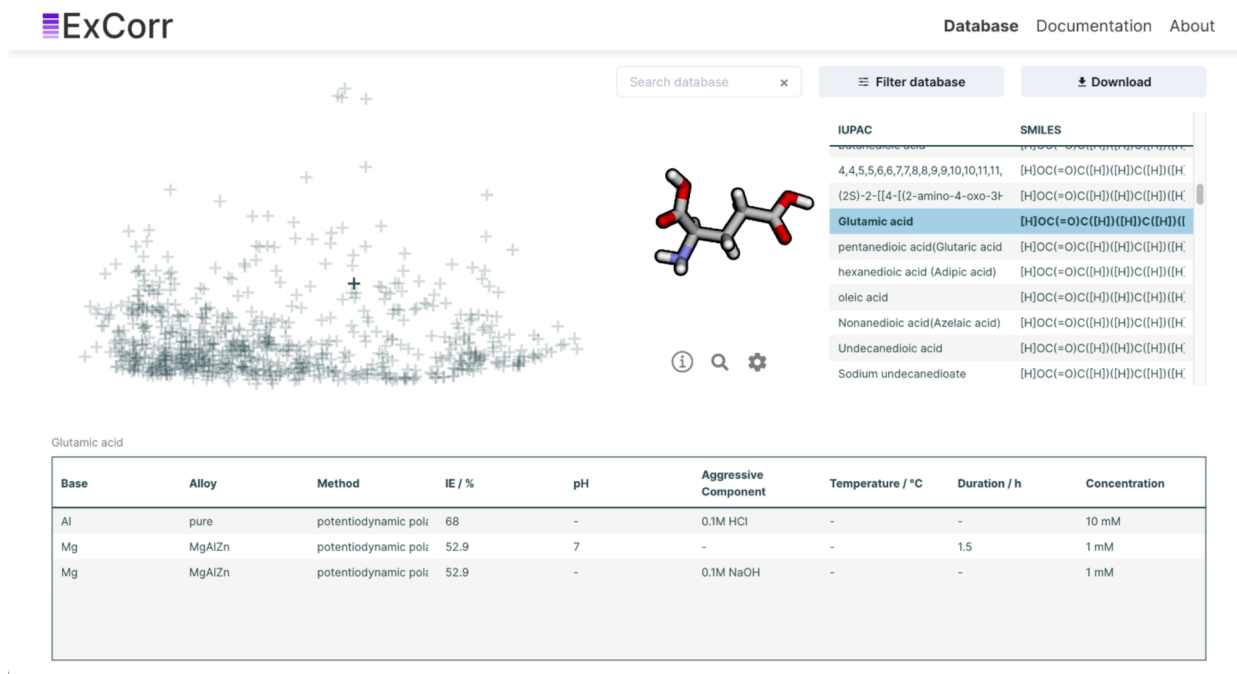
fittest molecules are subject to mutation operators such as point mutation (perturbing a single bit in the genome, local search), crossover (splitting two genomes at a random point and combining the fragments in new ways, entering new chemical space), and elitism (retaining the best solutions without change). Molecules corresponding to these mutated genomes are synthesized and assessed for fitness, with the cycle repeating until an acceptance criterion is met, or no further improvement results.

There are multiple advantages of using evolutionary methods to discover next-generation corrosion inhibitors. Evolutionary methods allow complex fitness functions to be defined that provide optimal solutions for multiple properties e.g., high corrosion inhibition, low toxicity, compatibility with coating formulations, lower cost. As mentioned, they also explore chemistry space more efficiently than other methods and work synergistically with design-of-experiments techniques to increase the size of chemical space explored. They can minimize the number of physical experiments that need to be performed, reducing cost and increasing the speed of discovery. They also work well with methods such as active learning (adaptive experimental design). As the evolutionary process operates, the accumulated experimental data can be used to train machine learning models of the fitness landscape, replacing the need to conduct experiments in some cases.

There are currently no examples of the application of evolutionary methods to discover corrosion inhibitors, but we expect this approach to be of increasing importance in the near term. Genetic and evolutionary algorithm methods have, however, been used to derive corrosion-rate expressions for steel and zinc [561], to detect corrosion profiles on steel matrices [562] as well as to forecast the aging of single base pollutants [563].

#### 5.4. Autonomous systems

More speculatively, there is growing interest in autonomous systems (self-driving labs) for the discovery of novel molecules and materials [564–572]. Here, automated chemical synthesis and testing are combined with evolutionary algorithms or generative machine learning methods that convert a predicted activity from a machine learning model into a synthesizable molecule. This creates a system that can be initiated by lead materials and will iterate a synthesis-characterization-mutation cycle, without a human in the loop, until molecules with the desired properties are achieved. This paradigm is clearly very applicable to the discovery of next-generation corrosion inhibitors. The challenge is that the performance of a corrosion inhibitor molecule typically differs significantly from one alloy to another even within one metallic substrate (e.g. compare inhibitor performance for E21 and AZ31 Mg alloys in [60] or AA2024 and AA7075 in [73]). Two-three “universal” inhibitors, effective for several alloys of the same base metal, were also found per 100 tested, e.g. 3-amino-5-mercapto-1,2,4- triazole and 1,2,4-triazole-3-thiol were highly ranked for AA2024 and AA7075 [73], benzotriazole suppressed Cu corrosion in pure and alloy forms [568], while 2,5- and 2,6-pyridine-dicarboxylates and fumarate were highly ranked for all nine tested Mg alloys [60]. Testing conditions, such as surface pretreatment, inhibitor concentration, initial bulk pH, electrolyte volume to surface area ratio, temperature, and medium composition and concentration also significantly influence measured inhibition efficiency. Thus, evolutionary methods will work best when all relevant metadata are captured in the genome. “Read across” methods for prediction of corrosion inhibition from one metal to another may also be useful, as other fields of technology



The screenshot displays the ExCorr web application interface. At the top left is the ExCorr logo. On the right, there are links for "Database", "Documentation", and "About". Below these are search and filter options: "Search database" with a clear button, "Filter database", and "Download". A 3D ball-and-stick model of a molecule is shown in the center. To the right of the model is a table with two columns: "IUPAC" and "SMILES". The table lists several acids, with "Glutamic acid" highlighted. Below the table, there is a table with the following data:

| Base | Alloy  | Method              | IE / % | pH | Aggressive Component | Temperature / °C | Duration / h | Concentration |
|------|--------|---------------------|--------|----|----------------------|------------------|--------------|---------------|
| Al   | pure   | potentiodynamic pol | 68     | -  | 0.1M HCl             | -                | -            | 10 mM         |
| Mg   | MgAlZn | potentiodynamic pol | 52.9   | 7  | -                    | -                | 1.5          | 1 mM          |
| Mg   | MgAlZn | potentiodynamic pol | 52.9   | -  | 0.1M NaOH            | -                | -            | 1 mM          |

**Fig. 31.** User interface of the web application *ExCorr* that enables browsing the database of corrosion inhibitors. Available online <https://excrrr.web.app/>.

such as nanomaterials, have shown these methods to have considerable value. Ideally, targeted screening for a particular alloy, tested under specified conditions, needs to be performed. The discovery of ‘universal’ corrosion inhibitors exhibiting the same performance as chromates, that perform equally well for a wide range of metallic substrates and microstructures, would be an important goal.

## 6. Diverse chemical classes of organic inhibitors

Hundreds of small organic molecules have been tested as corrosion inhibitors by a diverse range of methods and against the full spectrum of commercially important metals and alloys.

As outlined in Section 5 of this review, the databases containing corrosion inhibition entries should be the intermediate point, rather than the destination. Even the most efficient, automated experimental inhibitor screening will not be able to process 160 million compounds currently listed in the Chemical Abstracts Service database, let alone all hypothetically synthesizable small organic molecules. Given the size of chemical space, AI and Machine Learning models are the only feasible way to discover more robust and effective corrosion inhibiting small organic compounds tailored for specific alloys. The most prominent species identified by the experimental screening should be studied to unravel their inhibition mechanisms and to explore ways of incorporating inhibitors into metal protective coatings, their main application area.

We have compiled an extensive database comprising 1308 individual organic molecules, tested as corrosion inhibitors for Al-, Cu-, Zn, Mg-alloys and steels using different methods and operating concentrations etc., resulting in about 6000 database entries. This constitutes the largest data source so far for use by QSPR and other machine learning studies of organic corrosion inhibitors for diverse types of metal protection. To enable corrosion scientists to browse the database assembled as part of this review, and to render the data easily accessible for the community, we created a structure–property landscape which is available at <https://excrr.web.app/> (Fig. 31). This app summarizes the known organic corrosion inhibitors and their chemical diversity. The details of the experimental methods, measurement techniques, and inhibition efficiencies are also listed in the database. As an additional feature, a structure of interest in the given database can be selected by the user and the  $n$  most similar compounds from the underlying database are provided. Given that a structure–property relationship exists, the suggested compounds might be potent corrosion inhibitors for material of interest even if they have originally been tested for an entirely different material. First, the structures of all compounds in the database are encoded using the smooth overlap of atomic positions (SOAP) approach. Atoms are replaced by three-dimensional Gaussian functions and their rotationally and translationally invariant overlap is calculated between all local atomic environments using a defined cutoff radius around all atoms in the molecules. A global similarity matrix can be built from the resulting covariance matrix. To visualize this high-dimensional kernel as a 2D map, a dimension reduction method is applied (here we use kernel principal component analysis). Visualization is useful for checking operating concentration ranges, a specific material (Mg, Al, Cu, Zn, Steel) or testing method ( $H_2$  evolution, weight loss gravimetry, EIS, PP, etc.).

A visualization of the database of corrosion inhibitors is available as a Word document in the supporting information of this review. As machine learning algorithms require standardized input data, the authors created a machine-readable version of the reported corrosion inhibitors which is also provided as a supporting information file. To help keep the database up to date, the authors have provided a template to enable the community to add their own data in the future, to further expand data available for the training of machine learning models. The database behind ExCorr also contains less efficient or relatively novel species that have not been well studied to date. These nevertheless constitute highly relevant entities for machine learning algorithms as they extend the domains of applicability of the models. The <https://excrr.web.app/> will be regularly updated with newly constituted sets of data contributed by the corrosion community. Another database, CORDATA, (<https://datacor.shinyapps.io/cordata/>) has been recently created and is being updated by researchers from University of Aveiro, Portugal [540].

## 7. Summary and path forward for organic corrosion inhibitors

As was exemplified in Section 4.5.5 of this review, conflicting values of inhibition efficiency for many organic compounds exist in the literature and have been unselectively collected in the ExCorr or CORDATA databases. The discrepancies stem from varying experimental conditions that affect measured corrosion inhibition values in many ways. These include alloy composition and processing steps defining the microstructure, surface condition, composition and concentration of corrosive medium and inhibitor concentration, initial pH and sample surface to electrolyte volume ratio, electrolyte flow and thickness, aeration,  $CO_2$  content and temperature, to mention a few. These factors can significantly influence corrosion rate and inhibition mechanisms that impact the measured inhibition efficiency. Two general strategies for dealing with these discrepancies can be proposed: collecting databases with strictly controlled experimental conditions using robotic screening when possible; or collecting the most potent, universal, corrosion inhibitors under a wide range of varying conditions. Although discovering a single ecologically benign molecule as potent as chromate is unlikely, the latter approach may allow researchers to narrow down the set of universal inhibitor candidates with high inhibition efficiency for many metallic materials under diverse service conditions.

Most current inhibitor screening approaches consist of extensive testing of varying chemotypes on one metallic substrate, i.e. one specific alloy, under fixed conditions of surface preparation, inhibitor and corrosion medium concentration, testing time, etc. Exploring and defining the strategies for extending corrosion inhibition data within the same alloy family (e.g. Al containing Mg alloys, AZ31, AZ91, AM50) or across different alloy families (e.g. Al- or rare-earth-containing Mg alloys, AZ31 vs WE43) would significantly decrease the need for experimental [60] and computational [29,34] efforts and accelerate discovery of corrosion inhibitors with wide applicability. Lack of defined industry acceptance criteria is another hurdle on the way of adopting multiple successful, from academic standpoint, corrosion inhibitors into industrial practice. Comprehensive selection criteria for the inhibitors developed together by

academic and industrial researchers might shorten the path to industrial acceptance. Such selection criteria are unlikely to be common for a wide range of industries/applications due to a wide range of service conditions and hence performance validating tests. This results in a large variety of industrial standards per company, let alone the industry branch. Just like stand-alone inhibitors are prone to environmentally dependent performance, as demonstrated in Section 4.5.5 and Fig. 26, protective coatings incorporating such inhibitors possess the same property. Perhaps, the most practical solution is to aim at inhibitor-containing protective coatings for specific industrial applications, considering corresponding service conditions and industrial testing requirements.

Only a small fraction of service applications embodies full immersion of a metallic part in inhibitor-containing electrolyte. In most cases, metallic parts are exposed to intermittent atmospheric conditions, where corrosion inhibitors are combined with other protective strategies such as being distributed in polymeric or inorganic reservoirs, serving as inhibitor delivery system. They are typically added to primer coatings. Often, the inhibiting effect is retained when corresponding compounds are incorporated in the inhibitor delivering reservoirs distributed in a coating, but this cannot be taken for granted and needs to be verified for each specific coating-inhibitor combination. A loss of inhibitor capacity or deterioration of coating barrier properties have been reported [450,569] and are related to low local concentration of inhibitor upon leaching, local electrolyte conditions, interaction of inhibitors with the surrounding coating or reservoirs, or altered inhibition mechanism. Data related to protective performance of inhibitor-containing coatings are rarely reported and are much smaller (e.g. [570]), probably because testing is considerably longer, requires separation of the coating, reservoir and inhibitor effects, and is even more difficult to standardize owing to a wide variety of coating components. Nevertheless, given that the inhibitor-containing coating is closest to the real application, new high-throughput testing methods validating efficiency of corrosion inhibitor incorporated into protective coating, are urgently needed. These can include electrochemical testing (e.g. LPR [570]), new approaches to accelerated corrosion testing, combining purely experimental testing with machine learning methods [571] and developing models predicting coating behaviour under various atmospheric conditions (digital twins). Designing accelerated yet representative experimental workflows for testing stand-alone and coating-incorporated corrosion inhibitors will overcome the current bottlenecks holding back *in silico* screening of corrosion inhibitors. These include lack of reliable, representative and diverse experimental data for training machine learning models. Another approach is contributing to shared databases, following the best practice for data reporting (recording and disclosing experimental conditions including alloy type, composition, impurity level, grain size, surface preparation, type and concentration of corrosive medium, inhibitor concentration, initial and final pH, test duration, evaluation method, sample surface to electrolyte volume ratio, electrolyte flow and thickness, aeration, CO<sub>2</sub> content and temperature).

Although machine learning models for corrosion inhibition are available and are developing rapidly, another challenge stems from deciphering the language of corrosion inhibition. Evolution of language and notation often precedes major breakthroughs in science. A good example of this is Newton and Leibniz's definition of differential calculus, which started with a lack of language to describe the scientific problem of mechanics itself. After, this mathematical foundation enabled simpler understanding of a myriad of unsolved problems. Meanwhile the language of quantum mechanics also started with a new mathematical notation, which changed the understanding of all physical sciences. Similarly, we currently lack the best notation or description needed to digitize our experiments. This is critical in communicating our results to predictive machine learning models. To this end, finding the computational descriptors that best digitize corrosion inhibition is crucial. Currently, the literature contains many descriptor generation packages for quantitative-activity relationships. There are very promising new approaches that move beyond externally generated features by intrinsically defining molecules (graph neural networks, adjacency matrices, natural language embeddings of SMILES/SMARTS/SELFIES) [572]. Although initially developed solely for small organic molecules, in future, generalization of descriptor definitions would better capture the complex behaviour of inorganic inhibition systems such as Li, Ce, chromate systems, and later, interaction between different inhibitor chemicals, and components of coating systems. However, devising such a unified language is non-trivial [573]. Especially, the rise of the transformers (e.g. ChatGPT) in recent years bears high potential to usher a new era in the development of predictive models for corrosion inhibitor research as the self-attention mechanism at the core of their learning process can potentially connect hidden links between the experimental and computational realm.

The search for chromate-free corrosion inhibitors is an ongoing quest for at least two decades. Yet, the results are far from optimal. This made aerospace, automotive, construction and other industries appeal to environment regulatory bodies to extend (limited) use of hexavalent chrome inhibitors. While such extensions are often justified and granted, this holds back the progress in development of alternative corrosion inhibitors. Another issue is that environmental compatibility and toxicity of organic corrosion inhibitors are typically not properly addressed in publications dealing with corrosion inhibitor discovery. It is often done much later, at the industrial implementation stage. Clarifying hazardous properties at the inhibitor screening stage might save time and effort that otherwise would be put into a potentially dangerous compound. There is clearly a need for such pre-screening stage to be implemented before including any compound into a testing routine. Manual consulting of MSDS data of existing compounds, screening or estimating toxicity using existing apps linked to biomedical databases [574] might be a starting point.

So, what else is needed to move towards a bright future of machine learning in corrosion inhibition research? If the right data are available, machine learning is already proving to be an invaluable tool to predict the inhibition performance of, e.g., individual chemical compounds for a given base material. Machine learning models that predict the synergistic effects of mixtures also already exist, although mostly in other domains than corrosion inhibition as described in section 4.6 and 4.7. However, the necessary tools are available and combining them with a solid data foundation (for example, acquired by recently proposed droplet micro-array testing [575]) will help to accelerate the discovery of synergistic mixtures for corrosion inhibition. Atomistic simulations [576] bear the potential to increase the mechanistic understanding of investigated systems and mixtures, revealing relationships that can be incorporated into the modelling process to further increase the predictive performance. New molecular descriptors such as MolSets will further support the modelling process [577], whereas the rise of self-driving labs [578] will facilitate the reproducible collection of

large datasets. The huge design spaces that inevitably arise when dealing with complex systems or mixtures can be conquered by using adaptive sampling methods, such as Bayesian optimization [579]. First approaches towards the identification of advanced corrosion protection coatings [571] were already successful. Complementing the efficiency of self-driving labs with data architectures provided by electronic lab notebooks will also lay the foundation for more generally applicable machine learning models that work for a range of base materials, in contrast to just single alloys. Machine-readable databases (e.g., as provided with this review via ExCorr) provide a sound starting point for the development towards such material-independent foundation models for corrosion inhibitor selection.

Interdisciplinary collaboration is crucial in advancing the discovery of organic corrosion inhibitors, particularly as the complexity of materials in corrosion science and their interactions with the environment demands a diverse set of skills and perspectives. Simple trial-and-error approaches, guided by chemical intuition and slow-pace empirical testing are unlikely to lead to breakthroughs needed in corrosion science. High-throughput manual and robotic testing requires redesign of testing approaches making them suitable for automation. This calls for involving wide range of experts skilled in electrical engineering, optical image treatment, robotics engineering and programming to assist corrosion scientists and chemist. High-throughput testing leads to faster generation of large datasets and requires involvement of experts with a strong background in mathematics, machine learning and computer science. These advancements underscore the growing importance of cross-disciplinary teamwork in tackling some of the most complex challenges in materials science today.

Once good organic inhibitors are discovered and optimized, it will be necessary to manufacture at least 112,000 – 139,000 tons/annum (see section 1.1) to meet industry demand, assuming a one-to-one correspondence of inhibitor efficiency for the new inhibitor versus chromate. However, finding universal corrosion inhibitors similar in performance to chromate might not be possible and case-by-case solutions will need to be found for each alloy and service condition. Organic inhibitors can be derived from one or two routes: extraction from biomaterials or chemical synthesis. Many simple carboxylic acids can be derived by distillation from a range of sources. For example, acetic acid can be derived from fermentation and distillation. It can also be manufactured from the reaction of methanol with carbon monoxide with over 12.1 million tons produced via this route in 2012 and an estimated 16.3 million tons for 2018. Thus, the production of over 100,000 tons/annum of acetic acid seems achievable. However, this is only possible because acetic acid is used as a precursor for a range of other chemicals, with the largest quantity being vinyl acetate. Equally, heterocyclic compounds such as pyridine are also manufactured in bulk, again because it is a precursor for other reactions. On the other hand, organic inhibitors that show encouraging performance are likely to be derived from commodity chemicals and will therefore involve additional chemical steps, moving inhibitor manufacture from a bulk chemical to specialty chemical, which adds to the cost. The production routes of the most successful inhibitors might be further optimized, leading to decreased cost.

Finally, there is synergy and complementarity between screening for new organic corrosion inhibitors and the development of new battery technology additives. Highly efficient corrosion inhibitors discovered by experimental and *in silico* screening would potentially be invaluable for batteries too. Next-generation sustainable metal-air aqueous batteries (e.g. Zn-, Mg- and Al- secondary and primary cells) require electrolyte additives that minimize self-corrosion, prevent anode fouling with precipitated discharge products and control dendrite growth, leading to higher utilization efficiency and output voltages [60,429,580,581]. Such additives must inhibit the parasitic cathodic process on metallic anode without forming a dense adsorption or precipitation layer and trap metal ions into soluble complexes that can otherwise form detrimental precipitates. Small organic molecules have been demonstrated to be highly efficient electrolyte additives for Zn-, Mg- and Al- secondary and primary cells [429,552,580,587–589].

## 8. ORCID/Google Scholar/Scopus

Author Name: David Winkler  
ORCID ID: 0000-0002-7301-6076  
Author Name: Anthony Hughes  
ORCID ID: 0000-0003-3573-6344  
Author Name: Can Ozkan  
ORCID ID: 0000-0001-8029-806X  
Author Name: Arjan Mol  
ORCID ID: 0000-0003-1810-5145  
Author Name: Tim Würger  
ORCID ID: 0000-0003-0346-0371  
Author Name: Christian Feiler  
ORCID ID: 0000-0003-4312-7629  
Author Name: Dawei Zhang  
ORCID ID: 0000-0002-6546-6181  
Author Name: Sviatlana Lamaka  
ORCID ID: 0000-0002-0349-0899

## CRedit authorship contribution statement

**David A. Winkler:** Conceptualization, Data curation, Formal analysis, Project administration, Supervision, Writing – original draft, Writing – review & editing. **Anthony E. Hughes:** Writing – review & editing, Writing – original draft, Visualization, Supervision, Project administration, Data curation, Conceptualization. **Can Özkan:** Writing – review & editing, Writing – original draft. **Arjan Mol:**



Writing – review & editing, Writing – original draft, Investigation, Conceptualization. **Tim Würger**: Writing – review & editing, Writing – original draft, Visualization, Investigation, Formal analysis, Data curation. **Christian Feiler**: Writing – review & editing, Writing – original draft, Supervision, Formal analysis, Data curation. **Dawei Zhang**: Writing – review & editing, Writing – original draft. **Sviatlana V. Lamaka**: Writing – review & editing, Writing – original draft, Supervision, Project administration, Methodology, Formal analysis, Conceptualization.

### Declaration of competing interest

The authors declare that they have no known competing financial interests or personal relationships that could have appeared to influence the work reported in this paper.

### Acknowledgements

This work was partially supported by the funds provided by: the MMDi IDEA project (Modulators of Mg dissolution for biomedical applications) funded by Helmholtz-Zentrum Hereon; the AI2 project (Eyesight to AI: Discovery of efficient corrosion modulators via predictive machine learning models), funded by Helmholtz Association via Helmholtz AI project number ZT-I-PF-5-102; the Robust Design of Green Magnesium Dissolution Modulators project funded by the Deutscher Akademischer Austauschdienst (DAAD, German Academic Exchange Service) via Projektnummer 57511455; VIPCOAT (Virtual Open Innovation Platform for Active Protective Coatings Guided by Modelling and Optimisation) funded by Horizon 2020 research and innovation programme of the European Union by grant agreement no. 952903; Deutsche Forschungsgemeinschaft (DFG, German Research Foundation) – project number 535656357, OPTIMA (Identification of optimal corrosion inhibitors for bare and PEO coated magnesium alloy by combining machine learning and robotic testing).

### Data availability

No data was used for the research described in the article.

### References

- [2] Petrovic Z. Catastrophes caused by corrosion. *Vojnotehnicki glasnik* 2016;64:1048–64.
- [3] Raabe D, Tasan CC, Olivetti EA. Strategies for improving the sustainability of structural metals. *Nature* 2019;575:64–74.
- [4] Koch GH, Brongers MPH, Thompson NG, Virmani YP, Payer JH. Corrosion costs and preventative strategies in the United States. In: Department of Transport FHA, editor. Houston: NACE International; 2002.
- [5] NACE International EEB. IMPACT: International Measures of Prevention, Application, and Economics of Corrosion Technologies Study, <http://impact.nace.org/documents/Nace-International-Report.pdf>. 2016.
- [6] Iannuzzi M, Frankel GS. The carbon footprint of steel corrosion. *npj Mater Degrad* 2022;6:101.
- [7] Palanisamy G. Corrosion Inhibitors. In: Corrosion Inhibitors. IntechOpen; 2019. Available from: <https://doi.org/10.5772/intechopen.80542>.
- [8] Hughes AE. Conversion Coatings. In: Wandelt K, editor. *Encyclopedia of Interfacial Chemistry*. Oxford: Elsevier; 2018. p. 108–14.
- [9] Buchheit RG, Hughes AE. Chromate and Chromate-Free Coatings. In: Moosbrugger C, editor. *Corrosion: Fundamentals, Testing and Protection*. Materials Park, Oh, USA: ASM International; 2003. p. 720–35.
- [10] Sinko J. Challenges of chromate inhibitor pigments replacement in organic coatings. *Prog Org Coat* 2001;42:267–82.
- [11] Sax NI. *Dangerous Properties of Industrial Materials*. 5th ed. New York: Van Nostrand Reinhold Company; 1979.
- [12] LaPuma PT, Fox JM, Kimmel EC. Chromate concentration bias in primer paint particles. *Regul Toxicol Pharm* 2001;33:343–9.
- [13] den Braver-Sewradj SP, van Benthem J, Staal YCM, Ezendam J, Piersma AH, Hessel EVS. Occupational exposure to hexavalent chromium. Part II. Hazard assessment of carcinogenic effects. *Regul Toxicol Pharm* 2021;126:105045.
- [14] Hessel EVS, Staal YCM, Piersma AH, den Braver-Sewradj SP, Ezendam J. Occupational exposure to hexavalent chromium. Part I. Hazard assessment of non-cancer health effects. *Regul Toxicol Pharm* 2021;126.
- [15] Extensive Research, “Barium Chromate Market Size 2023 - 2030 Global Industrial Analysis, Key Geographical Regions, Market Share, Top Key Players, Product Types and Forecast”, LinkedIn, 31.10.2023. <https://www.linkedin.com/pulse/barium-chromate-market-size-2023-2030-global-industrial-f0hge/>, last accessed 06.06.2024, <https://archive.is/xRoK0> last accessed 24.06.2024.
- [16] S&P Global Commodity Insights, “Chromium Compounds, Inorganic”, Chemical Economics Handbook, December 2023, <https://www.spglobal.com/commodityinsights/en/ci/products/inorganic-chromium-chemical-economics-handbook.html>, last accessed 06.06.2024, <https://archive.is/EIOXS> last accessed 24.06.2024.
- [17] Visser P, Terry H, Mol JMC. Aerospace coatings. *Springer Ser Mater Sci* 2016;315–72.
- [18] Hughes AE, Mol JMC, Cole IS. The Cost and Availability of Rare Earth-Based Corrosion Inhibitors. In: Forsyth M, Hinton BRW, editors. *Rare Earth-based Corrosion Inhibitors*. Cambridge: Woodhead Publishing; 2014. p. 292–305.
- [19] O’Driscoll M. Supply Situation Report: Chromite in a tight spot. *Industrial Minerals*. September ed: Fastmarkets IM; 2011.
- [20] Papp JF. Chromium. United States Geological Survey (USGS). 2002.
- [21] Sorahan T. Cancer risks in chemical production workers exposed to 2-mercaptobenzothiazole. *Occup Environ Med* 2009;66:269.
- [22] Sillanpää M. Environmental Fate of EDTA and DTPA. In: Ware GW, editor. *Reviews of Environmental Contamination and Toxicology: Continuation of Residue Reviews*. New York, NY: Springer New York; 1997. p. 85–111.
- [23] Brycki BE, Kowalczyk I, Szulc A, Kaczerevska O, Pakiet M. Organic Corrosion Inhibitors. In: Mahmood A, editor. *Corrosion Inhibitors, Principles and Recent Applications*. Rijeka: IntechOpen; 2017. p. Ch. 1.
- [24] Fujita T, Winkler DA. Understanding the Roles of the “Two QSARs”. *J Chem Inf Model* 2016;56:269–74.
- [25] Winkler DA. Neural networks as robust tools in drug lead discovery and development. *Mol Biotechnol* 2004;27:139–67.
- [26] Winkler DA, Burden FR. Robust QSAR models from novel descriptors and Bayesian Regularised Neural Networks. *Mol Simulat* 2000;24:243–58.
- [27] Würger T, Feiler C, Musil F, Feldbauer GBV, Hoche D, Lamaka SV, et al. Data science based Mg corrosion engineering. *Front Mater* 2019;6:53.
- [28] Würger T, Mei D, Vaghefinazari B, Winkler DA, Lamaka SV, Zheludkevich ML, et al. Exploring structure-property relationships in magnesium dissolution modulators. *npj Mater Degrad* 2021;5:2.
- [29] Feiler C, Mei D, Vaghefinazari B, Würger T, Meissner RH, Luthringer-Feyerabend BJC, et al. In silico screening of modulators of magnesium dissolution. *Corros Sci* 2020;163:108245.

- [30] Schiessler EJ, Würger T, Lamaka SV, Meißner RH, Cyron CJ, Zheludkevich ML, et al. Predicting the inhibition efficiencies of magnesium dissolution modulators using sparse machine learning models. *npj Comput Mater* 2021;7:193.
- [31] Le TC, Winkler DA. A bright future for evolutionary methods in drug design. *ChemMedChem* 2015;10:1296–300.
- [32] Le TC, Winkler DA. Discovery and optimization of materials using evolutionary approaches. *Chem Rev* 2016;116:6107–32.
- [33] Winkler DA. Biomimetic molecular design tools that learn, evolve, and adapt. *Beilstein J Org Chem* 2017;13:1288–302.
- [34] Feiler C, Mei D, Luthringer-Feyerabend BJC, Lamaka SV, Zheludkevich ML. Rational design of effective Mg degradation modulators. *Corrosion* 2021;77:204–8.
- [35] Bohacek RS, McMartin C, Guida WC. The art and practice of structure-based drug design: A molecular modeling perspective. *Med Res Rev* 1996;16:3–50.
- [36] Micklus A, Muntner S. Biopharma deal-making in 2015: changing the pharma landscape. *Nat Rev Drug Discov* 2016;15:78–9.
- [37] Mullard A. The drug-maker's guide to the galaxy. *Nature* 2017;549:445–7.
- [38] Selekmán JA, Qiu J, Tran K, Stevens J, Rosso V, Simmons E, et al. High-throughput automation in chemical process development. *Ann Rev Chem Biomol Eng* 2017;8:525–47.
- [39] Devaraj NK, Finn MG. Introduction: click chemistry. *Chem Rev* 2021;121:6697–8.
- [40] Plutschack MB, Pieber B, Gilmore K, Seeberger PH. The Hitchhiker's guide to flow chemistry. *Chem Rev* 2017;117:11796–893.
- [41] Rasheed A, Farhat R. Combinatorial chemistry: a review. *Int J Pharm Sci Res* 2013;4:2502–16.
- [42] Singh MS, Chowdhury S, Koley S. Advances of azide-alkyne cycloaddition-click chemistry over the recent decade. *Tetrahedron* 2016;72:5257–83.
- [43] Kokalj A, Lozinsek M, Kapun B, Taheri P, Neupane S, Losada-Pérez P, et al. Simplistic correlations between molecular electronic properties and inhibition efficiencies: Do they really exist? *Corros Sci* 2021;179:108856.
- [44] He H, Garcia EA. Learning from imbalanced data. *IEEE Trans Knowl Data Eng* 2009;21:1263–84.
- [1] Kokalj A, Xie C, Milošev I, Crespo D. How relevant are molecular electronic parameters for predicting corrosion inhibition efficiency: imidazoles as corrosion inhibitors of Cu/Zr materials in NaCl solution. *Corros Sci* 2021;193:109900.
- [45] Mei D, Li Y, Tian Y, Zhang Q, Liu M, Zhu S, et al. The effect of selected corrosion inhibitors on localized corrosion of magnesium alloy: The expanded understanding of “inhibition efficiency”. *Corros Sci* 2024;226:111650.
- [46] Robinet L, Thickett D. A new methodology for accelerated corrosion testing. *Stud Conserv* 2003;48:263–8.
- [47] LeBozec N, Blandin N, Thierry D. Accelerated corrosion tests in the automotive industry: a comparison of the performance towards cosmetic corrosion. *Mater Corros* 2008;59:889–94.
- [48] Baldwin KR, Smith CJE. Accelerated corrosion tests for aerospace materials: current limitations and future trends. *Aircr Eng Aerosp Technol* 1999;71:239–44.
- [49] Dante J. Accelerated Dynamic Corrosion Test Method Development. SERDP WP-1673, 2017. Project report. 307 pp. <https://apps.dtic.mil/sti/tr/pdf/AD1053665.pdf>.
- [50] Dante J, Macha E, Fowler A, Matzdorf C, Rodrigues-Santiago V, Kovaleski K, et al. Accelerated Dynamic Corrosion Test Method Development SERDP WP-1673 / ESTCP; 2018.
- [51] Pennell SM, Sapper ED, Wallburg AG, Williams KS. Cyclic flexing salt-spray chamber and methods USA: Boeing Co 2018. US20180313745A1, US10436703B2.
- [52] Sapper ED, Bilodeau EN. Perturbed oscillatory kinetics electrochemistry systems and methods Boeing Co 2017. US20170212034A1 / US10145779B2.
- [53] Boerstler JT, Jokar M, Frankel GS. Corrosion of coated aluminium alloy 7075-T6 galvanic test assemblies, part I: Unscrubbed panels. *Corros Eng Sci Technol* 2020;55:268–80.
- [54] Russell J. Galvanic Corrosion Test Method for Coatings and Materials. ASETS Defense 2012: Workshop on Sustainable Surface Engineering for Aerospace and Defense August 27-30, 2012, San Diego, CA.
- [55] Valdez B, Ramirez J, Eliezer A, Schorr M, Ramos R, Salinas R. Corrosion assessment of infrastructure assets in coastal seas. *J Mar Eng Technol* 2016;15:124–34.
- [56] Valentinelli L, Vogelsang J, Ochs H, Fedrizzi L. Evaluation of barrier coatings by cycling testing. *Prog Org Coat* 2002;45:405–13.
- [57] ASTM. G 1-03(2017) e1. Standard Practice for Preparing, Cleaning, and Evaluating Corrosion Test Specimens. G0001-03R17E01. ASTM; 2017.
- [58] Song GL, Atrous A. Corrosion mechanisms of magnesium alloys. *Adv Eng Mater* 1999;1:11–33.
- [59] Wang C, Mei D, Wiese G, Wang LQ, Deng M, Lamaka SV, et al. High rate oxygen reduction reaction during corrosion of ultra-high-purity magnesium. *npj Mater Degrad* 2020;4:42.
- [60] Lamaka SV, Vaghefnazari B, Mei D, Petrauskas RP, Höche D, Zheludkevich ML. Comprehensive screening of Mg corrosion inhibitors. *Corros Sci* 2017;128:224–40.
- [61] Strelb M, Virtanen S. Real-time monitoring of atmospheric magnesium alloy corrosion. *J Electrochem Soc* 2019;166:C3001–9.
- [62] Kallip S, Bastos AC, Zheludkevich ML, Ferreira MGS. A multi-electrode cell for high-throughput SVET screening of corrosion inhibitors. *Corros Sci* 2010;52:3146–9.
- [63] Snihirova D, Taryba M, Lamaka SV, Montemor MF. Corrosion inhibition synergies on a model Al-Cu-Mg sample studied by localized scanning electrochemical techniques. *Corros Sci* 2016;112:408–17.
- [64] Coelho LB, Olivier MG. The inhibition efficiency of different species on AA2024/graphite galvanic coupling models depicted by SVET. *Corros Sci* 2018;136:292–303.
- [65] Ren C, Ma L, Zhang D, Li X, Mol A. High-throughput experimental techniques for corrosion research: A review. *Mater Genome Eng Adv* 2023;1:e20.
- [66] Chambers BD, Taylor SR, Kendig MW. Rapid discovery of corrosion inhibitors and synergistic combinations using high-throughput screening methods. *Corrosion* 2005;61:480–9.
- [67] Chambers BD, Taylor SR. The high throughput assessment of aluminium alloy corrosion using fluorometric methods. Part I - Development of a fluorometric method to quantify aluminium ion concentration. *Corros Sci* 2007;49:1584–96.
- [68] Chambers BD, Taylor SR. The high throughput assessment of aluminium alloy corrosion using fluorometric methods. Part II - A combinatorial study of corrosion inhibitors and synergistic combinations. *Corros Sci* 2007;49:1597–609.
- [69] Taylor SR, Chambers BD. The discovery of non-chromate corrosion inhibitors for aerospace alloys using high-throughput screening methods. *Corros Rev* 2007;25:571–90.
- [70] Taylor SR, Chambers BD. Identification and characterization of nonchromate corrosion inhibitor synergies using high-throughput methods. *Corrosion* 2008;64:255–70.
- [71] Garcia SJ, Muster TH, Ozkanat O, Sherman N, Hughes AE, Terryn H, et al. The influence of pH on corrosion inhibitor selection for 2024-T3 aluminium alloy assessed by high-throughput multielectrode and potentiodynamic testing. *Electrochim Acta* 2010;55:2457–65.
- [72] Muster TH, Hughes AE, Furman SA, Harvey T, Sherman N, Hardin S, et al. A rapid screening multi-electrode method for the evaluation of corrosion inhibitors. *Electrochim Acta* 2009;54:3402–11.
- [73] Winkler DA, Breedon M, White P, Hughes AE, Sapper ED, Cole I. Using high throughput experimental data and in silico models to discover alternatives to toxic chromate corrosion inhibitors. *Corros Sci* 2016;106:229–35.
- [74] White PA, Smith GB, Harvey TG, Corrigan PA, Glenn MA, Lau D, et al. A new high-throughput method for corrosion testing. *Corros Sci* 2012;58:327–31.
- [75] White PA, Hughes AE, Furman SA, Sherman N, Corrigan PA, Glenn MA, et al. High-throughput channel arrays for inhibitor testing: Proof of concept for AA2024-T3. *Corros Sci* 2009;51:2279–90.
- [76] Zabula AV, Dey S, Robinson JR, Cheisson T, Higgins RF, Bhargava G, et al. Screening of molecular lanthanide corrosion inhibitors by a high-throughput method. *Corros Sci* 2020;165:108377.
- [77] Mei D, Lamaka SV, Feiler C, Zheludkevich ML. The effect of small-molecule bio-relevant organic components at low concentration on the corrosion of commercially pure Mg and Mg-0.8Ca alloy: An overall perspective. *Corros Sci* 2019;153:258–71.
- [78] He J, Bahr J, Chisholm BJ, Li J, Chen Z, Balbyshev SN, et al. Combinatorial materials research applied to the development of new surface coatings X: A high-throughput electrochemical impedance spectroscopy method for screening organic coatings for corrosion inhibition. *J Comb Chem* 2008;10:704–13.
- [79] Shi P, Li B, Huo J, Wen L. A smart high-throughput experiment platform for materials corrosion study. *Sci Program* 2016.

- [80] Strebl M, Bruns M, Virtanen S. Editors' Choice—Respirometric in Situ Methods for Real-Time Monitoring of Corrosion Rates: Part I. Atmospheric Corrosion. *Journal of The Electrochemical Society*. 2020;167:021510.
- [81] Silva EL, Lamaka SV, Mei D, Zheludkevich ML. The reduction of dissolved oxygen during magnesium corrosion. *ChemistryOpen* 2018;7:664–8.
- [82] Ngo TD, Kashani A, Imbalzano G, Nguyen KTQ, Hui D. Additive manufacturing (3D printing): A review of materials, methods, applications and challenges. *Compos B Eng* 2018;143:172–96.
- [83] Barui S, Mandal S, Basu B. Thermal inkjet 3D powder printing of metals and alloys: Current status and challenges. *Curr Opin Biomed Eng* 2017;2:116–23.
- [84] Chen S, Tong Y, Liaw PK. Additive Manufacturing of High-Entropy Alloys: A Review. *Entropy* 2018;20:937.
- [85] Haghdadi N, Laleh M, Moyle M, Primig S. Additive manufacturing of steels: a review of achievements and challenges. *J Mater Sci* 2021;56:64–107.
- [86] Hoefler K, Nitsche A, Abtoss KG, Ertugrul G, Haelsig A, Mayr P. Multi-material additive manufacturing by 3D plasma metal deposition for graded structures of super duplex alloy 1.4410 and the austenitic corrosion resistant alloy 1.4404. *JOM* 2019;71:1554–9.
- [87] Lewandowski JJ, Seifi M. Metal additive manufacturing: a review of mechanical properties. In: Clarke DR, editor. *Annual Review of Materials Research*, Vol 46 2016. p. 151-86.
- [88] Murr LE, Gaytan SM, Ramirez DA, Martinez E, Hernandez J, Amato KN, et al. Metal fabrication by additive manufacturing using laser and electron beam melting technologies. *J Mater Sci Technol* 2012;28:1–14.
- [89] Rodrigues TA, Duarte V, Miranda RM, Santos TG, Oliveira JP. Current status and perspectives on wire and arc additive manufacturing (WAAM). *Materials* 2019;12:1121.
- [90] Ornek C. Additive manufacturing - a general corrosion perspective. *Corros Eng Sci Technol* 2018;53:531–5.
- [91] Laleh M, Sadeghi E, Revilla RI, Chao Q, Haghdadi N, Hughes AE, et al. Heat treatment for metal additive manufacturing. *Prog Mater Sci* 2023;133:101051.
- [92] Wang YM, Voisin T, McKeown JT, Ye J, Calta NP, Li Z, et al. Additively manufactured hierarchical stainless steels with high strength and ductility. *Nat Mater* 2018;17:63–71.
- [93] Shin W-S, Son B, Song W, Sohn H, Jang H, Kim Y-J, et al. Heat treatment effect on the microstructure, mechanical properties, and wear behaviors of stainless steel 316L prepared via selective laser melting. *Mater Sci Eng A* 2021;806:140805.
- [94] Nguyen QB, Zhu Z, Ng FL, Chua BW, Nai SML, Wei J. High mechanical strengths and ductility of stainless steel 304L fabricated using selective laser melting. *J Mater Sci Technol* 2019;35:388–94.
- [95] Ronneberg T, Davies CM, Hooper PA. Revealing relationships between porosity, microstructure and mechanical properties of laser powder bed fusion 316L stainless steel through heat treatment. *Mater Des* 2020;189:108481.
- [96] Suryawanshi J, Prashanth KG, Ramamurty U. Mechanical behavior of selective laser melted 316L stainless steel. *Mater Sci Eng A* 2017;696:113–21.
- [97] Saeidi K, Gao X, Zhong Y, Shen ZJ. Hardened austenite steel with columnar sub-grain structure formed by laser melting. *Mater Sci Eng A* 2015;625:221–9.
- [98] Bertsch KM, Meric de Bellefont G, Kuehl B, Thoma DJ. Origin of dislocation structures in an additively manufactured austenitic stainless steel 316L. *Acta Mater* 2020;199:19–33.
- [99] Skylar-Scott MA, Mueller J, Visser CW, Lewis JA. Voxellated soft matter via multimaterial multinozzle 3D printing. *Nature* 2019;575:330–5.
- [100] Reiser A, Lindén M, Rohner P, Marchand A, Galinski H, Sologubenko AS, et al. Multi-metal electrohydrodynamic redox 3D printing at the submicron scale. *Nat Commun* 2019;10:1853.
- [101] Hughes AE, MacRae C, Wilson N, Torpy A, Muster TH, Glenn AM. Sheet AA2024-T3: A new investigation of microstructure and composition. *Surf Interface Anal* 2010;42:334–8.
- [102] Chen GS, Gao M, Wei RP. Microconstituent-induced pitting corrosion in aluminum alloy 2024-T3. *Corrosion* 1996;52:8–15.
- [103] Bucci RJ, Warren CJ, Starke Jr EA. Need for new materials in aging aircraft structures. *J Aircr* 2000;37:122–9.
- [104] Birbilis N, Zhu YM, Kairy SK, Glenn MA, Nie JF, Morton AJ, et al. A closer look at constituent induced localised corrosion in Al-Cu-Mg alloys. *Corros Sci* 2016;113:160–71.
- [105] Boag A, Hughes AE, Wilson NC, Torpy A, MacRae CM, Glenn AM, et al. How complex is the microstructure of AA2024-T3? *Corros Sci* 2009;51:1565–8.
- [106] Lacroix L, Ressler L, Blanc C, Mankowski G. Combination of AFM, SKPFM, and SIMS to study the corrosion behavior of S-phase particles in AA2024-T351. *J Electrochem Soc* 2008;155:C131–7.
- [107] Lacroix L, Ressler L, Blanc C, Mankowski G. Statistical study of the corrosion behavior of Al2CuMg intermetallics in AA2024-T351 by SKPFM. *J Electrochem Soc* 2008;155:C8–15.
- [108] Cawley NR, Harlow DG. Spatial statistics of particles and corrosion pits in 2024-T3 aluminium alloy. *J Mater Sci* 1996;31:5127–34.
- [109] Mao Y, Gokhale AM, Harris J. Computer simulations of realistic microstructures of coarse constituent particles in a hot-rolled aluminum alloy. *Comput Mater Sci* 2006;37:543–56.
- [110] Chen FF, Cole I, Hughes AE, Glenn AM, Sapper E, Osborne J. Microstructure characterisation and reconstruction of intermetallic particles. *Mater Corros* 2014;65:664–9.
- [111] Boesenbergh U, Ryan CG, Kirkham R, Siddons DP, Alfeld M, Garrevoet J, et al. Fast X-ray microfluorescence imaging with submicrometer-resolution integrating a Maia detector at beamline P06 at PETRA III. *J Synchrotron Radiat* 2016;23:1550–60.
- [112] Choudhary K, DeCost B, Chen C, Jain A, Tavazza F, Cohn R, et al. Recent advances and applications of deep learning methods in materials science. *npj Comput Mater* 2022;8:59.
- [113] Raymond JL, Awale M. Exploring chemical space for drug discovery using the chemical universe database. *ACS Chem Neurosci* 2012;3:649–57.
- [114] Li JQ, Ballmer SG, Gillis EP, Fujii S, Schmidt MJ, Palazzolo AME, et al. Synthesis of many different types of organic small molecules using one automated process. *Science* 2015;347:1221–6.
- [115] Service RF. The synthesis machine. *Science* 2015;347:1190–3.
- [116] LeCun Y, Bengio Y, Hinton G. Deep learning. *Nature* 2015;521:436–44.
- [117] Ma JS, Sheridan RP, Liaw A, Dahl GE, Svetnik V. Deep neural nets as a method for quantitative structure-activity relationships. *J Chem Inf Model* 2015;55:263–74.
- [118] Walters FH. Use of statistical mixture designs to evaluate ternary mixtures of organics as corrosion-inhibitors. *Anal Lett* 1990;23:1783–90.
- [119] Le T, Epa VC, Burden FR, Winkler DA. Quantitative structure-property relationship modeling of diverse materials properties. *Chem Rev* 2012;112:2889–919.
- [120] Al-Amiery AA, Isahak WN, Al-Azzawi WK. Corrosion inhibitors: natural and synthetic organic inhibitors. *Lubricants* 2023;11:174.
- [121] Kokalj A. Corrosion inhibitors: physisorbed or chemisorbed? *Corros Sci* 2022;196:109939.
- [122] Dariva CG, Galio AF. Corrosion inhibitors – principles, mechanisms and applications. In: Aliofkhaizraei M, editor. *Developments in Corrosion Protection*. Rijeka: IntechOpen; 2014.
- [123] Kovačević N, Kokalj A. Chemistry of the interaction between azole type corrosion inhibitor molecules and metal surfaces. *Mater Chem Phys* 2012;137:331–9.
- [124] Altaf F, Qureshi R, Ahmed S. Surface protection of copper by azoles in borate buffers-voltammetric and impedance analysis. *J Electroanal Chem* 2011;659:134–42.
- [125] Otmacic H, Stupnisek-lisac E, Takenouti H. The influence of pH value on the efficiency of imidazole based corrosion inhibitors of copper. *Corros Sci* 2010;52:398–405.
- [126] Finšgar M, Lesar A, Kokalj A, Milošev I. A comparative electrochemical and quantum chemical calculation study of BTAH and BTAOH as copper corrosion inhibitors in near neutral chloride solution. *Electrochim Acta* 2008;53:8287–97.
- [127] Taheri P, Milo I, Kokalj A. On the importance of time-resolved electrochemical evaluation in corrosion inhibitor-screening studies. *npj Mater Degrad* 2020;4:12.
- [128] Ma H, Chen S, Yin B. Impedance spectroscopic study of corrosion inhibition of copper by surfactants in the acidic solutions. 2003;45:867-82.
- [129] Tavakoli H, Shahrabi T, Hosseini MG. Synergistic effect on corrosion inhibition of copper by sodium dodecylbenzenesulphonate (SDBS) and 2-mercaptobenzoxazole. *Mater Chem Phys* 2008;109:281–6.

- [130] Vaghefnazari B, Lamaka SV, Gazenbiller E, Yasakau K, Blawert C, Serdechnova M, et al. Corrosion inhibition of decylphosphonate on bare and PEO-coated Mg alloy. *Corros Sci* 2024;226:111651.
- [131] Arancibia A, Henriquez-Roman J, Páez MA, Padilla-Campos L, Zagal JH, Costamagna J, et al. Influence of 5-chloro and 5-methyl benzotriazole on the corrosion of copper in acid solution: an experimental and a theoretical approach. *J Solid State Electrochem* 2006;10:894–904.
- [132] Singh MM, Rastogi RB, Upadhyay BN, Yadav M. Thiosemicarbazide, phenyl isothiocyanate and their condensation product as corrosion inhibitors of copper in aqueous chloride solutions. *Mater Chem Phys* 2003;80:283–93.
- [133] Szakálos P, Hultquist G, Wikmark G. Corrosion of copper by water. *Electrochem Solid St* 2007;10:C63–7.
- [134] Mihajlović MBP, Milan MA. Copper corrosion inhibitors. Period 2008–2014. A review. *Int J Electrochem Sci*. 2015;10:1027–53.
- [135] Antonijević MM, Petrović MB. Copper corrosion inhibitors. A review. *Int J Electrochem Sci* 2008;3:1–28.
- [136] Antonijević MM, Milić SM, Petrović MB. Films formed on copper surface in chloride media in the presence of azoles. *Corros Sci* 2009;51:1228–37.
- [137] Finšgar M, Milošev I. Inhibition of copper corrosion by 1,2,3-benzotriazole: A review. *Corros Sci* 2010;52:2737–49.
- [138] Verma C, Ebenso EE, Quraishi MA. Corrosion inhibitors for ferrous and non-ferrous metals and alloys in ionic sodium chloride solutions: A review. *J Mol Liq* 2017;248:927–42.
- [139] Kuznetsov YL. Triazoles as a class of multifunctional corrosion inhibitors. A review. part I. 1,2,3-benzotriazole and its derivatives. Copper, zinc and their alloys. *Int Jo Corros Scale Inhibition* 2018;7:271–307.
- [140] Fateh A, Aliofkhaezai M, Rezvanian AR. Review of corrosive environments for copper and its corrosion inhibitors. *Arab J Chem* 2020;13:481–544.
- [141] Hultquist G, Szakálos P, Graham MJ, Belonoshko AB, Sproule GI, Gräsjö L, et al. Water corrodes copper. *Catal Lett* 2009;132:311–6.
- [142] Edwards M, Ferguson JF, Reiber SH. The pitting corrosion of copper. *J Am Water Works Assoc* 1994;86:74–90.
- [143] Hollander O, May RC. Chemistry of azole copper corrosion inhibitors in cooling water. *Corrosion* 1985;41:39–45.
- [144] Ye XR, Xin XQ, Zhu JJ, Xue ZL. Coordination compound films of 1-phenyl-5-mercaptopotetrazole on copper surface. *Appl Surf Sci* 1998;135:307–17.
- [145] Balcunaitė E, Petrasauskiene N, Alaburdaite R, Jakubauskas G, Paluckiene E. Formation and properties of mixed copper sulfide (Cu<sub>2</sub>S) layers on polypropylene. *Surf Interfaces* 2020;21:100801.
- [146] Frignani A, Tommesani L, Brunoro G, Monticelli C, Fogagnolo M. Influence of the alkyl chain on the protective effects of 1,2,3-benzotriazole towards copper corrosion. Part I: Inhibition of the anodic and cathodic reactions. *Corros Sci* 1999;41:1205–15.
- [147] Huynh N, Bottle SE, Notoya T, Schweinsberg DP. Inhibition of copper corrosion by coatings of alkyl esters of carboxybenzotriazole. *Corros Sci* 2002;44:2583–96.
- [148] Bartley J, Huynh N, Bottle SE, Flitt H, Notoya T, Schweinsberg DP. Computer simulation of the corrosion inhibition of copper in acidic solution by alkyl esters of 5-carboxybenzotriazole. *Corros Sci* 2003;45:81–96.
- [149] Tan YS, Srinivasan MP, Pehkonen SO, Chooi SYM. Effects of ring substituents on the protective properties of self-assembled benzenethiols on copper. *Corros Sci* 2006;48:840–62.
- [150] Kokalj A, Peljhan S, Finšgar M, Milošev I. What determines the inhibition effectiveness of ATA, BTAH, and BTAOH corrosion inhibitors on copper? *J Am Chem Soc* 2010;132:16657–68.
- [151] Gustinčić D, Kokalj A. A DFT study of adsorption of imidazole, triazole, and tetrazole on oxidized copper surfaces: Cu<sub>2</sub>O(111) and Cu<sub>2</sub>O(111)-w/o-CuCUS. *PCCP* 2015;17:28602–15.
- [152] Kokalj A, Gustinčić D, Poberžnik M, Lozinšek M. New insights into adsorption bonding of imidazole: A viable C2–H bond cleavage on copper surfaces. *Appl Surf Sci* 2019;479:463–8.
- [153] Kovačević N, Kokalj A. DFT study of interaction of azoles with Cu(111) and Al(111) surfaces: role of azole nitrogen atoms and dipole-dipole interactions. *J Phys Chem C* 2011;115:24189–97.
- [154] Kovacevic N, Kokalj A. The relation between adsorption bonding and corrosion inhibition of azole molecules on copper. *Corros Sci* 2013;73:7–17.
- [155] Lakshminarayanan V, Kannan R, Rajagopalan SR. Cyclic voltammetric behavior of certain copper-azole systems using carbon paste electrodes. *J Electroanal Chem* 1994;364:79–86.
- [156] Kovačević N, Kokalj A. Analysis of molecular electronic structure of imidazole- and benzimidazole-based inhibitors: A simple recipe for qualitative estimation of chemical hardness. *Corros Sci* 2011;53:909–21.
- [157] Milošev I, Kovačević N, Kovač J, Kokalj A. The roles of mercapto, benzene and methyl groups in the corrosion inhibition of imidazoles on copper: I. Experimental characterization. *Corros Sci* 2015;98:107–18.
- [158] Kovačević N, Milošev I, Kokalj A. The roles of mercapto, benzene, and methyl groups in the corrosion inhibition of imidazoles on copper: II. Inhibitor-copper bonding. *Corros Sci* 2015;98:457–70.
- [159] Sherif EM, Park SM. Effects of 2-amino-5-ethylthio-1,3,4-thiadiazole on copper corrosion as a corrosion inhibitor in aerated acidic pickling solutions. *Electrochim Acta* 2006;51:6556–62.
- [160] Sherif EM. Effects of 2-amino-5-(ethylthio)-1,3,4-thiadiazole on copper corrosion as a corrosion inhibitor in 3% NaCl solutions. *Appl Surf Sci* 2006;252:8615–23.
- [161] Sherif EM, Park SM. 2-Amino-5-ethyl-1,3,4-thiadiazole as a corrosion inhibitor for copper in 3.0% NaCl solutions. *Corros Sci* 2006;48:4065–79.
- [162] Baeza H, Guzmán M, Ortega P, Vera L. Corrosion Inhibition of copper in 0.5 M hydrochloric acid by 1,3,4-thiadiazole-2,5-dithiol. *J Chil Chem Soc* 2003;48:23–6.
- [163] Wu X, Wiame F, Maurice V, Marcus P. Molecular scale insights into interaction mechanisms between organic inhibitor film and copper. *npj Mater Degrad* 2021;5:1–8.
- [164] Ohsawa M, Suétaka W. Spectro-electrochemical studies of the corrosion inhibition of copper by mercaptobenzothiazole. *Corros Sci* 1979;19:709–22.
- [165] Marconato JC, Bulhões LO, Temperin ML. A spectroelectrochemical study of the inhibition of the electrode process on copper by 2-mercaptobenzothiazole in ethanolic solutions. *Electrochim Acta* 1997;43:771–80.
- [166] Chiter F, Costa D, Maurice V, Marcus P. Chemical interaction, self-ordering and corrosion inhibition properties of 2-mercaptobenzothiazole monolayers: DFT atomistic modelling on metallic copper. *Corros Sci* 2022;209:110658.
- [167] Sherif EM, Erasmus RM, Comins JD. Effects of 3-amino-1,2,4-triazole on the inhibition of copper corrosion in acidic chloride solutions. *J Colloid Interface Sci* 2007;311:144–51.
- [168] Sherif EM, Erasmus RM, Comins JD. Corrosion of copper in aerated synthetic sea water solutions and its inhibition by 3-amino-1,2,4-triazole. *J Colloid Interface Sci* 2007;309:470–7.
- [169] El Issami S, Bazzi L, Mihit M, Hammouti B, Kertit S, Addi EA, et al. Triazolic compounds as corrosion inhibitors for copper in hydrochloric acid. *Pigm Resin Technol* 2007;36:161–8.
- [170] Lalitha A, Ramesh S, Rajeswari S. Surface protection of copper in acid medium by azoles and surfactants. *Electrochim Acta* 2005;51:47–55.
- [171] Awad MK, Mustafa MR, Elnga MMA. Computational simulation of the molecular structure of some triazoles as inhibitors for the corrosion of metal surface. *J Mol Struct (Theochem)* 2010;959:66–74.
- [172] Sherif EM, El Shamy AM, Ramla MM, El Nazhawy AOH. 5-(Phenyl)-4H-1,2,4-triazole-3-thiol as a corrosion inhibitor for copper in 3.5% NaCl solutions. *Mater Chem Phys* 2007;102:231–9.
- [173] Ramesh S, Rajeswari S. Evaluation of inhibitors and biocide on the corrosion control of copper in neutral aqueous environment. *Corros Sci* 2005;47:151–69.
- [174] Jiang Y, Adams JB. First principle calculations of benzotriazole adsorption onto clean Cu(111). *Surf Sci* 2003;529:428–42.
- [175] Peljhan S, Kokalj A. DFT study of gas-phase adsorption of benzotriazole on Cu(111), Cu(100), Cu(110), and low coordinated defects thereon. *Phys Chem Chem Phys* 2011;13:20408–17.
- [176] Peljhan S, Koller J, Kokalj A. The effect of surface geometry of copper on adsorption of benzotriazole and Cl. Part I. *J Phys Chem C* 2014;118:933–43.
- [177] Kokalj A. Ab initio modeling of the bonding of benzotriazole corrosion inhibitor to reduced and oxidized copper surfaces. *Faraday Discuss* 2015;180:415–38.
- [178] Kokalj A, Peljhan S. Density functional theory study of adsorption of benzotriazole on Cu<sub>2</sub>O surfaces. *J Phys Chem C* 2015;119:11625–35.

- [179] Kokalj A, Peljhan S, Koller J. The effect of surface geometry of copper on dehydrogenation of benzotriazole. Part II. *J Phys Chem C* 2014;118:944–54.
- [180] Aruchamy A, Fujishima A, Ibrahim A, Loo BH. A surface-enhanced Raman spectroscopic study of benzotriazole and 6-tolyltriazole corrosion inhibitors on copper electrodes in alkaline solutions. *J Electroanal Chem Interfacial Electrochem* 1990;281:299–304.
- [181] Brusic V, Frisch MA, Eldridge BN, Novak FP, Kaufman FB, Rush BM, et al. Copper corrosion with and without inhibitors. *J Electrochem Soc* 1991;138:2253–9.
- [182] Tromans D, Soc JE, Tromans D. Aqueous potential - pH equilibria in copper - benzotriazole systems aqueous potential-pH equilibria in copper-benzotriazole systems. *J Electrochem Soc* 1998;145:42–5.
- [183] Törnkvist C, Thierry D, Bergman J, Liedberg B, Leygraf C. Methyl substitution in benzotriazole and its influence on surface structure and corrosion inhibition. *J Electrochem Soc* 1989;136:58–64.
- [184] Loo BH, Ibrahim A, Emerson MT. Analysis of surface coverage of benzotriazole and 6-tolyltriazole mixtures on copper electrodes from surface-enhanced Raman spectra. *Chem Phys Lett* 1998;287:449–54.
- [185] Aramaki K, Kiuchi T, Sumiyoshi T, Nishihara H. Surface enhanced Raman scattering and impedance studies on the inhibition of copper corrosion in sulphate solutions by 5-substituted benzotriazoles. *Corros Sci* 1991;32:593–607.
- [186] Elia A, De Wael K, Dowsett M, Adriaens A. Electrochemical deposition of a copper carboxylate layer on copper as potential corrosion inhibitor. *J Solid State Electrochem* 2012;16:143–8.
- [187] Hefter GT, North NA, Tan SH. Organic corrosion inhibitors in neutral solutions; Part 1 - inhibition of steel, copper, and aluminum by straight chain carboxylates. *Corrosion* 1997;53:657–67.
- [188] Quartarone G, Battilana M, Bonaldo L, Tortato T. Investigation of the inhibition effect of indole-3-carboxylic acid on the copper corrosion in 0.5 M H<sub>2</sub>SO<sub>4</sub>. *Corros Sci* 2008;50:3467–74.
- [189] Chang FH, Chen TY, Lee SH, Chen YH, Chen YJ, Lin JL. Corrosion inhibition of copper particles on ITO with 1,2,4-triazole-3-carboxylic acid. *Surf Interfaces* 2018;10:162–9.
- [190] Žerjav G, Milošev I. Carboxylic acids as corrosion inhibitors for Cu, Zn and brasses in simulated urban rain. *Int J Electrochem Sci* 2014;9:2696–715.
- [191] Damous M, Allal H, Belhocine Y, Maza S, Merazig H. Quantum chemical exploration on the inhibition performance of indole and some of its derivatives against copper corrosion. *J Mol Liq* 2021;340:117136 -.
- [192] Agafonkina MO, Kuznetsov YI, Andreeva NP. Inhibitor properties of carboxylates and their adsorption on copper from aqueous solutions. *Russ J Phys Chem A* 2015;89:1070–6.
- [193] Kuznetsov YI. Organic corrosion inhibitors: where are we now? A review. Part II. Passivation and the role of chemical structure of carboxylates. *Int J Corros Scale Inhib* 2016;5:282–318.
- [194] Kuznetsov YI, Agafonkina MO, Andreeva NP, Kazansky LP. Adsorption of dimegin and inhibition of copper dissolution in aqueous solutions. *Corros Sci* 2015;100:535–43.
- [195] Kumar D, Jain N, Jain V, Rai B. Amino acids as copper corrosion inhibitors: A density functional theory approach. *Appl Surf Sci* 2020;514:145905 -.
- [196] Barouni K, Bazzi L, Salghi R, Mihit M, Hammouti B, Albourine A, et al. Some amino acids as corrosion inhibitors for copper in nitric acid solution. *Mater Lett* 2008;62:3325–7.
- [197] Zhang DQ, Cai QR, Gao LX, Lee KY. Effect of serine, threonine and glutamic acid on the corrosion of copper in aerated hydrochloric acid solution. *Corros Sci* 2008;50:3615–21.
- [198] Zhang DQ, Cai QR, He XM, Gao LX, Zhou GD. Inhibition effect of some amino acids on copper corrosion in HCl solution. *Mater Chem Phys* 2008;112:353–8.
- [199] Amin MA, Khaled KF. Copper corrosion inhibition in O<sub>2</sub>-saturated H<sub>2</sub>SO<sub>4</sub> solutions. *Corros Sci* 2010;52:1194–204.
- [200] Barouni K, Kassale A, Bazzi L, Salghi R, Hammouti B, Albourine A, et al. Inhibition of corrosion of copper in nitric acid solution by four amino acids. *Res Chem Intermed* 2014;40:991–1002.
- [201] Matos JB, Pereira LP, Agostinho SML, Barcia OE, Cordeiro GGO, D'Elia E. Effect of cysteine on the anodic dissolution of copper in sulfuric acid medium. *J Electroanal Chem* 2004;570:91–4.
- [202] Moretti G, Guidi F. Tryptophan as copper corrosion inhibitor in 0.5 M aerated sulfuric acid. *Corros Sci* 2002;44:1995–2011.
- [203] Zhang DQ, Xie B, Gao LX, Joo HG, Lee KY. Inhibition of copper corrosion in acidic chloride solution by methionine combined with cetrimonium bromide/cetylpyridinium bromide. *J Appl Electrochem* 2011;41:491–8.
- [204] Zhang DQ, Hj Z, Zhang L, Liu P, Gao LX. Influence of oxygen and oxidant on corrosion inhibition of cysteine self-assembled membranes for copper. *Colloids Surf A Physicochem Eng Asp* 2014;445:105–10.
- [205] Scendo M. Corrosion inhibition of copper by purine or adenine in sulphate solutions. *Corros Sci* 2007;49:3953–68.
- [206] Scendo M. Inhibition of copper corrosion in sodium nitrate solutions with nontoxic inhibitors. *Corros Sci* 2008;50:1584–92.
- [207] Scendo M. The effect of purine on the corrosion of copper in chloride solutions. *Corros Sci* 2007;49:373–90.
- [208] Dafali A, Hammouti B, Mokhlisse R, Kertit S. Substituted uracils as corrosion inhibitors for copper in 3% NaCl solution. *Corros Sci* 2003;45:1619–30.
- [209] Hong Y, S-SL G, Hong Y, Roy D, Babu SV. Ammonium dodecyl sulfate as a potential corrosion inhibitor surfactant for electrochemical mechanical planarization of copper ammonium dodecyl sulfate as a potential corrosion inhibitor surfactant for electrochemical mechanical planarization of copper. *Electrochem Solid St* 2005;8:G297.
- [210] Scendo M, Uznanska J. The effect of ionic liquids on the corrosion inhibition of copper in acidic chloride solutions. *Int J Corros* 2011;718626.
- [211] Scendo M, Uznanska J. Inhibition effect of 1-butyl-4-methylpyridinium tetrafluoroborate on the corrosion of copper in phosphate solutions. *Int J Corros* 2011; 761418.
- [212] Vastag G, Shaban A, Vranes M, Tot A, Belic S, Gadzuric S. Influence of the N-3 alkyl chain length on improving inhibition properties of imidazolium-based ionic liquids on copper corrosion. *J Mol Liq* 2018;264:526–33.
- [213] Espinosa T, Sanes J, Jiménez AE, Bermúdez MD. Surface interactions, corrosion processes and lubricating performance of protic and aprotic ionic liquids with OFHC copper. *Appl Surf Sci* 2013;273:578–97.
- [214] More MS, Joshi PG, Mishra YK, Khanna PK. Metal complexes driven from Schiff bases and semicarbazones for biomedical and allied applications: a review. *Mater Today Chem* 2019;14:100195 -.
- [215] Ma H, Chen S, Niu L, Zhao S, Li S, Li D. Inhibition of copper corrosion by several Schiff bases in aerated halide solutions. *J Appl Electrochem* 2002;32:65–72.
- [216] Ehteshamzadeh M, Shahrabi T, Hosseini M. Innovation in acid pickling treatments of copper by characterizations of a new series of Schiff bases as corrosion inhibitors. *Anti-Corros Methods Mater* 2006;53:296–302.
- [217] De Souza FS, Giacomelli C, Gonçalves RS, Spinelli A. Adsorption behavior of caffeine as a green corrosion inhibitor for copper. *Mater Sci Eng C* 2012;32: 2436–44.
- [218] Fallavena T, Antonow M, Gonçalves RS. Caffeine as non-toxic corrosion inhibitor for copper in aqueous solutions of potassium nitrate. *Appl Surf Sci* 2006;253: 566–71.
- [219] Messaoudi H, Djazi F, Litim M, Keskin B, Slimane M, Bekhiti D. Surface analysis and adsorption behavior of caffeine as an environmentally friendly corrosion inhibitor at the copper/aqueous chloride solution interface. *J Adhes Sci Technol* 2020;34:2216–44.
- [220] Hadisaputra S, Purwoko AA, Savalas LRT, Prasetyo N, Yuanita E, Hamdiani S. Quantum chemical and monte carlo simulation studies on inhibition performance of caffeine and its derivatives against corrosion of copper. *Coatings* 2020;10:1–17.
- [221] Abd-El-Nabey BA, Abdel-Gaber AH, Ali MES, Khamis E, El-Housseiny S. Inhibitive action of cannabis plant extract on the corrosion of copper in 0.5 M H<sub>2</sub>SO<sub>4</sub>. *Int J Electrochem Sci* 2013;8:7124–37.
- [222] Sangeetha TV, Fredimoses M. Inhibition of mild copper metal corrosion in HNO<sub>3</sub> Medium by acid extract of *Azadirachta Indica* seed. *J Chem* 2011;8:S1–6.
- [223] Al-Qudah MA. Inhibition of copper corrosion by flavonoids in nitric acid. *J Chem* 2011;8:326–32.
- [224] Al Jahdaly BA, Maghraby YR, Ibrahim AH, Shouier KR, Taher MM, El-Shabasy RM. Role of green chemistry in sustainable corrosion inhibition: a review on recent developments. *Mater Today Sustain* 2022;100242.

- [225] Metal Handbook, American Society for Metals, ASM Materials Engineering Dictionary, ASM International, Ed. J.R.Davis, ISBN: 978-0-87170-447-1. 7th ed. Ohio 1992.
- [226] Suzuki S. Characterization of formation of ferrous and ferric oxides in aqueous solution from a multidisciplinary viewpoint. *ISIJ Int* 2022;62:800–10.
- [227] Nishimoto M, Muto I, Sugawara Y. Comparison of the pitting corrosion resistance of bainite and martensite in Fe-0.4C-1.5Si-2Mn Steel. *ISIJ Int* 2024;64:497–501.
- [228] Liu P, Zhang Q-H, Watanabe Y, Shoji T, Cao F-H. A critical review of the recent advances in inclusion-triggered localized corrosion in steel. *npj Mater Degrad* 2022;6:81.
- [229] Honeycombe RWK. *Steels: Microstructure and Properties, Metallurgy and Materials Science Series London: Edward Arnold; 1990.*
- [230] Aslam R, Serdaroglu G, Zehra S, Kumar Verma D, Aslam J, Guo L, et al. Corrosion inhibition of steel using different families of organic compounds: Past and present progress. *J Mol Liq* 2022;348:118373.
- [231] Misawa T, Hashimoto K, Shimodaira S. The mechanism of formation of iron oxide and oxyhydroxides in aqueous solutions at room temperature. *Corros Sci* 1974;14:131–49.
- [232] Xiao K, Dong C-f, Li X-g, Wang F-m. Corrosion products and formation mechanism during initial stage of atmospheric corrosion of carbon steel. *J Iron Steel Res Int* 2008;15:42–8.
- [233] Harvey TG, Hardin SG, Hughes AE, Muster TH, White PA, Markley TA, et al. The effect of inhibitor structure on the corrosion of AA2024 and AA7075. *Corros Sci* 2011;53:2184–90.
- [234] Mei L, Liao L, Wang Z, Xu C. Interactions between phosphoric/tannic acid and different forms of FeOOH. *Adv Mater Sci Eng* 2015;2015:e250836.
- [235] Ono S, Asoh H. Mechanism of hot water sealing of anodic films formed on aluminum. *Corros Sci* 2021;181:109221.
- [236] Mazumder MAJ, Al-Muallem HA, Faiz M, Ali SA. Design and synthesis of a novel class of inhibitors for mild steel corrosion in acidic and carbon dioxide-saturated saline media. *Corros Sci* 2014;87:187–98.
- [237] Shehnazdeep PB. A study on effectiveness of inorganic and organic corrosion inhibitors on rebar corrosion in concrete: A review. *Mater Today: Proc* 2022;65:1360–6.
- [238] El-Taib Heakl F, Tantawy NS, Shehata OS. Influence of cerium (III) ions on corrosion and hydrogen evolution of carbon steel in acid solutions. *Int J Hydrogen Energy* 2012;37:19219–30.
- [239] Mouanga M, Andreatta F, Druart M-E, Marin E, Fedrizzi L, Olivier M-G. A localized approach to study the effect of cerium salts as cathodic inhibitor on iron/aluminum galvanic coupling. *Corros Sci* 2015;90:491–502.
- [240] Verma C, Verma DK, Ebenso EE, Quraishi MA. Sulfur and phosphorus heteroatom-containing compounds as corrosion inhibitors: An overview. *Heteroatom Chemistry*. 2018;29.
- [241] Aiad I, Shaban SM, Elged AH, Aljoboury OH. Cationic surfactant based on alginate as green corrosion inhibitors for the mild steel in 1.0 M HCl. *Egypt J Pet* 2018;27:877–85.
- [242] Zhang QH, Li YY, Lei Y, Wang X, Liu HF, Zhang GA. Comparison of the synergistic inhibition mechanism of two eco-friendly amino acids combined corrosion inhibitors for carbon steel pipelines in oil and gas production. *Appl Surf Sci* 2022;583.
- [243] Lamaka SV, Zheludkevich ML, Yasakau KA, Montemor MF, Ferreira MGS. High effective organic corrosion inhibitors for 2024 aluminium alloy. *Electrochim Acta* 2007;52:7231–47.
- [244] Berdimurodov E, Kholikov A, Akbarov K, Guo L, Kaya S, Katin KP, et al. Novel gossypol–indole modification as a green corrosion inhibitor for low-carbon steel in aggressive alkaline–saline solution. *Colloids Surf A Physicochem Eng Asp* 2022;637:128207.
- [245] Kirkland NT, Schiller T, Medhekar N, Birbilis N. Exploring graphene as a corrosion protection barrier. *Corros Sci* 2012;56:1–4.
- [246] Ma F, Zhang Y, Wang H, Li W, Hou B. Inhibition behavior of chitooligosaccharide derivatives for carbon steel in 3.5% NaCl solution. *Int J Electrochem Sci* 2018;13:235–49.
- [247] Verma C, Quraishi MA, Ebenso EE. Quinoline and its derivatives as corrosion inhibitors: A review. *Surf Interfaces* 2020;21:100634.
- [248] Sukul D, Pal A, Saha SK, Satpati S, Adhikari U, Banerjee P. Newly synthesized quercetin derivatives as corrosion inhibitors for mild steel in 1 M HCl: Combined experimental and theoretical investigation. *PCCP* 2018;20:6562–74.
- [249] Verma C, Quraishi MA, Singh A. A thermodynamical, electrochemical, theoretical and surface investigation of diheteroaryl thioethers as effective corrosion inhibitors for mild steel in 1 M HCl. *J Taiwan Inst Chem Eng* 2016;58:127–40.
- [250] Wei H, Heidarsheenas B, Zhou L, Hussain G, Li Q, Ostrikov KK. Green inhibitors for steel corrosion in acidic environment: state of art. *Mater Today Sustain* 2020;10:100044.
- [251] Elaraby A, El-samad SA, Khamis EA, Zaki EG. Theoretical and electrochemical evaluation of tetra-cationic surfactant as corrosion inhibitor for carbon steel in 1 M HCl. *Sci Rep* 2023;13:942.
- [252] El Achouri M, Infante MR, Izquierdo F, Kertit S, Gouytaya HM, Nciri B. Synthesis of some cationic gemini surfactants and their inhibitive effect on iron corrosion in hydrochloric acid medium. *Corros Sci* 2001;43:19–35.
- [253] Azeze FA, Al-Rashed OA, Nazeer AA. Controlling of mild-steel corrosion in acidic solution using environmentally friendly ionic liquid inhibitors: Effect of alkyl chain. *J Mol Liq* 2018;265:654–63.
- [254] Yasakau KA, Zheludkevich ML, Lamaka SV, Ferreira MGS. Mechanism of corrosion inhibition of AA2024 by rare-earth compounds. *J Phys Chem B* 2006;110:5515–28.
- [255] Likhanova NV, Arellanes-Lozada P, Olivares-Xometl O, Hernández-Cocoletzi H, Lijanova IV, Arriola-Morales J, et al. Effect of organic anions on ionic liquids as corrosion inhibitors of steel in sulfuric acid solution. *J Mol Liq* 2019;279:267–78.
- [256] Zheng H, Shao Y, Wang Y, Meng G, Liu B. Reinforcing the corrosion protection property of epoxy coating by using graphene oxide–poly(urea–formaldehyde) composites. *Corros Sci* 2017;123:267–77.
- [257] Hamadi L, Mansouri S, Oulmi K, Kareche A. The use of amino acids as corrosion inhibitors for metals: A review. *Egypt J Pet* 2018;27:1157–65.
- [258] Khadam AA, Kadhim MM, Anae RA, Mahood HB, Mahdi MS, Salman AW. Theoretical evaluation of Citrus Aurantium leaf extract as green inhibitor for chemical and biological corrosion of mild steel in acidic solution: Statistical, molecular dynamics, docking, and quantum mechanics study. *J Mol Liq* 2021;343:116978.
- [259] Ali SA, El-Shareef AM, Al-Ghamdi RF, Saeed MT. The isoxazolindines: the effects of steric factor and hydrophobic chain length on the corrosion inhibition of mild steel in acidic medium. *Corros Sci* 2005;47:2659–78.
- [260] Hamani H, Daoud D, Benabid S, Douadi T. Electrochemical, density functional theory (DFT) and molecular dynamic (MD) simulations studies of synthesized three new Schiff bases as corrosion inhibitors on mild steel in the acidic environment. *J Indian Chem Soc* 2022;99:100492.
- [261] Fernandes CM, Pina VGSS, Alfaro CG, de Sampaio MTG, Massante FF, Alvarez LX, et al. Innovative characterization of original green vanillin-derived Schiff bases as corrosion inhibitors by a synergic approach based on electrochemistry, microstructure, and computational analyses. *Colloids Surf A Physicochem Eng Asp* 2022;641:128540.
- [262] Ansari KR, Chauhan DS, Quraishi MA, Mazumder MAJ, Singh A. Chitosan Schiff base: an environmentally benign biological macromolecule as a new corrosion inhibitor for oil & gas industries. *Int J Biol Macromol* 2020;144:305–15.
- [263] Solomon MM, Umoren SA, Quraishi MA, Salman M. Myristic acid based imidazoline derivative as effective corrosion inhibitor for steel in 15% HCl medium. *J Colloid Interface Sci* 2019;551:47–60.
- [264] Zhang C, Hu J, Yang Z, Zheng Z, Geng S, Zhong X. Effects of the number of imidazoline ring and the length of alkyl group chain of imidazoline derivatives on corrosion inhibition of carbon steel in HCl solution: Molecular simulation and experimental validation. *Petroleum* 2022;8:447–57.
- [265] Zheng Z, Hu J, Eliaz N, Zhou L, Yuan X, Zhong X. Mercaptopropionic acid-modified oleic imidazoline as a highly efficient corrosion inhibitor for carbon steel in CO<sub>2</sub>-saturated formation water. *Corros Sci* 2022;194:109930.
- [266] Hu J, Xiong Q, Chen L, Zhang C, Zheng Z, Geng S, et al. Corrosion inhibitor in CO<sub>2</sub>-O<sub>2</sub>-containing environment: Inhibition effect and mechanisms of bis(2-ethylhexyl) phosphate for the corrosion of carbon steel. *Corros Sci* 2021;179:109173.

- [267] Cao F, Wei J, Dong J, Ke W. The corrosion inhibition effect of phytic acid on 20SiMn steel in simulated carbonated concrete pore solution. *Corros Sci* 2015;100:365–76.
- [268] Mandal S, Singh JK, Lee D-E, Park T. Effect of phosphate-based inhibitor on corrosion kinetics and mechanism for formation of passive film onto the steel rebar in chloride-containing pore solution. *Materials* 2020;13.
- [269] Shaban A, Felhosi I, Telegdi J. Laboratory assessment of inhibition efficiency and mechanism of inhibitor blend (P22SU) on mild steel corrosion in high chloride containing water. *Int J Corros Scale Inhib* 2017;6:262–75.
- [270] Rahim AA, Rocca E, Steinmetz J, Jain KM. Inhibitive action of mangrove tannins and phosphoric acid on pre-rusted steel via electrochemical methods. *Corros Sci* 2008;50:1546–50.
- [271] Yan R, Gao X, Lv D, Ma H. A study on the differences in morphology and corrosion resistance performance between two different bis(2-ethylhexyl) phosphate self-assembled thin films prepared on an iron substrate in water and ethanol solvents. *RSC Adv* 2016;6:55936–45.
- [272] Gust J. Application of infrared spectroscopy for investigation of rust phase component conversion by agents containing Oak Tannin and Phosphoric Acid. *Corrosion* 1991;47:453–7.
- [273] Flores Merino S, Caprari JJ, Vasquez Torres L, Figueroa Ramos L, Hadzich GA. Inhibitive action of tara tannin in rust converter formulation. *Anti-Corros Methods Mater* 2017;64:136–47.
- [274] Cui M, Wang Z, Wang B. Survival Strategies of Mangrove (*Ceriops tagal* (per.) C. B. Rob) and the Inspired Corrosion Inhibitor. *Frontiers in Materials*. 2022;9.
- [275] Wang F, Zhang Z, Wu S, Jiang J, Chu H. Effect of inhibitor on adsorption behavior and mechanism of micro-zone corrosion on carbon steel. *Materials* 2019;12.
- [276] Zhang H-Y, Lei Y-Y, Li J-Y, Zhang Y-Z, Di Z-G, Wu P-P, et al. Electrochemical impedance spectroscopy, atomistic simulation, and quantum chemistry simulation of the mechanism of five inhibitors to prevent acidizing corrosion of N80 steel in 15% (wt) HCl solution. *Corros* 2019;75:809–23.
- [277] Zhang Z, Wang F, Liu Y, Wu S, Li W, Sun W, et al. Molecule adsorption and corrosion mechanism of steel under protection of inhibitor in a simulated concrete solution with 3.5% NaCl. *RSC Adv* 2018;8:20648–54.
- [278] Guo L, Qi C, Zheng X, Zhang R, Shen X, Kaya S. Toward understanding the adsorption mechanism of large size organic corrosion inhibitors on an Fe(110) surface using the DFTB method. *RSC Adv* 2017;7:29042–50.
- [279] Zakeri A, Bahmani E, Aghdam ASR. Plant extracts as sustainable and green corrosion inhibitors for protection of ferrous metals in corrosive media: A mini review. *Corros Commun* 2022;5:25–38.
- [280] Gowraraju ND, Jagadeesan S, Ayyasamy K, Olasunkanmi LO, Ebenso EE, Subramanian C. Adsorption characteristics of Iota-carrageenan and Inulin biopolymers as potential corrosion inhibitors at mild steel/sulphuric acid interface. *J Mol Liq* 2017;232:9–19.
- [281] Wang Q, Zheng H, Zhao C, Zhang Q, Liu L, Wu X, et al. Experimental and theoretical insights into Oxalis corniculata L. extract as a sustainable and eco-friendly corrosion inhibitor for carbon steel in acidic environments. *Mater Chem Phys* 2023;306:128075.
- [282] Maizia R, Zaabar A, Djermoune A, Amoura D, Martemianov S, Thomas A, et al. Experimental assessment and molecular-level exploration of the mechanism of action of Nettle (*Urtica dioica* L.) plant extract as an eco-friendly corrosion inhibitor for X38 mild steel in sulfuric acidic medium. *Arab J Chem* 2023;16:104988.
- [283] López DA, Simison SN, de Sánchez SR. Inhibitors performance in CO<sub>2</sub> corrosion: EIS studies on the interaction between their molecular structure and steel microstructure. *Corros Sci* 2005;47:735–55.
- [284] Zhang H-h, Pang X, Gao K. Localized CO<sub>2</sub> corrosion of carbon steel with different microstructures in brine solutions with an imidazoline-based inhibitor. *Appl Surf Sci* 2018;442:446–60.
- [285] Pourbaix M. Thermodynamics and corrosion. *Corros Sci* 1990;30:971–88.
- [286] Jeurgens LPH, Sloof WG, Tichelaar FD, Mittemeijer EJ. Growth kinetics and mechanisms of aluminum-oxide films formed by thermal oxidation of aluminum. *J Appl Phys* 2002;92:1649–56.
- [287] Jeurgens LPH, Sloof WG, Tichelaar FD, Mittemeijer EJ. Structure and morphology of aluminium-oxide films formed by thermal oxidation of aluminium. *Thin Solid Films* 2002;418:89–101.
- [288] Zhang XY, Kang QX, Wang Y. Theoretical study of N-thiazolyl-2-cyanoacetamide derivatives as corrosion inhibitor for aluminum in alkaline environments. *Comput Theor Chem* 2018;1131:25–32.
- [289] Poberžnik M, Chiter F, Milošev I, Marcus P, Costa D, Kokalj A. DFT study of n-alkyl carboxylic acids on oxidized aluminum surfaces: From standalone molecules to self-assembled-monolayers. *Appl Surf Sci* 2020;525:146156.
- [290] Masoud MS, Awad MK, Ali AE, El-Tahawy MMT. Molecular structure of amino alcohols on aluminum surface. *J Mol Struct* 2014;1063:51–9.
- [291] Sein LT, Wei Y, Jansen SA. Corrosion inhibition by aniline oligomers through charge transfer: a DFT approach. *Synth Met* 2004;143:1–12.
- [292] Chen S, Kar T. Theoretical investigation of inhibition efficiencies of some Schiff bases as corrosion inhibitors of aluminum. *Int J Electrochem Sci* 2012;7:6265–75.
- [293] Lashkari M, Arshadi MR. DFT studies of pyridine corrosion inhibitors in electrical double layer: solvent, substrate, and electric field effects. *Chem Phys* 2004;299:131–7.
- [294] Jamalizadeh E, Jafari AH, Hosseini SMA. Semi-empirical and ab initio quantum chemical characterisation of pyridine derivatives as HCl inhibitors of aluminium surface. *J Mol Struct (Theochem)* 2008;870:23–30.
- [295] Gravina R, Josse C, Viguier B, Laurino A, Alexis J, Hughes AE, et al. Corrosion behaviour of AA 1370 strands for wires: Identification of the critical metallurgical parameters. *Corros Sci* 2018;134:112–21.
- [296] Parvizi R, Hughes AE, Glenn AM, Cizek P, Tan MY, Forsyth M. Role of microstructure in corrosion initiation of a highly-deformed AA2024 wire. *Corros Sci* 2018;144:184–97.
- [297] Martinson CWB, Flodström SA. Oxygen adsorption on aluminum single crystal faces studied by AES, XPS and LEED. *Surface Sci* 1979;80:306–16.
- [298] Birbilis N, Buchheit RG. Investigation and discussion of characteristics for intermetallic phases common to aluminum alloys as a function of solution pH. *J Electrochem Soc* 2008;155:C117.
- [299] Scamans GM, Birbilis N, Buchheit RG. 3.08 - Corrosion of Aluminum and its Alloys. In: Cottis B, Graham M, Lindsay R, Lyon S, Richardson T, Scantlebury D, et al., editors. *Shreir's Corrosion*. Oxford: Elsevier; 2010. p. 1974–2010.
- [300] Birbilis N, Buchheit RG. Electrochemical characteristics of intermetallic phases in aluminum alloys. *J Electrochem Soc* 2005;152:B140.
- [301] Hughes AE, Parvizi R, Forsyth M. Microstructure and corrosion of AA2024. *Corros Rev* 2015;33:1–30.
- [302] Kosari A, Tichelaar F, Visser P, Zandbergen H, Terryn H, Mol JMC. Dealloying-driven local corrosion by intermetallic constituent particles and dispersoids in aerospace aluminium alloys. *Corros Sci* 2020;177:108947.
- [303] Zhang X, Zhou X, Nilsson J-O. Corrosion behaviour of AA6082 Al-Mg-Si alloy extrusion: The influence of quench cooling rate. *Corros Sci* 2019;150:100–9.
- [304] Ma Y, Wu H, Zhou X, Li K, Liao Y, Liang Z, et al. Corrosion behavior of anodized Al-Cu-Li alloy: the role of intermetallic particle-introduced film defects. *Corros Sci* 2019;158:108110.
- [305] Zhang X, Hashimoto T, Lindsay J, Zhou X. Investigation of the de-alloying behaviour of  $\theta$ -phase (Al<sub>2</sub>Cu) in AA2024-T351 aluminium alloy. *Corros Sci* 2016;108:85–93.
- [306] Ma Y, Zhou X, Thompson GE, Hashimoto T, Thomson P, Fowles M. Distribution of intermetallics in an AA 2099–T8 aluminium alloy extrusion. *Mater Chem Phys* 2011;126:46–53.
- [307] Li M, Seyeux A, Wiame F, Marcus P, Świątowska J. Localized corrosion induced surface modifications of Al-Cu-Li alloy studied by ToF-SIMS 3D imaging. *npj Mater Degrad* 2021;5:23.
- [308] Muster TH, Hughes AE, Thompson GE. *Copper Distributions in Aluminium Alloys*. New York: Nova Science Publishers; 2009.
- [309] Additive C. *Scalmalloy - Datasheet*. [https://www.carpenteradditive.com/hubs/Resources/Data%20Sheets/Scalmalloy\\_Datasheet.pdf](https://www.carpenteradditive.com/hubs/Resources/Data%20Sheets/Scalmalloy_Datasheet.pdf).
- [310] Aboulkhair NT, Simonelli M, Parry L, Ashcroft I, Tuck C, Hague R. 3D printing of aluminium alloys: additive manufacturing of aluminium alloys using selective laser melting. *Prog Mater Sci* 2019;106:100578.

- [311] Schimbäck D, Mair P, Bärtil M, Palm F, Leichtfried G, Mayer S, et al. Alloy design strategy for microstructural-tailored scandium-modified aluminium alloys for additive manufacturing. *Scr Mater* 2022;207:114277.
- [312] Oliveira GHM, Belei C, de Carvalho WS, Canto LB, Amancio-Filho ST. On the fully additive manufacturing of PC/AlSi10Mg hybrid structures. *Mater Lett* 2023;330:133378.
- [313] Gao M, Feng C, Wei RP. An analytical electron microscopy study of constituent particles in commercial 7075-T6 and 2024-T3 alloys. *Metall Mater Trans A* 1998;29:1145–51.
- [314] Ayer R, Koo JY, Steeds JW, Park BK. Microanalytical study of the heterogeneous phases in commercial Al-Zn-Mg-Cu alloys. *Metall Trans A* 1985;16:1925–36.
- [315] MacRae CM, Hughes AE, Laird JS, Glenn AM, Wilson NC, Torpy A, et al. An examination of the composition and microstructure of coarse intermetallic particles in AA2099-T8, including Li detection. *Microscopy Microanal* 2018;24:325–41.
- [316] Phragmen G. On the phases occurring in alloys of aluminium with copper, magnesium, manganese, iron, and silicon. *J Inst Met* 1950;77:489–551.
- [317] Mondolfo LF. *Aluminum Alloys: Structure and Properties* Butterworth-Heinemann; 1976.
- [318] Polmear I, St John D, Nie J-F, Qian M. *Light Alloys: Metallurgy of the Light Metals*. 5th ed: Butterworth-Heinemann; 2017.
- [319] Buchheit RG, Grant RP, Hlava PF, Mckenzie B, Zender GL. Local dissolution phenomena associated with S phase (Al<sub>2</sub>CuMg) particles in aluminum alloy 2024-T3. *J Electrochem Soc* 1997;144:2621–8.
- [320] Buchheit RG, Martinez MA, Montes LP. Evidence for Cu ion formation by dissolution and dealloying the Al<sub>2</sub>CuMg intermetallic compound in rotating ring-disk collection experiments. *J Electrochem Soc* 2000;147:119.
- [321] Lacroix L, Blanc C, Pèbère N, Thompson GE, Tribollet B, Vivier V. Simulating the galvanic coupling between S-Al<sub>2</sub>CuMg phase particles and the matrix of 2024 aerospace aluminium alloy. *Corros Sci* 2012;64:213–21.
- [322] Lacroix L, Ressler L, Blanc C, Mankowski G. Statistical study of the corrosion behavior of Al<sub>2</sub>CuMg intermetallics in AA2024-T351 by SKPFM. *J Electrochem Soc* 2008;155:C8–15.
- [323] Boag A, Hughes AE, Glenn AM, Muster TH, McCulloch D. Corrosion of AA2024-T3 Part I: localised corrosion of isolated IM particles. *Corros Sci* 2011;53:17–26.
- [324] Ehsani A, Shiri HM, Mahjani MG, Moshrefi R, Hadi M, Soltanpour N. Theoretical, common electrochemical and electrochemical noise investigation of inhibitory effect of new organic compound nanoparticles in the corrosion of stainless steel in acidic solution. *Trans Indian Inst Met* 2016;69:1519–27.
- [325] Nelson KJH, Hughes AE, Taylor RJ, Hinton BRW, Wilson L, Henderson M. Characterisation of aluminium alloys after HNO<sub>3</sub>/HF-NaOH-HNO<sub>3</sub>/HF pretreatment. *Mater Sci Technol* 2001;17:1211–21.
- [326] Hughes AE, Theodossiou G, Elliott S, Harvey TG, Miller PR, Gorman JD, et al. Study of deoxidation of 2024-T3 with various acids. *Mater Sci Technol* 2001;17:1642–52.
- [327] Toh SK, McCulloch DG, Du Plessis J, Paterson PJK, Hughes AE, Jamieson D, et al. An investigation of the native oxide of aluminum alloy 7475-T7651 using XPS, AES, TEM, EELS, GDOES and RBS. *Surf Rev Lett* 2003;10:365–71.
- [328] Harvey TG, Hughes AE, Hardin SG, Nikpour T, Toh SK, Boag A, et al. Non-chromate deoxidation of AA2024-T3: Sodium bromate-nitric acid (20–60°C). *Appl Surf Sci* 2008;254:3562–75.
- [329] Liu Y, Colin F, Skeldon P, Thompson GE, Zhou X, Habazaki H, et al. Enrichment factors for copper in aluminium alloys following chemical and electrochemical surface treatments. *Corros Sci* 2003;45:1539–44.
- [330] Liu Y, Arenas MA, Skeldon P, Thompson GE, Habazaki H, Shimizu K, et al. Generation of copper nanoparticles during alkaline etching of an Al-30at.%Cu alloy. *Corros Sci* 2006;48:1874–84.
- [331] Luo C, Albu SP, Zhou X, Sun Z, Zhang X, Tang Z, et al. Continuous and discontinuous localized corrosion of a 2xxx aluminium-copper-lithium alloy in sodium chloride solution. *J Alloy Compd* 2016;658:61–70.
- [332] Sukiman NL, Zhou X, Birbilis N, Hughes AE, Mol JMC, Garcia SJ, et al. Durability and corrosion of aluminium and its alloys: overview, property space, techniques and developments In: Ahmad Z, editor. *Aluminium Alloys - New Trends in Fabrication and Applications*. Rijeka: Intech Publications; 2012.
- [333] Kozlica DK, Kokalj A, Milošev I. Synergistic effect of 2-mercaptobenzimidazole and octylphosphonic acid as corrosion inhibitors for copper and aluminium – An electrochemical, XPS, FTIR and DFT study. *Corros Sci* 2021;182:109082.
- [334] HosseinpourRokni M, Naderi R, Soleimani M, Jannat AR, Pourfath M, Saybani M. Using plant extracts to modify Al electrochemical behavior under corroding and functioning conditions in the air battery with alkaline-ethylene glycol electrolyte. *J Ind Eng Chem* 2021;102:327–42.
- [335] Luo X, Dong C, Xi Y, Ren C, Wu J, Zhang D, et al. Computational simulation and efficient evaluation on corrosion inhibitors for electrochemical etching on aluminum foil. *Corros Sci* 2021;187:109492.
- [336] El Ghayati L, Sert Y, Sebbar NK, Ramli Y, Ahabchane NH, Talbaoui A, et al. Syntheses of novel 1,5-benzodiazepine derivatives: Crystal structures, spectroscopic characterizations, Hirshfeld surface analyses, molecular docking studies, DFT calculations, corrosion inhibition anticipation, and antibacterial activities. *J Heterocyclic Chem* 2021;58:270–89.
- [337] Hni B, Sebbar NK, Anouar EH, Ibrahim BE, Ellouz M, Hökelek T, et al. Syntheses, crystal structures, spectroscopic characterizations, DFT calculations, hirshfeld surface analyses and monte carlo simulations of novel long-chain alkyl-substituted 1,4-benzothiazine derivatives. *J Mol Struct* 2020;1221:128886.
- [338] Bulteau Y, Tarrat N, Pèbère N, Lacaze-Dufaure C. 8-Hydroxyquinoline complexes (Alq3) on Al(111): atomic scale structure, energetics and charge distribution. *New J Chem* 2020;44:15209–22.
- [339] Bourzi H, Oukhrif R, El Ibrahim B, Abou Oualid H, Abdellaoui Y, Balkard B, et al. Furfural analogs as sustainable corrosion inhibitors—predictive efficiency using DFT and Monte Carlo Simulations on the Cu(111), Fe(110), Al(111) and Sn(111) Surfaces in Acid Media. *Sustainability* 2020;12.
- [340] Allal H, Belhocine Y, Zouaoui E. Computational study of some thiophene derivatives as aluminium corrosion inhibitors. *J Mol Liq* 2018;265:668–78.
- [341] Tamilarasan R, Sreekanth A. Spectroscopic and DFT investigations on the corrosion inhibition behavior of tris(5-methyl-2-thioxo-1,3,4-thiadiazole)borate on high carbon steel and aluminium in HCl media. *RSC Adv* 2013;3:23681–91.
- [342] El Nemr A, Moneer AA, Khaled A, El Sikaily A, El-Said GF. Modeling of synergistic halide additives' effect on the corrosion of aluminum in basic solution containing dye. *Mater Chem Phys* 2014;144:139–54.
- [343] Zhang F, Liu Z-G, Zeng R-C, Li S-Q, Cui H-Z, Song L, et al. Corrosion resistance of Mg-Al-LDH coating on magnesium alloy AZ31. *Surf Coat Technol* 2014;258:1152–8.
- [344] Eddy NO, Momoh-Yahaya H, Oguzie EE. Theoretical and experimental studies on the corrosion inhibition potentials of some purines for aluminum in 0.1M HCl. *J Adv Res* 2015;6:203–17.
- [345] Wang D, Yang D, Zhang D, Li K, Gao L, Lin T. Electrochemical and DFT studies of quinoline derivatives on corrosion inhibition of AA5052 aluminium alloy in NaCl solution. *Appl Surf Sci* 2015;357:2176–83.
- [346] Awad MK, Mustafa MR, Abouelnga MM. Quantum chemical studies and atomistic simulations of some inhibitors for the corrosion of Al surface. *Prot Met Phys Chem* 2016;52:156–68.
- [347] Abd El-Rehim SS, Hassan HH, Deyab MAM, Abd El Moneim A. Experimental and theoretical investigations of adsorption and inhibitive properties of Tween 80 on corrosion of aluminium alloy (A5754) in alkaline media. *Z Phys Chem* 2016;230:67–78.
- [348] Naik UJ, Jha PC, Lone MY, Shah RR, Shah NK. Electrochemical and theoretical investigation of the inhibitory effect of two Schiff bases of benzaldehyde for the corrosion of aluminium in hydrochloric acid. *J Mol Struct* 2016;1125:63–72.
- [349] Naik UJ, Shah NK. Protection of aluminium in acidic environment and inhibition efficiency of aminophenol-N-benzylidene - theoretical and practical investigation. *ECS Trans* 2017;77:705–22.
- [350] El-Deeb MM, Alshammari HM, Abdel-Azeim S. Effect of ortho-substituted aniline on the corrosion protection of aluminum in 2 mol/L H<sub>2</sub>SO<sub>4</sub> solution. *Can J Chem* 2017;95:612–9.
- [351] Gece G, Bilgiç S. A quantum chemical insight into corrosion inhibition effects of moxifloxacin and betamethasone drugs. *Int J Corros Scale Inhib* 2018;7:710–7.
- [352] Ugin Inbaraj N, Venkatesa PG. Corrosion inhibition properties of paracetamol based benzoxazine on HCS and Al surfaces in 1M HCl. *Prog Org Coat* 2018;115:27–40.



- [353] Abdallah M, Gad EAM, Al-Fahemi JH, Sobhi M. Experimental and theoretical investigation by DFT on the some azole antifungal drugs as green corrosion inhibitors for aluminum in 1.0M HCl. *Prot Met Phys Chem* 2018;54:503–12.
- [354] Arjomandi J, Moghanni-Bavil-Olyaei H, Parvin MH, Lee JY, Chul Ko K, Joshaghani M, et al. Inhibition of corrosion of aluminum in alkaline solution by a novel azo-schiff base: experiment and theory. *J Alloy Compd* 2018;746:185–93.
- [355] Su P, Li L, Li W, Huang C, Wang X, Liu H, et al. Expired drug theophylline as potential corrosion inhibitor for 7075 aluminium alloy in 1M NaOH solution. *Int J Electrochem Sci* 2020;15:1412–25.
- [356] El Moll H, Alenezi KM, Abdel-Latif MK, Halouani H, EL-Deeb MM. Water-soluble calix [4] arenes as inhibitors for the corrosion of aluminium in 2 M H<sub>2</sub>SO<sub>4</sub> solution. *Int J Electrochem Sci* 2020;15:252–64.
- [357] Nardeli JV, Fugivara CS, Taryba M, Pinto ERP, Montemor MF, Benedetti AV. Tannin: A natural corrosion inhibitor for aluminum alloys. *Prog Org Coat* 2019; 135:368–81.
- [358] Sihem O, Abderrahim K, Sihem A, Bououdina M. In-depth investigation of cefalexin's action mechanism as Al-Cu alloy corrosion inhibitor in 0.5 M HCl medium. *Mater Res Express* 2018;5.
- [359] Elmi S, Foroughi MM, Shahraki M, Dehdab M, Shahidi M. Computational evaluation of N-thiazolyl-2-cyanoacetamide derivatives on corrosion inhibition of aluminum. *J Fail Anal and Preven* 2018;18:887–904.
- [360] Kokalj A. Formation and structure of inhibitive molecular film of imidazole on iron surface. *Corros Sci* 2013;68:195–203.
- [361] Chiter F, Bonnet M-L, Lacaze-Dufaure C, Tang H, Pèbère N. Corrosion protection of Al(111) by 8-hydroxyquinoline: a comprehensive DFT study. *PCCP* 2018; 20:21474–86.
- [362] Chiter F, Lacaze-Dufaure C, Tang H, Pebere N. DFT studies of the bonding mechanism of 8-hydroxyquinoline and derivatives on the (111) aluminum surface. *PCCP* 2015;17:22243–58.
- [363] Soliman HN. Influence of 8-hydroxyquinoline addition on the corrosion behavior of commercial Al and Al-HO411 alloys in NaOH aqueous media. *Corros Sci* 2011;53:2994–3006.
- [364] Yasakau KA, Zheludkevich ML, Karavai OV, Ferreira MGS. Influence of inhibitor addition on the corrosion protection performance of sol-gel coatings on AA2024. *Prog Org Coat* 2008;63:352–61.
- [365] Marcelin S, Pèbère N. Synergistic effect between 8-hydroxyquinoline and benzotriazole for the corrosion protection of 2024 aluminium alloy: A local electrochemical impedance approach. *Corros Sci* 2015;101:66–74.
- [366] 08 AD. D1654 – 08. Standard Test Method for Evaluation of Painted or Coated Specimens Subjected to Corrosive Environments. ASTM International.
- [367] Weder N, Alberto R, Koitz R. Thiourea derivatives as potent inhibitors of aluminum corrosion: atomic-level insight into adsorption and inhibition mechanisms. *J Phys Chem C* 2016;120:1770–7.
- [368] Gusieva K, Davies CHJ, Scully JR, Birbilis N. Corrosion of magnesium alloys: the role of alloying. *Int Mater Rev* 2015;60:169–94.
- [369] Esmaily M, Svensson JE, Fajardo S, Birbilis N, Frankel GS, Virtanen S, et al. Fundamentals and advances in magnesium alloy corrosion. *Prog Mater Sci* 2017;89: 92–193.
- [370] Makar GL, Kruger J. Corrosion of magnesium. *Int Mater Rev* 1993;38:138–53.
- [371] Pokrovsky OS, Schott J. Experimental study of brucite dissolution and precipitation in aqueous solutions: surface speciation and chemical affinity control. *Geochim Cosmochim Acta* 2004;68:31–45.
- [372] ASTM B951-11. Standard Practice for Codification of Unalloyed Magnesium and Magnesium- Alloys, Cast and Wrought. 2011.
- [373] Südholtz AD, Kirkland NT, Buchheit RG, Birbilis N. Electrochemical properties of intermetallic phases and common impurity elements in magnesium alloys. *Electrochem Solid St* 2011;14:C5.
- [374] Song G, Atrens A. Understanding magnesium corrosion—a framework for improved alloy performance. *Adv Eng Mater* 2003;5:837–58.
- [375] Atrens A, Song G-L, Liu M, Shi Z, Cao F, Dargusch MS. Review of recent developments in the field of magnesium corrosion. *Adv Eng Mater* 2015;17:400–53.
- [376] Jiang P, Blawert C, Scharnagl N, Zheludkevich ML. Influence of water purity on the corrosion behavior of Mg<sub>0.5</sub>ZnX (X=Ca, Ge) alloys. *Corros Sci* 2019;153: 62–73.
- [377] Yuwono JA, Birbilis N, Taylor CD, Williams KS, Samin AJ, Medhekar NV. Aqueous electrochemistry of the magnesium surface: thermodynamic and kinetic profiles. *Corros Sci* 2018.
- [378] Würger T, Feiler C, Vonbun-Feldbauer GB, Zheludkevich ML, Meißner RH. A first-principles analysis of the charge transfer in magnesium corrosion. *Sci Rep* 2020;10:15006.
- [379] Surendralal S, Todorova M, Finnis MW, Neugebauer J. First-Principles approach to model electrochemical reactions: understanding the fundamental mechanisms behind Mg corrosion. *Phys Rev Lett* 2018;120:246801.
- [380] Binns WJ, Zargarzadah F, Dehnavi V, Chen J, Noel JJ, Shoesmith DW. Physical and electrochemical evidence for the role of a Mg hydride species in Mg alloy corrosion. *Corrosion* 2019;75:58–68.
- [381] Seyeux A, Liu M, Schmutz P, Song G, Atrens A, Marcus P. ToF-SIMS depth profile of the surface film on pure magnesium formed by immersion in pure water and the identification of magnesium hydride. *Corros Sci* 2009;51:1883–6.
- [382] Wang C, Xu W, Höche D, Zheludkevich ML, Lamaka SV. Exploring the contribution of oxygen reduction reaction to Mg corrosion by modeling assisted local analysis. *J Magnesium Alloys* 2023;11:100–9.
- [383] Wang L, Shinohara T, Zhang B-P. Influence of deaerated condition on the corrosion behavior of AZ31 magnesium alloy in dilute NaCl solutions. *Mater Trans* 2009;50:2563–9.
- [384] Wang C, Xu W, Höche D, Zheludkevich ML, Lamaka SV. Exploring the contribution of oxygen reduction reaction to Mg corrosion by modeling assisted local analysis. *J Magnesium Alloys* 2023;11:100–9.
- [385] Ng M-F, Blackwood DJ, Jin H, Tan TL. First-principles investigation into the contributions of ORR and HER in magnesium corrosion. *J Electrochem Soc* 2023; 170:071501.
- [386] Rong-Chang Z, Zheng-Zheng Y, Xiao-Bo C, Dao-Kui X. Corrosion Types of Magnesium Alloys. In: Tomasz T, Wojciech B, Mariusz K, editors. *Magnesium Alloys*. Rijeka: IntechOpen; 2018. p. Ch. 3.
- [387] Wang L, Snihirova D, Deng M, Vaghefinazari B, Höche D, Lamaka SV, et al. Revealing physical interpretation of time constants in electrochemical impedance spectra of Mg via Tribo-EIS measurements. *Electrochim Acta* 2022;404:139582.
- [388] Wang L, Snihirova D, Deng M, Wang C, Vaghefinazari B, Wiese G, et al. Insight into physical interpretation of high frequency time constant in electrochemical impedance spectra of Mg. *Corros Sci* 2021;187:109501.
- [389] Atrens A, Song GL, Shi Z, Soltan A, Johnston S, Dargusch MS. Understanding the Corrosion of Mg and Mg Alloys. In: Wandelt K, editor. *Encyclopedia of Interfacial Chemistry*. Oxford: Elsevier; 2018. p. 515–34.
- [390] Atrens A, Shi Z, Mehreen SU, Johnston S, Song G-L, Chen X, et al. Review of Mg alloy corrosion rates. *J Magnesium Alloys* 2020;8:989–98.
- [391] Vaghefinazari B, Wierzbicka E, Visser P, Posner R, Arrabal R, Matykina E, et al. Chromate-free corrosion protection strategies for magnesium alloys - a review. Part III - Corrosion inhibitors and combining them with other protection strategies. *Materials* 2022;15:8489.
- [392] Umoren SA, Abdullahi MT, Solomon MM. An overview on the use of corrosion inhibitors for the corrosion control of Mg and its alloys in diverse media. *J Mater Res Technol* 2022;20:2060–93.
- [393] Hu J, Huang D, Zhang G, Song G-L, Guo X. Research on the inhibition mechanism of tetraphenylporphyrin on AZ91D magnesium alloy. *Corros Sci* 2012;63: 367–78.
- [394] Zucchi F, Grassi V, Zanotto F. Sodium monocarboxylates as inhibitors of AZ31 alloy corrosion in a synthetic cooling water. *Mater Corros* 2009;60:199–205.
- [395] Frignani A, Grassi V, Zanotto F, Zucchi F. Inhibition of AZ31 Mg alloy corrosion by anionic surfactants. *Corros Sci* 2012;63:29–39.
- [396] Li Y, Lu X, Wu K, Yang L, Zhang T, Wang F. Exploration the inhibition mechanism of sodium dodecyl sulfate on Mg alloy. *Corros Sci* 2020;168:108559.
- [397] Lu X, Li Y, Ju P, Chen Y, Yang J, Qian K, et al. Unveiling the inhibition mechanism of an effective inhibitor for AZ91 Mg alloy. *Corros Sci* 2019;148:264–71.
- [398] Semiletov AM, Kuznetsov YI, Chirkunov AA. Inhibition of magnesium corrosion by salts of higher carbonic acids. *Prot Met Phys Chem* 2017;53:1265–70.

- [399] Lin J, Battocchi D, Bierwagen GP. Inhibitors for prolonging corrosion protection of Mg-rich primer on Al alloy 2024–T3. *J Coat Technol Res* 2017;1–8.
- [400] Kartsonakis IA, Stanciu SG, Matei AA, Karaxi EK, Hristu R, Karantonis A, et al. Evaluation of the protective ability of typical corrosion inhibitors for magnesium alloys towards the Mg ZK30 variant. *Corros Sci* 2015;100:194–208.
- [401] Maltseva A, Lamaka SV, Yasakau KA, Mei D, Kurchavov D, Zheludkevich ML, et al. In situ surface film evolution during Mg aqueous corrosion in presence of selected carboxylates. *Corros Sci* 2020;171:108484.
- [402] Yang JJ, Blawert C, Lamaka SV, Yasakau KA, Wang L, Laipple D, et al. Corrosion inhibition of pure Mg containing a high level of iron impurity in pH neutral NaCl solution. *Corros Sci* 2018;142:222–37.
- [403] Fockaert LI, Wurger T, Unbehau R, Boelen B, Meissner RH, Lamaka SV, et al. ATR-FTIR in Kretschmann configuration integrated with electrochemical cell as in situ interfacial sensitive tool to study corrosion inhibitors for magnesium substrates. *Electrochim Acta* 2020;345:136166.
- [404] Menger FM, Keiper JS. Gemini surfactants. *Angew Chem Int Ed* 2000;39:1906–20.
- [405] Yang X, Pan FS, Zhang DF. A study on corrosion inhibitor for magnesium alloy. *Mater Sci Forum* 2009;610–613:920–6.
- [406] Dinodi N, Shetty AN. Alkyl carboxylates as efficient and green inhibitors of magnesium alloy ZE41 corrosion in aqueous salt solution. *Corros Sci* 2014;85:411–27.
- [407] Williams G, McMurray HN, Grace R. Inhibition of magnesium localised corrosion in chloride containing electrolyte. *Electrochim Acta* 2010;55:7824–33.
- [408] Song G, StJohn DH. Corrosion of magnesium alloys in commercial engine coolants. *Mater Corros* 2005;56:15–23.
- [409] Zeng R-C, Hu Y, Guan S-K, Cui H-Z, Han E-H. Corrosion of magnesium alloy AZ31: The influence of bicarbonate, sulphate, hydrogen phosphate and dihydrogen phosphate ions in saline solution. *Corros Sci* 2014;86:171–82.
- [410] Lamaka SV, Knörnschild G, Snihirova DV, Taryba MG, Zheludkevich ML, Ferreira MGS. Complex anticorrosion coating for ZK30 magnesium alloy. *Electrochim Acta* 2009;55:131–41.
- [411] Gao H, Li Q, Dai Y, Luo F, Zhang HX. High efficiency corrosion inhibitor 8-hydroxyquinoline and its synergistic effect with sodium dodecylbenzenesulphonate on AZ91D magnesium alloy. *Corros Sci* 2010;52:1603–9.
- [412] Hu J, Zeng D, Zhang Z, Shi T, Song G-L, Guo X. 2-Hydroxy-4-methoxy-acetophenone as an environment-friendly corrosion inhibitor for AZ91D magnesium alloy. *Corros Sci* 2013;74:35–43.
- [413] Ding C, Liu Y, Wang M, Wang T, Fu J. Self-healing, superhydrophobic coating based on mechanized silica nanoparticles for reliable protection of magnesium alloys. *J Mater Chem A* 2016;4:8041–52.
- [414] Konno H, Zhu Z, Nagayama M. Chemical and electrochemical modifications of zinc using organic compounds. *Plating Surf Finish.* 1987; 74: 40 - 44.
- [415] Cicileo GP, Rosales BM, Varela FE, Vilche JR. Inhibitory action of 8-hydroxyquinoline on the copper corrosion process. *Corros Sci* 1998;40:1915–26.
- [416] Niki K, Delnick FM, Hackerman N. Behavior of Salicylaldehyde and 8-Hydroxyquinoline at a Copper Electrode. *J Electrochem Soc* 1975;122:855.
- [417] Garrigues L, Pebere N, Dabosi F. An investigation of the corrosion inhibition of pure aluminum in neutral and acidic chloride solutions. *Electrochim Acta* 1996; 41:1209–15.
- [418] Isobe Y, Tanaka S, Hine F. Effects of Organic Inhibitors on Pitting Corrosion of Aluminum Alloys. *Corros Eng.* 1990;39:185–91.
- [419] Galio AF, Lamaka SV, Zheludkevich ML, Dick LFP, Müller IL, Ferreira MGS. Inhibitor-doped sol-gel coatings for corrosion protection of magnesium alloy AZ31. *Surf Coat Technol* 2010;204:1479–86.
- [420] Gnedenkov AS, Sinebryukhov SL, Mashtalyar DV, Gnedenkov SV. Localized corrosion of the Mg alloys with inhibitor-containing coatings: SVET and SIET studies. *Corros Sci* 2016;102:269–78.
- [421] Vaghefnazari B, Lamaka SV, Blawert C, Serdechnova M, Scharnagl N, Karlova P, et al. Exploring the corrosion inhibition mechanism of 8-hydroxyquinoline for a PEO-coated magnesium alloy. *Corros Sci* 2022;203:110344.
- [422] Lamaka SV, Höche D, Petrauskas RP, Blawert C, Zheludkevich ML. A new concept for corrosion inhibition of magnesium: Suppression of iron re-deposition. *Electrochem Commun* 2016;62:5–8.
- [423] Hoche D, Blawert C, Lamaka SV, Scharnagl N, Mendis C, Zheludkevich ML. The effect of iron re-deposition on the corrosion of impurity-containing magnesium. *Phys Chem Chem Phys* 2016;18:1279–91.
- [424] Eaves D, Williams G, McMurray HN. Inhibition of self-corrosion in magnesium by poisoning hydrogen recombination on iron impurities. *Electrochim Acta* 2012;79:1–7.
- [425] Mercier D, Światowska J, Zanna S, Seyeux A, Marcus P. Role of segregated iron at grain boundaries on Mg corrosion. *J Electrochem Soc* 2018;165:C42–9.
- [426] Lysne D, Thomas S, Hurley MF, Birbilis N. On the Fe enrichment during anodic polarization of Mg and its impact on hydrogen evolution. *J Electrochem Soc* 2015;162:C396–402.
- [427] Cain T, Madden SB, Birbilis N, Scully JR. Evidence of the enrichment of transition metal elements on corroding magnesium surfaces using rutherford backscattering spectrometry. *J Electrochem Soc* 2015;162:C228–37.
- [428] Yang L, Zhou X, Liang S-M, Schmid-Fetzer R, Fan Z, Scamans G, et al. Effect of traces of silicon on the formation of Fe-rich particles in pure magnesium and the corrosion susceptibility of magnesium. *J Alloy Compd* 2015;619:396–400.
- [429] Höche D, Lamaka SV, Vaghefnazari B, Braun T, Petrauskas RP, Fichtner M, et al. Performance boost for primary magnesium cells using iron complexing agents as electrolyte additives. *Sci Rep* 2018;8:7578.
- [430] Mercier D, Światowska J, Protopopoff E, Zanna S, Seyeux A, Marcus P. Inhibition of Mg corrosion by sulfur blocking of the hydrogen evolution reaction on iron impurities. *J Electrochem Soc* 2020;167:121504.
- [431] Williams G, Dafydd H-A-L, McMurray HN, Birbilis N. The influence of arsenic alloying on the localised corrosion behaviour of magnesium. *Electrochim Acta* 2016;219:401–11.
- [432] Birbilis N, Williams G, Gusieva K, Samaniego A, Gibson MA, McMurray HN. Poisoning the corrosion of magnesium. *Electrochem Commun* 2013;34:295–8.
- [433] Dong C-f, Xiao K, Liu Z-y, Yang W-j, Li X-g. Hydrogen induced cracking of X80 pipeline steel. *Int J Miner Metall Mater* 2010;17:579–86.
- [434] Zhang P, Laleh M, Hughes AE, Marceau RKW, Hilditch T, Tan MY. A systematic study on the influence of electrochemical charging conditions on the hydrogen embrittlement behaviour of a pipeline steel. *Int J Hydrogen Energy* 2023;48:16501–16.
- [435] Gore P, Fajardo S, Birbilis N, Frankel GS, Raja VS. Anodic activation of Mg in the presence of  $\text{In}^{3+}$  ions in dilute sodium chloride solution. *Electrochim Acta* 2019;293:199–210.
- [436] Yuwono JA, Birbilis N, Liu R, Ou Q, Bao Q, Medhekar NV. Aqueous electrochemical activity of the Mg surface: the role of group 14 and 15 microalloying elements. *J Electrochem Soc* 2017;164:C918–29.
- [437] Liu RL, Hurley MF, Kvrayan A, Williams G, Scully JR, Birbilis N. Controlling the corrosion and cathodic activation of magnesium via microalloying additions of Ge. *Sci Rep* 2016;6:28747.
- [438] Bao T, Hou L, Sun J, Liu X, Du H, Wei H, et al. Effect of indium on the negative difference effect for magnesium alloy. *J Electrochem Soc* 2021;168:031515.
- [439] Wang L, Snihirova D, Deng M, Wang C, Höche D, Lamaka SV, et al. Indium chloride as an electrolyte additive for primary aqueous Mg batteries. *Electrochim Acta* 2021;373:137916.
- [440] Zhang RF, Zhang SF, Yang N, Yao LJ, He FX, Zhou YP, et al. Influence of 8-hydroxyquinoline on properties of anodic coatings obtained by micro arc oxidation on AZ91 magnesium alloys. *J Alloy Compd* 2012;539:249–55.
- [441] Verma C, Ebenso EE, Quraishi MA. Ionic liquids as green and sustainable corrosion inhibitors for metals and alloys: An overview. *J Mol Liq* 2017;233:403–14.
- [442] Su H, Wang L, Wu Y, Zhang Y, Zhang J. Insight into inhibition behavior of novel ionic liquids for magnesium alloy in NaCl solution: Experimental and theoretical investigation. *Corros Sci* 2020;165:108410.
- [443] Su H, Liu Y, Gao X, Qian Y, Li W, Ren T, et al. Corrosion inhibition of magnesium alloy in NaCl solution by ionic liquid: Synthesis, electrochemical and theoretical studies. *J Alloy Compd* 2019;791:681–9.
- [444] Elsentriecy HH, Luo H, Meyer HM, Grado LL, Qu J. Effects of pretreatment and process temperature of a conversion coating produced by an aprotic ammonium-phosphate ionic liquid on magnesium corrosion protection. *Electrochim Acta* 2014;123:58–65.
- [445] Birbilis N, Howlett PC, MacFarlane DR, Forsyth M. Exploring corrosion protection of Mg via ionic liquid pretreatment. *Surf Coat Technol* 2007;201:4496–504.

- [446] Huang D, Hu J, Song G-L, Guo X. Inhibition effect of inorganic and organic inhibitors on the corrosion of Mg–10Gd–3Y–0.5Zr alloy in an ethylene glycol solution at ambient and elevated temperatures. *Electrochim Acta* 2011;56:10166–78.
- [447] Vaghefinazari B, Wierzbicka E, Visser P, Posner R, Arrabal R, Matykinia E, et al. Chromate-free corrosion protection strategies for magnesium alloys – a review: Part III. *Materials* 2022;15:8489.
- [448] Johari NA, Alias J, Zanurina A, Mohamed NS, Alang NA, Zain MZM. Recent progress of self-healing coatings for magnesium alloys protection. *J Coat Technol Res* 2022;19:757–74.
- [449] Upadhyay V, Bergseth Z, Kelly B, Battocchi D. Silica-based sol-gel coating on magnesium alloy with green inhibitors. *Coatings* 2017;7:86.
- [450] Vaghefinazari B, Wang C, Mercier D, Mei D, Seyeux A, Marcus P, et al. Adverse effect of 2,5PDC corrosion inhibitor on PEO coated magnesium. *Corros Sci* 2021;192:109830.
- [451] Wierzbicka E, Vaghefinazari B, Lamaka SV, Zheludkevich ML, Mohedano M, Moreno L, et al. Flash-PEO as an alternative to chromate conversion coatings for corrosion protection of Mg alloy. *Corros Sci* 2021;180:109189.
- [452] Song Y, Tang Y, Fang L, Wu F, Zeng X, Hu J, et al. Enhancement of corrosion resistance of AZ31 Mg alloys by one-step in situ synthesis of ZnAl-LDH films intercalated with organic anions (ASP, La). *J Magnesium Alloys* 2021;9:658–67.
- [453] Chen J, Fang L, Wu F, Xie J, Hu J, Jiang B, et al. Corrosion resistance of a self-healing rose-like MgAl-LDH coating intercalated with aspartic acid on AZ31 Mg alloy. *Prog Org Coat* 2019;136:105234.
- [454] Anjum MJ, Zhao J, Zahedi Asl V, Yasin G, Wang W, Wei S, et al. In-situ intercalation of 8-hydroxyquinoline in Mg-Al LDH coating to improve the corrosion resistance of AZ31. *Corros Sci* 2019;157:1–10.
- [455] Chen Y, Lu XP, Lamaka SV, Ju PF, Blawert C, Zhang T, et al. Active protection of Mg alloy by composite PEO coating loaded with corrosion inhibitors. *Appl Surf Sci* 2020;504:144462.
- [456] Ivanou DK, Yasakau KA, Kallip S, Lisenkov AD, Starykevich M, Lamaka SV, et al. Active corrosion protection coating for a ZE41 magnesium alloy created by combining PEO and sol-gel techniques. *RSC Adv* 2016;6:12553–60.
- [457] Mingo B, Guo Y, Leiva-Garcia R, Connolly BJ, Matthews A, Yerokhin A. Smart functionalization of ceramic-coated AZ31 magnesium alloy. *ACS Appl Mater Interfaces* 2020;12:30833–46.
- [458] Wu WX, Wang WP, Lin HC. A study on corrosion behavior of micro-arc oxidation coatings doped with 2-aminobenzimidazole loaded halloysite nanotubes on AZ31 magnesium alloys. *Surf Coat Technol* 2021;416:127116.
- [459] Aramaki K, Hackerman N. Inhibition mechanism of medium-sized polymethyleneimine. *J Electrochem Soc* 1969;116:568.
- [460] Kokalj A. Considering the concept of synergism in corrosion inhibition. *Corros Sci* 2023;212:110922.
- [461] Qiu Y, Tu X, Lu X, Yang J. A novel insight into synergistic corrosion inhibition of fluoride and DL-malate as a green hybrid inhibitor for magnesium alloy. *Corros Sci* 2022;199:110177.
- [462] Snihirova D, Lamaka SV, Taheri P, Mol JMC, Montemor MF. Comparison of the synergistic effects of inhibitor mixtures tailored for enhanced corrosion protection of bare and coated AA2024-T3. *Surf Coat Technol* 2016;303:342–51.
- [463] Udoh II, Shi H, Liu F, Han E-H. Synergistic effect of 3-Amino-1,2,4-triazole-5-thiol and cerium chloride on corrosion inhibition of AA2024-T3. *J Electrochem Soc* 2019;166:C185–95.
- [464] Dq Z, Lx G, Zhou Gd. Synergistic effect of 2-mercapto benzimidazole and KI on copper corrosion inhibition. *J Appl Electrochem* 2003;361–6.
- [465] Wu YC, Zhang P, Pickering HW, Allara DL. Effect of KI on improving copper corrosion inhibition efficiency of benzotriazole in sulfuric acid electrolytes. *J Electrochem Soc* 1993;140:2791–800.
- [466] Hosseini MG, Tavakoli H, Shahrabi T. Synergism in copper corrosion inhibition by sodium dodecylbenzenesulphonate and 2-mercaptobenzimidazole. *J Appl Electrochem* 2008;38:1629–36.
- [467] Okafor PC, Zheng Y. Synergistic inhibition behaviour of methylbenzyl quaternary imidazole derivative and iodide ions on mild steel in H<sub>2</sub>SO<sub>4</sub> solutions. *Corros Sci* 2009;51:850–9.
- [468] Okafor PC, Liu CB, Liu X, Zheng YG. Inhibition of CO<sub>2</sub> corrosion of N80 carbon steel by carboxylic quaternary imidazole and halide ions additives. *J Appl Electrochem* 2009;39:2535–43.
- [469] Arab ST, Al-Turkustani AM, Al-Dahiri RH. Synergistic effect of Azadirachta Indica extract and iodide ions on the corrosion inhibition of aluminium in acid media. *J Korean Chem Soc* 2008;52:281–94.
- [470] Bouklah M, Hammouti B, Aouniti A, Benkaddour M, Bouyanzer A. Synergistic effect of iodide ions on the corrosion inhibition of steel in 0.5 M H<sub>2</sub>SO<sub>4</sub> by new chalcone derivatives. *Appl Surf Sci* 2006;252:6236–42.
- [471] Jayaprabha C, Sathiyarayanan S, Venkatachari G. Influence of halide ions on the adsorption of diphenylamine on iron in 0.5 M H<sub>2</sub>SO<sub>4</sub> solutions. *Electrochim Acta* 2006;51:4080–8.
- [472] Jayaprabha C, Sathiyarayanan S, Venkatachari G. Co-adsorption effect of polyaniline and halide ions on the corrosion of iron in 0.5 M H<sub>2</sub>SO<sub>4</sub> solutions. *J Electroanal Chem* 2005;583:232–40.
- [473] Larabi L, Harek Y, Traisnel M, Mansri A. Synergistic influence of poly(4-vinylpyridine) and potassium iodide on inhibition of corrosion of mild steel in 1M HCl. *J Appl Electrochem* 2004;34:833–9.
- [474] Obot IB, Obi-Egbedi NO. Inhibition of aluminium corrosion in hydrochloric acid using nizoral and the effect of iodide ion addition. *E-J Chem* 2010;7:837–43.
- [475] Obot IB, Obi-Egbedi NO, Umoren SA. The synergistic inhibitive effect and some quantum chemical parameters of 2,3-diaminonaphthalene and iodide ions on the hydrochloric acid corrosion of aluminium. *Corros Sci* 2009;51:275–82.
- [476] El-Hashemy MA, Easton CD, Seeber A, Cole IS, Hughes AE. Electrochemical and surface characterisation of carbon steel exposed to mixed Ce and iodide electrolytes. *Metals* 2023;13:1553.
- [477] El-Hashemy MA, Hughes AE, Gengenbach T, Glenn AM, Cole IS. Combined influence of Ce(III) and iodide ions for corrosion protection of AA 2024–T3 in acidic to neutral chloride-rich environments: electrochemical and surface characterization studies. *J Rare Earths* 2022;41:309–20.
- [478] Muster TH, Sullivan H, Lau D, Alexander DLJ, Sherman N, Garcia SJ, et al. A combinatorial matrix of rare earth chloride mixtures as corrosion inhibitors of AA2024-T3: Optimisation using potentiodynamic polarisation and EIS. *Electrochim Acta* 2012;67:95–103.
- [479] Clark AM, Gedeck P, Cheung PP, Bunin BA. Using machine learning to parse chemical mixture descriptions. *ACS Omega* 2021;6:22400–9.
- [480] Buin A, Chiang HY, Gadsden SA, Alderson FA. Permutationally invariant deep learning approach to molecular fingerprinting with application to compound mixtures. *J Chem Inf Model* 2021;61:631–40.
- [481] Jirasek F, Hasse H. Combining machine learning with physical knowledge in thermodynamic modeling of fluid mixtures. *Ann Rev Chem Biomol Eng* 2023;14:31–51.
- [482] Duan QN, Hu Y, Zheng SR, Lee J, Chen JY, Bi SF, et al. Machine learning for mixture toxicity analysis based on high-throughput printing technology. *Talanta* 2020;207:120299.
- [483] Cipullo S, Snapir B, Prpich G, Campo P, Coulon F. Prediction of bioavailability and toxicity of complex chemical mixtures through machine learning models. *Chemosphere* 2019;215:388–95.
- [484] Zhang F, Wang Z, Peijnenburg W, Vijver MG. Machine learning-driven QSAR models for predicting the mixture toxicity of nanoparticles. *Environ Int* 2023;177:108025.
- [485] Chen YQ, Peng BL, Kontogeorgis GM, Liang XD. Machine learning for the prediction of viscosity of ionic liquid-water mixtures. *J Mol Liq* 2022;350:118546.
- [486] Liu YB, Hong WX, Cao BY. Machine learning for predicting thermodynamic properties of pure fluids and their mixtures. *Energy* 2019;188:116091.
- [487] Biloudeau C, Kazakov A, Mukhopadhyay S, Emerson J, Kalantar T, Muzny C, et al. Machine learning for predicting the viscosity of binary liquid mixtures. *Chem Eng J* 2023;464:142454.
- [488] Dobbelaere MR, Ureel Y, Vermeire FH, Tomme L, Stevens CV, Van Geem KM. Machine learning for physicochemical property prediction of complex hydrocarbon mixtures. *Ind Eng Chem Res* 2022;61:8581–94.

- [489] Hack HP. 2.07 - Galvanic Corrosion. In: Cottis B, Graham M, Lindsay R, Lyon S, Richardson T, Scantlebury D, et al., editors. *Shreir's Corrosion*. Oxford: Elsevier; 2010. p. 828-56.
- [490] ASTM. G 82 - 98. Standard Guide for Development and Use of a Galvanic Series for Predicting Galvanic Corrosion Performance. 1998.
- [491] Muster TH, Hughes AE, Thompson GE. *Cu Distributions in Aluminium Alloys*. 1st ed. New York: Nova Science Publishers; 2009.
- [492] Hatch JE. *Aluminium: Properties and Physical Metallurgy*: ASM International; 1984.
- [493] Ahmad Z. CHAPTER 4 - TYPES OF CORROSION: Materials and Environments. In: Ahmad Z, editor. *Principles of Corrosion Engineering and Corrosion Control*. Oxford: Butterworth-Heinemann; 2006. p. 120-270.
- [494] Gui F. 11 - Novel corrosion schemes for the aerospace industry. In: Benavides S, editor. *Corrosion Control in the Aerospace Industry*: Woodhead Publishing; 2009. p. 248-65.
- [495] Kallip S, Bastos AC, Yasakau KA, Zheludkevich ML, Ferreira MGS. Synergistic corrosion inhibition on galvanically coupled metallic materials. *Electrochem Commun* 2012;20:101-4.
- [496] Catubig RA, Tan YJ, Hughes AE, Cole IS, Hinton BR, Forsyth M. An Al-Cu multielectrode model for studying corrosion inhibition with praseodymium mercaptoacetate at intermetallic particles in AA2024. *J Electrochem Soc* 2021;168:071501.
- [497] Coelho LB, Mouanga M, Druart ME, Recloux I, Cossement D, Olivier MG. A SVET study of the inhibitive effects of benzotriazole and cerium chloride solely and combined on an aluminium/copper galvanic coupling model. *Corrosion Science* 2016;110:143-56.
- [498] Hughes AE, Glenn AM, Wilson N, Moffatt A, Morton AJ, Buchheit RG. A consistent description of intermetallic particle composition: An analysis of ten batches of AA2024-T3. *Surface and Interface Analysis*. 10 ed 2013. p. 1558-63.
- [499] Winkler DA. Predicting the performance of organic corrosion inhibitors. *Metals* 2017;7:553.
- [500] Engel T, Gasteiger J. *Chemoinformatics: Basic Concepts and Methods*: Wiley VCH; 2018.
- [501] Burden FR, Winkler DA. Optimal sparse descriptor selection for QSAR using Bayesian methods. *QSAR Comb Sci* 2009;28:645-53.
- [502] Muthukrishnan R, Rohini R. LASSO: A feature selection technique in predictive modeling for machine learning. 2016 IEEE International Conference on Advances in Computer Applications (ICACA)2016. p. 18-20.
- [503] Ouyang R, Curtarolo S, Ahmetcik E, Scheffler M, Ghiringhelli LM. SISSO: A compressed-sensing method for identifying the best low-dimensional descriptor in an immensity of offered candidates. *Phys Rev Mater* 2018;2:083802.
- [504] Bartok AP, De S, Poelking C, Bernstein N, Kermode JR, Csanyi G, et al. Machine learning unifies the modeling of materials and molecules. *Sci Adv* 2017;3:e1701816.
- [505] Butler KT, Davies DW, Cartwright H, Isayev O, Walsh A. Machine learning for molecular and materials science. *Nature* 2018;559:547-55.
- [506] Ramprasad R, Batra R, Paliani G, Mannodi-Kanakkithodi A, Kim C. Machine learning in materials informatics: recent applications and prospects. *npj Comput Mater* 2017;3:54.
- [507] Alexander DLJ, Tropsha A, Winkler DA. Beware of R<sup>2</sup>: simple, unambiguous assessment of the prediction accuracy of QSAR and QSPR models. *J Chem Inf Model* 2015;55:1316-22.
- [508] Moura Barbosa AJ, Del Rio A. Freely accessible databases of commercial compounds for high- throughput virtual screenings. *Curr Top Med Chem* 2012;12:866-77.
- [509] Tingle BI, Tang KG, Castanon M, Gutierrez JJ, Khurelbaatar M, Dandarchuluun C, et al. ZINC-22—a free multi-billion-scale database of tangible compounds for ligand discovery. *J Chem Inf Model* 2023;63:1166-76.
- [510] Fronzi M, Isayev O, Winkler DA, Shapter JG, Ellis AV, Sherrill PC, et al. Active learning in bayesian neural networks for bandgap predictions of novel van der Waals heterostructures. *Adv Intell Syst* 2021;3:2100080.
- [511] Winkler Le TC DA. Performance of deep and shallow neural networks, the Universal Approximation theorem, activity cliffs, and QSAR. *Mol Inf* 2016;36:1600118.
- [512] Jorgensen PB, Schmidt MN, Winther O. Deep generative models for molecular science. *Mol Inf* 2018;37:1700133.
- [513] Meyers J, Fabian B, Brown N. De novo molecular design and generative models. *Drug Discov Today* 2021;26:2707-15.
- [514] Sanchez-Lengeling B, Aspuru-Guzik A. Inverse molecular design using machine learning: Generative models for matter engineering. *Science* 2018;361:360-5.
- [515] Gong H, Fu Z, Ma L, Zhang D. Inhibitor\_Mol\_VAE: a variational autoencoder approach for generating corrosion inhibitor molecules. *npj Mater Degrad* 2024;8:102.
- [516] Ebenso EE, Verma C, Olasunkanmi LO, Akpan ED, Verma DK, Lgaz H, et al. Molecular modelling of compounds used for corrosion inhibition studies: a review. *Phys. Chem. Chem. Phys.* 2021;23:19987-20027.
- [517] Verma DK, Aslam R, Aslam J, Quraisi MA, Ebenso EE, Verma C. Computational modeling: theoretical predictive tools for designing of potential organic corrosion inhibitors. *J Mol Struc* 2021;1236.
- [518] Sastri VS, Perumareddi JR. Molecular orbital theoretical studies of some organic corrosion inhibitors. *Corrosion* 1997;53:617-22.
- [519] Ozcan M, Dehri I. Electrochemical and quantum chemical studies of some sulphur-containing organic compounds as inhibitors for the acid corrosion of mild steel. *Prog Org Coat* 2004;51:181-7.
- [520] Ozcan M, Dehri I, Erbil M. Organic sulphur-containing compounds as corrosion inhibitors for mild steel in acidic media: correlation between inhibition efficiency and chemical structure. *Appl Surf Sci* 2004;236:155-64.
- [521] Sastri VS, Elboudjaini M, Perumareddi JR. Utility of quantum chemical parameters in the rationalization of corrosion inhibition efficiency of some organic inhibitors. *Corrosion* 2005;61:933-42.
- [522] Bedair MA. The effect of structure parameters on the corrosion inhibition effect of some heterocyclic nitrogen organic compounds. *J Mol Liq* 2016;219:128-41.
- [523] Kokalj A. On the alleged importance of the molecular electron-donating ability and the HOMO-LUMO gap in corrosion inhibition studies. *Corros Sci* 2021;180:109016.
- [524] Winkler DA, Breedon M, Hughes AE, Burden FR, Barnard AS, Harvey TG, et al. Towards chromate-free corrosion inhibitors: structure-property models for organic alternatives. *Green Chem* 2014;16:3349-57.
- [525] Özkan C, Sahlmann L, Feiler C, Zheludkevich M, Lamaka S, Sewlikar P, et al. Laying the experimental foundation for corrosion inhibitor discovery through machine learning. *npj Mater Degrad* 2024;8:21.
- [526] Zheng P, Zubatyuk R, Wu W, Isayev O, Dral PO. Artificial intelligence-enhanced quantum chemical method with broad applicability. *Nat Commun* 2021;12:7022.
- [527] Feiler C, Mei D, Vaghefinazari B, Würger T, Meißner RH, Luthringer-Feyerabend BJC, et al. In silico screening of modulators of magnesium dissolution. *Corros Sci* 2020;163:108245.
- [528] Landrum G. *RDKit: Open-source cheminformatics*. . 2010.
- [529] Mauri A, Consonni V, Pavan M, Todeschini R. Dragon software: An easy approach to molecular descriptor calculations. *MATCH Commun. Math. Comput. Chem.* 2006;56:237-48.
- [530] Mauri A. alvaDesc: A Tool to Calculate and Analyze Molecular Descriptors and Fingerprints. In: Roy K, editor. *Ecotoxicological QSARs*. Springer, US: New York, NY; 2020. p. 801-20.
- [531] Fernandez M, Breedon M, Cole IS, Barnard AS. Modeling corrosion inhibition efficacy of small organic molecules as non-toxic chromate alternatives using comparative molecular surface analysis (CoMSA). *Chemosphere* 2016;160:80-8.
- [532] Horner L, Meisel K. Corrosion-inhibitors 23 (1) - Does there exist a structure-efficiency relation in organic inhibitors of aluminum corrosion. *Werkstoffe Und Korrosion-Materials and Corrosion* 1978;29:654-64.
- [533] Winkler; DA, Hughes; AE, Özkan; C, Mol; A, Würger; T, Feiler; C, et al. <https://excorr.web.app/database> 2024.
- [534] Jayalakshmi M, Muralidharan VS. Correlation between structure and inhibition of organic compounds for acid corrosion of transition metals. *Indian J Chem Technol* 1998;5:16-28.

- [535] Keshavarz MH, Esmailpour K, Golikand AN, Shirazi Z. Simple approach to predict corrosion inhibition efficiency of imidazole and benzimidazole derivatives as well as linear organic compounds containing several polar functional groups. *Z Anorg Allg Chem* 2016;642:906–13.
- [536] Zhang SG, Lei W, Xia MZ, Wang FY. QSAR study on N-containing corrosion inhibitors: quantum chemical approach assisted by topological index. *J Mol Struct-Theochem* 2005;732:173–82.
- [537] Liu Y, Guo Y, Wu W, Xiong Y, Sun C, Yuan L, et al. A machine learning-based QSAR model for benzimidazole derivatives as corrosion inhibitors by incorporating comprehensive feature selection. *Interdiscipl Sci-Comput Life Sci* 2019;11:738–47.
- [538] El Assiri EH, Driouch M, Lazrak J, Bensouda Z, Elhaloui A, Sfaira M, et al. Development and validation of QSPR models for corrosion inhibition of carbon steel by some pyridazine derivatives in acidic medium. *Heliyon* 2020;6:e05067.
- [539] Galvao TLP, Novell-Leruth G, Kuznetsova A, Tedim J, Gomes JRB. Elucidating structure-property relationships in aluminum alloy corrosion inhibitors by machine learning. *J Phys Chem C* 2020;124:5624–35.
- [540] Galvão TLP, Ferreira I, Kuznetsova A, Novell-Leruth G, Song C, Feiler C, et al. CORDATA: an open data management web application to select corrosion inhibitors. *npj Mater Degrad* 2022;6:48.
- [541] Obot IB, Umoren SA. Experimental, DFT and QSAR models for the discovery of new pyrazines corrosion inhibitors for steel in oilfield acidizing environment. *Int J Electrochem Sci* 2020;15:9066–80.
- [542] Costa SN, Almeida-Neto FWQ, Campos OS, Fonseca TS, de Mattos MC, Freire VN, et al. Carbon steel corrosion inhibition in acid medium by imidazole-based molecules: Experimental and molecular modelling approaches. *J Mol Liq* 2021;326:115330.
- [543] Sadik K, Byadi S, Hachim ME, Hamdani NE, Podlipnik C, Aboulmouhajir A. Multi-QSAR approaches for investigating the relationship between chemical structure descriptors of thiazole derivatives and their corrosion inhibition performance. *J Mol Struct* 2021;1240:130571.
- [544] Dai J, Fu D, Song G, Ma L, Guo X, Mol A, et al. Cross-category prediction of corrosion inhibitor performance based on molecular graph structures via a three-level message passing neural network model. *Corros Sci* 2022;209:110780.
- [545] Ma J, Dai J, Guo X, Fu D, Ma L, Keil P, et al. Data-driven corrosion inhibition efficiency prediction model incorporating 2D–3D molecular graphs and inhibitor concentration. *Corros Sci* 2023;222:111420.
- [546] Li X, Vaghefinazari B, Würger T, Lamaka SV, Zheludkevich ML, Feiler C. Predicting corrosion inhibition efficiencies of small organic molecules using data-driven techniques. *npj Mater Degrad* 2023;7:64.
- [547] Schiessler EJ, Würger T, Vaghefinazari B, Lamaka SV, Meißner RH, Cyron CJ, et al. Searching the chemical space for effective magnesium dissolution modulators: a deep learning approach using sparse features. *npj Mater Degrad* 2023;7:74.
- [548] Burden FR, Winkler DA. An optimal self-pruning neural network and nonlinear descriptor selection in QSAR. *QSAR Comb Sci* 2009;28:1092–7.
- [549] Bartók AP, Kondor R, Csányi G. On representing chemical environments. *Phys Rev B* 2013;87:184115.
- [550] De S, Bartok AP, Csanyi G, Ceriotti M. Comparing molecules and solids across structural and alchemical space. *Phys Chem Chem Phys* 2016;18:13754–69.
- [551] Musil F, De S, Yang J, Campbell JE, Day GM, Ceriotti M. Machine learning for the structure-energy-property landscapes of molecular crystals. *Chem Sci* 2018;9:1289–300.
- [552] Würger T, Wang L, Snihirova D, Deng M, Lamaka S, Winkler DA, et al. Data-driven selection of electrolyte additives for aqueous magnesium batteries. *J Mater Chem A* 2022;10:21672–82.
- [553] Aghaaminiha M, Mehrani R, Colahan M, Brown B, Singer M, Nestic S, et al. Machine learning modeling of time-dependent corrosion rates of carbon steel in presence of corrosion inhibitors. *Corros Sci* 2021;193:109904.
- [554] Sutojo T, Rustad S, Akrom M, Syukur A, Shidik GF, Dipojono HK. A machine learning approach for corrosion small datasets. *npj Mater Degrad* 2023;7:18.
- [555] Akrom M, Rustad S, Dipojono HK. A machine learning approach to predict the efficiency of corrosion inhibition by natural product-based organic inhibitors. *Phys Scr* 2024;99:036006.
- [556] Iyer RS, Iyer NS, P RA, Joseph A. Harnessing machine learning and virtual sample generation for corrosion studies of 2-alkyl benzimidazole scaffold small dataset with an experimental validation. *Journal of Molecular Structure*. 2024;1306:137767.
- [557] Biamonte J, Wittek P, Pancotti N, Rebentrost P, Wiebe N, Lloyd S. Quantum machine learning. *Nature* 2017;549:195–202.
- [558] von Burg V, Low GH, Häner T, Steiger DS, Reiher M, Roetteler M, et al. Quantum computing enhanced computational catalysis. *Phys Rev Res* 2021;3:033055.
- [559] Akrom M, Rustad S, Dipojono HK. Development of quantum machine learning to evaluate the corrosion inhibition capability of pyrimidine compounds. *Mater Today Commun* 2024;39:108758.
- [560] Airbus, BMW, AWS. Quantum Computing Challenge: The Quantum Mobility Quest. <https://qcc.thequantuminsider.com/#slide-32024>.
- [561] Marref A, Basalamah S, Al-Ghamdi R. Evolutionary computation techniques for predicting atmospheric corrosion. *Int J Corros* 2013;2013:805167.
- [562] Ridha M, Amaya K, Aoki S. Multistep genetic algorithm for detecting corrosion of reinforcing steels in concrete. *Corrosion* 2001;57:794–801.
- [563] Khalid F, Aslam MN, Ghani MA, Ahmad N, Abdullah SK. Aging prediction in single based propellants using hybrid strategy of machine learning and genetic algorithm. *Chemom Intel Lab Syst* 2024;245.
- [564] Burger B, Maffettone PM, Gusev VV, Aitchison CM, Bai Y, Wang X, et al. A mobile robotic chemist. *Nature* 2020;583:237–41.
- [565] Coley CW, Eyke NS, Jensen KF. Autonomous Discovery in the chemical sciences Part II: Outlook. *Angew Chem Intl Ed* 2020;59:23414–36.
- [566] Coley CW, Eyke NS, Jensen KF. Autonomous Discovery in the chemical sciences Part I: Progress. *Ange Chem-Inte Ed* 2020;59:22858–93.
- [567] Montoya JH, Winther KT, Flores RA, Bliigaard T, Hummelshøj JS, Aykol M. Autonomous intelligent agents for accelerated materials discovery. *Chem Sci* 2020;11:8517–32.
- [568] Finsgar M, Milosev I. Inhibition of copper corrosion by 1,2,3-benzotriazole: a review. *Corros Sci* 2010;52:2737–49.
- [569] Shchukin DG, Zheludkevich M, Yasakau K, Lamaka S, Ferreira MGS, Moehwald H. Layer-by-layer assembled nanocontainers for self-healing corrosion protection. *Adv Mater* 2006;18:1672–8.
- [570] White PA, Collis GE, Skidmore M, Breedon M, Ganther WD, Venkatesan K. Towards materials discovery: assays for screening and study of chemical interactions of novel corrosion inhibitors in solution and coatings. *New J Chem* 2020;44:7647–58.
- [571] Liu T, Chen Z, Yang J, Ma L, Mol A, Zhang D. Machine learning assisted discovery of high-efficiency self-healing epoxy coating for corrosion protection. *npj Mater Degrad* 2024;8:11.
- [572] Krenn M, Ai Q, Barthel S, Carson N, Frei A, Frey NC, et al. SELFIES and the future of molecular string representations. *Patterns* 2022;3:100588.
- [573] Jablonka KM, Schwaller P, Ortega-Guerrero A, Smit B. Leveraging large language models for predictive chemistry. *Nat Machine Intell* 2024;6:161–9.
- [574] Pu L, Naderi M, Liu T, Wu H-C, Mukhopadhyay S, Brylinski M. eToxPred: a machine learning-based approach to estimate the toxicity of drug candidates. *BMC Pharmacol Toxicol* 2019;20:2.
- [575] Ren C, Ma L, Luo X, Dong C, Gui T, Wang B, et al. High-throughput assessment of corrosion inhibitor mixtures on carbon steel via droplet microarray. *Corros Sci* 2023;213:110967.
- [576] Han P, He Y, Chen C, Yu H, Liu F, Yang H, et al. Study on synergistic mechanism of inhibitor mixture based on electron transfer behavior. *Sci Rep* 2016;6:33252.
- [577] Zhang H, Chen J, Rondinelli JM, Chen W. MolSets: Molecular Graph Deep Sets Learning for Mixture Property Modeling. *arXiv preprint arXiv:231216473*. 2023.
- [578] Abolhasani M, Kumacheva E. The rise of self-driving labs in chemical and materials sciences. *Nature Synthesis* 2023;2:483–92.
- [579] Takahashi A, Kumagai Y, Aoki H, Tamura R, Oba F. Adaptive sampling methods via machine learning for materials screening. *Sci Technol Adv Mater: Methods* 2022;2:55–66.
- [580] Vaghefinazari B, Höche D, Lamaka SV, Snihirova D, Zheludkevich ML. Tailoring the Mg-air primary battery performance using strong complexing agents as electrolyte additives. *J Power Sources* 2020;453:227880.
- [581] Zhang T, Tao Z, Chen J. Magnesium–air batteries: from principle to application. *Mater Horiz* 2014;1:196–206.

- [582] Hoeche D, Lamaka SV, Zheludkevich ML. Electrolyte additives for magnesium air batteries, 16187152.0, EP 3291361B1, JP 06932350B2, US 10637117B2, KR 10-2017-0100315 B1. 2016.
- [583] Wang LQ, Snihirova D, Deng M, Vaghefinazari B, Hoche D, Lamaka SV, et al. Enhancement of discharge performance for aqueous Mg-air batteries in 2,6-dihydroxybenzoate-containing electrolyte. *Chem Eng J* 2022;429:132369.
- [584] Wang L, Snihirova D, Deng M, Vaghefinazari B, Lamaka SV, Hoche D, et al. Tailoring electrolyte additives for controlled Mg-Ca anode activity in aqueous Mg-air batteries. *J Power Sources* 2020;460:228106.